IMA11 -11th Conference of the International Marangoni Association

19-22 June 2023

Bordeaux (France)

BOOK OF ABSTRACTS

Session 1 – Marangoni flows

Monday June 19, 9:30–10:30

"Inverse Marangoni" instability of an ink droplet on a bath

Milène Aubry[1] and Anaïs Gauthier[1]

[1] *Univ Rennes, CNRS, IPR (Institut de Physique de Rennes) - UMR 6251, F-35000 Rennes, France*
anais.gauthier@univ-rennes1.fr

We consider the pattern formed by the spreading of Indian ink on the surface of a water bath, in the spirit of the Japanese "suminagashi" paper marbling process (figure 1a).

Here, ink is deposited with a brush or with a syringe on a bath containing a controlled concentration of surfactants. When increasing the concentration of surfactant in the bath, we evidence a transition between the classical Marangoni spreading to a new kind of instability. The patch of ink initially floating on the bath surface spontaneously destabilize from the center and spreads, forming in the process a complex and intricate pattern (figure 1b). The pattern becomes denser and more complex with time (figure 1c), and when the spreading finally stops, it covers a large portion of the bath surface. Interestingly, this phenomenon is observed only when the surface tension of the bath is close or lower than the surface tension of the ink, *i.e.*, when the initial surface tension forces should prevent the spreading.

This phenomenon is robust and appears with multiple combinations of inks and surfactants. We determine the conditions of its apparition, characterize the spreading of the ink filaments and study the properties of the final pattern. We finally propose a model to explain its origin.

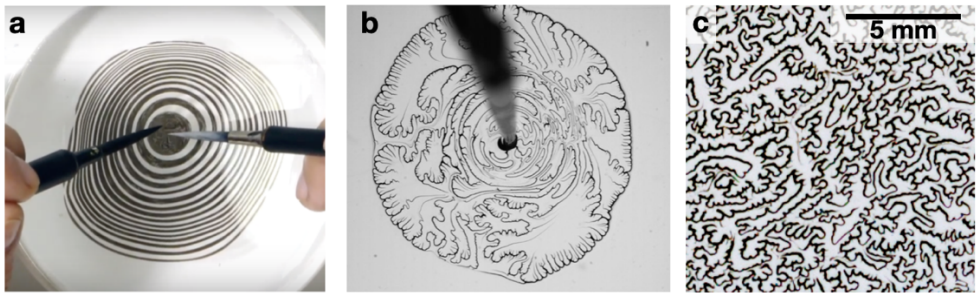

FIG. 1. **a)** Classical paper marbling: ink and soap are successively deposited on the surface of a water bath, forming rings **b)** Instability appearing when ink is deposited on a bath containing surfactants (here SDS, 10g/L). The surface tension of the bath is γ = 37 mN/m and the surface tension of ink is γ = 39 mN/m. **c)** Detail of the final pattern after the deposition of a drop of ink on the bath.

A single parameter can predict surfactant impairment of superhydrophobic drag reduction

Fernando Temprano-Coleto[1], Scott M. Smith[2], François J. Peaudecerf[3], Julien R. Landel[4], Frédéric Gibou[5] and Paolo Luzzatto-Fegiz[5]

[1]*Andlinger Center for Energy and the Environment, Princeton University, Princeton NJ 08544, USA*
ftempranocoleto@princeton.edu
[2]*Department of Chemical Engineering, University of Michigan, Ann Arbor, MI 48109, USA*
scmsmith@umich.edu
[3]*Institut de Physique de Rennes, Université de Rennes, UMR 6251, F-35000 Rennes, France*
francois.peaudecerf@univ-rennes1.fr
[4] *Department of Mathematics, Alan Turing Building, University of Manchester, Manchester M13 9PL, UK*
julien.landel@manchester.ac.uk
[5]*Department of Mechanical Engineering, University of California, Santa Barbara, CA 93106, USA*
fgibou@ucsb.edu pfegiz@ucsb.edu

Recent experimental and computational investigations have shown that trace amounts of surfactants, unavoidable in practice, can critically impair the drag reduction of superhydrophobic surfaces (SHSs), by inducing Marangoni stresses at the air–liquid interface [1 , 2, 3]. However, predictive models for realistic SHS geometries do not yet exist; this has limited the understanding and mitigation of these adverse surfactant effects. To address this issue, we derive a model for laminar, three-dimensional flow over SHS gratings (as sketched in Fig. 1A,B), as a function of geometry and soluble surfactant properties, which together encompass ten dimensionless groups [4]. We establish that the grating length g is the key geometric parameter, and predict that the ratio between actual and surfactant-free slip increases with g^2. Guided by our model, we perform synergistic numerical simulations and microfluidic

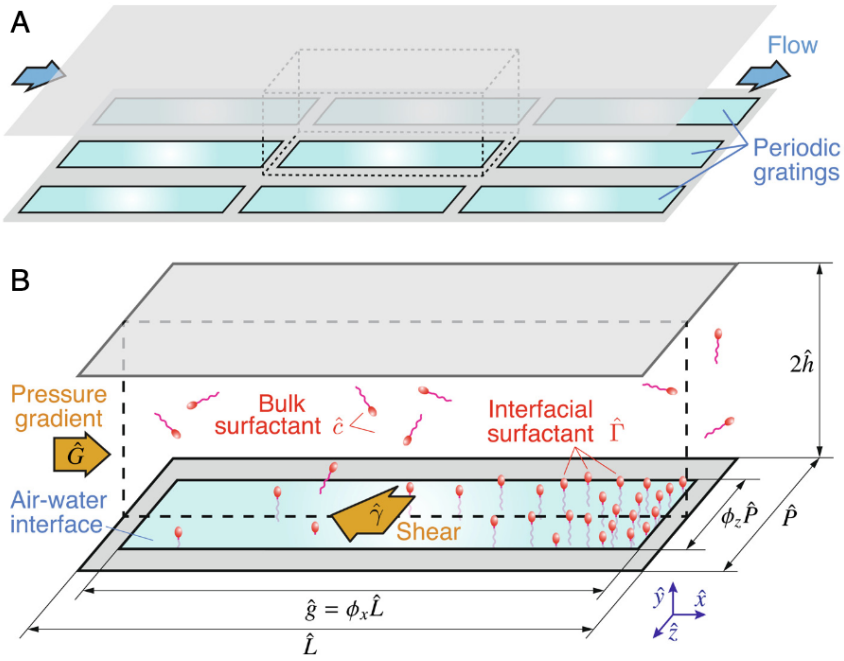

FIG. 1. (A) Channel flow arrangement studied, with an array of slender periodic streamwise gratings on the bottom. (B) Unit cell of the SHS (shown with dashed lines in A), illustrating the downstream accumulation of surfactant.

[1] D. Schäffel, K. Koynov, D. Vollmer, H. J. Butt, C. Schönecker, Local flow field and slip length of superhydrophobic surfaces. Phys. Rev. Lett. **116**, 134501 (2016).
[2] F. J. Peaudecerf, J. R. Landel, R. E. Goldstein, P. Luzzatto-Fegiz, Traces of surfactants can severely limit the drag reduction of superhydrophobic surfaces. Proc. Natl. Acad. Sci. U.S.A. **114**, 7254–7259 (2017). D.
[3] Song et al., Effect of a surface tension gradient on the slip flow along a superhydrophobic air- water interface. Phys. Rev. Fluids **3**, 033303 (2018).
[4] Temprano-Coleto, F., Smith, S. M., Peaudecerf, F. J., Landel, J. R., Gibou, F., & Luzzatto-Fegiz, P. (2023). A single parameter can predict surfactant impairment of superhydrophobic drag reduction. Proc. Natl. Acad. Sci. U.S.A. **120**(3), e2211092120.

experiments, finding good agreement with the theory as we vary surfactant type and SHS geometry, as shown in Fig. 2. Our model also enables the estimation, based on velocity measurements, of a priori unknown properties of surfactants inherently present in microfluidic systems. For SHSs, we show that surfactant effects can be predicted by a single parameter, representing the ratio between the grating length and the interface length scale beyond which the flow mobilizes the air–water interface, as shown in fig. 3 below. This "mobilization length" is more sensitive to the surfactant chemistry than to its concentration, such that even trace-level contaminants may significantly increase drag if they are highly surface active. These findings advance the fundamental understanding of realistic interfacial flows and provide practical strategies to maximize superhydrophobic drag reduction [4].

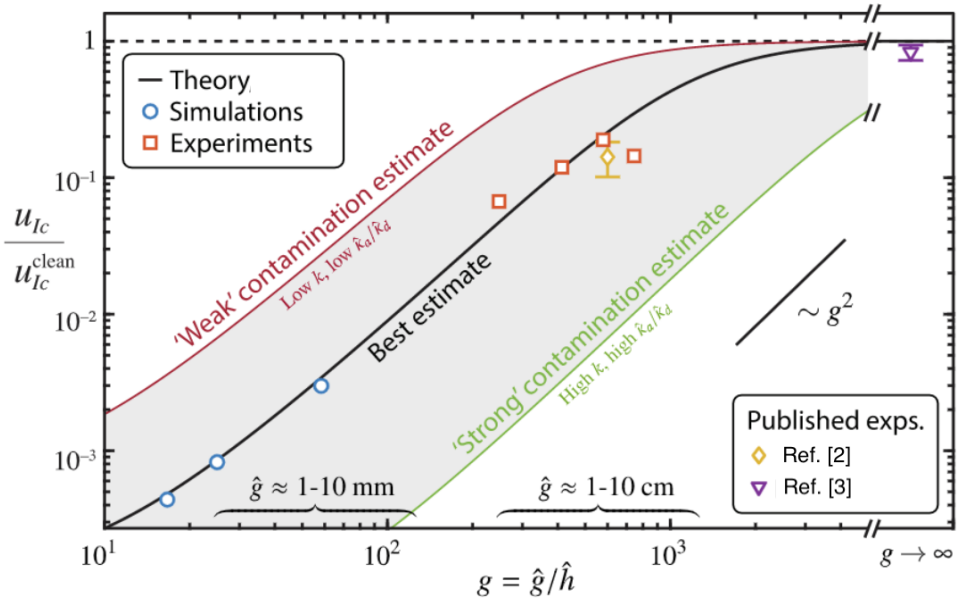

FIG. 2. Ratio between the actual centerline slip velocity and the surfactant-free value (i.e., "clean") from our theory, simulations, and experiments, as well as prior experiments of refs. [2] and [3]. Ref. [3] used an annular grating in a rheometer, with an effectively infinite groove length. The theoretical predictions from our model and simulations use a best-estimate of surfactant parameters, with the shaded region denoting a range of plausible levels of contamination within our estimates.

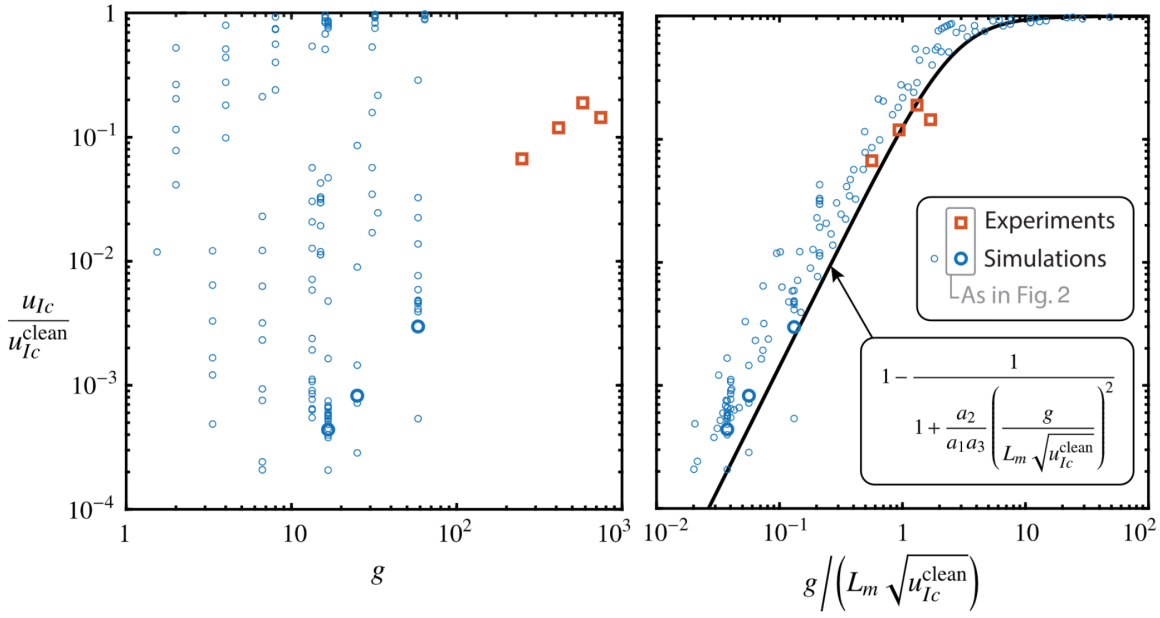

FIG. 3. Left: Experimental and numerical data for the slip velocity, plotted against dimensionless grating length, as one varies surfactant properties, flow velocity, and SHS geometry, together characterized by ten dimensionless groups. Right: normalizing g by the mobilization length L_m approximately collapses the same data onto a single curve, governed by only one dimensionless group.

Collective behavior of dichloromethane drops deposited on a surfactant solution

T. Roy[1], I. Tiwari[3], J. Sebilleau[2], J. Magnaudet[2], P. Parmananda[3], V. Pimienta[1]

[1] *Laboratoire des Interactions Moléculaires et Réactivités Chimiques et Photochimiques, Université Toulouse III - Paul Sabatier, 118 Route de Narbonne, 31062, Toulouse, France*
tanuroy.phy@gmail.com, veronique.pimienta@univ-tlse3.fr
[2] *Institut de Mécanique des Fluides de Toulouse (IMFT), Université de Toulouse, CNRS, Toulouse, France*
[3] *Department of Physics, IIT Bombay, Powai, Mumbai-400076, Maharashtra, India*

We examine the collective dynamics of dichloromethane (DCM) drops on an aqueous solution of cetyltrimethylammonium bromide (CTAB). A single drop of DCM is known to exhibit a rich variety of complex patterns governed by the Marangoni instability[1], sometimes associated with spontaneous symmetry breaking. The corresponding regimes include erratic drifts, pulsations[2], spinning motion[3], and are primarily selected by the molarity of the CTAB solution. To start exploring the collective behavior of multiple DCM drops, we separate two drops with a suitable barrier to avoid their coalescence. The properties of the barrier, especially its permeability, serve as an additional control parameter to tune the strength of the interactions in the neighborhood of each drop, thereby affecting the dynamics of the whole system. Our preliminary observations reveal that these interactions modify the preferably selected regime at a given surfactant concentration. For instance, in the case of two DCM drops on a 0.5 mM CTAB aqueous solution, the drops mostly exhibit spinning motions instead of pulsations which are the expected behavior of the system at this concentration. Schlieren visualizations and particle image velocimetry are used to provide detailed insights into the spatio-temporal evolution of the system.

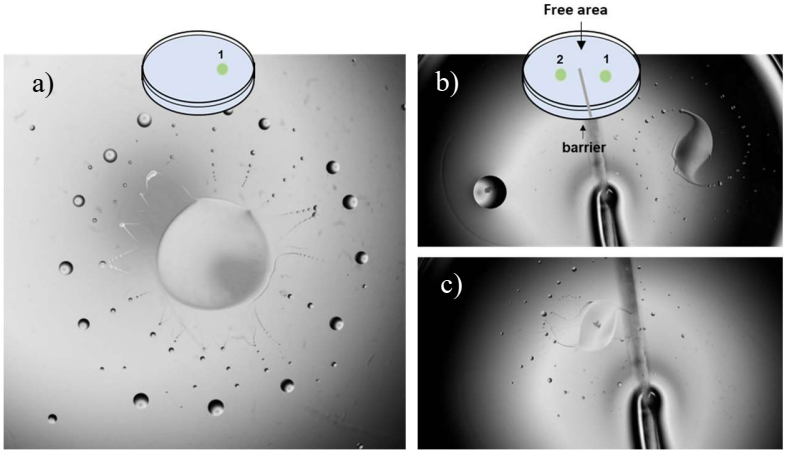

Figure 1 : a) Pulsations observed with a single drop on a 0.5 mM CTAB solution ; b) and c) spinning motion observed for two drops deposited simultaneously on a 0.5 mM CTAB solution. In (b), the presence of drop 1 inhibits the motion of drop 2 ; in (c), drop 1 has faded away while drop 2 exhibits spinning motion.

---

[1] V. Pimienta, M. Brost, N. Kovalchuk, S. Bresch, and O. Steinbock, Complex shapes and dynamics of dissolving drops of dichloromethane, Angewandte Chemie International Edition, **50**, 10728-10731 (2011).

[2] F. Wodlei, J. Sebilleau, J. Magnaudet, and V. Pimienta, Marangoni-driven flower-like patterning of an evaporating drop spreading on a liquid substrate, Nature Communications, **9**, 820 (2018).

[3] D. Boniface, J. Sebilleau, J. Magnaudet, and V. Pimienta, Spontaneous spinning of a dichloromethane drop on an aqueous surfactant solution, Journal of Colloid and Interface Science, **625**, 990-1001 (2022).

How self-propelled droplets adapt to changes in the surroundings by altering their motility

Ranabir Dey[1,2], Carola M. Buness[3,2], Babak Vajdi Hokmabad[4,2] and Corinna C. Maass[5,2]

[1] *Department of Mechanical and Aerospace Engineering, Indian Institute of Technology Hyderabad, Kandi, Telengana- 502285, India, ranabir@mae.iith.ac.in*

[2] *Max Planck Institute for Dynamics and Self-Organization, Am Fassberg 17, 37077 Goettingen, Germany*

[3] *Karlsruhe Institute of Technology, 76131 Karlsruhe, Germany, carola.buness@kit.edu*

[4] *Department of Chemical and Biological Engineering, Princeton University, Princeton, NJ 08544, United States, bv5267@princeton.edu*

[5] *Physics of Fluids Group, Max Planck Center for Complex Fluid Dynamics and J. M. Burgers Center for Fluid Dynamics, University of Twente, PO Box 217, 7500AE Enschede, Netherlands, c.c.maass@utwente.nl*

Biological microswimmers have developed various locomotion strategies to adapt to different changes in their micro-environment. For example, bacteria like *E. coli* and *Vibrio alginolyticus* exhibit run-and-tumble[1] and switch-and-flick[2] motility in response to the changing physico-chemical cues from their immediate surrounding; bacteria and sperm cells also exhibit unique swimming trajectories ranging from linear and helical to oscillatory to adapt to external flows in confined environments[3,4]. Here, we show that self-propelling artificial microswimmers also exhibit autonomous changes in their motility to adapt to changes in their surroundings, by considering active droplets as a model system. These active droplets are oil droplets that are slowly dissolving in supramicellar aqueous solutions of ionic surfactants. The droplets spontaneously develop self-sustaining gradients in interfacial surfactant coverage, resulting in Marangoni stresses which lead to self-propulsion[5].

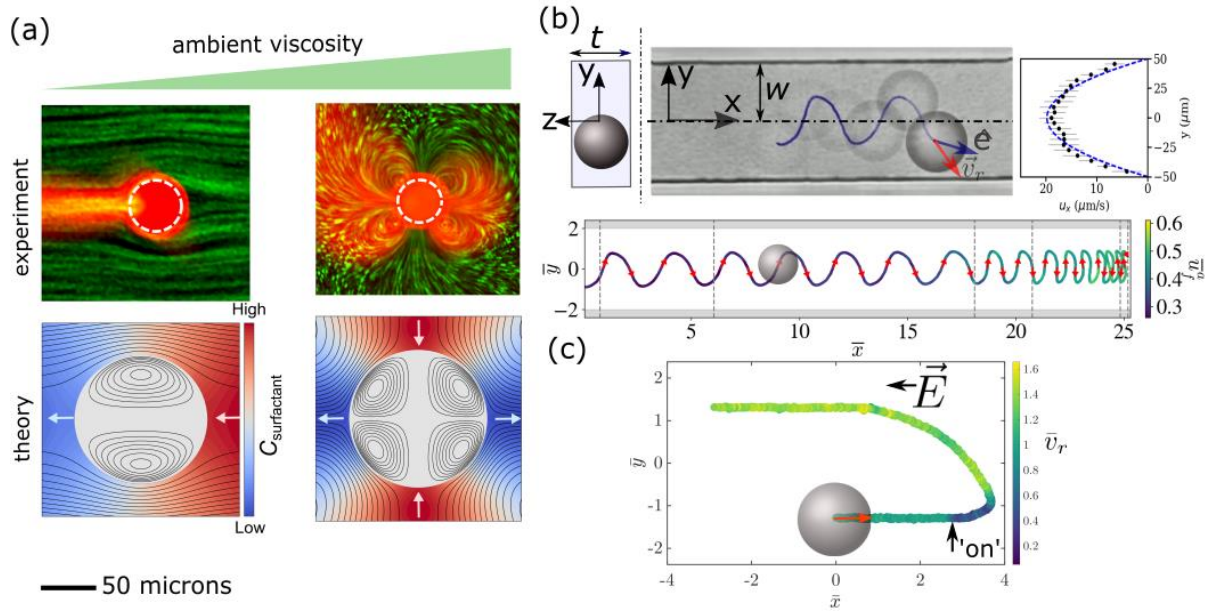

Fig. 1 (a) Emergence of higher hydrodynamic modes (dipolar to quadrupolar) in an active droplet (red) with increasing viscosity of the surrounding medium (green). The interaction of the active droplet with the self-generated chemical gradient, in presence of the higher hydrodynamic mode, results in the emergence of bimodal

[1] H. C. Berg and D. A. Brown, Chemotaxis in Escherichia coli analysed by three-dimensional tracking, Nature **239**, 500-504 (1972).

[2] L. Xie, T. Altindal, S. Chattopadhyay and X-L Wu, Bacterial flagellum as a propeller and as a rudder for efficient chemotaxis, PNAS **108,** 2246-2251 (2011).

[3] V. Kantsler, J. Dunkel, M. Blayney and R. E. Goldstein, Rheotaxis facilitates upstream navigation of mammalian sperm cells, eLife **3**, e02403 (2014).

[4] A. J. Mathijssen, N. Figueroa-Morales, G. Junot, E. Clément, A. Lindner and A. Zöttl, Oscillatory surface rheotaxis of swimming E. coli bacteria, Nature Communications **10(1)**, (2019).

[5] S. Herminghaus, C. C. Maass, C. Krüger, S. Thutupalli, L. Goehring and C. Bahr, Interfacial mechanisms in active emulsions, Soft Matter **10**, 7008 (2014).

motility. **(b)** Time-lapse superposition from bright-field microscopy, showing an active droplet oscillating upstream, in a microchannel flow. The oscillatory trajectory of the active droplet, as it swims upstream, under increasing imposed flow rate ($\bar{u}_a^f$) is also shown here. **(c)** Swimming trajectory of an active droplet showing its reorientation (initially self-propelling towards right; red arrow) on application of an external electric field (directed towards the left; black arrow). The trajectory is color-coded with the instantaneous velocity of the microswimmer.

We show that the self-propelled active droplets adapt to increase in the viscosity of the swimming medium by gradually exhibiting a bimodal swimming strategy instead of the inherent quasi-ballistic motion[6] (Fig. 1(a)). We demonstrate that the bimodal motility at high viscosity emerges from the non-linear coupling between hydrodynamics and the transport of chemical species (surfactants in the case of active droplets) for autophoretic microswimmers. Furthermore, we show that an active droplet navigates upstream of an external flow in a microchannel in an oscillatory trajectory, reminiscent of many biological microswimmers[7] (Fig. 1(b)). Comparing our experiments to a purely hydrodynamic theory model, we explain that the oscillatory upstream swimming of the droplet is primarily governed by the interaction of the finite-sized microswimmer with all four microchannel walls, and the shear flow characteristics. Finally, we demonstrate that these active droplets alter the direction of their inherent quasi-ballistic swimming in response to an external electric field. The active droplets reorient to self-propel along the direction of the applied electric field, thereby exhibiting a directional bias (Fig. 1(c)).

Our results demonstrate that self-propelled artificial microswimmers, like the Marangoni stress driven active droplets, are capable of altering their swimming dynamics in response to external cues due to their physico-chemical and hydrodynamic interactions with the surrounding. Understanding these alterations in swimming strategy for artificial microswimmers (model systems) serves two main purpose- one, it provides better insight into the underlying adaptation mechanisms which to a certain extent are applicable even for biological microswimmers; two, it helps in devising accurate methodologies for possible control of active particles swimming in confinements as relevant in many biotechnology/biomedical applications.

[6] B. V. Hokmabad, R. Dey, M. Jalaal, D. Mohanty, M. Almukambetova, K. A. Baldwin, D. Lohse and C. C. Maass, Emergence of bimodal motility in active droplets, Physical Review X **11 (1)**, 011043 (2021).

[7] R. Dey, C. M. Buness, B. V. Hokmabad, C. Jin and C. C. Maass, Oscillatory rheotaxis of artificial swimmers in microchannels, Nature Communications **13 (1)**, 1-10 (2022).

Session 2 – Wetting and contact lines

Monday June 19, 11:00–12:30

Partial wetting on a horizontal solid surface: beyond Young's equation

Marc Medale[1] and David Brutin[2]

[1] *Aix-Marseille Université, IUSTI, CNRS UMR 7343, Marseille, France,* marc.medale@univ-amu.fr

[2] *Aix-Marseille Université, IUSTI, CNRS UMR 7343, Marseille, France,* david.brutin@univ-amu.fr

I. INTRODUCTION

The equation that governs the equilibrium shape of a liquid drop in contact with a solid substrate remains a topical scientific question. Indeed, Young's equation [1] determines the value of the macroscopic contact angle as a function of the surface tensions at the solid-liquid, solid-gas and gas-liquid interfaces, only. However, it solves for a unique equilibrium value, meanwhile most experiments report a contact angle hysteresis between advancing and receding contact lines. Finally, most of the assumptions involved in its derivation have never been clearly stated and several questions therefore remain open. What is its domain of validity? Could other physical contributions such as line tension and/or gravity have some influence on the value of the macroscopic contact angle?

II. DEVELOPED MODEL AND RESULTS

To contribute to answer these questions, we have derived a macroscopic model based on the physico-chemical equilibrium condition of the system, which corresponds to the minimization of the total energy of the solid-liquid-gas system [2]. This approach leads to deal in a unified formalism with either gravity-assisted wetting (sessile drop) or opposing one (pendant drop), along with weightlessness as a particular case. The latter case leads to an analytical governing equation, which is trigonometric, thanks to the spherical cap model [3]. On the other hand, in a gravity field assuming the solid substrate to be horizontal endows the problem with a rotational symmetry that leads to a set of six differential-algebraic equations to be solved numerically.

The main outcomes of the proposed approach are: i) in weightlessness, line tension does influence the macroscopic contact angle in a $1/r$ trend (r being the dimensionless wetted radius), as long as r is lower than roughly one thousand. Above this value the macroscopic contact angle asymptotically tends towards the value given by the Young's equation; ii) in a gravity field the macroscopic contact angle also depends on the Bond number over a broad range of values, cf. fig. 1 and 2.

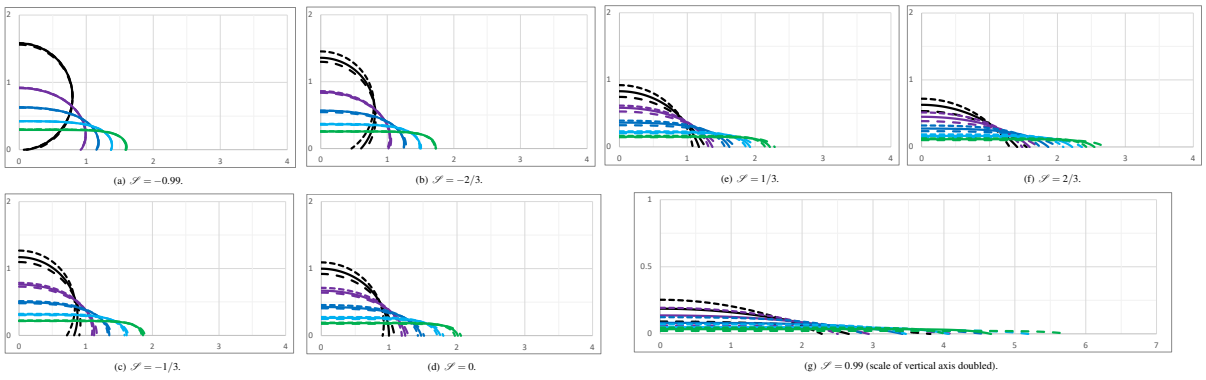

FIG. 1. Sessile drops in a gravity field for Bond number ranging from 0-4 (step of 1) and seven dimensionless ratios of surface free energies $S=(\gamma_{sg}- \gamma_{sl})/\gamma_{lg}$. Solid lines refers to the solution with no line tension, short and long dashed lines refer to advancing and receding contact lines, respectively.

Thus, the range of validity of Young's equation is the one that simultaneously satisfies two conditions: i) large wetting radius (when the relative influence of line tension is negligible compared to that of surface tensions) and ii) small drop size compared to the capillary length (low Bond number). It follows that in many situations in earth gravity where these two conditions cannot be simultaneously satisfied,

the surface tensions deduced from Young's equation could be incorrectly evaluated.

So to conclude, in a gravity field the Young's equation can be only an approximate relationship for the macroscopic contact angle. In the present work, all surface and line tension were assumed to be independent on the drop shape. Therefore, in the next steps, this work will also consider the case where line tension could depend on the macroscopic contact angle.

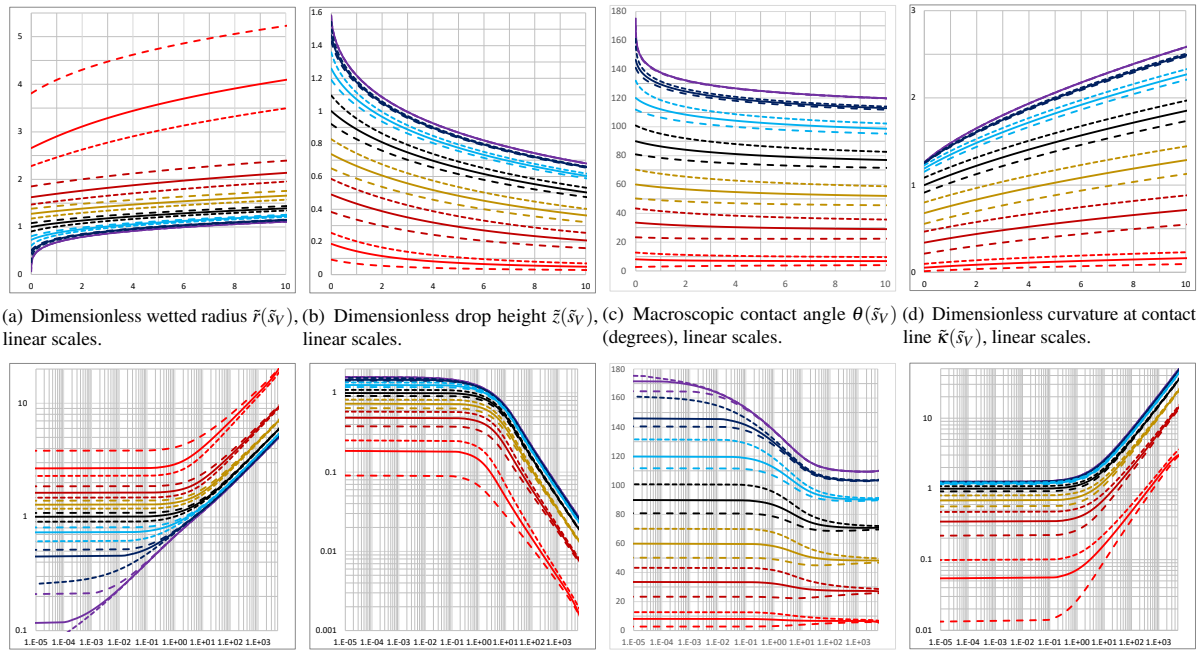

(a) Dimensionless wetted radius $\tilde{r}(\tilde{s}_V)$, linear scales. (b) Dimensionless drop height $\tilde{z}(\tilde{s}_V)$, linear scales. (c) Macroscopic contact angle $\theta(\tilde{s}_V)$ (degrees), linear scales. (d) Dimensionless curvature at contact line $\tilde{\kappa}(\tilde{s}_V)$, linear scales.

(e) Dimensionless wetted radius $\tilde{r}(\tilde{s}_V)$, logarithmic scales. (f) Dimensionless drop height $\tilde{z}(\tilde{s}_V)$, logarithmic scales. (g) Macroscopic contact angle $\theta(\tilde{s}_V)$ (degrees), linear-logarithmic scales. (h) Dimensionless curvature at contact line $\tilde{\kappa}(\tilde{s}_V)$, log scales.

FIG. 2. Sessile drops in a gravity field for various Bond number and seven dimensionless ratios of surface free energies S=-0.99 (purple), -2/3 (dark blue), -1/3 (light blue), 0 (black), 1/3 (gold), 2/3 (dark red), 0.99 (red). Solid lines refers to the solution with no line tension, short and long dashed lines refer to advancing and receding contact lines, respectively.

[1] Young, T. *An Essay on the Cohesion of Fluids*. Philos. Transactions, Roy. Soc. Lond. 95, 65-87 (1805).

[2] Gibbs, J. W. *Scientific Papers of Josiah Willard Gibbs*, vol. 1 (Longmans, Green, And Co., New York and Bombay) (1906).

[3] Medale, M., Brutin, D. *Sessile drops in weightlessness: an ideal playground for challenging Young's equation*. npj Microgravity 7, 30, DOI: 10.1038/s41526-021-00153-9 (2021).

Particle Dispersion and Deposition in Evaporating Two-Dimensional Sessile Droplets

Ali Kerem Erdem[1], Fabian Denner[2], Luca Biancofiore[1]

[1] *Department of Mechanical Engineering, Bilkent University, 06800, Ankara, Turkey,* luca@bilkent.edu.tr
[2] *Chair of Mechanical Process Engineering, Otto von Guericke University, 39106, Magdeburg, Germany,* fabian.denner@ovgu.de

I. INTRODUCTION

Evaporating sessile droplets containing dispersed particles, are used in different technological applications, such as coating, printing, and medicine. For these applications, it is needed to accurately predict both the motion and deposition of the particles. Furthermore, the interaction between the droplet and the surface where it lies down must be considered: in particular, the motion of the contact line has to be carefully modeled [1]. In literature, we have found that most of the works assume only one contact line regime either pinned or moving. This assumption is made to simplify the model and the numerical methods. However, both scenarios, i.e., moving and pinned contact line regimes, are observed during the whole evaporation process [2]. Therefore, in this work, both regimes are taken into consideration together with the particle motion and deposition. We have developed a numerical algorithm which solves the pinned contact line regime until a determined contact angle limit is reached. After exceeding this limit, the contact line starts to move, and we follow the droplet evolution until most of the initial particle mass is deposited.

II. MATHEMATICAL AND NUMERICAL MODELS

The one-sided model [3] is used to simplify the multiphase problem and ignoring contribution of the vapor phase. Our mathematical model describes how the droplet's height (h), the particle concentration (c), both the radius and contact angle of the droplet (a, Θ, respectively), and the deposited particle density (ρ_{dep}) spatio-temporally evolve. The Navier-Stokes equations, the advection-diffusion equation, the constitutive equation for particle deposition, and the relevant boundary conditions are all utilized in our mathematical model. Scaling and simplifications are made within the lubrication theory [4, 5] and the rapid vertical diffusion assumptions [6]. As in Karapetsas et al. [7], the viscosity depends on the particle concentration. We consider the effect of both the evaporation and the contact angle on the contact line motion [4]. We assume that there is a linear relation between the particle concentration and their deposition [8], and this relation is implemented into the transport equation for the concentration. As a result, we can derive the temporal evolution equations for $h, c,$ and a. The important parameters of our model are: (i) the Marangoni number M, which measures the thermocapillary strength, (ii) the evaporation number E, that compares the evaporative and viscous time scales, (iii) the Damköhler number Da, comparing the particle deposition and diffusion, and (iv) the Peclet number Pe, i.e., ratio between particle diffusion and advection.

The described mathematical model is solved with the finite difference method. The transient terms are discretized with Runge-Kutta 4th order method (RK4) and the spatial domain is discretized with 4th order central and backward difference methods. The algorithm development is divided into to two sub-cases; (i) the first sub-algorithm concerns the moving contact line without considering the particles concentration; (ii) the second sub-algorithm focused on the pinned contact line regime where both particle motion and deposition are present. Finally, these two sub-algorithms are combined to cover both contact line regimes, in which particles are present. The validation of the two sub-algorithms is achieved

[1] J. H. Snoeijer and B. Andreotti, Annual Review of Fluid Mechanics **45**, 269–292, (2013).
[2] H. Hu and R. G. Larson, The Journal of Physical Chemistry B **106**, 1334-1344, (2002).
[3] J. P. Burelbach, S.G. Bankoff, and S.H. Davis, Journal of Fluid Mechanics **195**, 463-494, (1988).
[4] D. M. Anderson, and S. H. Davis, Physics of Fluids **7**, 248-265, (1995).
[5] P. Ehrhard and S. H. Davis, Journal of Fluid Mechanics **229**, 365 - 388, (1991).
[6] O. E. Jensen and J. B. Grotberg, Physics of Fluids A: Fluid Dynamics **5**, 58 - 68, (1993).
[7] G. Karapetsas, K. C. Sahu, and O. K. Matar, Langmuir **32**, 6871-6881, (2016).
[8] E. Widjaja, and M. T. Harris, AIChE Journal **54**, 2250-2260, (2008).

by successfully comparing our results to previous works found in literature [4, 9, 10].

III. RESULTS

In figure 1, how h, c and ρ_{dep} evolve with time is shown for our test case. The droplet height decreases in the pinned part and, after exceeding the contact angle limit (Θ_{lim}=2°) [2], the droplet continues to shrink also in the moving contact line regime. For this test case, the particle concentration increases near the contact line in the pinned configuration, showing the particle accumulation near the contact line. This trend affects also the particle deposition. Figure 1c shows that most of the particles are deposited near the contact line during the pinning regime. Conversely, in the moving contact line regime, the remaining particles are deposited along the other parts of the domain. As a result of this, the final pattern left by the pattern recall the famous *coffee ring effect* [11].

Furthermore, we analyzed the influence on the droplet evolution of the different parameters (i.e., M, E, Da, Pe). By increasing the Marangoni number, we decrease the particle accumulation near the contact line and more particles are deposited near the center of the droplet. By increasing the evaporation number, an increase in the particle accumulation near the contact line is observed, while a larger (smaller) Damköhler (Peclet) number causes more uniform final patterns left by the deposited particles.

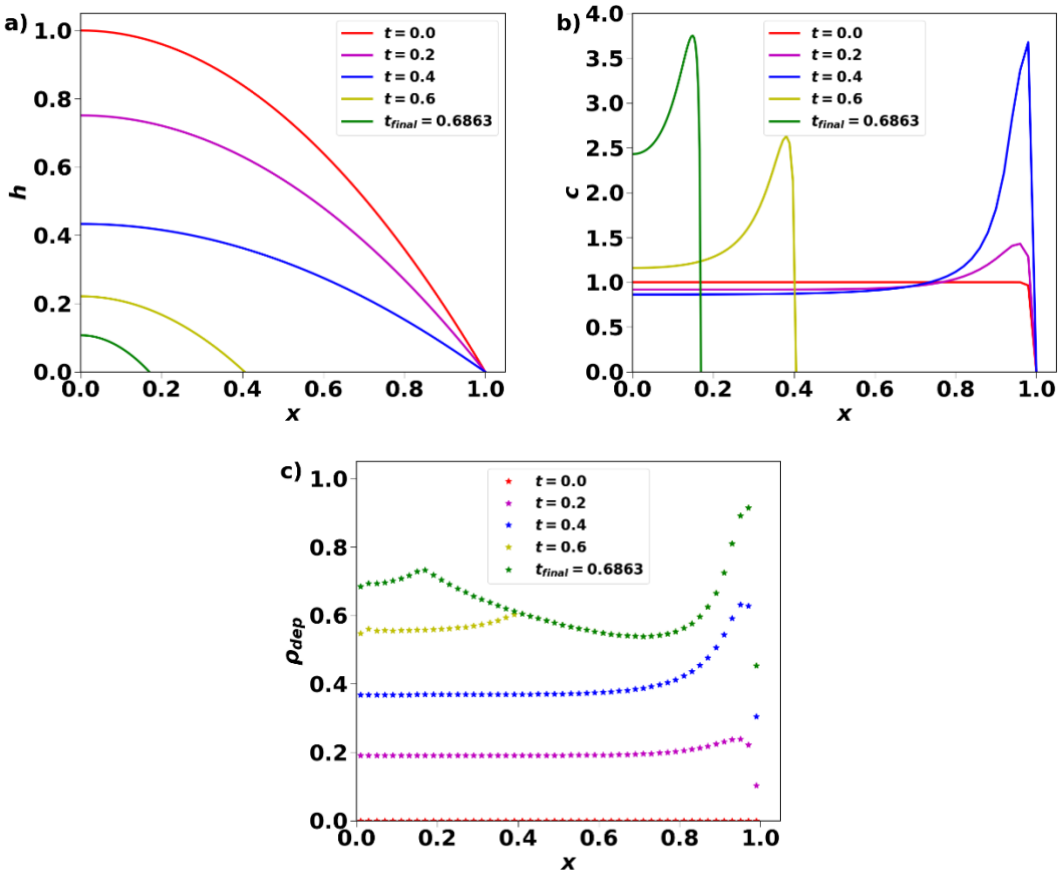

FIG. 1. Droplet evolution for M=1.0, E=0.5, Da=1.0, Pe=10.0. a) Droplet height; b) Particle concentration; c) Particle deposition.

[9] B. J. Fischer, Langmuir **18**, 60-67, (2002).

[10] Y. Y. Tarasevich, I. V. Vodolazskaya, and O. P. Isakova, Colloid and Polymer Science **289**, 1015-1023, (2011).

[11] R. D. Deegan, O. Bakajin, T. F. Dupont, G. Huber, S. R. Nagel, and T. A. Witten, Nature **389**, 827 - 829, (1997).

Anomalous flow fields near a moving contact line

Charul Gupta[1], Lakshmana Chandrala Dora[2] and Harish N Dixit[3]

[1]*Dept. of Mechanical & Aerospace Engineering, IIT Hyderabad, India,* me18resch11001@mae.iith.ac.in
[2]*Dept. of Mechanical & Aerospace Engineering, IIT Hyderabad, India,* lchandrala@mae.iith.ac.in
[3]*Dept. of Mechanical & Aerospace Engineering, IIT Hyderabad, India,* hdixit@mae.iith.ac.in

I. INTRODUCTION

The study of a moving contact line is a classical problem in fluid mechanics. According to viscous theory of Huh & Scriven[1] developed in the early 70s, it is shown that application of conventional no-slip boundary condition on the moving solid results in a stress singularity with a logarithmic divergence of dissipation. Nevertheless, the viscous theory predicts flow fields in the vicinity of a moving contact line which can be broadly divided into three categories as shown in fig. 1 depending on the value of the viscosity ratio ($\lambda = \mu_A/\mu_B$) and dynamic contact angle (θ_d, measured in phase B), with A and B corresponding to the receding and advancing phases respectively. Several theoretical models have been developed to regularize the singularity and are summarised in excellent reviews[2] and monographs[3]. The major focus of the theoretical models has been to predict the relationship between the dynamic contact angle, θ_d, the capillary number, $Ca = \mu_B U/\gamma$. Further, the theoretical models assume that the Huh & Scriven's solution is valid in the *'outer'* region, i.e., away from the moving contact line where the no-slip condition can be applied. This makes is possible to test contact line models by measuring the contact angle and flow fields away from the contact line. A key prediction of the viscous theory is that the flow field in the more viscous fluid is of the rolling-type as shown in fig. 1a. Such a flow field has been commonly observed in droplets rolling down an inline plane as shown in the seminal work of Dussan & Davis[4]. Most of the earlier experimental observations of flow fields were restricted to $\theta_d > 90°$ such as the advancing tube experiments of Chen et al.[5] and were found to be broadly consistent with viscous theory. One exception is the study of Savelski *et al*.[6] who questioned the validity of viscous theory since the observed flow fields were opposite to the predictions of viscous theory. It is important to note that the advancing contact angle for a rolling drop seldom falls below 90°.

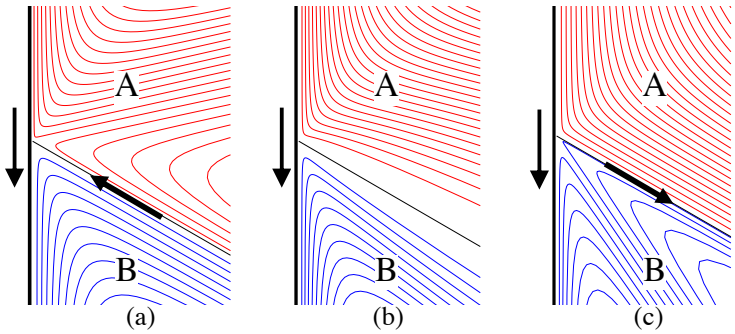

FIG. 1. Flow patterns based on the viscous theory of Huh & Scriven, (a) Rolling motion in B and split-streamline in A, (b) rolling motion in both the fluids, (c) split-streamline motion in B and rolling motion in A.

To have better control on the speed and angle of a moving contact line, we use plate advancing PIV experiments as shown schematically in fig 2. Using different combinations of fluids such as air-water, air-silicone oils, silicone oil-sugar water mixtures, air-glycerol water mixtures, we vary the viscosity ratio in our experiments. Surface treatment of the dipping plate as well as speed of the advancing plate allows us to access a wide range of dynamic contact angles. By operating at low speeds, we conduct a systematic study at low Reynolds and capillary numbers resulting in a comprehensive survey of the parameter space in the $\lambda - \theta_d$ plane.

II. RESULTS

Two key results from our study are shown in fig. 3. In the case of silicone oil, the flow is always found to be of the rolling-type which is consistent with viscous theory. In this case, the dynamic contact angle is also found to be in good agreement with slip-based models such as the Cox model[7,8]. But with sugar-

water mixtures with an advancing angle less than 90°, the flow field resembles a split-streamline flow in contradiction with the predictions of the viscous theory. To achieve such an acute angle, the advancing glass substrate is coated with a hydrophilic layer. Similar contradiction is also observed when using glycerol-water mixtures. Our experiments provide detailed information of flow field and interface shapes which can be used to develop and validate new contact line models. The anomalous nature of the flow fields suggests that viscosity ratio and dynamic contact angle are alone not sufficient to predict the flow fields near a moving contact line.

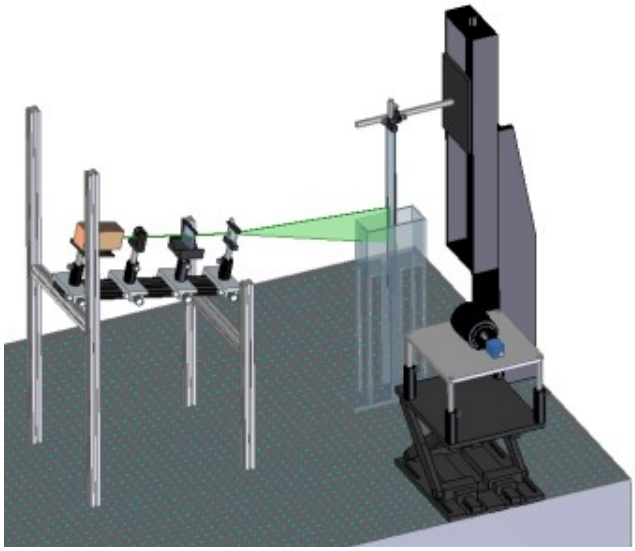

FIG. 2. Schematic of the PIV experimental set-up

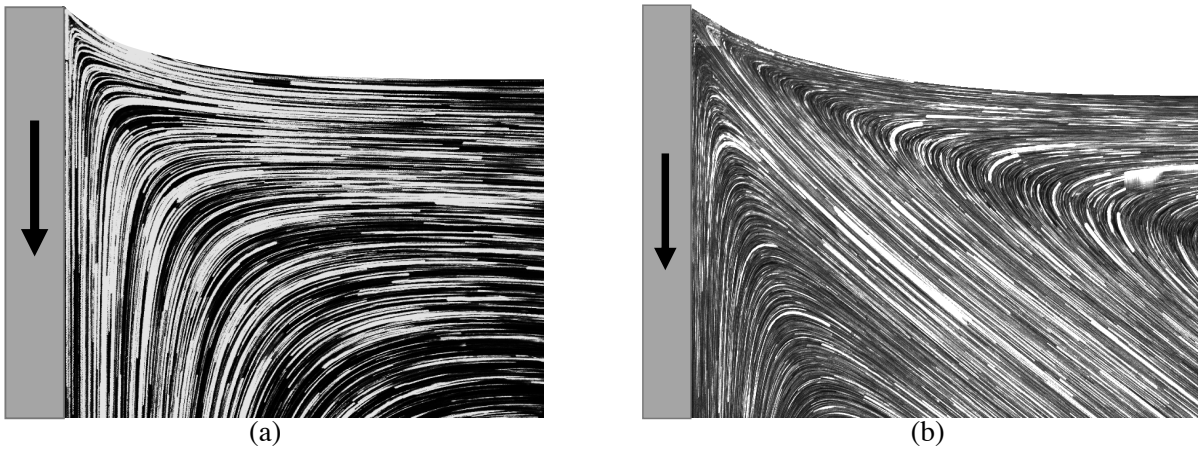

(a) (b)

FIG. 3. (a) Rolling motion in a 5 cSt silicone oil-air interface at $Re = 0.016$ and $Ca = 4.19 \times 10^{-3}$, (b) split-streamline motion for a 48% w/w sugar-water mixture at $Re = 9.61 \times 10^{-3}$ and $Ca = 1.13 \times 10^{-3}$.

[1]. C. Huh and L. E. Scriven, Hydrodynamic model of steady movement of a solid/liquid/fluid contact line, J. Coll. Interface Sci. **35(1)**, 85-101 (1971).

[2]. J. H. Snoeijer and B. Andreotti, Moving contact lines: scales, regimes, and dynamical transitions, Ann. Rev. Fluid Mech. **45**, 269-292 (2013).

[3]. Y. D. Shikhmurzaev, *Capillary flows with forming interfaces*, Chapman & Hall/CRC (2008).

[4]. E. B. Dussan and S. H. Davis, On the motion of a fluid-fluid interface along a solid surface, J. Fluid Mech. **65**, 71-95 (1974).

[5]. Q. Chen, E. Ramé and S. Garoff, The velocity field near moving contact lines, J. Fluid Mech. **337**, 49-66 (1997).

[6]. M. J. Savelski, S. A. Shetty, W. B. Kolb and R. L. Cerro, Flow patterns associated with the steady movement of a solid/liquid/fluid contact line, J. Coll. Interface Sci. **176**, 117-127 (1995).

[7]. R. G. Cox, The dynamics of the spreading of liquids on a solid surface. Part 1. Viscous flow, J. Fluid Mech. **168**, 169-194 (1986).

[8]. N. Le Grand, A. Daerr and L. Limat, Shape and motion of drops sliding down an inclined plane, J. Fluid Mech. **541**, 293-315 (2005).

Capillary desorption of molecules induced by a moving contact line

Sylvain Franiatte, Philippe Tordjeman and Thierry Ondarçuhu

Institut de Mécanique de Fluides de Toulouse, 31400 Toulouse, France. thierry.ondarcuhu@imft.fr

It is well established that the wetting properties of a surface by a given liquid largely depend on the topographic and chemical nature of the substrate, down to the nanometer scale. The coupling with the liquid can also trigger a modification of the substrate properties leading to complex situations of adaptative wetting [1]. In this context, the interplay between the substrate modification by the liquid and the dynamics of the drop is an open question in wetting science, which requires new specific experiments at the molecular scale.

Atomic force microscopy (AFM) is a unique tool to study the dynamics of contact line or nanomeniscus at the nanometer scale [2,3]. The monitoring of the capillary force exerted by the liquid on a nanoneedle carved at the apex of the AFM tip allows one to distinguish the effects of topographical and chemical defects and to monitor minute changes of the needle surface properties.

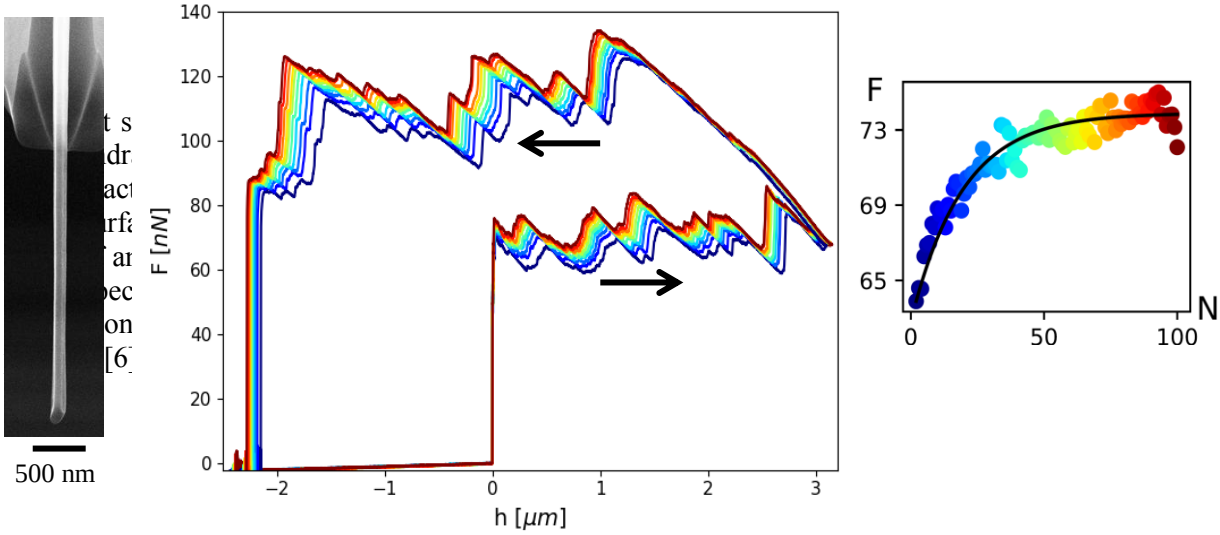

FIG. 1. Left: Scanning electron microscopy image of a nanoneedle carved at the extremity of an AFM tip; center: capillary forces F measured as a function of the immersion depth h for a nanoneedles dipped in (increasing h) and withdrawn (decreasing h) from a liquid bath, for successive dipping cycles (from blue to red); right: evolution of the force associated with a given peak of the force curve as a function of the number N of cycles.

In recent studies [4,5], we evidenced a change of wettability when the tip is continuously dipped in and withdrawn from the liquid a large number of times. We demonstrate that this leads to a decrease of the contact angle down to a constant value while keeping the topography intact. Interestingly, the

[1] Butt, H.-J., Berger, R., Steffen, W., Vollmer, D. and Weber, S. A. L. Adaptive Wetting—Adaptation in Wetting. *Langmuir* **34**, 11292–11304 (2018).

[2] Delmas, M., Monthioux, M. and Ondarçuhu, T. Contact Angle Hysteresis at the Nanometer Scale. *Phys. Rev. Lett.* **106**, 136102 (2011).

[3] Mortagne, C., Lippera, K., Tordjeman, P., Benzaquen, M. and Ondarçuhu, T. Dynamics of anchored oscillating nanomenisci. *Phys. Rev. Fluids* **2**, 102201 (2017).

[4] Franiatte, S., Tordjeman, P. and Ondarçuhu, T. Molecular Desorption by a Moving Contact Line. *Phys. Rev. Lett.* **127**, 065501 (2021).

[5] Franiatte, S., Tordjeman, P. and Ondarçuhu, T. Wetting at the Nanoscale: Molecular Mobility Induced by Contact Line Forces. *Langmuir* **38**, 2614–2625 (2022).

initial surface properties can be recovered when leaving the tip in air. We interpret these results as the result of an adsorption of airborne contaminants on the tip surface and their desorption by the liquid. Using specific experiments, we unambiguously demonstrate that the desorption mechanism is induced at the contact line, a result of the capillary force on the molecules, as already observed on particles [6]. Using a large range of liquids, tips and velocities, we present a comprehensive study of this effect and show its applications for monitoring molecules adsorption and desorption with a sub-second time resolution or for cleaning of surfaces.

[6] Sharma, P., Flury, M. & Zhou, J. Detachment of colloids from a solid surface by a moving air–water interface. *J. Colloid Interf. Sci.* **326**, 143–150 (2008).

Vertical Impact of a Liquid jet on an Over-heated Plate

Alice Germa[1], Aurélien Goerlinger[1], Farzam Zoueshtiagh[1] and Alexis Duchesne[1]

[1] *Univ. Lille, UMR 8520 - IEMN- Institut d'Electronique de Microélectronique et de Nanotechnologie, F-59000 Lille, France* alexis.duchesne@univ-lille.fr

When a liquid jet impinges vertically on a horizontal hot surface, one can observe different phenomena from film boiling to hydraulic jump formation and wetting [1]. In the present study, we perform experiments, with identical configuration, of a liquid jet normally impinging on a hot surface but with jets of sub-millimetric diameters. To this end, we produce water jets using commercially available needles of diameters of 0.11 mm to 0.45 mm. The impinged horizontal hot plate is maintained at a constant temperature, ranging from 350 to 530°C. The jet radius R and the liquid speed V are systematically varied. As first experimental results, we demonstrate that the temperature (in the selected range) has almost no influence and that the phenomenology could be rationalized using solely the Weber number. This dimensionless number is defined in our experiments as $We = \frac{\rho V^2 R}{\gamma}$ where ρ is the liquid density and γ the air-water surface tension.

Experiments show that in the low We (<30) regime (see FIG 1 a.), a liquid puddle in film boiling/Leidenfrost state is formed around the impact position of the jet with the hot plate.

For higher We (see FIG 1 b.), we observe the formation of a small patch where the liquid is in contact with the plate and surrounded at its periphery by a crown of ejected liquid droplets. The results show that these drops are ejected at a constant angle from the plate that depends on the We number value: it decreases from 30° to 4-5° when We increases from 30 up to 450.

(a) 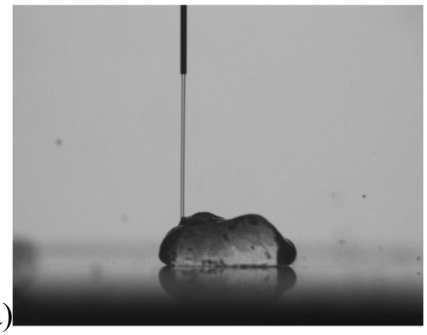 (b) 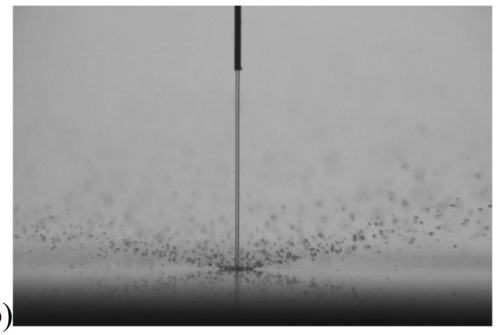

FIG 1: Vertical water (R=0.15 mm) jet impinging a 350°C hot plate. (a) low We regime: a levitating liquid puddle is formed (b) high We regime: liquid solid patch and drop ejection at constant angle are observed.

[1] C. Agrawal, Surface quenching by jet impingement– a review , Steel Res. Int., **90**, no 1, p. 1800285 (2019).

Session 3 – Solutocapillary flows

Monday June 19, 14:00–15:45

Effect of interfacial kinetics on the settling of a drop in a viscous medium

Sayali N. Jadhav[1] and Uddipta Ghosh[2]

[1] *Discipline of Mechanical Engineering, Indian Institute of Technology Gandhinagar, Palaj, Gujarat 382055, India,* sayali.jadhav@iitgn.ac.in

[2] *Discipline of Mechanical Engineering, Indian Institute of Technology Gandhinagar, Palaj, Gujarat 382055, India,* uddipta.ghosh@iitgn.ac.in

Multiphase emulsions, such as drops in a continuous medium tend to have surfactant-like impurities present at the interfaces, either naturally or introduced artificially for stability, which may influence the flow field and hence alter the motion of the drops through a host of different mechanisms. Here, we carry out a robust analysis to characterize multiple aspects of such interfacial phenomena, by studying the settling of a drop in a quiescent viscous medium. The surface active agents are assumed to be bulk-insoluble and non-ideal, while the interface itself is assumed to have its own rheology, described by the Boussinesq-Scriven model. The diffusive fluxes of the surfactants are expressed in a thermodynamically consistent manner as proportional to the chemical potential gradient, which results in concentration dependent diffusivity. We subsequently derive semi-analytical solutions for approximately spherical drops without any other restrictions on the transport processes. Our results reveal that stresses originating from interfacial rheology tend to decrease the settling velocity and at the same time make the surfactant concentration uniform across the surface. Remarkably, this settling velocity is revealed to be independent of the choice of the free-energy isotherms and the extent of packing of the surfactants, when a variable diffusivity is correctly accounted for. These insights will be helpful in better understanding of the underlying dynamics of surfactant-laden drops, having potential applications in microfluidic devices, food and pharmaceutical industries and separation processes.

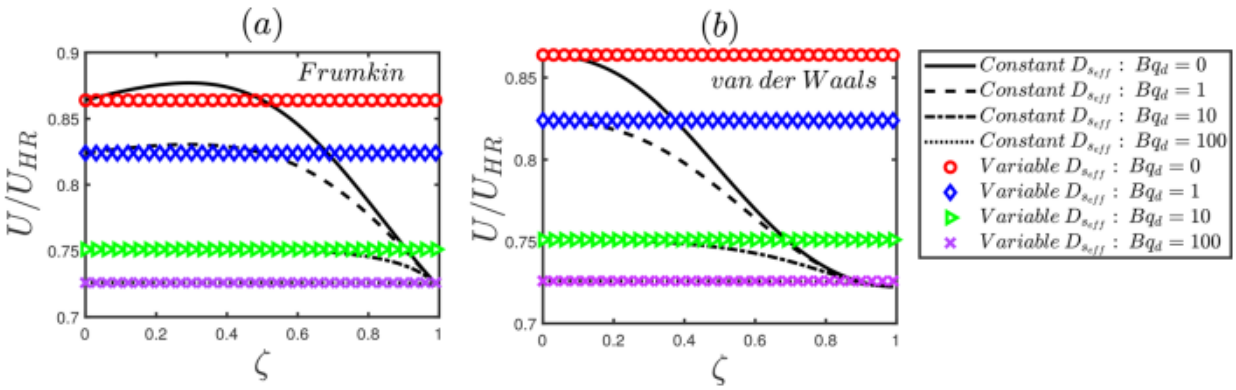

FIG. 1. Droplet velocity ($U = U/U_{HR}$) vs surfactant packing factor (ζ), for different Boussinesq dilatational numbers ($Bq_d = 0,1,10,100$), for Frumkin (a) and van der Waals (b) isotherms. The lines and markers represent the constant and variable diffusivity ($D_{S_{eff}}$) analysis respectively. Other relevant parameters are: $Ca = 0.04$, $Pe_s = 0.1$, $\chi = 2$, $\lambda = 0.2$, $Bq_s = 5$, $\beta = 0.5$.

The abstract is based upon the work done by our research group cited below [1].

[1] S. N. Jadhav and U. Ghosh, Effect of interfacial kinetics on the settling of a drop in a viscous medium, Physics of Fluids 34, 042007 (2022); https://doi.org/10.1063/5.0086538.

Exact solutions for viscous Marangoni spreading

François Detcheverry[1] and Thomas Bickel[2]

University of Lyon, Université Claude Bernard Lyon 1, CNRS, Institut Lumière Matière, F-69622 Villeurbanne, France, francois.detcheverry@univ-lyon1.fr

Univ. Bordeaux, CNRS, Laboratoire Ondes et Matière d'Aquitaine, F-33400 Talence, France, thomas.bickel@u-bordeaux.fr

When surface-active molecules are released at an air-liquid interface, their spreading dynamics is controlled by the induced Marangoni ows. Though such Marangoni spreading was investigated in a variety of limits, exact solutions for this process have remained very few.

Here we consider the spreading of an insoluble surfactant along the interface of a deep uid layer. For two-dimensional Stokes ows, it was recently demonstrated that the non-linear transport problem can be exactly mapped to a complex Burgers equation [1] . We rst present a very simple derivation of this mapping. We then provide fully explicit solutions and nd that changing the form of the initial surfactant distribution -- pulse, hole, or periodic – leads to very distinct spreading behaviors. We discuss the in uence of surfactant at the interface by nding the fundamental solution. We identify situations where spreading can be approximated as an e ective di usion process but observe that this description is not valid in general. Finally, we brie y consider the case of a three-dimensional ow with axial symmetry. Our results [2] provide reference solutions for Marangoni spreading and may be put to test in experiments with uorescent or photoswitchable surfactants.

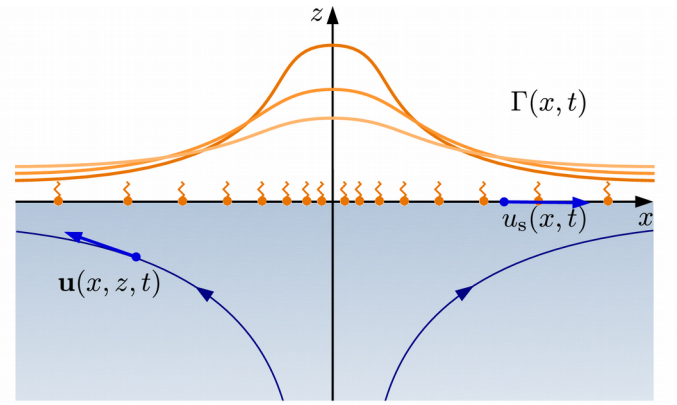

FIG. 1. Spreading of an insoluble surfactant above a semi-in nite liquid layer with Stokes two-dimensional ow. We provide a mathematically exact description of this process.

[1] D. G. Crowdy. Viscous Marangoni ow driven by insoluble surfactant and the complex Burgers equation. *SIAM J. Appl. Math.*, **81** 2526 (2021).

[2] T. Bickel, F. Detcheverry, Exact solutions for viscous Marangoni spreading, Physical Review E **106** 045107 (2022).

Modelling laminar drag reduction in surfactant-contaminated superhydrophobic channels

Samuel Tomlinson[1], Frederic Gibou[2], Paolo Luzzatto-Fegiz[2], Fernando Temprano-Coleto[3], Oliver Jensen[1] and Julien Landel[1]

[1] *Department of Mathematics, University of Manchester, Oxford Road, Manchester M13 9PL, UK*
samuel.tomlinson@manchester.ac.uk

[2] *Department of Mechanical Engineering, University of California, Santa Barbara, CA 93106, USA*

[3] *Andlinger Center for Energy and the Environment, Princeton University, Princeton, NJ 08544, USA*

Although superhydrophobic surfaces (SHSs) show promise for drag reduction applications, their performance can be compromised by traces of surfactant that accumulate at liquid-gas interfaces, generating Marangoni stresses that increase drag [1]. This question is addressed for soluble surfactant in a three-dimensional laminar channel flow, with periodic SHSs made of long finite-length streamwise grooves located on both walls. We consider the regime in which bulk diffusion is sufficiently strong for cross-channel concentration gradients to be small. Seeking solutions that are periodic in the streamwise and spanwise directions, and exploiting a long-wave theory that accounts for rapid spanwise Marangoni-driven flow and shear-dispersion effects, we reduce this high-dimensional problem to a one-dimensional model for the surfactant distribution. Our one-dimensional model allows us to predict the drag reduction and surfactant distribution across the parameter space, which includes 9 dimensionless groups. The system exhibits multiple regimes where asymptotic solutions can be constructed (see FIG. 1), which compare favourably with numerical simulations. Some are characterised by advection- (A) or diffusion-dominated (D) processes, where the liquid-gas interface exhibits near shear-free behaviour and the drag reduction is at its maximum. In contrast, others are dominated by Marangoni effects (M), where the liquid-gas interface exhibits near no-slip behaviour and the drag reduction vanishes. Our closed-form theoretical predictions of the drag reduction, which do not contain any empirical fitting parameters, compare well with results from the literature solving numerically the full three-dimensional transport problem [2]. Our atlas of maps across the parameter space provides a comprehensive analytical guide for designing surfactant-contaminated channels with SHSs, to maximise the drag reduction in small-scale applications, such as microfluidic or micro-cooling [3].

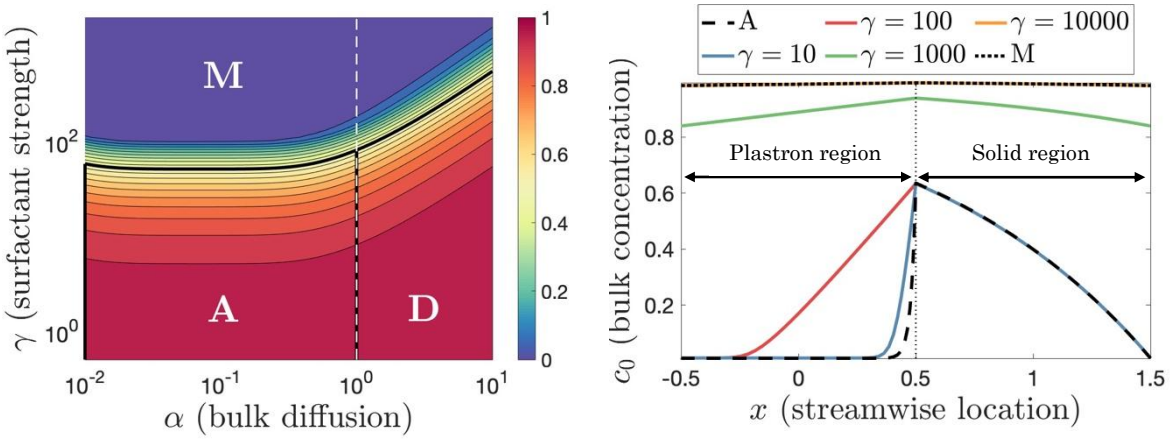

FIG. 1. Left: contour plot of the drag reduction (*DR*), where *DR* = 0 exhibits a no-slip SHS and *DR* = 1 exhibits a shear-free plastron; Right: plot of the bulk surfactant concentration for varying surfactant strength. We have defined regions that are dominated by Marangoni (M), advection (A) or diffusion (D) effects.

[1] F. J. Peaudecerf, J. R. Landel, R. E. Goldstein and P. Luzzatto-Fegiz, *Traces of surfactants can severely limit the drag reduction of superhydrophobic surfaces*, Proc. Natl. Acad. Sci. USA 114 (28), 7254–7259, (2017).

[2] F. Temprano-Coleto, S. M. Smith, F. J. Peaudecerf, J. R. Landel, F. Gibou and P. Luzzatto-Fegiz, *A single parameter can predict surfactant impairment of superhydrophobic drag reduction*, Proc. Natl. Acad. Sci. 120 (3), e2211092120 (2023).

[3] S. D. Tomlinson, F. Gibou, P. Luzzatto-Fegiz, F. Temprano-Coleto, O. E. Jensen and J. R. Landel, *Laminar drag reduction in surfactant-contaminated superhydrophobic channels*, arXiv preprint arXiv:2209.04834 (2022).

Microfluidic tensiometer based on interface instabilities: study of the kinetics of surfactants mass transfer

Marie Marsiglia (Moiré)[1], Yannick PEYSSON[1], Benjamin HERZHAFT[1], Nicolas PANNACCI[1],

Annie COLIN[2] and Christine DALMAZZONE[1]

[1] *IFPEN, 1 et 4 avenue de Bois Préau, 92 852 Rueil-Malmaison, France,* marie.marsiglia@ifpen.fr
[2] *ESPCI, 10, rue Vauquelin, 75 005 Paris, France,* annie.colin@espci.fr

I. Context

Emulsions are commonly found in daily life and industrial processes. Whether to stabilize or destabilize them depends on the desired application. One of the crucial parameters in understanding the kinetics of emulsion stabilization and destabilization is the dynamic interfacial tension, *ie.* the interfacial tension value measured during the transfer of amphiphilic molecules to and across the interfaces. This transfer primarily takes place within milliseconds or sub-milliseconds, which can only be measured by microfluidic tensiometers (such as [1], [2], [3], [4]). Among the available microfluidic tensiometers, only a few can measure dynamic interfacial tension over four orders of magnitude in pressure and temperature conditions that are present in industrial processes. In this conference, we will present the development of one of these microfluidic tensiometers, based on the Rayleigh-Plateau instability [5]. We will also give a preliminary insight into the study of mass transfer [6].

II. Methods

This tensiometer consists of two coaxial capillaries, with the inner capillary ending inside the outer capillary. Two immiscible liquids are injected into the capillaries, one in the inner capillary and one in the outer capillary. The flow rate applied to each liquid will result in different flow types observed at the end of the inner capillary, which can be classified into two categories: "drop" flows and "jet" flows. The transition between these two flow types is based on the Rayleigh-Plateau instability ([5]). The dominance of hydrodynamic forces results in a jet flow, while the dominance of interfacial forces leads to the formation of drops. At the transition point between the drop and jet regimes, hydrodynamic and interfacial forces are equal. By conducting a linear stability analysis of the basic flow through the theory of convective and absolute instabilities, the interfacial tension can be calculated ([6], [5], [7]).

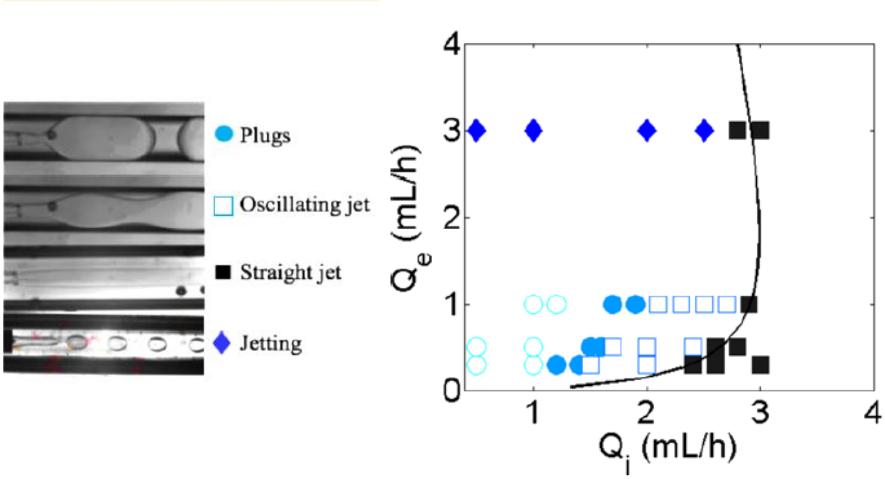

FIG. 1. From flow regime observation to interfacial tension calculation. Left: Different flow types of a cylindrical coaxial coflow. From top to bottom: plugs (filled circles), oscillating jets (open squares), straight jet (filled squares), jetting (filled diamonds) ; Right: Flow diagram representing the dripping to jetting transition of a solution containing DTAB (70.3×10^{-3} mol/L) and glycerol and of a silicone oil. Note that the open circle corresponds to the observation of droplets. The black line corresponds to the best fit of the transition using the linear stability analysis (cov = 0.9788) [6].

Note that the measurement is taken at the formation time of a droplet just before the transition from the dripping to the jetting regime. In the presence of surfactants in one or both phases, the transport and adsorption of surfactants at the interface occurs during the formation time of a droplet. After this time, the drop detaches, and the formation of a jet is no longer possible. This allows for a dynamic measurement at millisecond or sub-millisecond timescales and the determination of the amount of surfactants adsorbed at the interface during that time.

III. Results

Coupling this method with the work of Wang and Alvarez [8], [9] enables us to examine the kinetics of Triton X100 and DTAB mass transfer toward interfaces for different concentrations, and it has been found that while mass transfer occurs in less than 40 ms for DTAB (for all tested concentrations), 100 ms are not enough for Triton X100 to diffuse to the interface (for all tested concentrations).

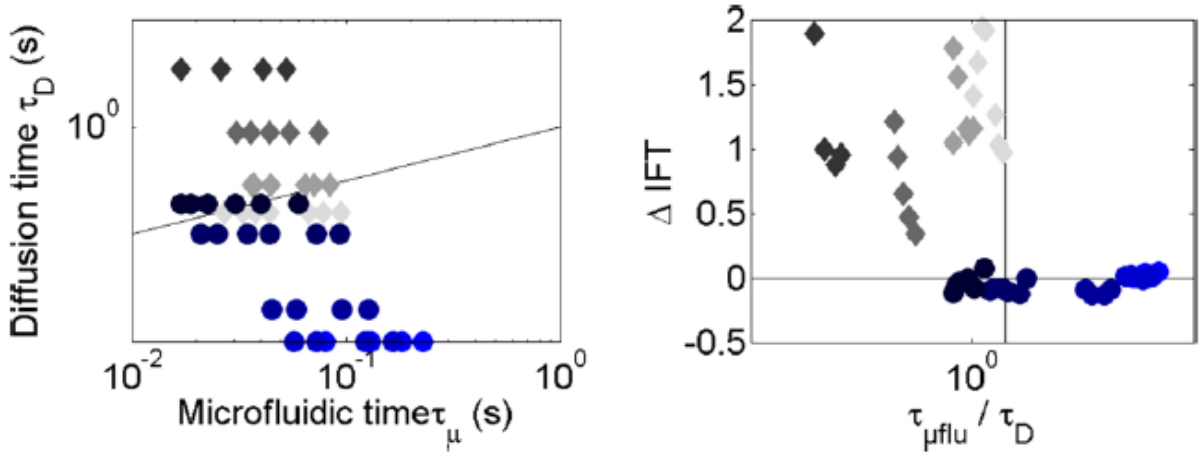

FIG. 2. Left: Comparison between the time at which microfluidic measurement is made and the diffusion time of the surfactants (diamonds: Triton X-100 – circles: DTAB). Right: impact of the difference between the diffusion time and the microfluidic measurement time on the difference between the IFT measured with the microfluidic tensiometer and the IFT measured at equilibrium with a pendant drop tensiometer. Note that the legend for the surfactants' concentrations can be found in reference [6].

III. Prospects

This tensiometer, which is fully suitable for studying surfactant mass transfer in industrial conditions across four orders of magnitude, is now used to gain a deeper understanding of surfactant mass transfer and construct related, reliable models at the millisecond time scale.

[1] Brosseau *et al.* Microfluidic dynamic interfacial tensiometry, J. of Soft Matter, 10, 3066−3076 (2014).
[2] Muijlwijk *et al.,* Interfacial tension measured at high expansion rates and within milliseconds using microfluidics, Journal of colloid and interface science, 470, 71-79 (2016).
[3] Steegmans *et al.* Dynamic interfacial tension measurements with microfluidic Y-junctions, Langmuir, 25 (17), 9751-9758 (2009).
[4] Deng *et al.,* Capillary pressure-based measurement of dynamic interfacial tension in a spontaneous microfluidic sensor, Lab on a chip, Advance Article (2022).
[5] Guillot *et al.,* Stability of a Jet in Confined Pressure-Driven Biphasic Flows at Low Reynolds Numbers, Phys. Rev. Lett., 99, 1−4 (2007).
[6] Moiré *et al.,* Ultralow interfacial tension measurement through jetting/dripping transition, Langmuir, 33, 10, 2531–2540 (2017).
[7] W. Van Saarloos, Front propagation into unstable states. ii. linear versus nonlinear marginal stability and rate of convergence, Phys. Rev. A, 39, 6367–6390 (1989).
[8] K. Wang *et al.* Mass-transfer-controlled dynamic interfacial tension in microfluidic emulsification processes, Langmuir, 32, 3174-3185 (2016).
[9] N. Alvarez *et al.* Using bulk convection in a microtensiometer to approach kinetic-limited surfactant dynamics at fluid-fluid interfaces. J. colloid interface sci., 372, 183-191 (2012).

Interaction between a particle and a liquid surface covered by a surfactant

Alexander Nepomnyashchy

Department of Mathematics, Technion – Israel Institute of Technology, 32000, Haifa, Israel,
nepom@technion.ac.il

The interaction of a particle with a liquid interface takes place in many engineering processes including flotation and colloidal self-assembly. When the liquid surface is covered by a surfactant, the liquid motion induces a Marangoni stress that acts on the flow and particle motion.

We consider the motion of a spherical particle rising in a viscous fluid towards a surface covered by a surfactant, in the framework of the Stokes equation. The presence of the surfactant modifies the flow significantly and changes the particle mobility. Upon the particle attachment to the surface, the dominant factors become the action of the Brownian forces and the spatial inhomogeneity of the wetting properties on the particle surface. The latter factor strongly enhances the duration of the system equilibration.

Marangoni swimmer in a flow

Camille Perret, Cécile Cottin-Bizonne, Francois Detcheverry, Christophe Ybert
Univ Lyon, Université Claude Bernard Lyon 1 ,
CNRS, Institut Lumière Matière, F-69622 Villeurbanne, France

Interfacial swimmers are objects that self-propel at an interface by generating a surface tension gradient, often through the continuous release of surfactant. While asymmetric swimmers have long been studied, experiments have shown that symmetric swimmers can also exhibit spontaneous motion [1]. The description of their propulsion induced by a symmetry-breaking mechanism is now well established [2 ,3]. However, we lack a characterization of the interactions between the swimmer and its environment. In particular, the role of Marangoni flows remains to be clarified. While a series of recent works investigated Marangoni flows around a fixed source [4 ,5 ,6], there is only a few investigations of the flow induced by a mobile source of surfactant [3, 7].

We address this problem by holding the swimmer fixed and submitting it to an externally imposed homogeneous velocity which thus becomes a fully controlled parameter (see FIG. 1 left). This allows to visualize the water flow around the swimmer in a stationary state and measure the force for an extensive range of flow velocities. We observe different regimes. For low flow velocities we measure a positive force and the swimmer exhibits an ellipsoidal trajectory whose amplitude decreases when increasing the flow. Then at a flow velocity equal to the spontaneous swimming speed the force vanishes at a stable point. For high flow velocity, the force is negative. In all cases, the presence of the swimmer strongly modifies the flow field with the formation of a large wake behind the swimmer and a stagnation point in front (see FIG. 1 right) . We discuss the relation with numerical simulations.

This work provides new hints on the interplay between swimming velocity, Marangoni flows and chemical release involved with interfacial swimmers. Moreover, it can be readily extended to address more complex situations such as swimmer-swimmer or swimmer-wall interactions.

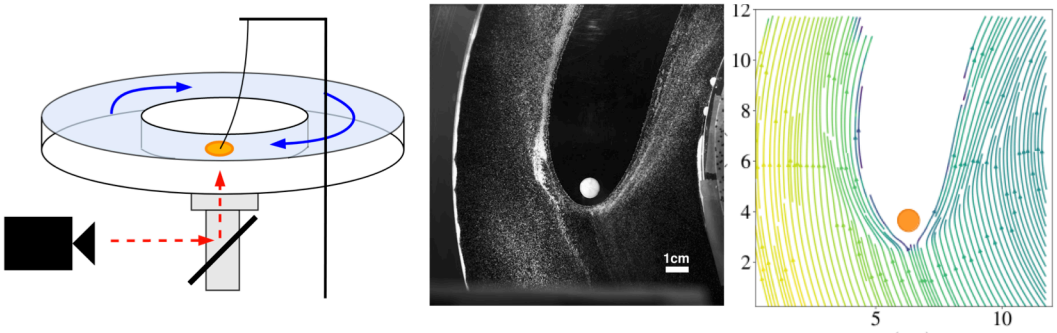

FIG. 1. Left: experimental setup. Middle: experimental image of a swimmer in an imposed flow with tracers. Right: streamlines obtained with a particle image velocimetry algorithm.

[1] N. J. Suematsu, S. Nakata, Frontispiece: Evolution of Self-Propelled Objects: From the Viewpoint of Nonlinear Science, Chem. Eur. J. 24, 6308 (2018).
[2] D. Boniface, C. Cottin-Bizonne, R. Kervil, C. Ybert, F. Detcheverry, Physical Review E 99, 062605 (2019)
[3] H. Ender, A.-K. Froin, H. Rehage, and J. Kierfeld, Eur. Phys. J. E (2021)
[4] M. Roché, Z. LI, I. M. Griffiths, S. Le Roux, I. Cantat, A. Saint-James, H. A. Stone, Marangoni Flow of Soluble Amphiphiles Physical Review Letters 112, 208302 (2014)
[5] M. M. Bandi, V. S. Akella, D. K. Singh, R. S. Singh, S. Mandre Physical, Hydrodynamic Signatures of Stationary Marangoni-Driven Surfactant Transport, Review Letters 119, 264501 (2017)
[6] A.Mizev, A.Shmyrov, A.Shmyrova, On the shear surfactant layer instability, Journal of Fluid Mechanics 939 (2022)
[7] S. Sur, H. Masoud, and J.P. Rothstein, Translational and rotational motion of disk-shaped Marangoni surfers Physics of Fluids 31, 102101 (2019)

Numerical model of the transport phenomena in the absorption of LiBr-H_2O + surfactant mixtures

PF. Arroiabe[1], Manex Martinez-Agirre[1], M. Mounir Bou-Ali[1] and Valentina Shevtsova[1,2]

[1] *Fluid Mechanics Group, Faculty of Engineering, Mondragon Unibertsitatea, Loramendi 4, Arrasate-Mondragon 20500, Gipuzkoa, Spain,* parroiabe@mondragon.edu

[2] *Ikerbasque, Basque Foundation for Science, Bilbao, Spain,* x.vshevtsova@mondragon.edu

I. INTRODUCTION

Most of the efforts to enhance the performance of the absorbers have been made using surfactants in working fluids. Several experimental studies have demonstrated the enhancement on the heat and mass transfer mechanisms by incorporating surfactants into both the vapor and liquid phases, the effect being stronger when the surface-active agents are incorporated to the vapor phase. This growth has been attributed to the secondary flows driven by the surface tension gradient (Marangoni convection). Two possible elucidations have been discussed in the literature. Some authors attribute the change in the sign of the surface tension variation ($d\sigma/dw$) from positive to negative with the LiBr mass fraction due to addition of the surfactant, (called "salting out" mechanism)[1]. Others consider that the enhancement is due to surfactant in the vapor reaching the liquid interface, which causes rivulets due to the generated surface tension gradient (called vapor-surfactant theory)[2]. However, the nature of the improvement remains unclear. Therefore, the present study aims to study the transport phenomena occurring in the absorption of water vapor by the water-lithium bromide (LiBr-H_2O) + additive mixtures by using 2D numerical models, based on the Finite Volume Method.

II. PROBLEM FORMULATION

The numerical model is based on the following assumptions: laminar flow and Newtonian fluid, liquid-vapor equilibrium at the interface and constant thermophysical properties. FIG 1 shows the geometry and boundary conditions of the numerical model. Currently, the computational domain consists only of the liquid phase. At the initial state, LiBr- H_2O is motionless at a constant mass fraction and temperature. When the process starts, the water vapor is absorbed at the interface (top face). As a result, the mass fraction in LiBr (w) of the interface decreases and, due to the generated heat of absorption, its temperature grows.

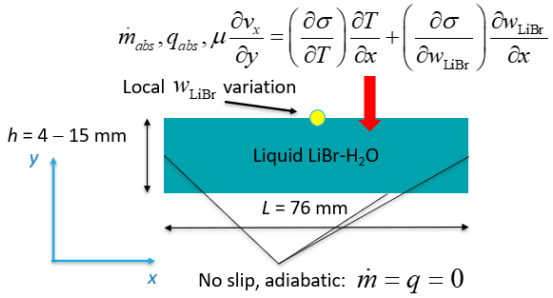

FIG 1: Computational domain and boundary conditions of the model

The problem of absorption is described by the Navier–Stokes, heat, and mass transfer equations:

$$\mathrm{div}\,(\mathbf{v}) = 0 \tag{1}$$

$$\frac{\partial \mathbf{v}}{\partial t} + \mathbf{v}\cdot\nabla\mathbf{v} = -\frac{1}{\rho_0}\nabla p + \nu\Delta\mathbf{v} + \mathbf{g}\left(-\beta\left(T - T_0\right) - \alpha\left(w - w_0\right)\right) \tag{2}$$

$$\frac{\partial T}{\partial t} + \mathbf{v}\cdot\nabla T = \frac{k}{\rho_0 c_p}\nabla T \tag{3}$$

[1] Daiguji, H., Hihara, E. & Saito, T. *Mechanism of absorption enhancement by surfactant*. Int J Heat Mass Transf **40**, 1743–1752 (1997).

[2] Kulankara, S. & Herold, K. E. *Theory of heat/mass transfer additives in absorption chillers*. HVAC and R Research **6**, 369–380 (2000).

$$\frac{\partial w}{\partial t} + \mathbf{v} \cdot \nabla w = -\frac{1}{\rho_0} \nabla \mathbf{J} \tag{4}$$

here **v,** *p, T, t* are the velocity, the pressure, the temperature and time, **g** is the gravity, β is the thermal expansion coefficient, and α is the mass expansion coefficient, ρ is the density, v is the kinematic viscosity, c_p is the specific heat, k is the thermal conductivity, and **J** is the the diffusion flux of LiBr. Since thermodiffusion effects are not considered then the mass flux is $\mathbf{J} = -\rho D \nabla w$.

The boundary conditions on the left, right and bottom faces are: no slip and adiabatic walls. Vapor-liquid equilibrium in presence of absorption leads to the coupling of the heat and mass fluxes (H_{abs} is the heat of absorption).

$$k\ \partial_y T = \dot{m}_{abs} H_{abs} \tag{5}$$

The absorbed mass flux is determined considering two different types of diffusion at the interface: 2D diffusion: $\dot{m}_{abs} = -\rho\ D\ \partial_y w$ and 1D diffusion: $\dot{m}_{abs} = -\rho\ D\ \partial_y w / w$ (also referred as Eckert–Schneider relation)[3].

Equilibrium conditions at the interface suggest a linear relationship between mass fraction and temperature for each working pressure[4] ($T_{if} = k_1 + k_2 w_{if}$). To initiate the Marangoni convection, local variation in the LiBr mass fraction at the interface is given. The presence of local variation of LiBr concentration on interface leads to change of the surface tension (σ), which causes the Marangoni convection:

$$\mu\ \partial_y \mathbf{v}_x = \partial_T \sigma\ \partial_x T + \partial_w \sigma\ \partial_x w \tag{6}$$

The governing equations are solved using Ansys Fluent 2023R1 software based on the Finite Volume**.**

III. RESULTS AND DISCUSSION

First, the problem is considered without the Marangoni effect to validate the numerical code by comparison with literature data. Using the selected mesh, the absorption of water vapor in the LiBr-H_2O system is studied with and without surfactant considering both 1D and 2D diffusion at the interface. Once the most appropriate is selected, the changes in the heat and mass transport phenomena caused by the Marangoni convection are investigated. The problem is multi-parametric and the target is to reach the highest mass flux of absorbent. To do this, the problem is examined for several liquid heights, initial mass fractions, various surfactants, and different variations in the LiBr mass fraction at the interface and changing locations of their maxima. Figure 2 shows the temperature and velocity field when a mass fraction perturbation was imposed in the middle of the interface, which initiated Marangoni convection. Considering the relatively deep layer, on the small times convection affects only limited liquid volume and the temperature varies only within the boundary layer near the interface.

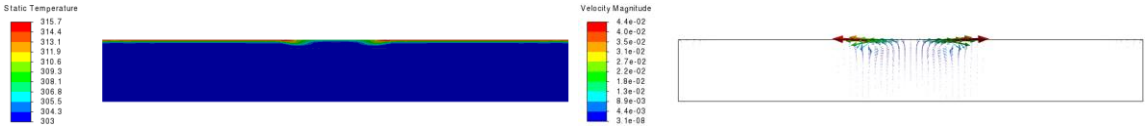

FIG 2: Temperature and velocity field in the LiBr system when Marangoni convection is caused by appearance of a surfactant locally at the interface.

Acknowledgements

This work is supported by Gipuzkoa Provincial Council under Grant No. 2022-CIEN-000052-01 (Hoztikor), Research Group Program of the Basque Government under Grant No. . IT1505-22 and GE-MICINN-TED of the Spanish Government Grant No. PID2021-124232OB-I00 (Treated).

[3] P. F. Arroiabe, M. Martinez-Agirre, and M. M. Bou-ali, Numerical analysis of different mass transfer models for falling film absorbers, *Int J Heat Mass Transf*, vol. **182**, 121892, 2022

4 Grossman, G. (1983). G. Grossman, "Simultaneous heat and mass transfer in film absorption under laminar flow," *Int J Heat Mass Transf*, vol. **26,** (3), 357–371, 1983

Session 4 – Drops and spreading

Monday June 19, 16:15–17:45

Gradient Dynamics Model for Drops on Elastic Substrates

Christopher Henkel[1] , Martin H. Essink[2], Ambre Bouillant[2], Uwe Thiele[1,3], Jacco H. Snoeijer[2]

Institute for Theoretical Physics, WWU, 48149, Münster, Germany, c_henk08@wwu.de
Physics of Fluids Group, University of Twente, 7500 AE, Enschede, Netherlands, m.h.essink@utwente.nl
[3]*Center for Nonlinear Science (CeNoS), WWU, 48149, Münster, Germany,* u.thiele@uni-muenster.de

While the wetting behaviour of liquids on rigid substrates has been extensively studied within the past decades, investigations of wetting on soft substrates have just recently gained momentum and increasingly attract attention. We present a mesoscopic gradient dynamics model for drops on elastic substrates that incorporates a simpli ed Winkler foundation type elasticity. We show that the model recovers fundamental e ects like the double-transition in contact angles with increasing softness and viscoelastic braking at moving contact lines [1] . Furthermore, the model allows one to e ortlessly treat even large drop ensembles as evidenced by a study of the dependence of droplet coarsening on substrate softness [1]. Finally, we show that the versatility of a gradient dynamics approach permits us to adapt it to more complex settings like the incorporation of condensation and of the Shuttleworth e ect [2].

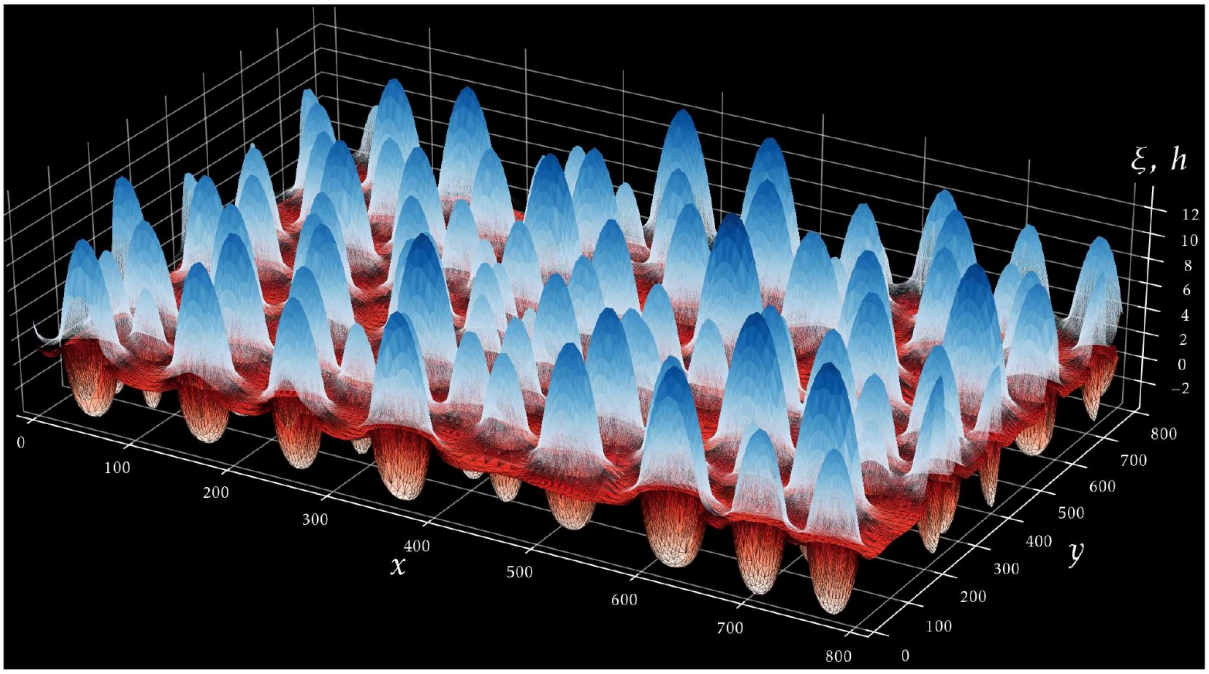

FIG. 1. Snapshot of a time simulation for condensing and coarsening drops on an elastic substrate

[1] Henkel C., Snoeijer J. H., Thiele U. *Gradient-dynamics model for liquid drops on elastic substrates.* Soft Matter 17, 10359–10375 (2021)

[2] Henkel C., Essink M. H., Hoang T., van Zwieten G. J., van Brummelen E. H., Thiele U., Snoeijer J. H. *Soft wetting with (a)symmetric Shuttleworth e ect*. Proc. R. Soc. A 478: 20220132. (2022)

Drop control and propulsion with applications in microfluidics and microgravity

Rodica Borcia, Ion Dan Borcia, Michael Bestehorn[1]

[1] *Institut für Physik, Brandenburgische Technische Universität Cottbus, Germany*

We study numerically the propulsion of a microdroplet with applications for microfluidics and microgravity. The investigation will be done via a phase field model earlier developed for describing static and dynamic contact angles [1–3]. The density field is nearly constant in every bulk region ($\rho = 1$ in the liquid phase, $\rho \approx 0$ in the vapor phase) and varies continuously from one phase to the other with a rapid but smooth variation across the interface. Complicated explicit boundary conditions along the interface are avoided and capturated implicitly by gradient terms of ρ in the hydrodynamic basic equations. The contact angle θ is controlled through the boundary condition for the density at the solid substrate ρ_S, a free parameter varying between 0 and 1.

Two different mechanisms will be presented and discussed:

- the droplet is placed on a homogeneous substrate vibrated harmonically both in lateral and vertical directions;
- the droplet is placed on a heterogeneous ratchet–structured substrate vibrated harmonically in lateral direction.

---

[1] R. Borcia, I.D. Borcia, M. Bestehorn, Drops on an arbitrarily wetting substrate: A phase field description. Phys. Rev. E **78**, 066307 (2008).

[2] R. Borcia, I.D. Borcia, M. Bestehorn, Can vibrations control drop motion? Langmuir **30**, 14113–14117 (2014).

[3] R. Borcia, I.D. Borcia, M. Bestehorn, Dancing drops over vibrating substrates. Eur. Phys. J. Special Topics **266**, 1297–1306 (2017).

Email address of the presenting's author: borciar@b-tu.de

Self-induced Flows Enhance the Levitation of Leidenfrost Drops on Liquid Baths

Benjamin Sobac[1,5], Laurent Maquet[2], Alexis Duchesne[2,3], Hatim Machrafi[4], Alexey Rednikov[1], Pierre Dauby[4], Pierre Colinet[1] and Stéphane Dorbolo[2]

[1] TIPs Lab, Université libre de Bruxelles, Brussels, Belgium
[2] GRASP, Université de Liège, Liège, Belgium
[3] Department of Physics, Technical University of Denmark, Lyngby, Denmark
[4] TPI, Université de Liège, Liège, Belgium
[5] Current Affiliation : LFCR UMR 5150 CNRS – Université de Pau et des Pays de l'Adour, Anglet, France,
benjamin.sobac@cnrs.fr

The Leidenfrost effect, classically associated with drops levitating on their own vapor over hot solid surfaces, can also be observed over hot baths of nonvolatile liquids [1 , 2] (see Fig. 1 Left). In view of substrate fluidity, heat transfer through the bath to the drop should most certainly be dominated by convection and not by only conduction as in the solids, which may be instrumental for an efficient heat supply to the drop given typically poor thermal conductivity of the liquids. Here, we undertake an experimental and numerical study of the flow in a bath of silicone oil V20 induced by an overlying Leidenfrost drop, highlighting that a toroidal vortex is formed underneath the drop whose direction of circulation turns out to be different for drops of different liquids (see Fig. 1 Right). We show that this is due to a shift in a delicate interplay between three mechanisms pulling in different directions: (i) shear stresses exerted by the vapor escaping from the gap between the bath and the drop, as well as (ii) buoyancy action and (iii) thermocapillary (Marangoni) stresses, both due to local evaporative cooling of the bath by the drop. Whatever the structure of this locally induced convection, its crucial heat transfer enhancing efficiency is readily confirmed in numerical simulations as favoring levitation [3].

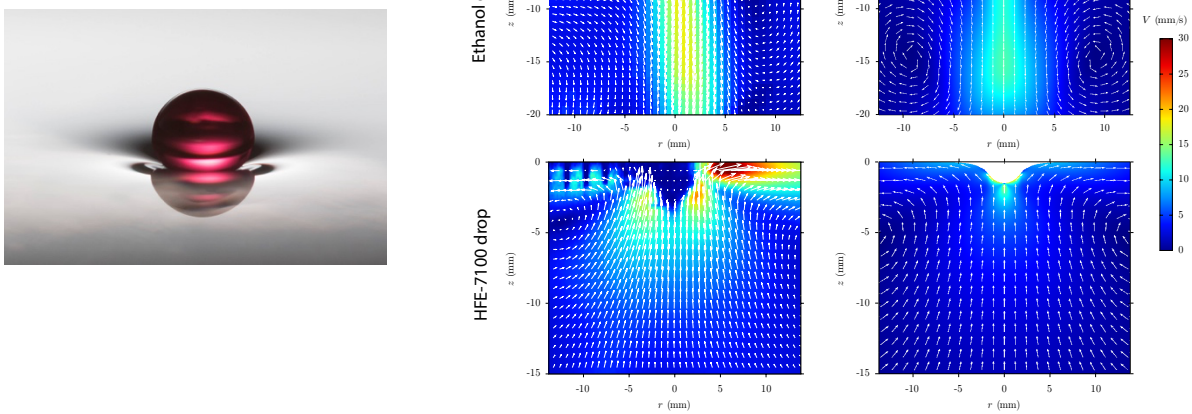

FIG. 1. Left. An ethanol drop (with red dye) of radius R=1.2 mm levitates in the Leidenfrost state over a bath of silicone oil V20 with a superheat ΔT=1K (Image credit: Florence Cavagnon). Right. Experimental and numerical flow fields in the bath under levitating ethanol (top) and HFE-7100 (bottom) Leidenfrost drops, both of radius R/lc=2 and subject to a superheat ΔT=19°C.

[1] L. Maquet, B. Sobac, B. Darbois-Texier, A. Duchesne, M. Brandenbourger, A. Rednikov, P. Colinet and S. Dorbolo, Leidenfrost drop on a heated liquid pool, Phys. Rev. Fluids **1** 053902 (2016).
[2] M. A. J. van Limbeek, B. Sobac, A. Rednikov, P. Colinet and J. Snoejier, Asymptotic theory for a Leidenfrost drop on a liquid pool, J. Fluid Mech. 863, 1157 – 1189 (2019).
[3] B. Sobac, L. Maquet, A. Duchesne, H. Macrafi, A. Rednikov, P. Dauby, P. Colinet and S. Dorbolo, Self-induced flows enhanced the levitation of Leidenfrost drops on liquid baths, Phys. Rev. Fluids **5**, 062701(R) (2020).

Asymmetric Compound Drops

Jan Diekmann[1] and Uwe Thiele[2]

[1] *Institute of Theoretical Physics , WWU, 48149, Münster, Germany,* j_diek07@uni-muenster.de
[2] *Institute of Theoretical Physics, WWU, 48149, Münster, Germany,* u.thiele@uni-muenster.de

We consider sessile compound drops of two immiscible liquids on rigid solid substrate. After establishing a mesoscopic model (amending [1]) consistent with the macroscopic description of [2 ,3], we use numerical continuation techniques to show for one-dimensional (1D) substrates that asymmetric compound drops can be energetically favoured. Furthermore, we investigate selected dewetting and coarsening processes and discuss emerging steady compound drops for two-dimensional (2D) substrates. This allows us to discuss the relation of 1D and 2D results.

[1] L. Mahadevan, M. Adda-Bedia, and Y. Pomeau. “Four-phase merging in sessile compound drops”. J. Fluid Mech. 451, pp. 411–420 (2002).
[2] M. J. Neeson et al. “Compound sessile drops”. Soft Matter 8, 11042–11050 (2012).
[3] A. Pototsky et al. “Morphology changes in the evolution of liquid two-layer films”. J. Chem. Phys. 122, p. 224711 (2005).
[4] Uwe Thiele et al. “Equilibrium contact angle and adsorption layer properties with surfactants”. Langmuir 34.24, pp. 7210–7221 (2018).

Sliding and dripping of liquid drops on porous and non-porous fibres

Atefeh Pour Karimi[1], Hossein Askarizadeh[1], Wilko Rohlfs[2], Benoit Scheid[3], Reinhold Kneer[1]

[1] *WSA, RWTH Aachen University, Augustinerbach 6, 52056 Aachen, Germany,* pour@wsa.rwth-aachen.de, askarizadeh@wsa.rwth-aachen.de, kneer@wsa.rwth-aachen.de

[2] *Department of Thermal and Fluid Engineering, University of Twente, Drienerlolaan 5, 7522 NB Enschede, Netherlands.* w.rohlfs@utwente.nl

[3] *TIPs, Université Libre de Bruxelles, Avenue F.D. Roosevelt 50, Bruxelles, 1050, Belgium.* bscheid@ulb.ac.be

Fog is a source of clean water, and the dramatic increase in potable water depletion on our planet, especially in arid areas, has made fog and dew harvesting a possible viable solution in the current decade. In recent years, numerous research projects have been carried out on the subject of fog harvesting [1,2,3]. Most previous works have examined the influence of general mesh topology (i.e. mesh fiber diameter or the commonly mentioned shade coefficient which is the proportion of the projected area covered by the solid mesh fiber), surface wettability, and fiber's material composition on the fog collecting efficiency. There has been little attention paid to a more detailed study of fiber angular alignments and its best possible inclination inside the mesh. This study focuses on the fiber inclination and show how the movement of liquid droplets on the fiber and their onset of dripping can be affected by variation in fiber inclination. Previous investigations on the tilted plastic fibers with silicon oil have shown that the inclination can even have a stabilizing effect up to a certain mass flow rate and a certain critical inclination, meaning that at higher inclinations, regular sequence of droplets of the same size and frequency flows along the fiber over even higher range of measured mass flow rates [4]. In this study, quantitative results on water film flows along fabric fibers such as woven polyolefin fibers, which is a standard material used in the fog harvesting nets are presented. This results will manifest how the inclination can influence the dynamics of the flow and dripping onset and consequently the overall efficiency of the water collection rate. In a fog harvesting mesh, when the droplets collide with the fiber, a minimum critical volume must be reached in order for gravity to overcome the adhesion forces at the solid-liquid interface and the retained droplet flow down along the mesh and eventually be collected. It can be assume that by having an appropriate fiber slope within the mesh, suitable to the selected fiber diameter, smaller critical water volumes are required for the droplets to slide down until collection. Therefore the collection efficiency can be increased.

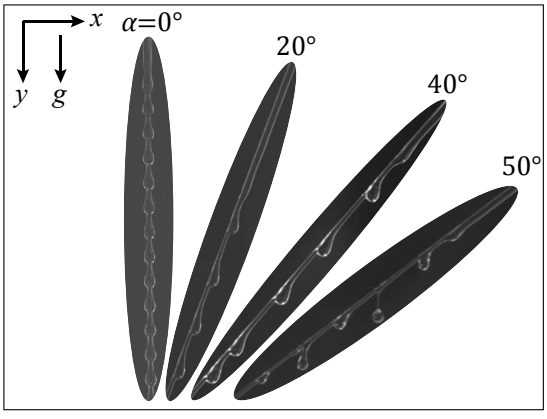

[1] Seo, D., Lee, J., Lee, C. et al. The effects of surface wettability on the fog and dew moisture harvesting performance on tubular surfaces. Sci Rep 6, 24276 (2016)

[2] Kyoo-Chul Park, Shreerang S. Chhatre, Siddarth Srinivasan, Robert E. Cohen, and Gareth H. McKinley Optimal design of permeable fiber network structures for fog harvesting. Langmuir 29 (43), 13269 (2013)

[3] Knapczyk-Korczak, J., Szewczyk, P., Ura, D., Berent, K., Stachewicz, U. Hydrophilic nanofibers in fog collectors for increased water harvesting efficiency. RSC Advances 10 (2020)

[4] Pour Karimi, A., Rietz, M., Rohlfs, W., Scheid, B., Kneer, R. Experimental study of dripping, jetting and drop-off from thin film flows on inclined fibers. EPJ Special Topics (2023). (Recently Accepted)

Evaporation of Sessile Binary Mixture Droplets: influence of concentration

Jun Qin[1,3], Glushchuk Andrey[2], Christoph Minetti[2], Yu-Qun Tao[1],, Qiu-Sheng Liu[1,3*]
[1] *Institute of Mechanics, Chinese Academy of Sciences, Beijing 100190, China*
[2] *Service Chimie-Physique, Université Libre de Bruxelles, 1050 Brussels, Belgium*
[3] *University of Chinese Academy of Sciences, Beijing 100049, China*
*liu@imech.ac.cn

The present study experimentally investigates the effects of concentration and volatility on the evaporation characteristics of the sessile droplet of binary mixtures. Three different volatile liquids: HFE7100, ethanol, and Isopropyl alcohol are used to make three different combinations. For the components with large differences in volatility (HFE-Eth), as shown in Fig.1, the evaporation process can be divided into three stages. In the first stage, the evaporative behavior is more like that of the pure HFE. This is because the more volatile component HFE evaporates ten times faster than that of the other component and dominates the whole evaporation. As time goes by, the concentration of HFE reaches a small value and the evaporation enters the second stage, which behaves like a smooth curve. Until the concentration decreased to zero, the other component (Eth) completely dominates the evaporation. Hence in the final stage, the behavior is closer to the less volatile liquid. For the components with small differences in volatility, the evaporation behavior is like that of pure substance. It means that selective evaporation only occurs where the two components have huge different volatility. We also calculate the evaporation rate of different stages. For the HFE-Eth mixtures, the evaporation rate in stage 1 is generally larger than the pure HFE for all concentrations. It seems that introducing another less volatile component (Eth) can facilitate evaporation in the early stage compared to the single-component drop. And in stage 3, the evaporation rate corresponds to that of the less component but is relatively higher. It means that HFE evaporation is always present throughout the droplet lifetime.

The effect of concentration is also studied in this paper. Five different compositions of the binary mixtures (20%+80%), (40%+60%), (50%+50%), (60%+40%), and (80%+20%) have been considered in this study. The evaporative behavior of drops including volume, height, contact radius, and contact angle is dependent on the concentration of the components. For the relatively high and low concentrations (80% and 20%), these parameters are clearly different from the other three combinations. Their behaviors are more like that of pure substance. Whereas for the intermediate concentrations (40%, 50%, 60%), the variation of concentrations has less impact on the droplet shape parameter, but a significant effect on the duration of stages.

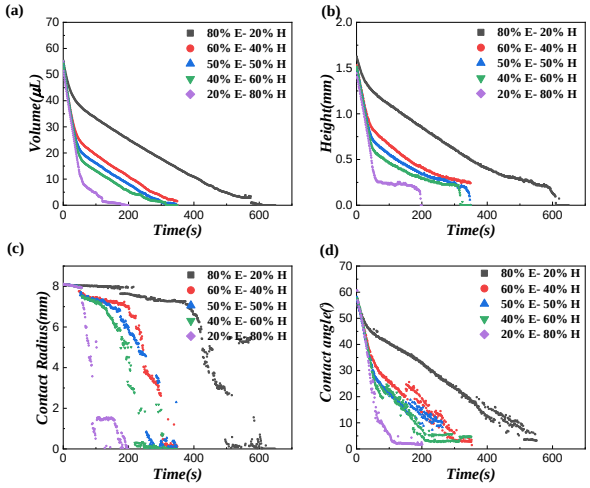

FIG. 1. The variations of shape parameters with time for the Eth-HFE mixture

ACKNOWLEDGEMENTS : This research was financially supported by the framework for utilization on the International Space Station (ISS) of China Space Station (CSS) of European Space Agency (ESA) and the China Manned Space Agency (CMSA) and the China's Manned Space Program (MT-TPSR).

Session 5 – Thermocapillary flows

Tuesday June 20, 9:00–10:30

Phase separation patterns of a binary mixture using Marangoni stresses

Marc Pascual, Axelle Amon and Marie-Caroline Jullien

Institut de Physique de Rennes, Rennes, France, marie-caroline.jullien@univ-rennes.fr

I. INTRODUCTION

The presentation focuses on thermosensitive binary systems consisting of water and ionic liquids (ILs) that have proven useful for several applications such as water desalination by direct osmosis [1-3], and low-grade heat valorization [4,5]. For all these techniques, temperature is used as a control parameter to trigger phase separation and recover the IL-rich phase of interest on demand. We propose to take advantage of capillary effects, which are known to improve the phase separation kinetics of binary systems [6-8], as demonstrated by Beysens *et al.* with pure CO_2 [9].

II. RESULTS

In our experiments, the centre of a cylindrical microcavity (50 µm thick and 1 mm in diameter) is heated locally, leading to a radial temperature profile in the cavity. The binary mixture is composed of water and an ionic liquid (IL) of different initial concentration. This binary mixture has the property to phase separate above a critical temperature (LCST solution type), leading to two phases: a water-enriched one and an ionic liquid (IL) enriched one whose compositions depends on the temperature, see Fig. 1. An important property is that the surface tension between the two phases increases with the temperature. Consequently, placed in a temperature gradient, we expect the Marangoni effects to play a key role in the separation of the two phases. We show that the separation pattern evolves along the phase diagram of the binary mixture composition, see Fig. 1. More precisely, the coupling of Marangoni stresses and of the wetting properties of the walls leads to three characteristic separation patterns.

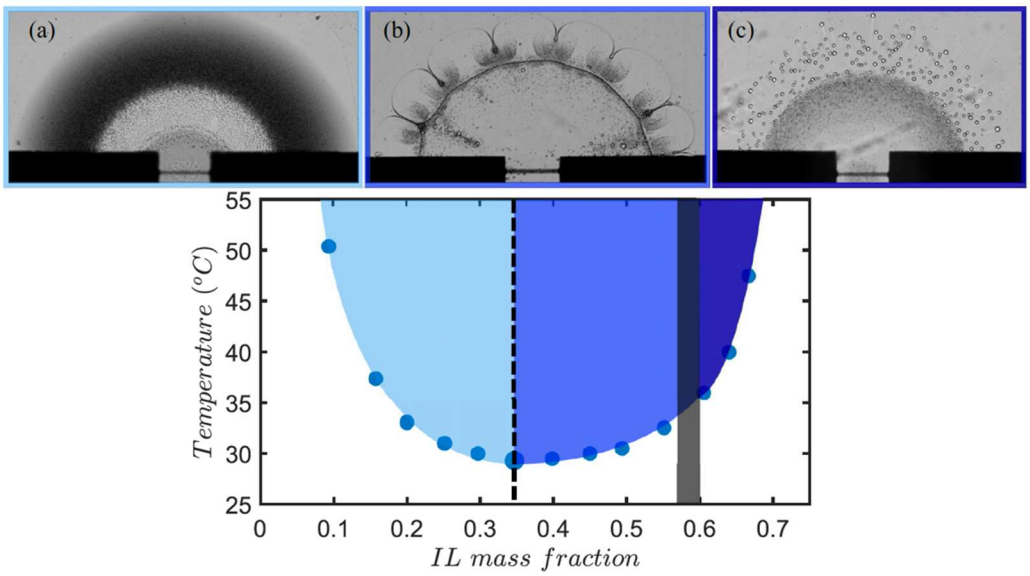

FIG. 1. Phase diagram of the solution used as a function of the initial mass fraction of ionic liquid, the other phase being water. To the left of the critical point, the emulsion is composed of droplets of IL in water the latter being the continuous phase. To the right of this point, *i.e.* for a higher mass fraction of IL, the emulsion is reversed, so water droplets are obtained and the ionic liquid is the continuous phase. As both phases have similar dynamic properties, the separation line between the two demixing regimes is almost vertical. The figures above the phase diagram represent the observed separation patterns which have been described and rationalized in [12,13] and which we will describe in the presentation.

The initial composition of the solution dictates the phase separation pattern [10,11], two of which result in a selective accumulation of the IL-rich phase in the hottest part of the cavity. The three separation regimes are presented in order of increasing IL mass fraction.

The first regime, in which water is the main component, has a 3D structure in which droplets of ionic liquid are expelled towards the outside due to thermocapillary stresses, see Fig 1 top left. These droplets, denser than the water forming the continuous phase, sediment and eventually form a film on the bottom of the cavity. This film, subjected to a temperature gradient is driven towards the centre of the cavity, where a drop of ionic liquid grows.

The second regime, beyond the consolute point of the binary mixture, generates an unexpected periodic pattern of the Bénard-Marangoni type, see Fig 1 top middle. We interpret this regime as a thermocapillary stress-driven instability, whose mechanisms involved are in fact different from the classical Bénard-Marangoni instability. This regime is analyzed in detail and the model allows us to recover the wavelength of the instability that is observed experimentally.

The third regime, well beyond the consolute point of the binary mixture, is easily explained and is of less interest for selective separation, see Fig 1 top right. This regime is rationalized by the thermocapillary migration of water-enriched drops into the IL compound phase.

All three regimes could be modelled using classical approaches and will be presented during the presentation [12,13]. At the end, we discuss the relevance of the three regimes for IL recovery applications.

IV. REFERENCES

[1] X. Fan, H. Liu, Y. Gao, Z. Zou, V. S. Craig, G. Zhang, and G. Liu, Forward-osmosis desalination with poly (ionic liquid) hydrogels as smart draw agents, Adv. Mater. **28**, 4156 (2016).
[2] C.-H. Hsu, C. Ma, N. Bui, Z. Song, A. D.Wilson, R. Kostecki, K. M. Diederichsen, B. D.McCloskey, and J. J. Urban, Enhanced forward osmosis desalination with a hybrid ionic liquid/hydrogel thermoresponsive draw agent system, ACS Omega **4**, 4296 (2019).
[3] E. Kamio, A. Takenaka, T. Takahashi, and H. Matsuyama, Fundamental investigation of osmolality, thermo-responsive phase diagram, and water-drawing ability of ionic-liquid-based draw solution for forward osmosis membrane process, J. Membr. Sci. **570**, 93 (2019).
[4] Y. Cai, W. Shen, J. Wei, T. H. Chong, R. Wang, W. B. Krantz, A. G. Fane, and X. Hu, Energy-efficient desalination by forward osmosis using responsive ionic liquid draw solutes, Environ. Sci.: Water Res. Technol. **1**, 341 (2015).
[5] A. Z. Haddad, A. K. Menon, H. Kang, J. J. Urban, R. S. Prasher, and R. Kostecki, Solar desalination using thermally responsive ionic liquids regenerated with a photonic heater, Environ. Sci. Technol. **55**, 3260 (2021).
[6] H. Tanaka, Wetting Dynamics in a Confined Symmetric Binary Mixture Undergoing Phase Separation, Phys. Rev. Lett. **70**, 2770 (1993).
[7] K. Binder, Spinodal decomposition in confined geometry, J. Non-Equilib. Thermodyn. **23**, 1 (1998).
[8] H. Tanaka, Interplay between wetting and phase separation in binary fluid mixtures: Roles of hydrodynamics, J. Phys.: Condens. Matter **13**, 4637 (2001).
[9] D. Beysens, Y. Garrabos, V. Nikolayev, C. Lecoutre-Chabot, J.-P. Delville, and J. Hegseth, Liquid-vapor phase separation in a thermocapillary force field, Europhys. Lett. **59**, 245 (2002).
[10] E. D. Siggia, Late stages of spinodal decomposition in binary mixtures, Phys. Rev. A 20, 595 (1979).
[11] D. A. Beysens, Kinetics and morphology of phase separation in fluids: The role of droplet coalescence, Physica A **239**, 329 (1997).
[12] M. Pascual, A. Poquet, A. Vilquin, and M.-C. Jullien, Phase separation of an ionic liquid mixture assisted by a temperature gradient, Phys. Rev. Fluids **6**, 024001 (2021).
[13] M. Pascual, A. Amon, and M.-C. Jullien, Thermocapillary instability of an ionic liquid-water mixture in a temperature gradient, Phys. Rev. Fluids **6**, 114203 (2021).

Thermocapillary effects on viscoelastic droplet suspended in another viscoelastic pressure driven axisymmetric flow

Malay Vyas[1] and Uddipta Ghosh[2]

[1] *Mechanical Engineering Discipline, Indian Institute of Technology, Gandhinagar, India*
vyas_malay@iitgn.ac.in

[2] *Mechanical Engineering Discipline, Indian Institute of Technology, Gandhinagar, India*
uddipta.ghosh@iitgn.ac.in

I. GENERAL GUIDELINES

This work explores the dynamics and deformation of a viscoelastic drop in another immiscible viscoelastic medium for a pressure driven base flow with an imposed temperature gradient. Refer to Fig. 1 for the schematic of the problem. Both of the fluids are described by the linear Phan-Thien-Tanner (l-PTT) model which accounts for shear thinning behaviour and predicts a non-zero first normal stress coefficient. The base flow thus has quartic (fourth power of the radius) variation in contrast with the Newtonian Poiseuille flow. We use an asymptotic framework [1, 2] to solve the problem analytically in small Deborah and Capillary number limits. A combination of regular perturbation and domain perturbation [2] is used to achieve the asymptotic solutions. We report the first two corrections to the Newtonian droplet behaviour. The effects of viscosity ratio, elongational properties, relaxation time, deformability, and applied temperature gradient are investigated in depth for their contribution in the behaviour of the droplet.

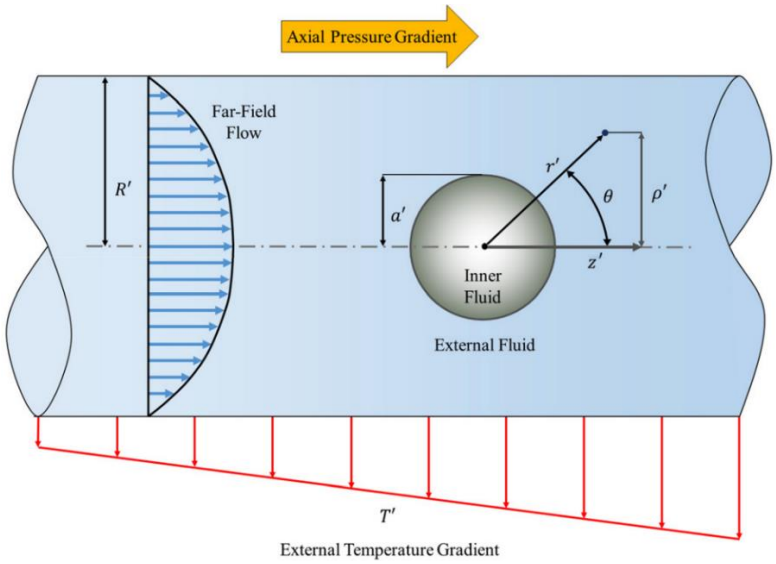

Figure 1: Schematic of the problem

We find that the characteristics of the inner fluid play a major role in governing the deformation and migration velocity of the droplet. The analysis discloses that a strongly viscoelastic droplet phase compared to the suspending medium can achieve a maximum migration velocity at intermediate viscosity ratios. This trend has been shown in Fig. 2.

[1] S. Das, S. Mandal, S. Som, and S. Chakraborty, Migration of a surfactant-laden droplet in non-isothermal Poiseuille flow, Phys. Fluids 29, 012002 (2017)

[2] L. G. Leal, *Advanced Transport Phenomena: Fluid Mechanics and Convective Transport Processes Vol. 7.*, Cambridge University Press (2007).

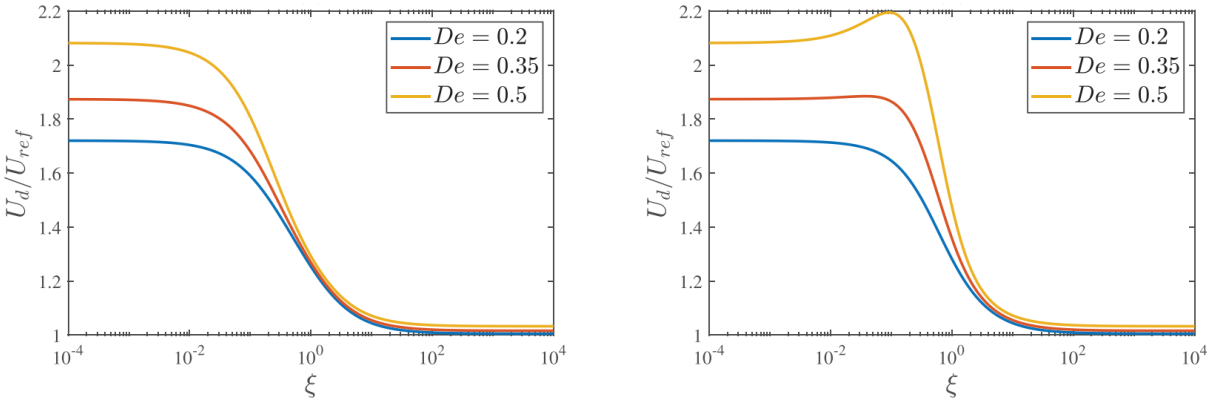

Figure 2: Normalized migration velocity of the droplet vs Viscosity ratio. Left: Mildly viscoelastic droplet. Right: Strongly viscoelastic droplet

Furthermore, we calculate the critical temperature gradient required to halt the motion of the migrating drop and investigate the effects of viscoelasticity on the same. We also delineate the consequence of viscoelastic stresses in altering the shape of the droplet. The shape changes between prolate and oblate depending upon the nature and strength of the viscoelastic stresses. Fig. 3 and Fig. 4 show the critical Marangoni number (non-dimensional temperature gradient) and deformation factor (Oblate: $D_f > 1$, Prolate: $D_f < 1$)

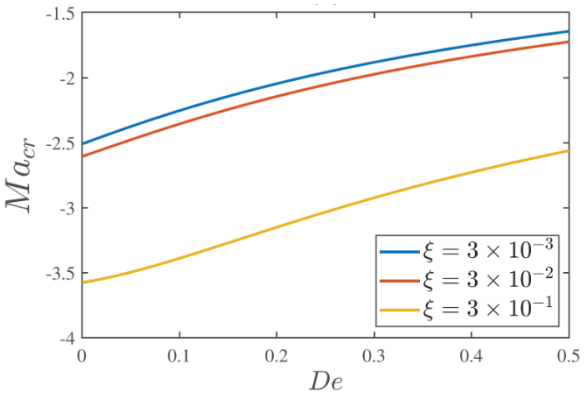

Figure 4: Critical Marangoni number vs Deborah number for different viscosity ratios

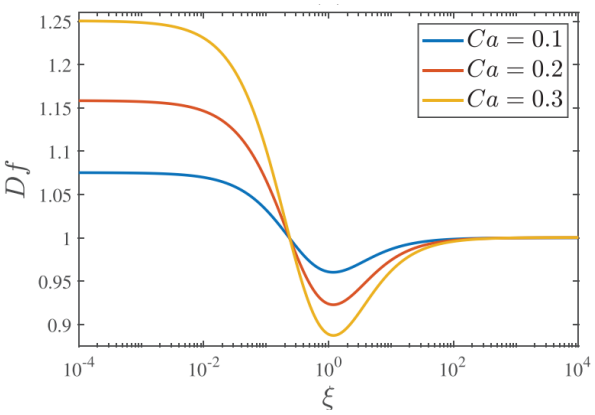

Figure 3: Deformation factor vs Viscosity ratio for different Capillary numbers

These findings have implications for several applications - for example, polymer processing and in medical and pharmaceutical fields.

Correlation between traveling wave of hydrothermal wave and azimuthal motion of particle forming coherent structure in liquid bridges

Shogo Sensui[1], Shin Noguchi[1], Kizuku Kurose[2], and Ichiro Ueno[2]

[1] *Div. of Mech. Aerospace Eng. Graduate School of Science and Technology, Tokyo Univ. Science, Japan*
7522532@ed.tus.ac.jp

[2] *Dept. of Mech. Aerospace Eng, Faculty of Science and Technology, Tokyo Univ. Science, Japan*
ich@rs.tus.ac.jp

We investigate experimentally the phenomenon of particle accumulation structures (PAS), as first described by Schwabe et al. [1], in which small tracer particles accumulate to form coherent structures under specific conditions within the half-zone liquid bridge (see **Fig. 1.**). A designated temperature difference ΔT $(\equiv T_h - T_c)$ is imposed between the two end surfaces of the liquid bridge in order to induce thermocapillary-driven flow on the free surface. As ΔT is increased, the convection field within the liquid bridge transitions from a two-dimensional "steady" state to a three-dimensional "oscillatory" one. Since the pioneering work [1], the spatial-temporal structure of PASs and their occurring conditions have been investigated through both experimental [2-6] and numerical [7-9] approaches. These unique structures have been observed despite the presence of gravitational acceleration [2,3,6]. It has been suggested that PASs exhibit a closed structure with an azimuthal wave number consistent with that of the oscillatory flow resulting from hydrothermal wave instability [2]. However, the mechanism of their formation remains unclear. Two major models have been proposed: the particle-free surface interaction (PSI) model [10] and the phase locking model [11]. The former posits that the formation of PAS is governed by the transfer of streamlines near the free surface, while the latter suggests that "synchronization" between the turnover motion of particles and the azimuthal traveling flow within the liquid bridge is responsible for particle accumulation.

In the present investigation, we implement a series of terrestrial experiments to examine the correlation between the rotational motion of particles and the thermal flow that travels with the spatial-temporal data of the particles that constitute the coherent structure within the O (1mm) sized liquid bridge, in an effort to overcome static pressure under normal gravitational conditions. The spatial-temporal dynamics of the suspended particles that comprise the PASs of various m's are monitored through the utilization of particle tracking velocimetry (**Fig. 2(a).**). We assess the Doppler shift [11] and examine the validity of the model through the analyzed experimental data (**Fig. 2(b).**). Additionally, we further investigate the correlation between the azimuthally traveling motion of the particles forming the coherent structures and the traveling-wave-type convection in the liquid bridge.

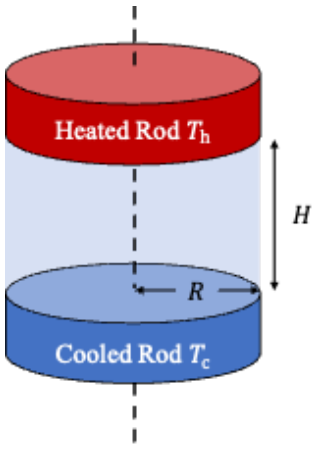

FIG. 1. Schematic diagram of liquid bridge

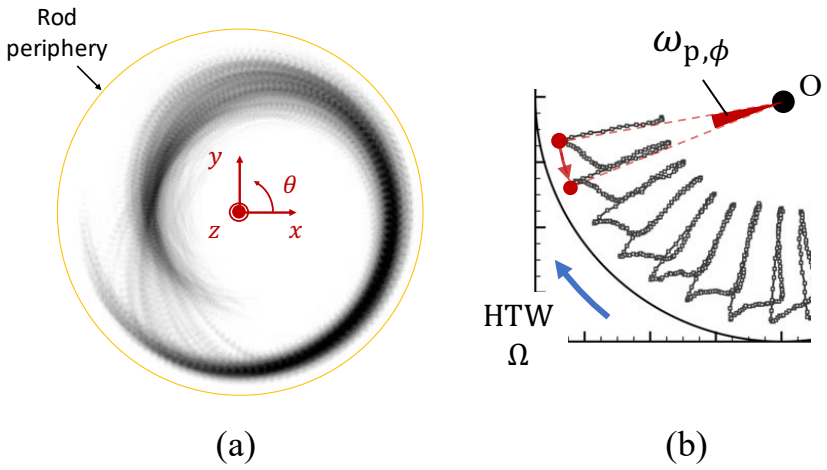

FIG. 2. (a) Particle image taken from above liquid bridge in rotating frame of reference (black dots: particles, yellow circle: rod periphery) and (b) two-dimensional trajectry in PAS in laboratory frame. $\omega_{p,\phi}$ is amount of azimuthal movement when the particle makes single turnover in the azimuthal convection with angular velocity Ω.

Acknowledgements : This work was partially supported from the Japan Society for the Promotion of Science (JSPS) by Grant-in-Aid for Challenging Research (Exploratory) (grant number: 20K20977).

[1] D. Schwabe, New feature of thermocapillary convection in floating zones revealed by tracer particle accumulation structure (PAS), Microgravity Sci. Technol, **9** (1996) 163.

[2] S. Tanaka, H. Kawamura, I. Ueno and D. Schwabe, Flow structure and dynamic particle accumulation in thermocapillary convection in a liquid bridge, Physics of Fluids, **18** (2006) 067103, DOI : 10.1063/1.2208289.

[3] D. Schwabe, A. I. Mizev, M. Udhayasankar, and S. Tanaka, Formation of dynamic particle accumulation structures in oscillatory thermocapillary flow in liquid bridges, Phys. Fluids, **19** (2007) 072102, DOI : 10.1063/1.2742304.

[4] M. Gotoda, A. Toyama, M. Ishimura, T. Sano, M. Suzuki, T. Kaneko and I. Ueno, Experimental study of coherent structures of finite-size particles in thermocapillary liquid bridges, Phys. Rev. Fluids, **244** (2019) 299, DOI : 10.1103/PhysRevFluids.4.094301.

[5] T. Oba, A. Toyama, T. Hori and I. Ueno, Experimental study on behaviors of low-stokes number particles in weakly chaotic structures induced by thermocapillary effect within a closed system with a free surface, Phys. Rev. Fluids, **4** (2019) 104002, DOI : 10.1103/PhysRevFluids.4.104002.

[6] T. Sakata, S. Terasaki, H. Saito, S. Fujimoto, I. Ueno, T. Yano, K. Nishino, Y. Kamotani and S. Matsumoto, Coherent structures of m = 1 by low-Stokes-number particles suspended in a half-zone liquid bridge of high aspect ratio: Microgravity and terrestrial experiments, Phys. Rev. Fluids, **7** (2022) 014005, DOI : 10.1103/PhysRevFluids.7.014005.

[7] I. Barmak, F. Romano and H. C. Kuhlmann, Finite-size coherent particle structures in high Prandtl-number liquid bridges, Phys. Rev. Fluids, **33** (2021) 19, DOI : 10.1103/PhysRevFluids.6.084301.

[8] P. Capobianchi and M. Lappa, On the influence of gravity on particle accumulation structures in high aspect-ratio liquid bridges, J. Fluid Mech., **908** (2021) A29, DOI : 10.1017/jfm.2020.882.

[9] D. Melnikov, D. Pushkin, and V. Shevtsova, Accumulation of particles in time dependent thermocapillary flow in a liquid bridge: modeling and experiments, Euro. Phys. J. Spec. Topics, **192** (2011) 29, DOI : 10.1140/epjst/e2011-01357-7

[10] H. C. Kuhlmann and E. Hofmann, The mechanics of particle accumulation structures in thermo-capillary flows, Euro. Phys. J. Spec. Topics, **192** (2011) 3, DOI : 10.1140/epjst/e2011-01355-9.

[11] D. Pushkin, D. Melnikov and V. Shevtsova, Ordering of small particles in one-dimensional coherent structures by time-periodic flows, Phys. Rev. Lett., **106** (2011) 234501, DOI : 10.1103/PhysRevLett.106.234501

Suppressing Marangoni instability using parametric forcing

I. B. Ignatius[1], B. Dinesh[2], Georg Dietze[3] and R. Narayanan[1]

[1]Department of Chemical Engineering, University of Florida, Gainesville, FL 32601, USA,
igin.ignatius@ufl.edu, ranga@ufl.edu
[2]IIT BHU, Varanasi, UP, 221005, India, dineshbh6@gmail.com
[3]Université Paris-Saclay, CNRS, FAST, 91405 Orsay, France, georg.dietze@universite-paris-saclay.fr

I. ABSTRACT

Marangoni instability occurs when a fluid layer is heated from below beyond a critical temperature gradient due to the action of surface tension gradients. The Marangoni effect at the interface can form either long-wave patterns or short-wave patterns, depending on the aspect ratio of the container. Experiments and theoretical calculations performed by Vanhook et.al. [1] show that a long-wave Marangoni instability will lead to the dry-out of thin films. In this study, we examine how and when this instability and the ensuing dry-out may be suppressed by the action of resonance. Resonant instability in the absence of any heating occurs when a fluid layer in a container is vertically oscillated at an amplitude greater than a critical value.

In the current study calculations show that through the application of parametric forcing, a long-wave Marangoni instability can be stabilized but not a short-wave Marangoni instability. If oscillated at a low frequency, linear stability calculations show that this system will transition to a stable regime with a flat interface beyond a critical amplitude. Further increase in amplitude beyond a second threshold will result in the onset of saturated oscillatory waves on account of resonance. At high frequencies of oscillation, the free surface directly transitions to saturated oscillatory waves beyond a critical amplitude, circumventing any transition to a stable state. The effect of parametric forcing on dry-outs is also studied by tracking the interface using a powerful reduced-ordered model developed using the weighted residual integral boundary layer method (WRIBL). Analysis using this model shows suppression of dry-outs in thin films at both low and high frequencies of oscillation. Our studies are placed in the context of other works on the combined effects of parametric forcing and surface-tension gradient induced instability [2, 3].

The suppression of dry-outs in thin films is important due to its relevance in coating industries for the manufacture of thin optical films and in additive manufacturing of metals in microgravity environments for human habitation in space.

II. ACKNOWLEDGEMENTS

The authors gratefully acknowledge funding from NSF via grant number CBET-2025117 and NASA via grant numbers 80NSSC20M0093 and 80NSSC23K0457.

[1] S. J. VanHook, M. F. Schatz, J. B. Swift, W. D. Mccormick, and H. L. Swinney, “Long-wavelength surface-tension-driven Bénard convection: experiment and theory,” Journal of Fluid Mechanics, vol. 345, p. 45–78, 1997.
[2] U. Thiele, J. M. Vega and E. Knobloch, “Long-wave Marangoni instability with vibration”, Journal of Fluid Mechanics 546, 61–87, 2006.
[3] A. A. Nepomnyashchy and I. B. Simanovskii, “The influence of vibration on Marangoni waves in two-layer films”, Journal of Fluid Mechanics 726, 476–496, 2013.

Maragoni effect in Phase Change Materials: enhanced melting and micro-energy harvesting

Santiago Madruga[1] and Carolina Mendoza[2]

[1]*Universidad Polite´cnica de Madrid, Aerospace Engineering School, Plaza Cardenal Cisneros 3, Madrid, 28040, Spain* santiago.madruga@upm.es
[2]*Universidad Antonio de Nebrija, Escuela Polite´cnica Superior, Departamento Escuela de Ingenieros, Santa Cruz de Marcenado, 27, 28015 Madrid, Spain*

The Phase Change Materials (PCM) take advantage of the latent heat of the solid/liquid phase change to store large amounts of thermal energy during melting or release it to the ambient during solidification. In addition to ground applications on energy storage and thermal management, the temperature cycles of operation of devices onboard spacecraft in microgravity suit well with the usage of latent heat during melting and solidification of PCMs [1, 2].

We show the melting dynamics of PCM under thermocapillary driving. The interplay between conduction and convection-dominated regions within the liquid phase determines relevant heat transfer features. Notably, some magnitudes follow power laws: position of the surface melting front, time to complete melting, energy stored, and dynamic Marangoni number with respect to the Nusselt number [3].

$$\mu \frac{\partial u_h}{\partial n} = -\epsilon \gamma \nabla_s T$$

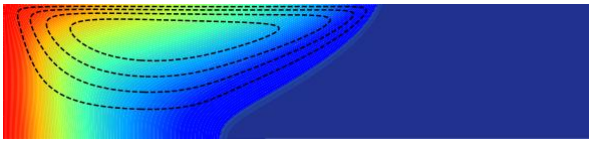

FIG. 1: Streamlines and temperature field of a Phase Change Material driven by thermocapillarity. The left side is a conductive wall held above PCM melting temperature; the rest of the boundaries are adiabatic. The upper boundary is a flat surface where the Marangoni effect induces flow motions at the liquid phase of the Phase Change Material. Dark blue: solid region.

We show the heat transfer, thermal energy storage, and flow dynamic generated by Marangoni flow in PCMs embedded in a metallic foam [8]. We present a full hydrodynamics model based on the Darcy–Brinkman–Forchheimer bulk equations and a linear shear stress boundary condition on porosity. The porous matrix weakens the Marangoni effect by decreasing the surface shear stress. Reduction of the porosity leads to shorter melting times and more efficiency in thermal energy storage due to the higher effective conductivity at low aspect ratios. However, increasing the aspect ratio, these enhancements decay, and the Marangoni flows are strong enough for high aspect ratios to offset the advantage of high thermal effective conductivity at high volumes of the metallic foam. The non-Darcy effects are strong for high aspect ratios. The optimum configurations correspond to high porosities and permeability to suppress less thermocapillary flows. The position of the surface melting front follows a power law for square geometries. In addition to this, we show how the introduction of metallic nanoparticles can enhance the performance of PCM systems driven by thermocapillarity through different mechanisms as using metallic foams [4]

Finally, we show how it is possible to use the Marangoni effect to boost the conversion of ambient thermal fluctuations into electric power. We show how coupling PCMs with thermoelectric devices increases the electric energy output an order of magnitude with respect to conventional designs in micro-energy harvesters to power sensors in spacecraft [5, 6]. For usual thermal conditions in satellites, we show how thermocapillarity can enhance the conversion rate of TEG/PCM micro-energy harvester and

produce enough power to feed low-consumption sensors. We show that most of the augmented energy production with respect to conductive transport occurs during the PCM heating phase when Marangoni flows are strongest [7].

[1] S. Madruga and C. Mendoza. Heat transfer performance and melting dynamic of a phase change material subjected to thermocapillary effects. *Int. J. Heat Mass Transf.*, 109:501–510, 2017.

[2] S. Madruga and C. Mendoza. Enhancement of heat transfer rate on phase change materials with thermocapillary flows. *Eur. Phys. J. Special Top.*, 226:1169–1176, 2017.

[3] S. Madruga and C. Mendoza. Scaling laws during melting driven by thermocapillarity. *Int. J. Heat Mass Transf.*, 163:120462, 2020.

[4] S. Madruga and C. Mendoza. Heat transfer performance and thermal energy storage in nano-enhanced phase change materials driven by thermocapillarity. *Int. Commun. Heat Mass Transf.*, 129:07351933, 2021.

[5] S. Madruga. Thermoelectric energy harvesting in aircraft with porous phase change materials. *IOP Conf. Ser.: Earth Environ. Sci.*, 354:012123, 2019.

[6] S. Madruga. Modeling of enhanced micro-energy harvesting of thermal ambient fluctuations with metallic foams embedded in Phase Change Materials. *Renew. Energy*, 168:424–437, 2021.

[7] S. Madruga and C. Mendoza. Introducing a new concept for enhanced micro-energy harvesting of thermal fluctuations through the Marangoni effect. *Appl. Energy*, 306:117966, 2022.

[8] S. Madruga. Modeling and simulations of the Marangoni effect in phase change materials embedded in metallic foams. *Appl. Therm. Eng.*, 219:119413, 2023.

Nonlinear dynamics of phase change material at the melting stage.

B. Seta[1], D. Dubert[2], Jna. Gavaldà[2], J. Massons[2], M. M. Bou-Ali[3], X. Ruiz[2] and V. Shevtsova[3,4]

[1] *Technical University of Denmark, Produktionstorvet, Lyngby, 2800, Denmark, berse@mek.dtu.dk*
[2] *Department of Universitat Rovira i Virgili, Tarragona, 43003, Spain, josepxavier.ruiz@urv.cat*
[3]*Faculty of Engineering, Mondragon University, 20500 Mondragon, Spain, mbouali@mondragon.edu*
[4]*IKERBASQUE, Basque Foundation for Science, Bilbao, 48009 Spain, x.vshevtsova@mondragon.edu*

I. INTRODUCTION

Phase change materials (PCMs) can store and release a large amount of thermal energy during melting or solidification, without changing the temperature. In terrestrial applications, the presence of convective flows in the liquid phase helps to solve heat transfer problems of PCMs with low thermal conductivities. However, this approach is not applicable in microgravity. Then, an alternative strategy is the use of the thermocapillary effect, in which a non-uniform temperature induces surface tension gradients that drive convective motion. Since the thermal gradients along PCM/air interface are large, with an increase in the PCM liquid phase, the system is prone to oscillatory instability. These are due to the onset and propagation of hydrothermal disturbances, whose combination can result in a variety of waveforms, ranging from simple standing waves to more complex time-dependent states due to the superposition of traveling waves with different wavenumbers.

II. PROBLEM DESCRIPTION AND MATHEMATICAL MODEL

We investigate a series of Marangoni flow bifurcations in a melting bridge made of a phase change material that is initially solid and then undergoes a transition to a liquid state as a result of fixed temperatures set on the supporting disks. The temperature of both supports is greater than the melting point of the material, although the top one just marginally, see geometry in FIG.1 (left side). These non-linear transitions are extremely sensitive to the transport of heat in the radial direction, which is taken into account in terms of the Biot number.

The system is considered in a microgravity environment. The phase change is modelled using an enthalpy-porosity formulation of the Navier-Stokes equations that describes the co-existing solid and liquid states as a continuum. The three-dimensional flow dynamics of the system is described by the momentum and continuity equations for incompressible Newtonian fluids, with a sink term in the momentum equation, which differentiates the velocity between the solid and liquid phases. This last term of the momentum equation represents the Carman-Kozeny model for a moving solid-liquid interface as a porous mushy layer where solid and liquid phases may coexist. As soon as melt reaches the interface, the Marangoni convection starts driven by the temperature gradients. A detailed description of the problem can be found in recent publications [1 , 2]. The properties of hydrothermal waves, such as traveling or standing patterns and azimuthal wave numbers, are studied using a recently developed approach adapted to the present PCM system [3].

III. RESULTS

One of the most important parameters in the thermal performance of PCM is the amount of heat that can be removed from the hot source at a given time interval. In order to quantify the performance of

[1] B. Seta, D. Dubert, J. Massons, Jna. Gavalda, M.M. Bou-Ali, X. Ruiz, Effect of Marangoni induced instabilities on a melting bridge under microgravity conditions. Int. J. Heat Mass Transfer 179, 121665 (2021).
[2] B. Seta, D. Dubert, J. Massons, Jna. Gavalda, M.M. Bou-Ali, X. Ruiz, V. Shevtsova, V. Transitions between nonlinear regimes in melting and liquid bridges in microgravity. Int. J. Heat Mass Transfer 193, 122984 (2022).
[3] Y. Gaponenko, V. Yasnou, A. Mialdun, A. Nepomnyashchy, V. Shevtsova, Hydrothermal waves in a liquid bridge subjected to a gas stream along the interface. J. Fluid Mech. 908, A34 (2021).

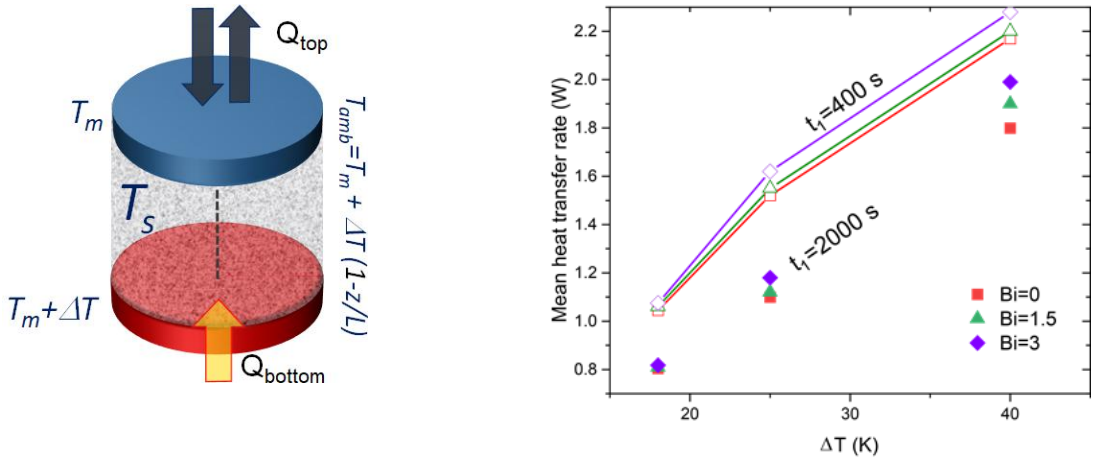

FIG.1 (left) Sketch of the system; (right) Mean heat transfer rate, Q_{mean}, through the lower (hot) support at different stages of the melting process (t_1= 400 s and 2000 s) as a function of the ΔT and Biot number. The line-connected open symbols correspond to t_1=400 s, and the solid symbols without a guideline correspond to t_1=2000 s.

the heat extraction in melting bridge geometry, we propose to determine the mean heat transfer rate through the hot (lower) support during a given time. Two values of the time interval are analyzed: (1) t_1 = 400 s to study the system in the initial phase of melting, when a significant part of the PCM is still solid; (2) t_1=2000 s to evaluate the long-term performance, i.e., to determine the amount of heat removed from the system when the PCM is completely melted. The results in FIG.1 (right side) present an interesting finding, that the mean heat transport decreases at longer times, reflecting the efficiency reduction as the PCM becomes more melted. These observations suggest the advantage of removing the melting bridge from a source of heat before the complete melting is achieved. This strategy can improve the performance of heat removal by up to 20%. The role of the Biot number at large times, i.e., at t_1=2000 s, is more pronounced than at t_1=400 s.

An example of time evolution on the system's non-linear dynamics during the melting process is shown in FIG.2 in terms of trajectories in the phase plane for the adiabatic case. The oscillations appearing near the onset of instability correspond to a hydrothermal wave with azimuthal wavenumber m=1, the trajectory of m=1 is a straight line passing through the origin of the phase plane, which is the signature of the standing wave. In course of time, the standing wave is attenuated and a spiral wave is originated, the development of which leads to the formation of a TW with m=2, as depicted in the central panel of FIG.2. Later, see FIG.2 (left panel), a uniform traveling wave (TW) with m=2 is established, which is characterized by the trajectory in the form of a circle centered at the origin of the coordinate. The counter-clockwise traveling wave is the final state of the system.

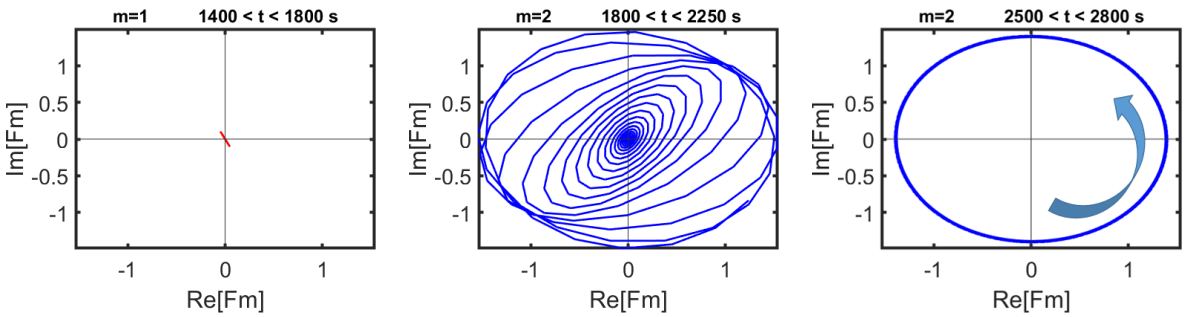

FIG.2. Trajectories of the dynamic system at different time intervals when Bi=0 and ΔT=25K illustrating: (left) standing wave m=1, (central) transition between dynamic states and (right) developed TW with m=2.

Session 6 – Instabilities

Tuesday June 20, 11:00–12:30

INSTABILITY OF A THIN FILM OF CHEMOTACTIC ACTIVE SUSPENSION

Nishanth Murugan[1] and Anubhab Roy[1]

[1]*Department Applied Mechanics, Indian Institute of Technology Madras, Chennai, India, Email:* anubhab@iitm.ac.in

The collective behavior of motile chemotactic swimmers is rich in its dynamical behavior and plays a critical role in its survival. Experiments by [4] involving the aerotactic bacterium *B. subtilis* revealed the presence of hydrodynamic instabilities in dilute suspensions of swimmers, resulting in the creation of dense regions of swimmers that are depleted of the attractant or nutrient. To explain this instability, [1] considered a suspension of swimmers in a channel with an imposed attractant gradient. The effects of an evolving attractant field on the stability characteristics of the system was considered in a recent work [2]. Through a continuum model, it was shown that the induced bias in the tumbling frequency in response to the presence of an attractant gradient, gives rise to an anisotropic active stress that serves to destabilize the system. In this work [3], we extend this by accounting for the presence of a free interface, which is more representative of the experiments by [4].

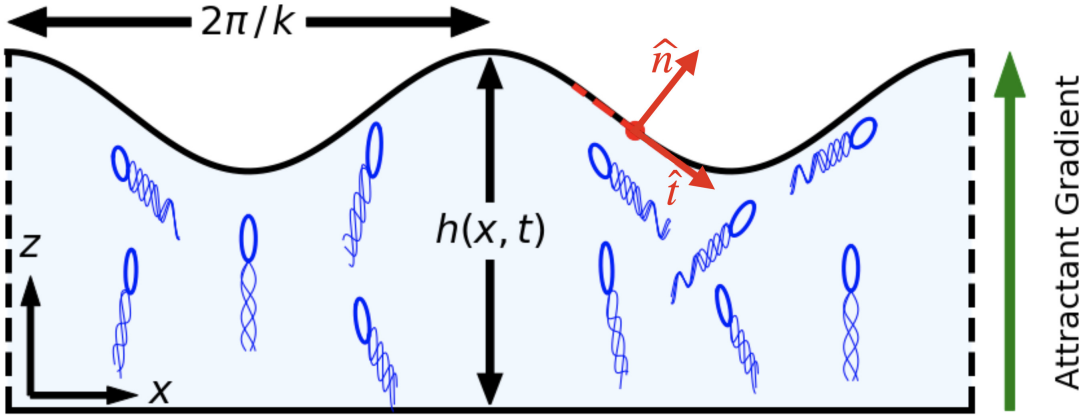

FIG. 1: Schematic of the thin film problem with an attractant gradient pointed towards the interface [3]. The swimmers bias their random walk so as to align their mean swimming orientation along the gradient.

The presence of the free interface results in symmetry breaking and gives rise to quantitatively different stability characteristics. We start by using long-wave stability calculation to analytically showcase the presence of a new mode of instability associated with the free interface which we term as an interface mode. This new mode is found to trigger an instability at far lesser threshold of the activity number than the predictions by [1] (which we term as a density mode). Furthermore, it is found that the coupling between the interface and density modes is capable of destabilizing a suspension of pullers, a system shown by [1] to be unconditionally stable. We use the eigenfucntions associated with the velocity fields to identify the density and interface modes of instability. It is found that the interface mode drives a local shear flow by means of a jump in viscous stress at the interface, whilst the density mode results in circulatory regions in the velocity field as shown by [1]. The calculation is then extended to classifying the stability of the system subject to finite wavenumber perturbations numerically using a spectral solver. Finally, we write down a set of non-linear long-wave equations that govern the evolution of the film. We verify the mechanism associated with these instabilities by numerically solving the equations and

comparing with the results of the linear stability analysis.

---

[1] T. Kasyap and D. L. Koch. Chemotaxis driven instability of a confined bacterial suspension. *Physical Review Letters*, 108(3):038101, 2012.

[2] N. Murugan and A. Roy. Instability of an autochemotactic active suspension. *Journal of Fluid Mechanics*, 934, 2022.

[3] N. Murugan and A. Roy. Instability of a thin film of chemotactic active suspension. *Journal of Fluid Mechanics*, 955:A11, 2023.

[4] A. Sokolov, R. E. Goldstein, F. I. Feldchtein, and I. S. Aranson. Enhanced mixing and spatial instability in concentrated bacterial suspensions. *Physical Review E*, 80(3):031903, 2009.

Instability in the thermocapillary migration of a flat droplet

Kai-Xin Hu[1] and Dan Wu[2]

[1] *Faculty of Mechanical Engineering and Mechanics, Ningbo University, 315211, Ningbo, China,* hukaixin@nbu.edu.cn

[2] *Faculty of Mechanical Engineering and Mechanics, Ningbo University, 315211, Ningbo, China,* wudan@nbu.edu.cn

The instability in the thermocapillary migration of an attached drop on a plate is examined for the Newtonian and Oldroyd-B fluids. The droplet, flattened by the gravity, is susceptible to two kinds of instabilities: the convective instability(CI)[1], which is independent of surface deformation; and the surface wave instability (SWI)[2], which only occurs when the Galileo number and the surface-tension number are not too large. The wave number of the latter is much smaller than that of the former, while the reverse is true for the wave speed. The mode includes the streamwise and oblique waves. Energy analysis suggests that the energy of long-wave mode comes from the shear stress induced by the surface deformation, the energy source for the mode with finite wavelength is the work done by Marangoni forces, while the energy from the basic flow is only important in some cases at small Prandtl numbers. For the Oldroyd-B fluid, a small elasticity slightly changes the critical Marangoni number of SWI, while larger elasticity changes the preferred mode from the SWI to the CI.

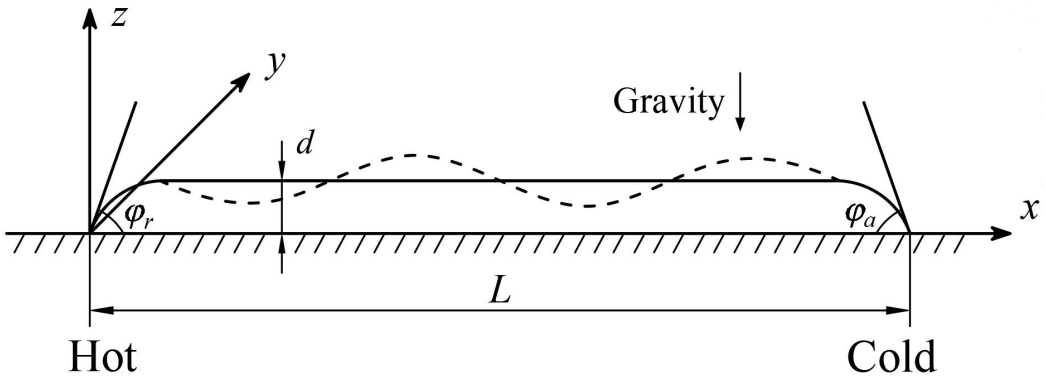

FIG. 1. The side view of thermocapillary migration for a thin droplet on a solid plane.

[1] Kai-Xin Hu, Chen-Yi Yan and Qi-Sheng Chen, Instability of thermocapillary – buoyancy convection in droplet migration, Phys. Fluids **31**, 122101 (2019).

[2] Kai-Xin Hu, Shao-Neng Zhang and Qi-Sheng Chen, Surface wave instability in the thermocapillary migration of a flat droplet, J. Fluid Mech. (2023), Accepted.

Influence of Insoluble Surfactant on Modulational Instability of Marangoni Wave Patterns

Alexander B. Mikishev[1] and Alexander A. Nepomnyashchy[2]

[1] *Department of Eng. Technology, Sam Houston State University, 77341, Huntsville, TX, USA,* amik@shsu.edu
[2] *Department of Mathematics, Technion, 32000, Haifa, Israel, nepom@technion.ac.il*

Pattern formation in Marangoni convection is determined by the interaction of Marangoni stresses caused by the thermocapillary effect, and surface deformation. The patterns grow beyond the instability threshold characterized by critical wavenumber k_c and, in the case of an oscillatory instability, by critical frequency ω_c[1]. Two sorts of patterns are possible, stationary patterns and oscillatory ones. Hexagons, rolls, and squares belong to the first group, the typical oscillatory (wave) patterns are traveling waves. When the surface-active agent is added to the surface, the selected patterns are changed.

The wavenumber selection of patterns is determined by their stability with respect to longwave modulation. In our previous works[2,3], we considered the stability of stationary structures to longwave modulation and the influence of spread insoluble surfactant on the modulational instability. Here we investigate the influence of surfactant on the modulation of Marangoni waves in a thin liquid layer between the media with low heat conductivity.

Using the Newell-Whitehead approach to the problem, we obtain a significant modification of the complex Ginzburg-Landau equation, that leads to the change of the criterion of the longitudinal phase-modulation instability similar to the Benjamin-Feir instability. The stability maps on the parameter plane (β, G) are plotted (β is the Biot number and G is the Galileo number) for different values of surfactant concentration, characterized by the elasticity parameter, N.

Acknowledgement: The study was partly supported by the Israel Science Foundation (Grant # 843/18).

[1] M.C. Cross and P.C. Hohenberg, Pattern formation outside the equilibrium, Rev. Mod. Phys. **65**, 851 (1993).

[2] A.B. Mikishev and A.A. Nepomnyashchy, Patterns and their large-scale distortions in Marangoni convection with insoluble surfactant, Fluids 6, 282 (2021).

[3] A.B. Mikishev and A.A. Nepomnyashchy, Marangoni patterns in a non-isothermal liquid with deformable interface covered by insoluble surfactant, Colloids Interfaces 6(4), 53 (2022).

Vibrational Dynamics of Liquids Interface in Rotating Cavities

Victor Kozlov[1], Nikolai Kozlov[1] and Antonio Viviani[2]

[1] *Laboratory of Vibrational Hydromechanics, PSHPU, 614045, Perm, Russia, kozlov@pspu.ru*
[2] *Dipartimento di Ingegneria, Università degli Studi della Campania, 81031, Aversa, Italy, Antonio.VIVIANI@unicampania.it*

The report presents the results of experimental study and theoretical analysis of vibrational dynamics of the interface of two immiscible liquids in a vertical Hele-Show cell subject to modulated rotation [1 , 2, 3]. The high contrast of liquids viscosity is a characteristic feature of the system under consideration. The results of experiments with different liquid pairs (when liquid that is more viscous has lower density and vise-verse) are discussed.

The cell has an axisymmetric circular lateral boundary and performs a modulated rotation around a horizontal axis, that is perpendicular to the layer plane, according the low $\Omega = \Omega_{\text{rot}}(1+\varepsilon\cos(\Omega_{lib}t))$, where Ω_{rot} is an average velocity and Ω_{lib} is a librations radian frequency. The equilibrium shape and stability of the interphase boundary is investigated. In the absence of librations, under the action of centrifugal force the boundary has an axisymmetric shape. It is found that at certain frequency ratios $\Omega_{\text{lib}}/\Omega_{\text{rot}} = 1,1/2,...$ the librations lead to a violation of the axisymmetric equilibrium location of the interface: in the cavity reference frame it is displaced in the radial direction (Fig. 1, left). This phenomenon is determined by the average action of the gravitational field; the results of experiments and theory are consistent. The experiments reveal that with an increase in the amplitude of the rotation velocity modulation ε the circular interface loses stability in a threshold manner, which manifest itself in a development of an azimuthal-periodic relief on the interface. The relief is quasi-stationary in the cavity reference frame (Fig. 1, right). It is shown that the appearance of a "frozen" relief is associated with the development of the Kelvin-Helmholtz instability against the background of tangential oscillations of a less viscous liquid near the interface. A dimensionless parameter that determines the stability of the interface in the limit of a high dimensionless libration frequency (when a less viscous fluid performs inviscid oscillations) is determined. It is found that the stability threshold grows with decreasing the dimensionless libration frequency.

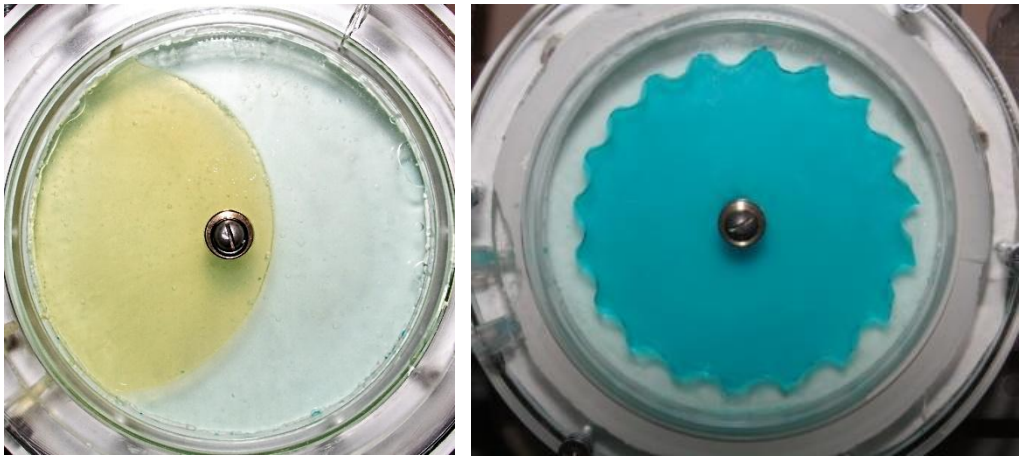

FIG. 1. A quasi-stationary shape of an interface. Left: industrial oil and silicon oil PMS-1000 at $\Omega_{\text{lib}} = \Omega_{\text{rot}} = 6.28\ \text{s}^{-1}$, $\varepsilon = 0.41$; Right: glycerol and fluorinert FC40 at $\Omega_{\text{rot}} = 15.7\ .\text{s}^{-1}\ \Omega_{\text{lib}} = 37.7\ \text{s}^{-1}\ \varepsilon = 0.22$.

Funding. The research is supported by the Russian Science Foundation (project 18-71-10053).

[1] V. G. Kozlov, J. S. Dementieva, V. S. Kobeleva and M. A. Petukhova, Stability of interface between liquids with high viscosity contrast in unevenly rotating cavity, J. Phys.: Conf. Ser. **1809**, 012022 (2021).
[2] V. G. Kozlov and M. A. Petukhova, Liquid free boundary in vertical gap subject to modulated rotation, J. Phys.: Conf. Ser. **2317**, 012008 (2022).
[3] V. Kozlov, M. Petukhova and N. Kozlov, Dynamics of liquids with high viscosity contrast in unevenly rotating Hele-Shaw cell, Phil. Trans. R. Soc., A 20220082 (2023).

Chaotic flow in a microtube: transition to plug flow

Philippe Beltrame[1]

[1]*UMR EMMAH, Avignon Université, Avignon, France,*
philippe.beltrame@univ-avignon.fr

This study investigates the 3D free surface flow in a cylindrical microtube taking into account the tube wettability (Fig. 1a). This type of problem is found in many contexts, whether industrial such as oil recovery by water injection [13] or physiological such as flow in human pulmonary capillaries [9] or agronomic such as water transfer in earthworm galleries [17]. Depending on the average amount of water, there are different types of flow. Near saturation of the microtube, a Taylor flow of air bubbles trapped in a plug flow occurs. Many works on microfluidic devices involve this type of flow and are studied in literature as in [7, 18]. If the microtube is weakly saturated, then a thin-film flow without a liquid bridge may appear. Due to the azimuthal curvature, thin films of uniform thickness are unstable, leading to a unduloid shape flow [11]. Moreover, for tubes with a sufficient large radius and thick enough films, the inertia terms play a relevant role in the dynamics and a rich scenario of traveling waves occurs [7, 12] and [6].

The aim of this paper is to study the transition from a thin film flow regime to the emergence of liquid bridge (plugs). Most of recent literature having studied the formation of liquid bridges have neglected the wettability [4, 5, 10]. However, in [5], a viscous blocking mechanism that drastically delays the onset of flooding in thin films has been identified. This mechanism results from buckling between two liquid collars generating two troughs of very thin films where dissipation is enhanced. Consequently, very thin films can appear spontaneously, which suggests that wettability is not negligible. This outcome is similar to the conclusion in [16] for flows on a fiber, that the thickness can become so thin that the intermolecular forces are no longer negligible and the wettability of the fiber has to be taken into account.

Recently, we focused on the wettability effect by studying microtube with very thin film in inertialess limit [1, 2]. We have highlighted specificities of the annular flow compared to the one-dimensional ridge flow on a plane. First, for tube radius small enough a periodic emission of pearls in the tail drop may occur, similar of pearls in the tail of a 3D drop [15]. The second specificity of annular flow is a dynamical complete wetting regime for large enough driving force and for small tube radius: A sliding ridge coexists with a thick film (compared to the precursor film). This regime is the analogue of the Landau-Levich film when a plate is removed from a liquid bath [8]. The latter regime may become unstable for specific long microtube. Then a flow regime by train of drops that consists of a clustering of drops without coalescence appear [2]. This regime is in contrast to 1D flows on a flat substrate where the flow takes place as a single very spread out drop, called pancake [19]. Therefore, for thin films in a long microtube, we do not expect a single coarse drop dynamic that would cause a liquid bridge.

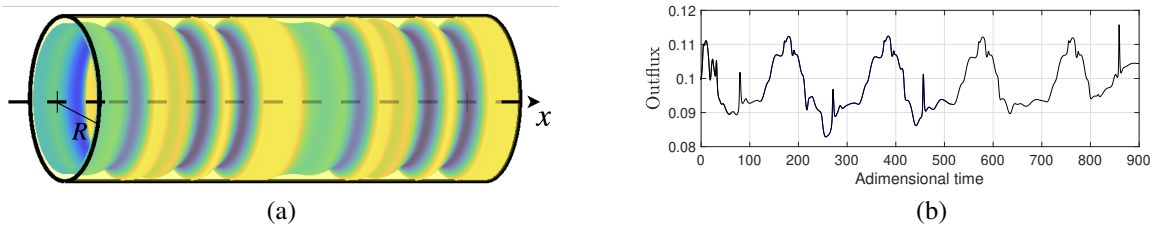

(a) (b)

FIG. 1: (a) Flow profile in a microtube of R radius .(b) Aperiodic time evolution of the outflux.

To study the transitions leading to the emergence of liquid bridge, partial wetting is taken into account using an effective interaction energy combining destabilizing short-range and stabilizing long-range interactions [14]. A constant flux at the inlet is imposed, in contrast to the periodic boundary conditions of the flow studied in [2, 3]. Thus, a richer dynamic behavior arises. Using time integration and path-following method, we study the different flow regimes and bifurcations. In particular, the traveling waves of the drop train flows become unstable and a competition between coalescence and fragmentation of drops takes place (Fig. 1). For long enough tube, aperiodic dynamics take place and intermittent and chaotic behaviors are brought to light (Fig. 1b). For an inertialess flow, this chaotic flow is noteworthy. An increase in inflow leads to strange attractor crises. These crises appear to be a precursor to the formation of liquid bridges, i.e. plug flow.

---

[1] P. Beltrame. Partial and complete wetting in micro-tube. *Europhys. Lett.*, 121:64002, 2018.

[2] P. Beltrame. Drop train flow in a microtube. *Eur. Phys. J. Spec. Top.*, 2023.

[3] Ph. Beltrame. Absolute negative mobility in ratchets: Symmetry, chaos and noise. *Journal of Chaotic Modeling and Simulation*, 1:101–114, 2018.

[4] Roberto Camassa, H. Reed Ogrosky, and Jeffrey Olander. Viscous film flow coating the interior of a vertical tube. part 1. gravity-driven flow. *Journal of Fluid Mechanics*, 745:682–715, 2014.

[5] G. F. Dietze and C. Ruyer-Quil. Films in narrow tubes. *Journal of Fluid Mechanics*, 762:68–109, 001 2015.

[6] C. Duprat, C. Ruyer-Quil, and F. Giorgiutti-Dauphiné. Spatial evolution of a film flowing down a fiber. *Phys. Fluids*, 21(4):042109, 2009.

[7] T.S. Fouilland, D.F. Fletcher, and B.S. Haynes. Film and slug behaviour in intermittent slug-annular microchannel flows. *Chemical Engineering Science*, 65:5344–5355, 2010.

[8] M. Galvagno, D. Tseluiko, H. Lopez, and U. Thiele. Continuous and discontinuous dynamic unbinding transitions in drawn film flow. *Phys. Rev. Lett.*, 112:137803, Apr 2014.

[9] James B. Grotberg. Respiratory fluid mechanics. *Phys. Fluids*, 23:021301, 2011.

[10] Oliver E. Jensen. Draining collars and lenses in liquid-lined vertical tubes. *Journal of Colloid and Interface Science*, 221(1):38–49, 2000.

[11] S. Kalliadasis and H.-C. Chang. Drop formation during coating of vertical fibres. *J. Fluid Mech.*, 261:135–168, 1994.

[12] V. Kerchman. Strongly nonlinear interfacial dynamics in core annular flows. *J. Fluid Mech.*, 290:131–166, 05 1995.

[13] W. L. Olbricht. Pore-scale prototypes of multiphase flow in porous media. *Annu. Rev. Fluid. Mech.*, 28(1):187–213, 1996.

[14] Len M. Pismen and Yves Pomeau. Disjoining potential and spreading of thin liquid layers in the diffuse-interface model coupled to hydrodynamics. *Phys. Rev. E*, 62:2480–2492, Aug 2000.

[15] T. Podgorski, J.-M. Flesselles, and L. Limat. Corners, Cusps, and Pearls in Running Drops. *Phys. Rev. Lett.*, 86((3)):036102, 2001.

[16] D. Quéré. Fluid coating on a fiber. *Annual Review of Fluid Mechanics*, 31(1):347–384, 1999.

[17] Sammartino S., Lissy A., Bogner C., Bogaert R. V. D., Capowiez Y., Ruy S., and Cornu S. Identifying the functional macopore network related to preferential flow in structured soils. *Vadose Zone J.*, 14(10):1–16, 2015.

[18] V. P. Schulz, N. Abbaspour, T. Baumeister, and T. Röder. Lattice-boltzmann simulation and experimental validation of a microfluidic t-junction for slug flow generation. *ChemEngineering*, 3(2), 2019.

[19] U. Thiele, K. Neuffer, M. Bestehorn, Y. Pomeau, and M.G. Velarde. Sliding drops on an inclined plane. *Colloids and Surfaces A*, 206:87–104, 2002.

Effect of a deep corrugated wall on the natural frequencies and the Faraday instability of a fluid interface

B. Dinesh[1], N. Brosius[2], T. Corbin[2] and R. Narayanan[2]

[1] *Department of Chemical Engineering and Technology, Indian Institute of Technology-BHU, Varanasi, UP 221005, India* dinesh.che@iitbhu.ac.in

[2] *Department of Chemical Engineering, University of Florida, Gainesville, FL 32611, USA,* ranga@ufl.edu

I. ABSTRACT

The natural frequency of an interface between a bilayer of immiscible fluids is shown to depend on the morphology of the bottom wall in addition to the density difference of the fluids, the interfacial tension, the fluid depths, and the disturbance wave number. To study the effect of deep wall-wave amplitude and fluids viscosities, a reduced-order method is employed that assumes the thickness of the bilayer to be small in comparison to the container width. The wavy wall is shown to lower the natural frequencies unless the number of waves of the wall pattern is twice that of the number of waves at the interface. These theoretical findings carry over to the resonant frequency determined by parametric excitation i.e., Faraday excitation. The theoretical results are qualitatively validated by physical experiments that use Faraday excitation over frequency ranges to obtain different interfacial modes under conditions that approximate slippery walls. An important outcome of the study is that the shift in the resonant frequency leads to a shift in the instability regions when fluid layers are subject to Faraday excitation. This work finds application in mixing and in heat transfer with resonant flows.

II. Acknowledgements

The authors gratefully acknowledge funding from NSF via grant numbers CBET-2025117 and EEC-1852111 for an REU.

Session 7 – Electric fields and EHD

Wednesday June 21, 9:00–10:30

Interfacial Instability due to Electrodeposition

Shreyanshu Agrawal[1], Ranga Narayanan[1], Kirk J. Ziegler[1], Farzam Zoueshtiagh[2] and Diwakar S. V.[3]

[1] *Department of Chemical Engineering, University of Florida, Gainesville, Florida 32611, USA*
s.agrawal@ufl.edu, ranga@ufl.edu, kziegler@che.ufl.edu
[2] *University of Lille, CNRS, UMR 8520, IEMN, F-59000 Lille, France*
farzam.zoueshtiagh@univ-lille.fr
[3] *Engineering Mechanics Unit, JNCASR, Bengaluru, India 560064* diwakar@jncasr.ac.in

Abstract

In this work, we develop a general model that predicts the onset of interfacial instability at the cathodic surface when an electrical potential difference is applied across a cell, which is composed of two metal electrodes separated by a dilute aqueous metallic solution. The instability takes the form of interfacial patterns as depicted in Figure 1. For this instability, the growth rate vs wavenumber curve reaches a maximum value for a particular wavenumber which depends on the scaled potential difference, the scaled mean concentration of the metal solution and the scaled surface energy. This model is compared to an approximate model where local electroneutrality was assumed and where domain dynamics are ignored. The predictions made by this model are also compared with experiments done for copper electrodes that span a gap containing dilute copper sulfate solution. This instability resembles many other interfacial instabilities like Rayleigh-Taylor instability and Marangoni instability, where growth rate is principally controlled by interfacial dynamics.

Acknowledgment: We acknowledge funding from NSF 2004527

Figure 1: A typical electrodeposition experiment in which top electrode is anode (higher potential) while bottom electrode is cathode (lower potential). Images were taken at different times. (a) Initial flat surface. (b) Cellular formation starts which can be seen as roughening of cathode. (c) Cells continue to grow and form dendrites. cf Ref [1]

[1] S. K. Gopalakrishnan et al., "Isolation of competing morphological patterns during microfluidic electrodeposition: Experimental confirmation of theory," *Electrochim Acta*, vol. 398, Dec. 2021, doi: 10.1016/j.electacta.2021.139205.

Dynamics of dendrites arising during electrodeposition

Pinar Eribol[1], Salah Mohand Moussa[1], Sarathy Gopalakrishnan[2], Diwakar Seyyanur Venkatesan[3], Abdelkrim Talbi[1], Kirk Ziegler[2], Ranga Narayanan[2], Farzam Zoueshtiagh[1]

[1] *Univ. Lille, CNRS, Centrale Lille, Univ. Polytechnique Hauts-de-France, UMR 8520, IEMN, F59000 Lille, France*
[2] *University of Florida, Department of Chemical Engineering, 32611, Gainesville, FL, US,*
[3] *Engineering Mechanics Unit, JNCASR, Jakkur, Bangalore, 560064, India*

Even though electrolysis is considered a basic process that is taught as early as in high schools, it appears that many associated phenomena are still not fully understood. One of them is the instability of electrodeposits that arise during such process. The morphological instability phenomenon is responsible for the non-uniform and wavy electrodeposition patterns at the cathode. The origin of this instability arises from the potential gradient across the electrodes that causes random disturbances. The wavelengths of the resulting instability patterns are governed by the interfacial surface energy and diffusion gradients transverse to the pattern development direction. In this work, the aim is to study the patterns that are observed to develop during electrodeposition on the cathode in the different cell configurations. An image analysis method is developed and the electrodeposition process is examined in terms of the growth rate of dendrites and wavelength. In particular, the physical characteristics of the dendrites are investigated with respect to the spacing between the electrodes and the orientation of the latter to gravity. This study demonstrated the influence of gravity on the wavelengths of the patterns developed but also on their growth rate. It is shown that the convectional flow can be decreased depending on the orientation of the electrochemical cell with respect to gravity and alter the kinetics of the deposition process (Fig. 1).

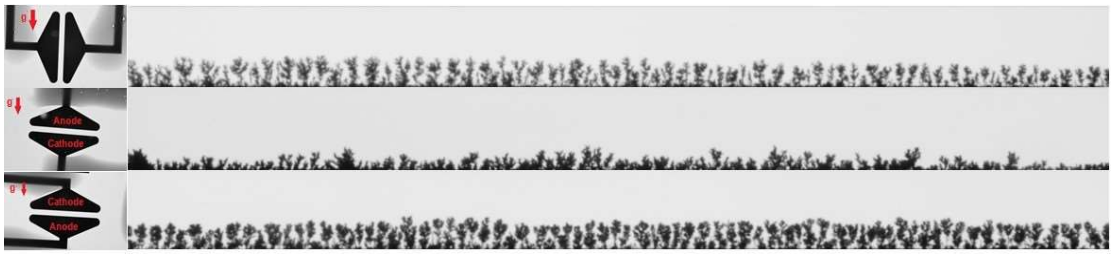

Figure 1 Effect of direction of the gravity on the developed patterns for ΔV=1.5V and an electrode spacing of 250µm.

Experimental Study on Micro Droplet Formation and Electrohydrodynamic Instability of Three Immiscible Liquids Flowing in a Microchannel

Eda N. Soysal[1] and A. Kerem Uguz[2]

[1]Department of Chemical Engineering, Bogazici University,
34342, Istanbul, Turkey eda.n.soysal@gmail.com
[2]Department of Chemical Engineering, Bogazici University,
34342, Istanbul, Turkey kerem.uguz@boun.edu.tr

Applying an electric field to the interface between immiscible liquids flowing in a microchannel is known to be an active method to generate monodispersed-sized micro droplets [1, 2, 4]. However, with this method, it is observed that it is not possible to switch the droplet and continuous phases. Eribol et al. [3] determined numerically that when a liquid is sandwiched between another immiscible liquid, it is possible to switch the droplet phase by manipulating the depth ratios of the liquids, i.e., the volumetric flow rates. The aim of this work is to test the results outlined in [3]. For that purpose, a liquid, surrounded by another immiscible liquid, will be pumped into the microchannel. A DC electric field will be applied in the normal direction to the flat interfaces between the liquids. The stability of the interfaces and the droplet formation as a function of various practical parameters such as the applied voltage, the volumetric flow rates, and the viscosities of the liquids will be investigated. The experiments will be compared to the numerical results [3].

[1] Altundemir, S., (2017), Experimental study on the electrohydrodynamic instability between two immiscible liquids flowing in a microchannel, Master Thesis, Boğaziçi University.
[2] Altundemir S, Eribol P, Uguz A (2018) Droplet formation and its mechanism in a microchannel in the presence of an electric field. Fluid Dyn Res 50:051404
[3] Eribol P., Kaykanat S., Ozan S. C., Uğuz, K., (2022), Electrohydrodynamic instability between three immiscible fluids in a microchannel: lubrication analysis. Microfluidics and Nanofluidics. 26.
[4] O. Ozen, N. Aubry, D.T. Papageorgiou, and P.G. Petropoulos (2006), Monodisperse drop formation in square microchannels, Phys. Rev. Lett. 96, 144501

Interfacial hydrodynamics of coaxial electrospray

Raj Agarwal[1] and Pradipta Kumar Panigrahi[2]

[1] *Department of Mechanical Engineering, I.I.T. Kanpur, Kanpur-208016, U.P., India,* rajagrwl@iitk.ac.in
[2] *Department of Mechanical Engineering, I.I.T. Kanpur, Kanpur-208016, U.P., India,* panig@iitk.ac.in

ABSTRACT

Coaxial electrospray is an efficient method for the generation of capsules for drug delivery and the manufacturing of several other products. The present study is aimed at understanding the effect of various interfacial forces on cone-jet generated from a coaxial nozzle in the presence of electric field. Coaxial jet formation (FIG. 1a.) under electric field is a consequence of equilibrium between mechanical and electrical forces. These forces are primarily interfacial in nature. As opposed to single nozzle electrospray, coaxial electrospray is not well understood in terms of its regimes and interplay between various non-dimensional parameters arising out of geometry, flow properties, electrical properties, actuation voltage. Existing numerical models for coaxial jets deal with steady state assumptions and has not yet showcased the effect of electrical properties on the interfacial space charge density distribution, surface tension distribution, electrical body force distribution which in turn are responsible for various stable regimes observed experimentally in coaxial electrospray [1]. The stability of a coaxial electrospray process can be attributed to the pressure variation in the flow field, which is difficult to obtain experimentally. Thus, we resort to numerical studies for understanding the pressure variations, which, as per our knowledge, are being discussed for the first time in literature. In the present work attempt has been made to understand the tradeoff between various EHD forces, specifically at the interfaces. This understanding will allow better controllability of the encapsulated drops in terms of shell fluid thickness, dripping frequency. This work will demonstrate the capability of coaxial electrospray in efficient generation of encapsulated droplets by the control of electrical properties and actuation potential.

Flow of three fluids is involved in the coaxial electrospray, which necessitates the use of Cahn-Hilliard equations for numerically tracking the two interfaces. The finite element-based commercial software 'COMSOL Multiphysics 6.0' is used for the simulation studies. The formulated methodology has been validated extensively with existing literature. Firstly, the deformation of a leaky dielectric droplet into an oblate shape in the presence of electric field is studied. The deformation is confirmed with the numerical study [2] and theoretic study [3]. Further, pinch-off phenomenon of glycerin in air is studied in the absence of electric field. The diameter of the droplet is found to be the same as reported in the numerical study [4] and the experimental study [5]. Additionally, the dripping to jetting transition is studied for the various Ohnesorge numbers and Weber numbers, which represent the dominance of viscous force and inertia force, respectively. The effect of the electric field on the pinch-off process is studied for validation of the EHD methodology. Additionally, space charge density distribution, electric field distribution, and electric body force distribution are analysed in the dripping and jetting regimes. The aforementioned analysis enabled us to understand the importance of model selection (dielectric/ leaky dielectric) for fluid and its coupling with corresponding interface tracking and the momentum equations. To understand the underlying fundamental difference between two-phase flow simulation (single nozzle) and three-phase flow simulation (coaxial nozzle), a compound droplet is considered in an electric field. A compound droplet is suspended in silicone oil, and the deformation behaviour is studied. Several regimes have been identified, differing in terms of flow circulation, space charge density distribution, and nature of deformation. These regimes are a function of viscosity ratio, density ratio, electrical conductivity ratio, and permittivity ratio [6].

Attempt has been made to capture the drop encapsulation process from a coaxial jet numerically (FIG. 1b.). Alternating space charge density patterns have been observed for the first time numerically at both the liquid interfaces in a coaxial jet (FIG. 2.). Due to the application of high potential the pinch-off of the encapsulated droplet from the jet is suppressed and is tested for several electrical property combinations (FIG. 3.). At low applied potential the magnitude of electrical body forces are two orders of magnitude less and pinch-off occurs due to the dominance of surface tension forces (FIG. 4.). These results have been obtained using dielectric model for the fluids. Detailed parametric study using leaky-dielectric model is under consideration focusing on practical fluids in order to thoroughly understand the coaxial electrospray phenomena.

[1] Gupta, Archana, and P. K. Panigrahi. "Alternating current coaxial electrospray for micro-encapsulation." *Experiments in Fluids* 61.2 (2020): 1-22.
[2] Lin, Yuan. "Two-phase electro-hydrodynamic flow modeling by a conservative level set model." *Electrophoresis* 34.5 (2013): 736-744.
[3] Taylor, Geoffrey Ingram. "The circulation produced in a drop by an electric field." *Proceedings of the Royal Society of London. Series A. Mathematical and Physical Sciences* 291.1425 (1966): 159-166.
[4] Borthakur, Manash Pratim, Gautam Biswas, and Dipankar Bandyopadhyay. "Formation of liquid drops at an orifice and dynamics of pinch-off in liquid jets." *Physical Review E* 96.1 (2017): 013115.
[5] Subramani, Hariprasad J., et al. "Simplicity and complexity in a dripping faucet." *Physics of fluids* 18.3 (2006): 032106.
[6] Behjatian, Ali, and Asghar Esmaeeli. "Electrohydrodynamics of a compound drop." *Physical Review E* 88.3 (2013): 033012.

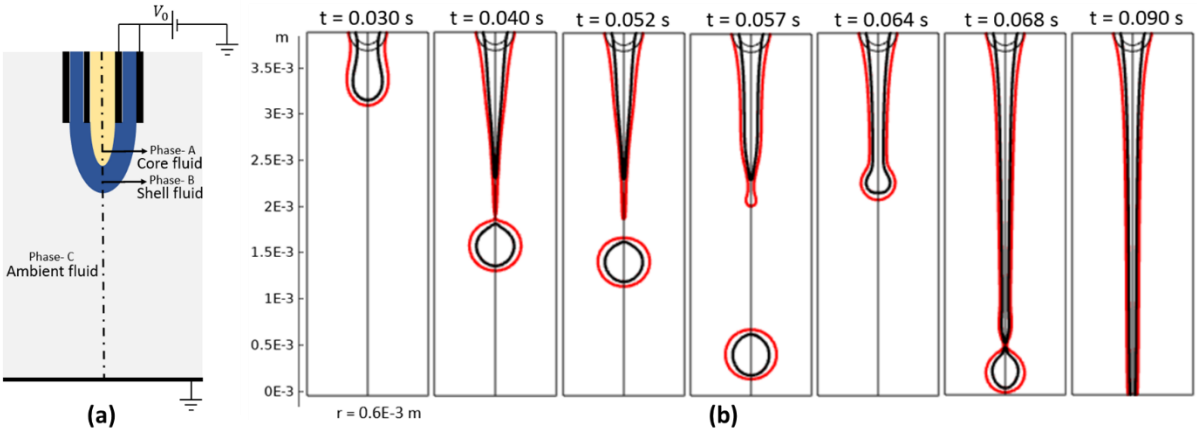

FIG. 1. (a) Schematic of Coaxial Electrospray. (b) Inertia driven encapsulation: Coaxial pinch-off process of Water (core fluid), Tributyl Phosphate (shell fluid) system at low potential (~ 100 V). Black contours correspond to the core-shell interface and red contours correspond to the shell-air interface.

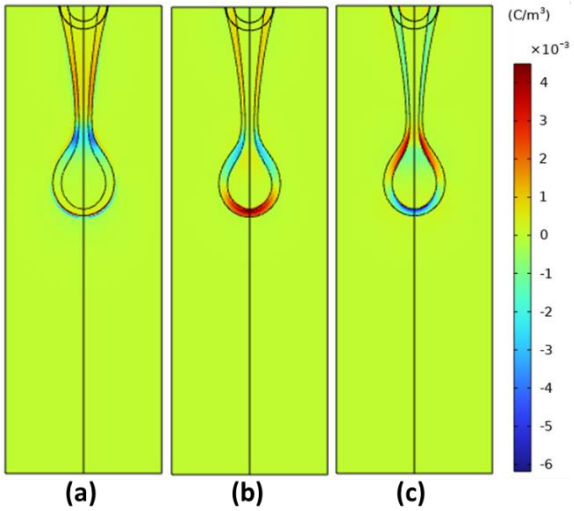

FIG. 2. Regimes in coaxial electrospray based on permittivity ratios of the fluids (10 V).
(a) $\epsilon_{ambient} = 1,\ \epsilon_{core} = 40,\ \epsilon_{shell} = 80.$
(b). $\epsilon_{ambient} = 60,\ \epsilon_{core} = 40,\ \epsilon_{shell} = 80.$
(c). $\epsilon_{ambient} = 60,\ \epsilon_{core} = 80,\ \epsilon_{shell} = 40.$

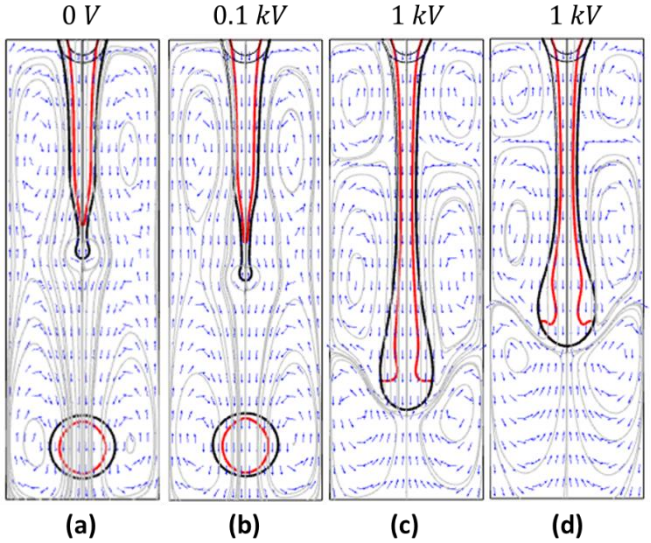

FIG. 3. Influence of applied potential, di-electric constant on the encapsulation and the jet formation process. Contours represent the interfaces. Normalized velocity vector fields are represented along with streamlines.
$\epsilon_{ambient} = 1,\ \epsilon_{shell} = 20,\ \epsilon_{core} = 10$ for (a), (b), (c).
$\epsilon_{ambient} = 1,\ \epsilon_{shell} = 10,\ \epsilon_{core} = 20$ for (d).

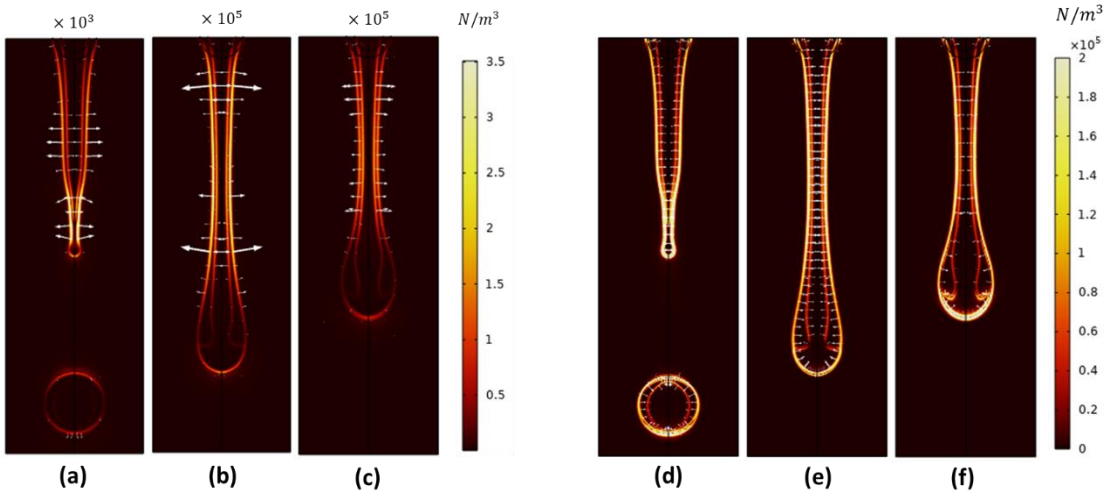

FIG. 4. (a) - (c) Variation of magnitude of electrical body forces with respect to change in applied potential, dielectric constant. (d) - (f) Variation of magnitude of surface tension forces with respect to change in applied potential, dielectric constant. (a), (d) $\epsilon_{ambient} = 1,\ \epsilon_{shell} = 20,\ \epsilon_{core} = 10; \mathrm{V_{applied}} = 100\ V$. (b), (e) $\epsilon_{ambient} = 1,\ \epsilon_{shell} = 20,\ \epsilon_{core} = 10; \mathrm{V_{applied}} = 1000\ V$. (c), (f) $\epsilon_{ambient} = 1,\ \epsilon_{shell} = 10,\ \epsilon_{core} = 20; \mathrm{V_{applied}} = 1000\ V$.

Electrostatically Forced Faraday Instability in Microgravity

Jason Livesay[1] and Ranga Narayanan[2]

[1] *Department of Chemical Engineering, UF, Gainesville, Florida, United States* livesayj@ufl.edu
[2] *Department of Chemical Engineering, UF, Gainesville, Florida, United States*, Ranga@ufl.edu

This talk presents a possible technique to measure interfacial tension and viscosity using electrostatic induced resonance of fluid bilayers. Here, AC electrostatic fields are imposed across a bi-layer of fluids and interfacial patterns are excited as a signal of resonance-induced instability. The idea is to determine the critical voltage and patterns at the resonant state and then correlate this to interfacial tension and viscosity via theoretical models. The presented work addresses two hypotheses. First, electrostatic forced oscillations of an interface between two fluids result in resonant conditions. Second, a reduced gravity environment reduces the critical voltage allowing for excitation of higher order modes increasing the possibility for self-benchmarking capability and isolating the effects of interfacial tension. Ground and reduced gravity experiments will be shown for a model two-fluid system clearly showing patterns at the onset and the reduced voltage at microgravity. The comparison of ground and flight data will be presented along with key plans for extending to liquid metals.

Acknowledgement: NASA 80NSSC 21K0352 and NSF 2025117. Robert Singiser and Zachary Karpinski for their contribution to experimentation during parabolic flight campaigns.

Marangoni stress-driven morphological instability in porous anodic oxides

Sajal Wankhede[1] and Dipin S. Pillai[2]

[1] *Department of Chemical Engineering, IIT Kanpur, 208016, Kanpur, India,* wankhede@iitk.ac.in

[2] *Department of Chemical Engineering, IIT Kanpur, 208016, Kanpur, India,* dipinsp@iitk.ac.in

ABSTRACT

Spontaneous formation of nanoscale pores in an oxide film growing at a metal-electrolyte interface during anodization has been observed for several metals such as aluminium, titanium, and tin. Under specific operating conditions, these films evolve into a well-ordered hexagonally array of parallel cylindrical pores with submicron diameters. In this work, we investigate the weakly non-linear behaviour of Marangoni stress-driven growth mechanism of porous anodic films. The study extends the results of Houser and Hebert's [1] model to the weakly nonlinear regime, which incorporates electrical migration and viscous flow contributions for the transport of metal and oxygen ions in the anodic oxide film. The flow is induced due to non-uniform compressive stresses at the oxide-solution interface that results from differential rates of anion adsorption at surface growth sites. Linear stability analysis suggests that the instability results from a competition between the destabilizing flow of oxide and stabilizing oxide formation, resulting in a wavelength selection that determines the inter-pore distance. This anodic instability is analogous to the classical Marangoni instability driven by gradients in surface tension at a fluid interface. The results of the weakly nonlinear analysis reveal that the solutions emerging from the critical state are supercritical at all wavenumbers (FIG.1) for the entire range of investigated control parameters.

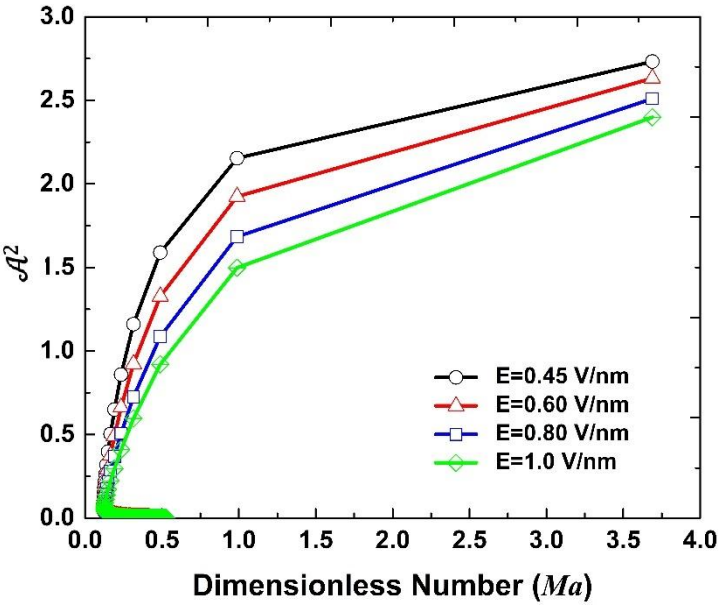

FIG. 1 $\mathcal{A}^2$ vs. effective Marangoni number (*Ma*) for different value of electric field E, obtained from weakly nonlinear analysis.

REFERENCES

[1] J. E. Houser and K. R. Hebert, "The role of viscous flow of oxide in the growth of self-ordered porous anodic alumina films," *Nat Mater*, vol. 8, no. 5, pp. 415–420(2009)

Session 8 – Waves

Wednesday June 21, 11:00–12:30

Wave breaking: spilling versus plunging

Ratul Dasgupta and Vinod Kadari

Department of Chemical Engineering, IIT Bombay, Powai, Mumbai, Maharashtra 400076, India

Breaking of wind generated surface waves causes entrainment of air into the upper layer of the ocean **[1]**. A typical cylinder-shaped entrained air column trapped beneath the free surface of a breaking wave, breaks rapidly into smaller parcels as a result of the unsteady (and often turbulent) flow around it, as well as due to the Rayleigh-Plateau instability, generating a spectrum of air bubbles of various sizes **[2]**. The splash generated due to breaking as well as the accompanying bursting of the rising bubbles at the air-water interface, causes ejection of water droplets into air leading to the formation of sea-salt aerosols in the atmosphere **[1]**. One broadly distinguishes between two qualitatively distinct kinds of wave breaking viz. spilling breaking involving instabilities of the wave crest and plunging breaking **[4]** where the entire wave is unstable. In this study, we study the bubble entrainment and droplet production due to this complex multiphase process initiated from a finite amplitude Stokes wave. The stability analysis by **[3]** of a Stokes wave to super-harmonic perturbations, provide a critical steepness of the Stokes wave beyond which it is linearly unstable. We generate spilling and plunging breaking by varying the steepness ε of the Stokes wave in our numerical simulations.

In figure 1, results from Direct Numerical Simulations (DNS) of two-phase 3-D breaking Stokes wave are shown, using the open source code Basilisk **[5]**. We simulate a Stokes wave with primary wavelength 24 cm, Bond number Bo = 200, Reynolds number Re = 40000, density ratio = 1/850 and viscosity ratio= 1.96e-2. The initial condition is taken to be a finite depth Stokes wave correct up to third order in the steepness parameter ε. In figure 1(a) and 1(b), we depict plunging breaking (ε=0.55) and spilling breaking (ε=0.4). It may be seen that plunging breaking is a more energetic event compared to spilling breaking. Notably plunging breaking occurs at an earlier non-dimensional time compared to spilling breaking (note that the Stokes wave is a nonlinear travelling wave whose time period depends on the primary wavelength as well as its amplitude). In figure 1(c), we show total energy dissipation as function of time for plunging breaking, benchmarking our results with that of **[6]**. For comparison, we also show the energy evolution as function of time for spilling breaking, depicting a clear difference between the two. In figure 1(d), total number of bubbles produced by both plunging (red curve) versus spilling wave breaking (black curve) is depicted as function of time. Expectedly, it is seen that plunging breaking produces many more bubbles compared to spilling breaking. In fig. 1(e), we show the total number of droplets produced by plunging and spilling breaking as a function of time. This figure makes it clear that plunging breaking also produces a larger number of droplets compared to spilling breaking. This is mainly due to production of a greater number of bubbles. Fig. 1(f) visualizes the bubbles generated as a result of plunging breaking. The detailed physics of these processes will be discussed at the meeting.

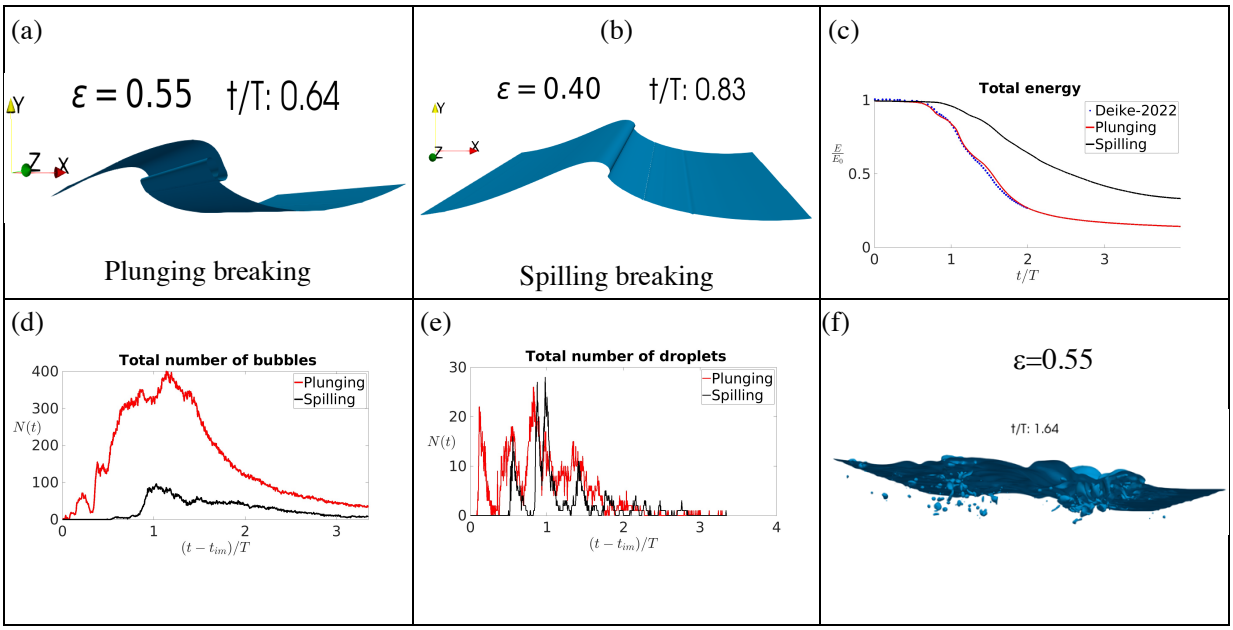

REFERENCES

1. Veron, Fabrice. "Ocean spray." Annual Review of Fluid Mechanics 47 (2015): 507-538.

2. Gao, Q., Deane, G. B., & Shen, L. (2021). Bubble production by air filament and cavity breakup in plunging breaking wave crests. *Journal of Fluid Mechanics*, *929*, A44.

3. Longuet-Higgins, Michael Selwyn. "The instabilities of gravity waves of finite amplitude in deep water I. Superharmonics." Proceedings of the Royal Society of London. A. Mathematical and Physical Sciences 360.1703 (1978): 471-488.

4. Longuet-Higgins, M. S. "Progress toward understanding how waves break." *21st Symposium on Naval Hydrodynamics*. Vol. 7. National Academic, Trondheim, Norway, 1997.

5. http://basilisk.fr

6. Mostert, W., Popinet, S., & Deike, L. (2022). High-resolution direct simulation of deep water breaking waves: transition to turbulence, bubbles and droplets production. *Journal of Fluid Mechanics*, *942*, A27.

Acknowledgements

Financial support from DST-SERB, Govt. India grants #CRG/2020/003707, #SPR/2021/000536 and #MTR/2019/001240 are gratefully acknowledged. The Ph.D. fellowship of V.K. is supported by a grant from Ansys, Inc. and is gratefully acknowledged.

Wave focusing and jet formation in pure capillary and pure gravity waves

Lohit Kayal [1] and Ratul Dasgupta[2]

[1] *Department of Chemical Engineering, IIT Bombay, India* kayal.lohit@gmail.com

Summary: We study the mechanism of jet formation from large amplitude, pure capillary and pure gravity waves, in the inviscid limit. The study is motivated by observations of such jets from a bursting bubble [1], spray formation in ultrasonic atomization [2] and at much larger scales, axisymmetric `spike' waves [3]. In recent analysis [4,5], we have studied this theoretically and demonstrated that such jets are also obtained by exciting an eigenmode at t=0 (Bessel function in radial geometry). It is known that these jets form due to the focusing of waves at the axis of symmetry. We observe this wave focusing in pure capillary (small scales) as well as pure gravity waves (large scales) for modal initial conditions. This initial condition allows us to solve the initial value problem (IVP) up to quadratic and cubic order in the small parameter (initial wave steepness ϵ). We find very good agreement between theory and numerical simulations in the weakly nonlinear regime. In the strongly nonlinear regime and for pure gravity waves, we compare our numerical results with the theory of Longuet-Higgins [7] also finding good agreement [6].

I. Jets and wave focusing (pure capillary waves)

Jet formation from a bursting bubble has long been known and studied [1]. A bursting bubble at low Bond number, Bo << 1 produces a sharply shooting jet, but has a highly deformed shape, not amenable to modal analysis. In recent studies [4,5], we surmount this restriction by showing that a modal initial condition can also generate similar jets. Due to this choice of initial condition, the problem becomes accessible to modal analysis beyond linear order. Using the Lindstedt-Poincare perturbation technique (method of stretched coordinates) we solve the IVP up to third order in the small parameter ϵ for a single eigenmode excited initially. This analytical solution is able to capture the inception of a dimple, the precursor to the jet, at moderate ϵ. We show using numerical simulations (*basilisk.fr*) that when $\epsilon \gg 1$ a sharp shooting jet develops from an initially perturbed axisymmetric Bessel mode $\hat{\eta} = \hat{a}_0 J_0\left(\frac{\hat{l}_q}{\hat{R}_0}\hat{r}\right)$, where $\hat{\eta}, \hat{a}_0, \hat{l}_q, \hat{R}_0$ are interface, initial amplitude, q^{th} nontrivial root of $J_1(*)$ and radius of the domain respectively. $\epsilon = \frac{\hat{a}_0 \hat{l}_q}{\hat{R}_0}$ is the measure of initial nonlinearity. Fig.1 shows the process of wave focusing generated from a single mode in a cylindrical domain of size 0.4 cm. As seen, two humps (sky blue) approach against each other indicated by red arrows and as a result a jet (pink) emerges at the symmetry axis. As reference, in the lower panel we show how wave focusing gives birth to a similar jet from a bursting bubble (Fig. 2).

FIG. 1. Wave focusing and jet formation in Bessel mode ($\epsilon = 2.3$)

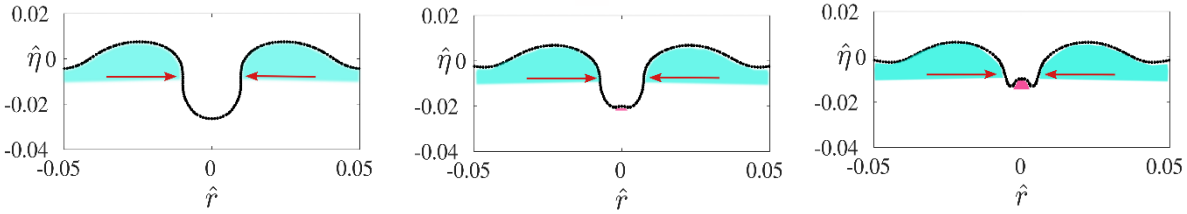

FIG. 2. Wave focusing and jet formation from a bubble ($Bo = 0.001$)

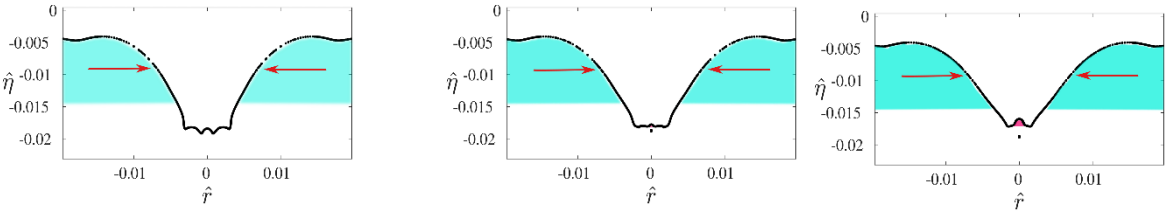

II. Jets and wave focusing (pure gravity waves)

Analogous to the previous section, we now consider waves at larger length scales. Consider a radial domain of radius $\hat{R}_0 = 600\ cm$ (>>> the pure capillary case treated earlier). Like before, an axisymmetric Bessel mode is excited at t=0 and we ask if a jet may also be observed here, when the modal initial amplitude is large. Fig 3 shows that the answer is in the affirmative, depicting the formation of a sharply shooting jet for $\epsilon = 1.6,\ l_{35} = 110.74$.

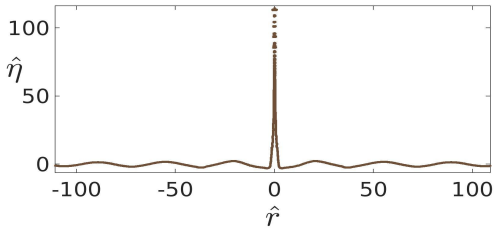

Fig 3. Jet formation for $\epsilon = 1.6,\ l_{35}$

We use the multiple scale method to solve the weakly nonlinear initial value problem for pure surface gravity wave. Solution up to $O(\epsilon^2)$ is indicated below in non-dimensional form [**6**],

$$\eta(r, T_0, T_2) = \epsilon\eta_1(r, T_0, T_2) + \epsilon^2\eta_2(r, T_0, T_2) + O(\epsilon^3) \quad , \text{ Here } T_0 \equiv t,\ T_2 \equiv \epsilon^2 t$$

$$\eta_1(r, T_0, T_2) = \left[a_{1p}(T_2)\sin T_0 - b_{1p}(T_2)\cos T_0\right] J_0(r)$$

$$\eta_2(r, T_0, T_2) = \sum_{j=1}^{\infty}\left[\zeta^1_{j,q}\cos(\omega_{j,q}T_0) + \zeta^2_{j,q}(T_2)\cos(2T_0) + \zeta^3_{j,q}(T_2)\sin(2T_0) + \zeta^4_{j,q}(T_2)\right] J_0(\alpha_{j,q}r)$$

$$\text{Where } \zeta^2_{j,q}, \zeta^3_{j,q}, \zeta^4_{j,q} \equiv f^{2,3,4}\left(a_{1p}(T_2), b_{1p}(T_2)\right)$$

Fig 4 shows the comparison of linear theory, weakly nonlinear theory and simulation at different time instants. Fig 4d shows the overshoot , the z=1 line is shown in pink dashes (max. initial height), and our weakly nonlinear theory can capture this quite well. Comparisons with the theory of Longuet-Higgins [7] will be presented at the meeting.

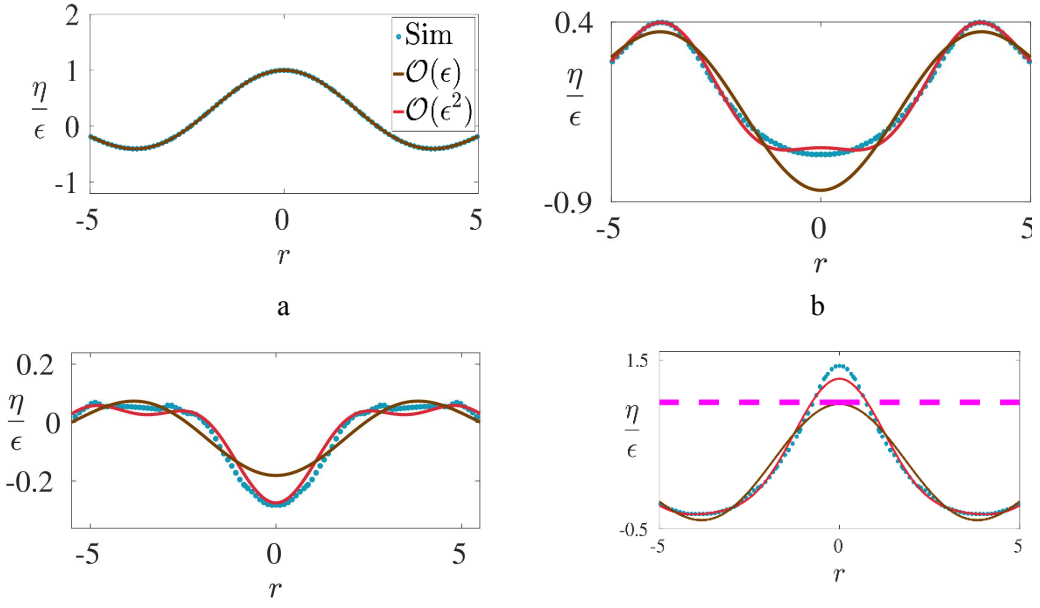

Fig 4. Comparison with simulation at various instants for $\epsilon = 0.5,\ l_{35}$

III. REFERENCES

[1] D. C. Blanchard. The electrification of the atmosphere by particles from bubbles in the sea. Progress in oceanography, 1:73–202, 1963
[2] Rajan, Raghavachari, and Aniruddha B. Pandit. "Correlations to predict droplet size in ultrasonic atomisation." Ultrasonics 39.4 (2001): 235-255.
[3] McAllister, M. L., et al. "Wave breaking and jet formation on axisymmetric surface gravity waves." Journal of Fluid Mechanics 935 (2022): A5.
[4]. Kayal, L., Basak, S., & Dasgupta, R. (2022). Dimples, jets and self-similarity in nonlinear capillary waves. Journal of Fluid Mechanics, 951, A26.
[5] Basak, Saswata, Palas Kumar Farsoiya, and Ratul Dasgupta. "Jetting in finite-amplitude, free, capillary-gravity waves." Journal of Fluid Mechanics 909 (2021): A3.
[6] Jet from a large surface gravity wave (To be submitted), Lohit Kayal & Ratul Dasgupta, 2023.
[7] Longuet-Higgins, M. (1983). Bubbles, breaking waves and hyperbolic jets at a free surface. Journal of Fluid Mechanics, 127, 103-121. doi:10.1017/S0022112083002645

IV. Acknowledgements

- We thank Dr. Vatsal Sanjay (University of Twente) for his help to generate the bubble shape.
- Financial support from DST-SERB grants CRG/2020/003707 and EMR/2016/000830 and IRCC (IIT Bombay) are gratefully acknowledged. L.K. acknowledges support from the Prime Minister's Research Fellowship (PMRF), Government of India.

The ThermoSlosh experiment: “Thermocapillary-based control of a free surface in microgravity”

U. Martínez, D. Gligor, I. Torres, J. Plaza, P. Salgado Sánchez, J. M. Ezquerro and J. Porter

E-USOC, Center for Computational Simulation, Escuela Técnica Superior de Ingeniería Aeronáutica y del Espacio, Universidad Politécnica de Madrid, Madrid, Spain. pablo.salgado@upm.es

Current as well as future challenges of space exploration require improved fluid management strategies. The “Thermocapillary-based control of a free surface in microgravity” (ThermoSlosh) experiment [1] aims to investigate the effectiveness of thermal forcing for controlling fluids in reduced gravity. The experiment proposes to analyze the dynamics of a free surface in a cylindrical cell, half filled with a low-viscosity silicone oil [2] and subjected to controlled temperatures and accelerations (see the left panel of Fig. 1). Results from a two-dimensional numerical model (see the right panel of Fig. 1) suggest that the thermocapillary effect can be used in microgravity to control the orientation of the free surface within the cell. We first analyze the free surface response to a steady applied thermal gradient, which can be effectively characterized using the rise and stabilization times and the overshoot; these quantities also help evaluate the effectiveness of the applied thermal forcing. In addition, the use of supplemental vibrations of amplitude A and frequency ω is investigated and shown to improve the overall performance of the thermal control, notably increasing the responsiveness of the system. We then extend the analysis to include classical feedback control. The strategy is evaluated in different scenarios of relevance for space science. In particular, the ability of thermocapillary-based control to reduce sloshing motion during the scenario of a real ISS re-boosting maneuver [3] is assessed.

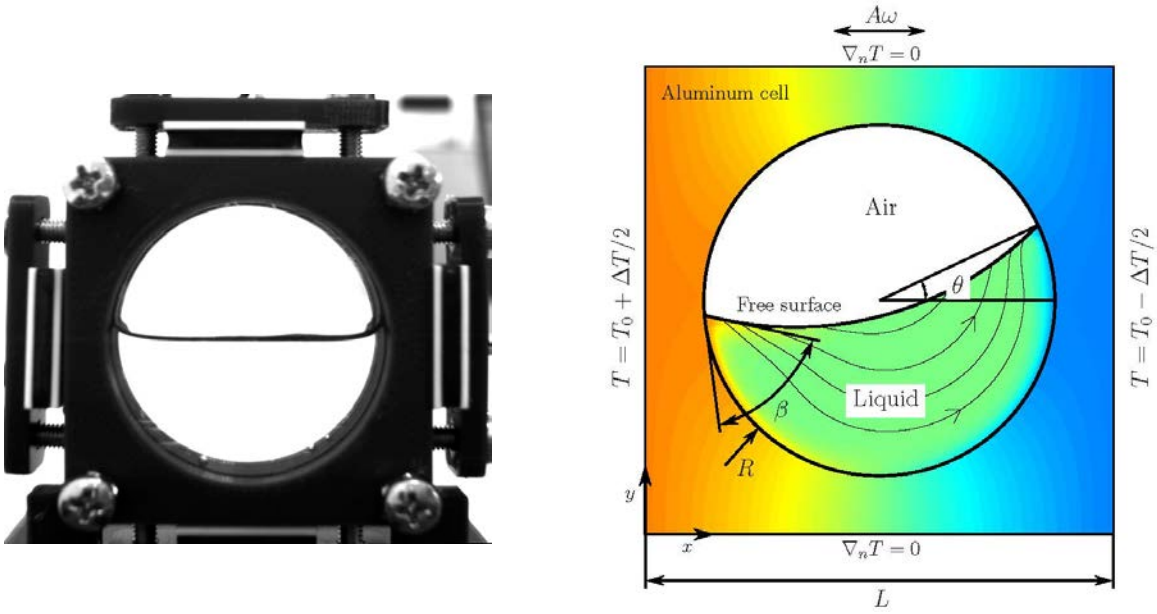

FIG. 1. Left: Snapshot of the experiment cell prototype showing the free surface position on ground. Right: Sketch of the set-up of the two-dimensional numerical model.

[1] P. Salgado Sánchez, U. Martínez, D. Gligor, I. Torres, J. Plaza, and J. M. Ezquerro. The “Thermocapillary-based control of a free surface in microgravity” experiment. Submitted to *Acta Astronautica*, under review.

[2] D. Gligor, P. Salgado Sánchez, J. Porter, and I. Tinao. Thermocapillary-driven dynamics of a free surface in microgravity: response to steady and oscillatory thermal excitation. *Physics of Fluids* **34**, 042116 (2022).

[3] D. Gligor, P. Salgado Sánchez, J. Porter, and J. M. Ezquerro. Thermocapillary-driven dynamics of a free surface in microgravity: control of sloshing. *Physics of Fluids* **34**, 072109 (2022).

Resonant surface waves in an oscillating periodic tank with a submerged hill

Franz-Theo Schön,[1] Uwe Harlander,[1] Ion Dan Borcia,[2]
Rodica Borcia,[2] Sebastian Richter,[2] and Michael Bestehorn[2]

[1]*Department of Fluid Mechanics, BTU, 03046, Cottbus, Germany*
[2]*Department of Theoretical Physics, BTU, 03046, Cottbus, Germany*

Sloshing of fluid layers is a well known research topic in fluid dynamics. The phenomenon has applications in engineering, geophysics, biology and microfluidics. Experimental studies are often done in rectangular tanks with fixed boundaries. In the present project, a 4.76 m long circular channel is used. This geometry allows experiments with periodic boundaries. Sloshing waves are excited due to a submerged hill and a harmonic oscillation of the tank. Experimental measurements are made with 18 ultrasonic probes, evenly distributed over the channel to track the wave propagation. For comparison, the authors developed a 2D numerical solution using the Karman-Pohlhausen approach.

The mountain sloshing gives a highly complex wave field. Different wave types like solitary waves, undular bores and standing waves are observed. The wave amplitudes show resonance peaks around certain eigenfrequencies, which fit with linear sloshing theory. Resonant reflection and transmission of solitary waves by the hill is observed. This represents a remarkable difference from fixed boundary sloshing experiments, where only reflecting wave resonance is possible. The experiments are of interest for tidal flows over bottom topography. In the future we plan an extension of the experiment using a stratified fluid in view of oceanic application.

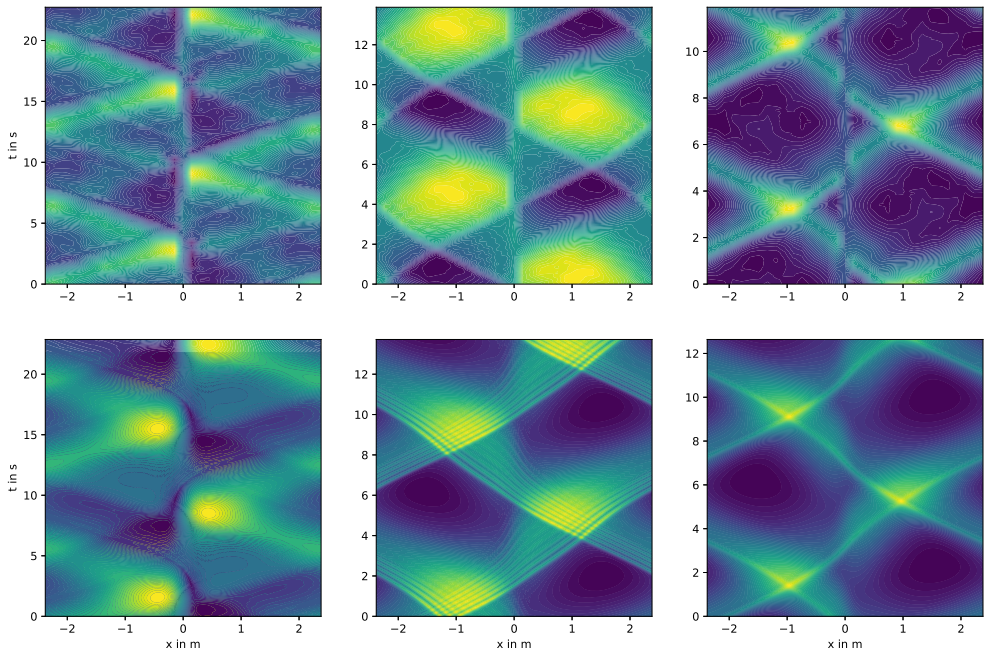

FIG. 1: Hovmöller diagrams of surface waves over an submerged hill. A comperison between experiment (top) and numerics (bottom). Excitation frequency increase from left to the right. The hill is half as high as the surface and is located at $x = 0\ m$. Left: reflected waves. Middle: undular bore. Right: transmitted waves.

Temporal and spatial ratchet for surface waves in a circular channel

Ion Dan Borcia,[1] Franz-Theo Schön,[2] Uwe Harlander,[2]
Sebastian Richter,[1] Rodica Borcia,[1] and Michael Bestehorn[1]

[1]*Institute of Physics, BTU, 03046, Cottbus, Germany* borciai@b-tu.de, bestehorn@b-tu.de, borciar@b-tu.de, sebastian.richter@b-tu.de

[2]*Department of Fluid Mechanics, BTU, 03044, Cottbus, Germany* haruwe@b-tu.de, shoefra@b-tu.de

We excite surface waves in a ring channel with the mean radius of 0.7575 m and 80 mm width. The ring is placed on a rotating table that can librate symmetrically (harmonic oscillation of the rotation velocity) or non-symmetrically (ratchet excitation) [1–3]. On the bottom of the periodic boundary channel we placed a symmetrical or non-symmetrical (ratchet shaped) mountain.

Two combination of the spatial/temporal setups are studied: symmetrical mountain with ratchet excitation and ratchet mountain with symmetrical excitation. We will compare the effects due to the temporal and spatial asymmetry. The resonance curve is firstly plotted. For frequency values close to the resonance bore like waves moving in one direction have much higher elevation (see Fig. 1). At these frequencies the transport effect is important and it will be studied in both experiment (using floating tracers and PIV) and simulation.

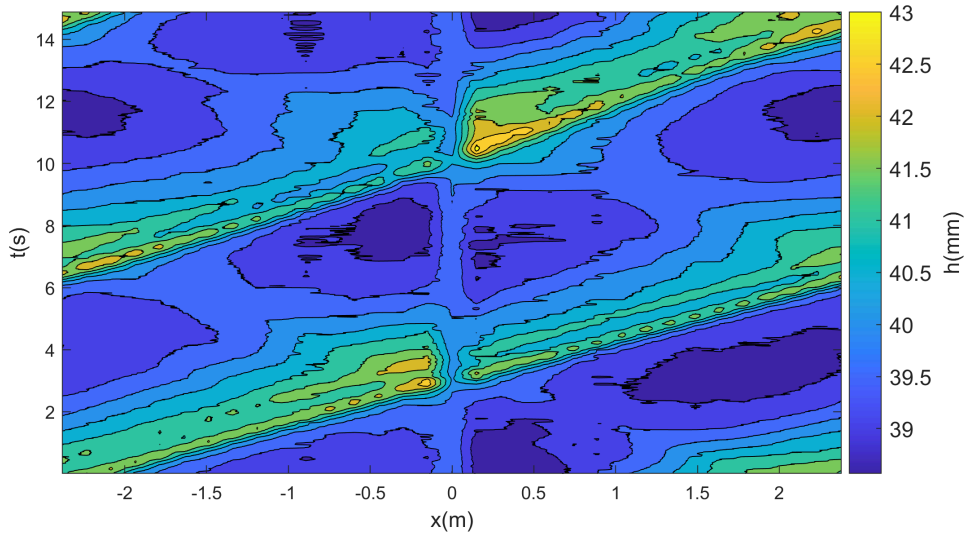

FIG. 1: Water surface elevation h for 20 mm height symmetrical mountain, 40 mm undisturbed water depth and ratchet excitation at f=0.07 Hz.

[1] I. D. Borcia, R. Borcia, W. Xu, M. Bestehorn, S. Richter, and U. Harlander, "Undular bores in a large circular channel," Eur. J. Mech. B Fluids **79**, 2020.

[2] I. D. Borcia, R. Borcia, S. Richter, W. Xu, M. Bestehorn, and U. Harlander, "Horizontal faraday instability in a circular channel", PAMM **19**, 2019.

[3] I. D. Borcia, S. Richter, R. Borcia, F.-T. Schön, U. Harlander, and M. Bestehorn, "Wave propagation in a circular channel - sloshing and resonance", Eur. Phys. J. Special Topics, accepted, 2023.

Mass transport in a horizontally vibrated thin fluid layer with a ratchet ground

M. Bestehorn[1], I. D. Borcia[1], R. Borcia[1], S. Richter[1], F.-T. Schön[2], U. Harlander[21]

[11] *Department of Theoretical Physics,* [2] *Department of Fluid Mechanics*
BTU Cottbus-Senftenberg, 03044 Cottbus, Germany

Applying longwave approximation, a reduced description for a thin liquid layer with a deformable surface including inertia effects was derived earlier [1]. The model is extended to the case of an arbitrarily shaped substrate (figure). If the fluid is periodically vibrated in horizontal direction, it turns out that an averaged mean flow either to the right or to the left side occurs, depending on the symmetry of the substrate and on the strength of excitation.

We show solutions for different shapes of the ground and several amplitudes below and above the critical ones where for a flat ground a surface instability emerges. It is interesting to note that a net flux only exists if inertia terms in the thin film equation are present.

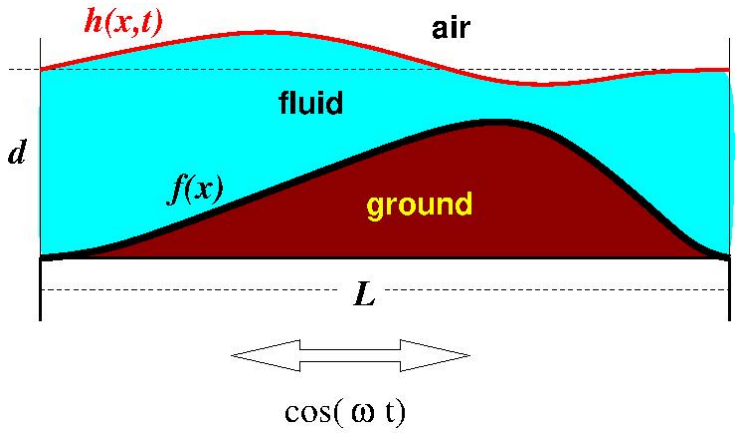

FIG. 1: Horizontally vibrated layer with mean depth d and variable ground $f(x)$. The local depth of the liquid is $\eta(x,t) = h(x,t) - f(x)$.

[1] M. Bestehorn, *Laterally extended thin liquid films with inertia under external vibrations*, Phys. Fluids 25, 114106 (2013)

Session 9 – Soap films

Wednesday June 21, 14:00–15:45

Horizontal soap film thinning: efficiency of Marangoni forces

Isabelle Cantat [1], A. Bussonnière[2] , A. Gros [1], T. Lenavetier [1], R. Poryles [4], C. Trégouët [5]

[1]Univ Rennes, CNRS, IPR (Institut de Physique de Rennes) – UMR 6251,
F – 35000 Rennes, France isabelle.cantat@univ-rennes1.fr

[2] *MSC, Paris, France*

[4] *Oniris, Nantes, France*

[5] *ESPCI, Paris, France*

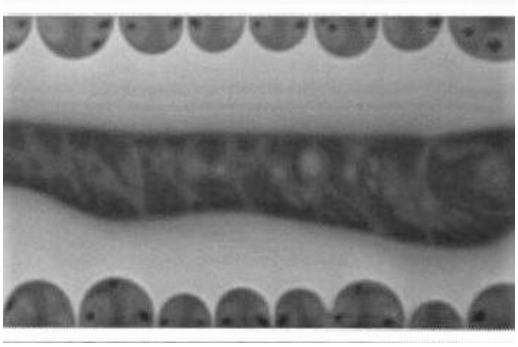

FIG. 1. Horizontal soap film, observed by fluorescence emission so that the brightness indicates the film thickness. Menisci at the top and bottom of the image (white stripes) re-adsorb the thickest part of the film (light grey domains) by capillary succion, by marginal regeneration.

The thinning of the liquid films separating bubbles in a foam or in a bubbly liquid controls the coalescence process and the foam stability, and is highly relevant in many industrial processes. The evolution of the film thickness is governed by highly nonlinear equations, whose solutions are still mostly unknown. For a flat horizontal film in contact with a meniscus at a lower pressure, a classical theoretical solution is the appearance, deepening and widening of a groove, close to the meniscus and invariant by translation along the meniscus.

We show experimentally that this theoretical film thickness profile is unstable, and we measure the instability wavelength along the meniscus [3]. This initial instability triggers the so called "marginal regeneration" [1,2]. This peculiar hydrodynamic instability is usually associated to the gravity and to the patches produced at the bottom of vertical soap films and slowly rising to the top [4,5]. Our experiment shows that it also occurs in a horizontal film and, as the gravity-induced rising motion of the patches is suppressed in this case, we are able to study its long times dynamics [6].

The marginal regeneration process is illustrated in the Figure 1. We first produce a domain of well controlled thickness by simply stretching the film and thus extracting some new pieces of film (light grey, thickness 3 microns) from the menisci (white stripes at the top and bottom of the Figure). When we stop stretching the film, the flow destabilises: thin film (the half-disk-shaped dark patches, thickness 300 nm) are extracted from the meniscus at slow velocity and the thick film flows into the meniscus, in the small channels between the spots.

[1] Mysels, Karol J., Stanley Frankel, and Kozo Shinoda. *Soap films: studies of their thinning and a bibliography*. Pergamon press, 1959.

[2] Bruinsma, R. "Theory of hydrodynamic convection in soap films." *Physica A: Statistical Mechanics and its Applications* 216.1-2 (1995): 59-76.

[3] Trégouët, C., and I. Cantat. "Instability of the one-dimensional thickness profile at the edge of a horizontal foam film and its Plateau border." *Physical Review Fluids* 6.11 (2021): 114005.

[4] Poulain, S., E. Villermaux, and L. Bourouiba. "Ageing and burst of surface bubbles." *Journal of fluid mechanics* 851 (2018): 636-671.

[5] Miguet, Jonas, et al. "Marginal regeneration-induced drainage of surface bubbles." *Physical Review Fluids* 6.10 (2021): L101601.

[6] Gros, A., A Bussonnière, S Nath, I Cantat, "Marginal regeneration in a horizontal film: Instability growth law in the nonlinear regime." *Physical Review Fluids* 6.2 (2021): 024004.

We show that this flow is controlled by strong surface tension gradients, associated to the high Gibbs elasticity of the films. We predict the patch growth with a simple model, that revisits and extends the initial interpretation of marginal regeneration proposed in [1].

The marginal regeneration instability observed here makes this drainage much more efficient than the Poiseuille flow drainage obtained in absence of flow destabilization.

Study of a pinch in the vicinity of a meniscus in a thin liquid film

Alice Etienne-Simonetti[1], Isabelle Cantat[2], Frédéric Restagno[1], Emmanuelle Rio[1]

[1] *Laboratoire de Physique des Solides, Orsay, France*
[2] *Institut de Physique de Rennes, Rennes, France*
alice.etienne-simonetti@universite-paris-saclay.fr

In a thin liquid film connected to a meniscus, the meniscus creates a capillary suction that generates a thinner zone where the meniscus connects to the film. This thin zone called “pinch” is the origin of the phenomenon of marginal regeneration (see Fig.1 Left) observed in the 1960s by Mysels in soap films [1]. It has been shown recently [2] that marginal regeneration is of major importance to describe the thinning of films over time. This thinning is in turn essential to predicting the lifetime of films therefore their stability.

We study the pinch dynamics in a horizontal film of silicone oil deposited on a solid surface by spin-coating. The meniscus is created by depositing a capillary tube vertically on the film. We measure the thickness of the film in the region of the pinch, perpendicular to the capillary, using a hyperspectral camera. We obtain thickness profiles along time, from which we can extract the pinch position (Fig.1 Right) and the pinch thickness and then compare them with the theoretical model of the pinch dynamics established by Aradian [3].

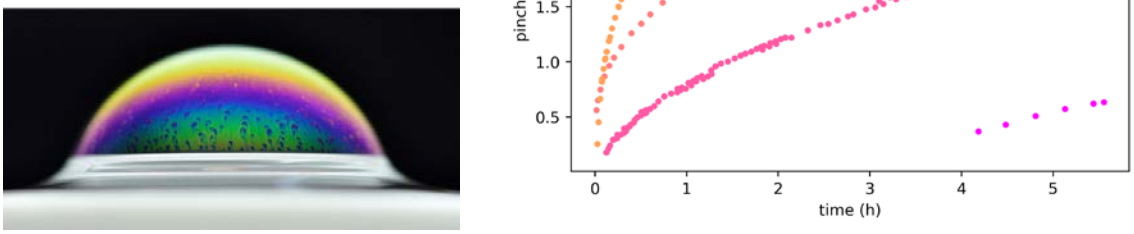

FIG. 1. Left: Photograph of a surface bubble illustrating marginal regeneration: thin circular patches rise while the rest of the thicker film falls [2]. Right: Position of the pinch for films of initial thickness 5 micrometers to 14 micrometers.

[1] K.J. Mysels, S. Frankel, K. Shinoda, *Soap films : studies of their thinning and a bibliography*, Pergamon press, (1959)

[2] J. Miguet, M. Pasquet, F. Rouyer, Y. Fang, E. Rio, Marginal regeneration-induced drainage of surface bubbles, Phys. Rev. Fluids **6**, L101601 (2021).

[3] A. Aradian, E. Raphaël, P.-G. de Gennes, “Marginal pinching” in soap films, Europhys. Lett. **55**, 834 (2001).

Soap film bursting: Is the flapping instability triggered by Marangoni flows?

Alexandre Guillemot[1], Juliette Pierre[1] and Adrien Bussonnière[2]

[1]*Institut ∂'Alembert, Sorbonne Université, CNRS UMR 7190, 75005 Paris, France, alexandre.guillemot@dalembert.upmc.fr*

[2] *Matière et Systèmes Complexes, Université Paris Cité, CNRS UMR 7057, 75013, Paris, France*

When a thin liquid film is punctured, a hole appears and grows at a well-defined speed called Taylor-Culick velocity, resulting from the balance between surface tension forces and inertia [1]. During the film bursting, the hole edge, called rim, starts flapping like a flag and the rim breaks into several droplets [2].

The triggering mechanism of the flapping instability (Kelvin-Helmotz like) remains unclear as a significant flow within the film is needed for its growth [3]. Indeed, the rim is moving at Taylor-Culick velocity, which is under the required speed to give rise to the instability. However, in soap film the rim is preceded by a Marangoni flow arising from the fast surfactant compaction at the interface (the film area decreases and vanishes in few ms) [4,5]. This flow is localized in a region called aureole where the surface tension decreases and the film thickens as shown in figure 1 (left) by the change in the color around the hole (curved stripes). To know if such Marangoni flows are fast enough to trigger the instability, a dedicated setup has been built to study the aureole.

We first create a vertical fluorescent soap film of 20 centimeters from the top to the lower meniscus and then puncture it. The entire thickness field is measured by the brightness of fluorescence emission with a high-speed camera during the opening, figure 1 (right). Combining the mass and momentum conservation equations and the thickness measurement, we can estimate the local flow and surface tension during the bursting.

In this talk, we will present if such rapid Marangoni flows can indeed trigger the flapping instability. Moreover, we foresee that this experimental setup will allow us to explore the rapid reorganization of surfactant and its dependency on surfactant concentration and types.

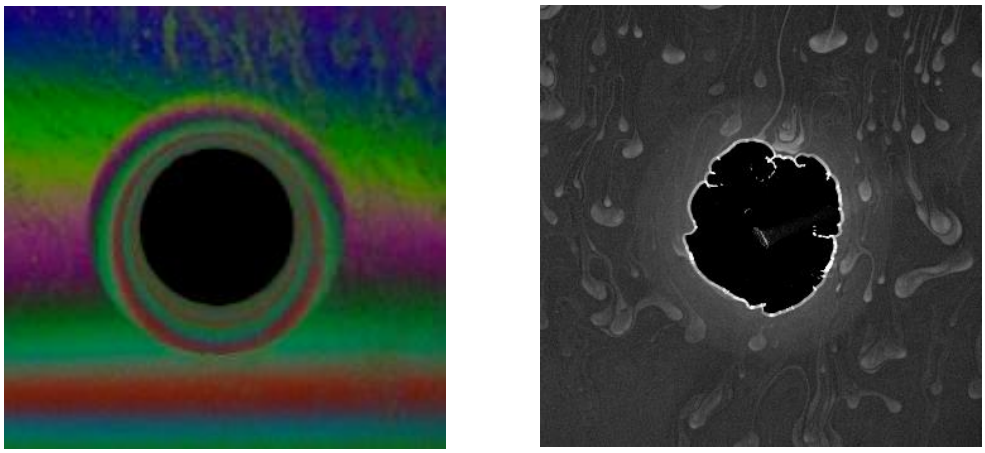

FIG. 1. Left: Vertical soap film observed during bursting. The color cycle is directly related to the thickness. The hole, in black, is surrounded by the aureole where the film is thicker; Right: Fluorescent soap film observed during bursting with a high-speed camera. The brightness indicates the thickness.

[1] F. E. C. Culick, Comments on a ruptured soap film, J. Appl. Phys. **31**, 1128 (1960)

[2] H. Lhuissier, E.Villermaux, Soap Films Burst Like Flappings Flags, Physical Review Letters **103**, 054501 (2009)

[3] H. B. Squire, Investigation of the instability of a moving liquid film, Br. J. Appl. Phys. **4**, 167, (1953)

[4] W. R. McEntee, K. J. Mysels, The Bursting of Soap Films. I. An Experimental Study, J. Phys. Chem., **73**, 3018 (1969)

[5] S. Frankel, K. J. Mysels, The Bursting of Soap Films. II. Theoretical Considerations, J. Phys. Chem., **73**, 3028 (1969)

Bursting of non-aqueous suspended liquid films induced by Marangoni-driven spreading of emulsified droplets

Léa Delance[1,2], Nicolas Passade-Boupat[2,3], Emilie Verneuil[1], François Lequeux[1,2] and Laurence Talini [4]

[1] *CNRS, SIMM, ESPCI Paris, PSL Research University, Sorbonne Université, Paris, France*
lea.delance@espci.fr
[2] *Laboratoire PIC, ESPCI, Paris, Bâtiment CHEMSTARTUP, Lacq, France*
[3] *Total Energies S.A., 64170 Lacq, France*
[4] *CNRS, SVI, Saint-Gobain, Aubervilliers, France*

Liquid mixtures can foam [1] owing the enhanced stability of the thin liquid films trapped between bubbles. As compared to pure liquids, this stability was recently ascribed to the difference in the molecules partition between the bulk and the film interfaces with air. This results in a thickness-dependent surface tension for liquid mixtures. Consequently, in foams, thickness gradients between the films and their edge translate into surface tension gradients that contribute to feed the films and impair their drainage. Hence, the lifetimes of thin suspended films and foams of liquid mixtures are larger than that of pure liquids.

As a practical consequence, industrial processes involving mixtures of non-aqueous liquids often face unwanted foaming issues. This problem is generally solved by adding anti-foaming agents, which are low-surface tension oils that are dispersed in the liquid as microdroplets. In the case of aqueous foams, the mechanisms responsible for the destabilization of the foam by these droplets have been extensively studied [2]. However, the effect of antifoaming agents on oil foams is still poorly understood [3].

We have shown previously [4] that Polydimethylsiloxane-rich (PDMS-rich) microdroplets dispersed in an oil mixture coalesce and spread at the air/liquid interface causing a decrease of surface tension. In this talk, I will present how these microdroplets induce the bursting of thin liquid oil films. Using a microfluidic set-up, we create suspended thin liquid films. Observing the films by interferometry allows for the measurement of the film thickness and reveals the presence of depressions (see FIG.1), whose thickness is about 50 nm, in a fraction of the films. Occurrence of these depressions correlates well with shorter lifetimes, demonstrating that the film bursting occurs earlier in the life of the film when a microdroplet is trapped in the film. Our results suggest that microdroplets spread at the film interface through a Marangoni effect which causes the film to thin down faster. The effect of PDMS viscosity on the destabilization of thin films is also studied.

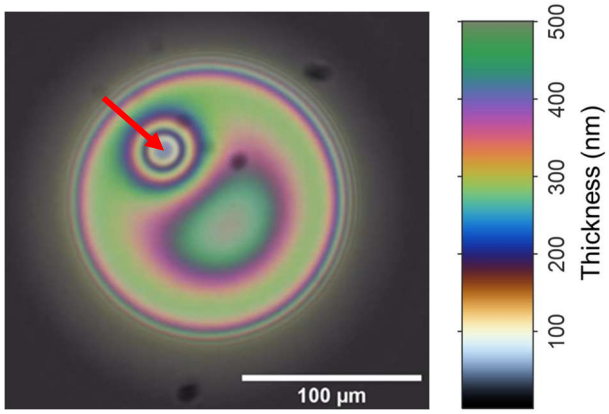

FIG.1. Observation of a liquid film by interferometry, allowing for the reconstruction of the thickness profile: a depression (arrow) appears in the film which bursts when the thickness at the depression center reaches 50nm.

[1] H.-P. Tran, M. Arangalage, L. Jørgensen, N. Passade-Boupat, F. Lequeux, and L. Talini, Understanding Frothing of Liquid Mixtures: A Surfactantlike Effect at the Origin of Enhanced Liquid Film Lifetimes, Phys. Rev. Lett., **125**, 178002 (2020).

[2] N. D. Denkov, Mechanisms of foam destruction by oil-based antifoams, Langmuir, **20**, 9463–9505, (2004).

[3] V. Chandran Suja, A. Kar, W. Cates, S. M. Remmert, and G. G. Fuller, Foam stability in filtered lubricants containing antifoams, Journal of Colloid and Interface Science, **567**, 1–9 (2020).

[4] L. Delance, C. Veillon, N. Passade-Boupat, F. Lequeux, L. Talini, and E. Verneuil, Uptake kinetics of spontaneously emulsified microdroplets at an air–liquid interface, Soft Matter, **18**, 5060–5066, (2022).

Dissipative processes in an elementary foam

Théo Lenavetier, Raphaël Poryles, Adrien Bussonnière, Emmanuel Schaub and Isabelle Cantat

Institut de Physique de Rennes, Univ Rennes, CNRS – UMR 6251, F- 35000 Rennes, France
theo.lenavetier@univ-rennes1.fr

In many consumer goods and industrial processes, liquid foams are notably used for their viscoelastic behaviour. Given that their liquid matrices are Newtonian fluids with viscosities lower by several orders of magnitude, their strong dissipative properties are surprising. Recent advances have shown that they may originate from a very localized zone near the junctions between the foam films associated to the transfer of surfactants from one film to its neighbours. To further investigate the different mechanisms involved there, and inspired by previous studies ([1-4]), we designed a special frame allowing us to create and observe three soap films connected together with a meniscus. We can control the lengths of the films using three synchronized motors to explore different geometries of deformation.

Using a fluorescent dye along with a photobleaching setup, hyperspectral cameras and tracking the position of the meniscus, we can have access to the thickness and velocity fields in the fluid, as well as the difference of surface tension between the films, thus characterizing the flow entirely.

In particular, it allows us to compare the amounts of surfactants going in and out of the meniscus during the imposed deformations. We show that the soap films exchange surfactants between them without exchanging with the meniscus as they are deformed, which is a key information to add to our model describing the rheology of this elementary foam.

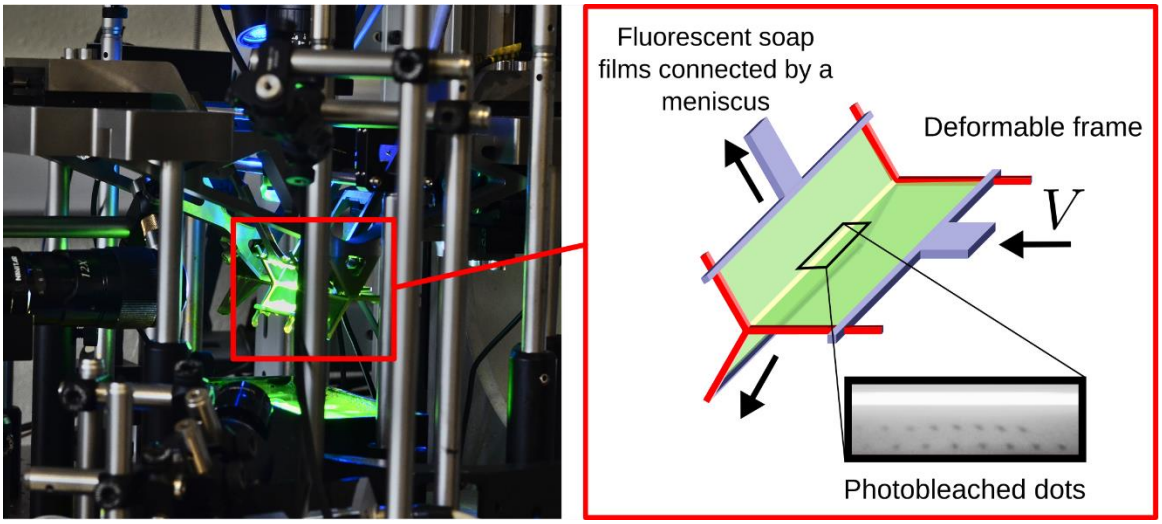

FIG. 1 : This elementary foam provides a robust basis to build a consistent model of foam viscosity

[1] M. Durand & H.A. Stone, *Relaxation time of the topological T1 process in a two-dimensional foam*, Physical Review Letters (2006).

[2] A-L Biance, A. Delbos & O. Pitois, *How topological rearrangements and liquid fraction control liquid foam stability*, Physical Review Letters (2011).

[3] J. Seiwert, B. Dollet & I. Cantat, *Theoretical study of the generation of soap films: role of interfacial visco-elasticity*, Journal of Fluid Mechanics (2013).

[4]. A. Bussonnière & I. Cantat, *Local origin of the visco-elasticity of a millimetric elementary foam*, Journal of Fluid Mechanics (2021).

Characterizing the gravity drainage of mobile soap films

Antoine Monier *[1], François-Xavier Gauci[1], Cyrille Claudet[1], Franck Celestini[1], Christophe Brouzet[1], and Christophe Raufaste[1,2]
[1]*Université Côte dAzur, CNRS, Institut de Physique de Nice, 06200 Nice, France*
[2]*Institut Universitaire de France (IUF), 75005 Paris, France*

The life time of a foam is a crucial quantity to predict for many applications ranging from food processing to water recycling [1]. The foam stability is proven to be highly related to the propreties of the soap films that connect its neighboring bubbles. These films are subject to evaporation, which has been recently adressed [2], and drainage. In fact, soap films drain and thin under the effect of gravity, which can be easily observed with single soap films supported by a solid frame. In this geometry, for soap films with mobile interfaces, Mysels *et al.* [3] showed the existence of an instability along the border of the frame called marginal regeneration. On the lateral sides of the frame, thin fluid patches rise, with a velocity V^+ (as seen in Figure 1 (a)) in opposite direction of the global drainage, with a velocity V^-, that measures the advection of the colored fringes of equal thickness. [4]. This complex motion governs the film drainage and needs to be further understood.

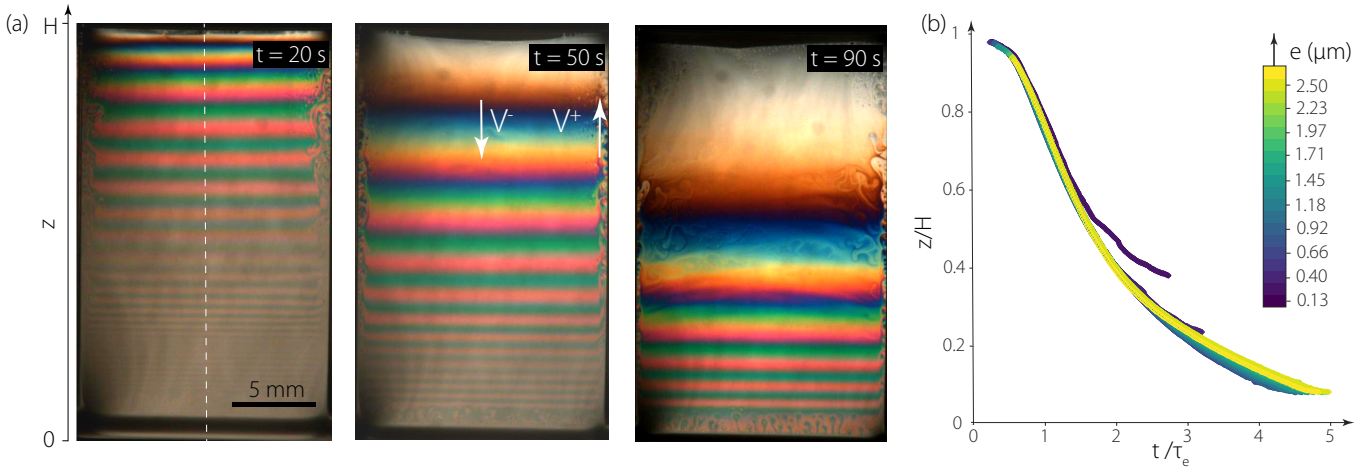

FIGURE 1 – (a) Snapshots of an experiment for three different times. The film drains from top to bottom and colors correspond to the film thickness. (b) Rescaled fringes profile showing the self-affinity. Colors code for the film thickness.

To do so, we study experimentally the drainage of mobile soap films supported by a solid frame and record the dynamics with a color camera. Figure 1 (a) presents a typical experiment at different times. To quantify the drainage dynamics, we propose to follow the thinning of the soap film at the center (dashed line in Figure 1 (a)). We thus track over time the fringes of equal thickness for a given wavelength $\lambda = 660\,\mathrm{nm}$. We find that all the fringes follow the same trend. In Figure 1 (b), we plot the rescaled fringe position z/H, with H the film height, as a function of a normalised time t/τ_e, with τ_e the dilatation time that depends of the fringe thickness : the thicker the fringe, the smaller τ_e. As a result, we are able to aggregate all our datas making a self-affinity hypothesis in Figure 1 (b) with no thickness dependency (given by the different colors). Morover, computing the velocity of the fringes, we show that the thicker the fringe the faster the its drainage velocity.

Finally, changing the control parameters (effective gravity, frame geometry, solution properties) evidences that the drainage is limited by the bulk friction of the rising patches close to the frame borders. These results pave the way towards a global understanding of mobile soap film drainage and thus foam life times.

[1] P. Stevenson, *Foam engineering : fundamentals and applications*. John Wiley & Sons, 2012.
[2] L. Champougny, J. Miguet, R. Henaff, F. Restagno, F. Boulogne, and E. Rio, "Influence of evaporation on soap film rupture," *Langmuir*, vol. 34, no. 10, pp. 3221–3227, 2018.
[3] K. J. Mysels, S. Frankel, and K. Shinoda, *Soap films : studies of their thinning and a bibliography*. Pergamon press, 1959.
[4] J. Seiwert, R. Kervil, S. Nou, and I. Cantat, "Velocity field in a vertical foam film," *Physical Review Letters*, vol. 118, no. 4, p. 048001, 2017.

*Corresponding author. E-mail : amonier@unice.fr.

Freezing a foam

Krishan Buma[1] , Juliette Pierre[1], Thomas Seon[1] and Axel Huerre[2]

[1] *Insitut d'Alembert, CNRS-Sorbonne Université, Paris, France*

[2] *MSC, CNRS- Université Paris-Cité, Paris, France,* axel.huerre@cnrs.fr

Liquid foam freezing is an essential and unavoidable processing to obtain solid foam. Here, we study experimentally the solidification dynamics of a model aqueous foam in contact with a cold substrate. The substrate temperature, the foam bubble radius and the liquid fraction are changed.

We will explore two configurations for the foam. In the first part, we will discuss the solidification of a foam in a container (Figure 1a). The foam is dyed with fluorescein to allow for a good contrast at the solidification front. We show that the freezing dynamics always starts by following a self similar square root of time diffusive dynamics. Figure 1b presents a compilation of pictures taken during the freezing of the foam. The liquid part is green and the frozen part is purple.

This early dynamics can be predicted as a function of the control parameters using a 1D diffusion model and by treating the foam as a homogeneous fluid with equivalent thermophysical properties (density, thermal conductivity and specific heat). In particular, we build a new expression for the foam conductivity. We show a good experimental and theoretical agreement in this experiment.

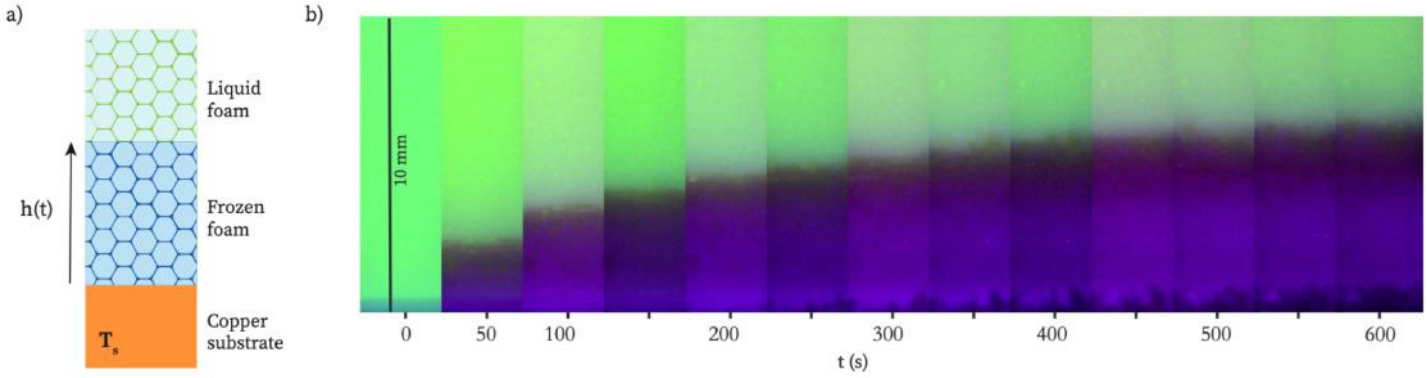

Figure 1: Experimental observation of a freezing foam. a) Schematics of the experimental setup. b) Compilation of experimental pictures showing the evolution of the freezing front dynamics during the solidification process.

In a second part, we will discuss a similar experiment but this time with a container-free foam (see figure 2). As can be clearly seen, the ascent of the freezing front is linked to a dramatic change the total volume of the foam. We are able to experimentally characterize this change for a various set of parameters and found a dependence with the mean radius of the bubbles composing the liquid foam. We build a physical model to describe the flow of water and gas coupled to the solidification process which could lead to such a dramatic change. This model is then numerically solved and is able to reproduce our experimental findings.

The processes at play in this complex system are key ingredients to control the freezing of the foam and the characteristics of the solid formed.

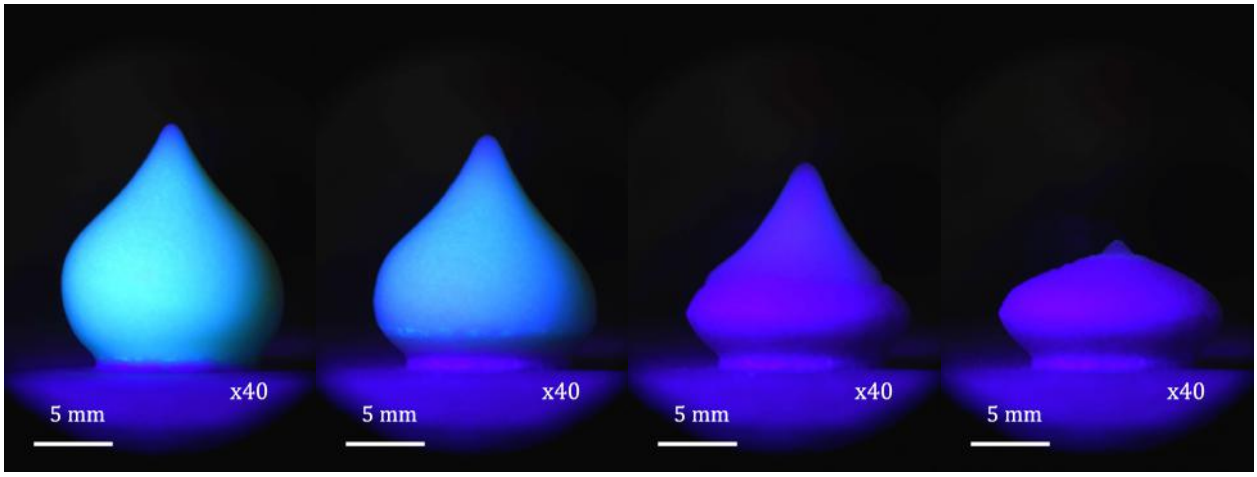

Figure 2: Change of volume when the freezing occurs in a container-less foam. The front evolution is linked to a collapse of the foam.

Session 10 – Evaporation and condensation

Wednesday June 21, 16:30–18:15

Flows inside a drop evaporating on a soluble substrate: From Marangoni to coffee-stain

Alexandra Mailleur[1], Jean Colombani[1], Christophe Pirat[1], Charlotte Rivière[1] and Irina Vodolazskaya[2]

[1] *Institut Lumière Matière ; Université de Lyon ; Université Claude Bernard Lyon 1 ; CNRS UMR 5306 ; Campus de la Doua, F-69622 Villeurbanne, France,* jean.colombani@univ-lyon1.fr
[2] *Laboratory of Mathematical Modeling, Astrakhan State University, Astrakhan, 414056, Russia*

I. CONTEXT

When a pure water drop evaporates on a soluble substrate, the final ring deposit may take the form of an inclined wall or of a hollow rim, depending on the initial sessile diameter and contact angle of the drop (see Fig. 1)[1]. This growth of these unprecedented hollow peripheral deposits is not a consequence of particular thermal or chemical conditions but of the geometry of the experiments, where the role of nucleation site played by the salt substrate is a necessary condition for the hollow or inclined rim to appear. Oppositely, the evaporation of a salty water drop on an inert substrate, where the nucleation may occur at all points of the liquid-air interface, leads to the growth of unstructured deposits[2].

This phenomenon can be interpreted as a molecular coffee-stain effect during which the dissolved salt is advected toward the pinned contact line where an increased evaporation takes place. The subsequent salt supersaturation in the vicinity of the triple-line due to this advection drives the nucleation and growth of the shell at this three-phase line. The contact line subsequently leaves its initial position and follows the growing edge of the shell. The progressive shrinkage of the evaporating drop gives the shell its characteristic half-toric shape[1].

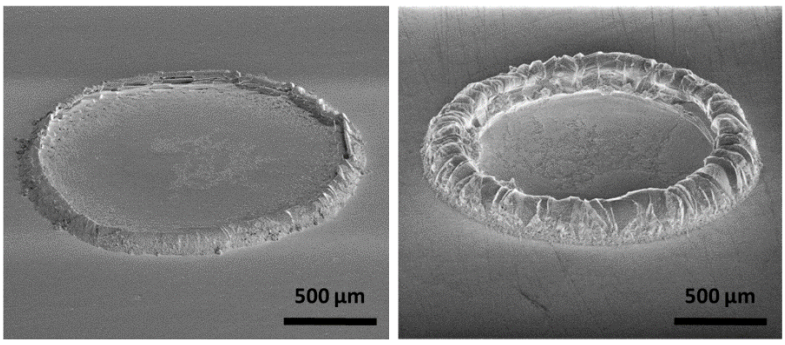

FIG. 1. Scanning electron microscopy images of the two characteristic morphologies of the ring deposit obtained after evaporation on a NaCl single crystal of a water drop: inclined walls (left) and hollow rim (right).

II. METHODOLOGY

In order to better understand the formation of these peculiar patterns, and validate the above-mentioned interpretation, we present here both experimental and numerical investigations of the inner flows during the evaporation of a drop of pure water on a salt substrate (NaCl single crystals). The velocity field is measured experimentally by a micro particle image velocimetry technique, the water drop being seeded with 1 µm fluorescent beads, and is simulated using the hydrodynamics equations

[1] A. Mailleur, C. Pirat, O. Pierre-Louis and J. Colombani, Hollow rims from water drop evaporation on salt substrates, *Phys. Rev. Lett.*, **121**, 214501 (2018).

[2] A. Mailleur, C. Pirat, G. Simon, R. Fulcrand, and J. Colombani, Ring shells obtained from pure water drops evaporating on a soluble substrate, *Colloids Surf. A*, **651**, 129724 (2022).

solved by the finite-elements method, using the lubrication approximation[3].

II. FLOWS INSIDE A DROP EVAPORATING ON A SOLUBLE SUBSTRATE

Surprisingly, an inward motion at the beginning of the evaporation characterizes the flow. This one is rapidly replaced by an outward motion, which lasts until the end of the evaporation. The transition between the two flow regions takes the form of a stagnation line, where the radial component of the velocity vanishes (see Fig. 2). This line migrates from the periphery toward the center of the drop, inducing the progressive reversal of the flow. The comparison between the experiments and simulations leads to the following interpretation of this flow inversion. The dissolution of the substrate induces the creation of a surface tension gradient at the drop free surface, leading to an outward Marangoni flow along the drop surface and an inward flow near the substrate. As the diffusion progressively makes the concentration more uniform, this surface-driven convection stops, and is replaced by the standard coffee-stain outward capillary flow, driven by the evaporation rate non uniformity, which eventually contribute to the growth of the hollow rims.

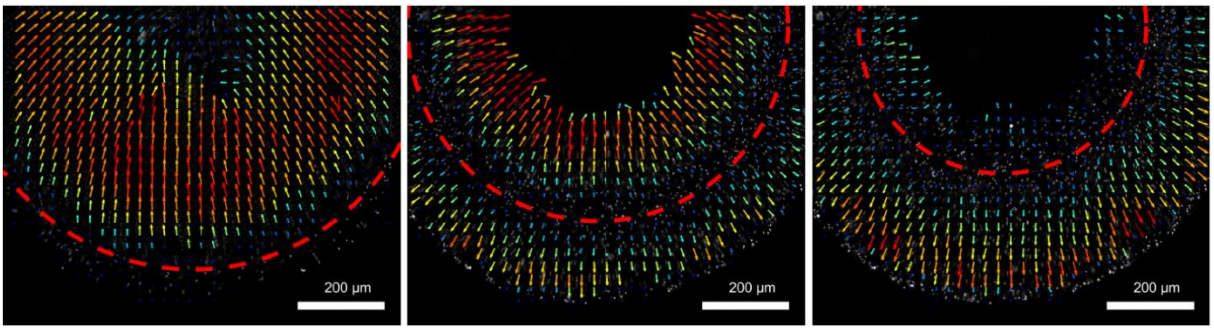

FIG. 2. Velocity field just above the bottom of a drop of pure water seeded with fluorescent beads evaporating on a NaCl single crystal, from left to right, 10, 27, and 33 s after deposition. The length of the arrows and their color indicate the magnitude of the velocity. The red dashed line shows the stagnation line, sharing the centripetal and centrifugal velocities.

[3] A. Mailleur, J. Colombani, C. Pirat, C. Rivière and I. Vodolazskaya, Flow reversal inside a drop evaporating on a soluble substrate, *Phys. Rev. Fluids,* **7**, 093605 (2022).

Flow and Temperature Visualization in a Nonisothermal Sessile Droplet

Fei Duan[1]

[1]*School of Mechanical and Aerospace Engineering, Nanyang Technological University, Singapore, 639798* feiduan@ntu.edu.sg

The onset of circumferentially distributed thermal patterns at the interface of a volatile sessile droplet has collected interests with the help of the thermographic measurement, the observed phenomena were reported as hydrothermal waves at the evaporating droplets under the transient conditions or steady state conditions. However, the mechanism to induce the nonisothermal temperature and complex thermal pattern is still not completely understood. The local interfacial temperature nonuniform affects the droplet phase change and can generate the complicated flow. The theoretical explanations are in lack of support from direct flow field measurement. We, thus, used the thermographic and optical microscopic measurements to present linking of the nonisothermal interface temperature and the flow field at a sessile ethanol droplet on a heated substrate. The constant contact radius mode was maintained for the droplet on a 5mm-in-diameter stage with a sharp edge. The thermographic imaging was performed for the droplet in a stainless chamber with infrared observation windows at the top. The measurements from particle image velocimetry (PIV) were also conducted from the top view by using the hollow glass spheres and fluorescent beads as the seeding particles. Figure 1(a) shows the evolution of temperature distribution at the interface of the evaporating ethanol droplet with the initial contact angle is around 59°. The thermal patterns indicate that the evaporation process haso four stages. In the first stage at τ = 0~0.3, the temperature increment near the edge is much higher than that in the inner part due to substrate heating and thereby a hot ring pattern is formed. In the second stage at τ = 0.3~0.5, there exists a transition from the uniformly circumferential temperature distribution to the regular petal-like thermal patterns. In the third stage at τ = 0.5~0.7, the petal patterns grow fast, and their number correspondingly decreases. Although the global temperature distribution is quasi-steady, the local unstable merging and splitting of petals are also noted. In the final stage at τ =0.7~1, the petals convert into cell-like patterns and then the temperature distribution becomes irregular. The corresponding global flow field of the four stages are shown in Fig.1(b) from the PIV measurement. At τ = 0.12, trajectories of microspheres are radial circulation of the capillary flow and the Marangoni reversal flow in the droplet. At τ = 0.37, small vortical flow structures emerge near the edge, and form in pairs with counter rotating directions. With the continuous phase change, the vortical structures grow inwards rapidly, while trajectories in the inner part remain radial. During the final stage, the aforementioned vortical structures convert into conventional Bénard-Marangoni cells. Further qualitative comparison between the infrared camera measurement and the flow visualization reveals that the regular thermal patterns at the interface of the evaporating droplet can be a result of the vortical flow structures near the edge. The capillary flow near the substrate separates at the interface and rolls up into a pair of counter rotating vortices. Since the capillary flow has a higher temperature than the above liquid, a hot region can be formed at the interface,which is the petal pattern observed through thermography. These vortices develop along the interface, from the edge to the apex. The agreements between the direct thermographic and the PIV measurements indicates infers that the thermal patterns are a result of the deformed Bénard -Marangoni convection cells in the sessile droplet illustrated in Fig.1(c).

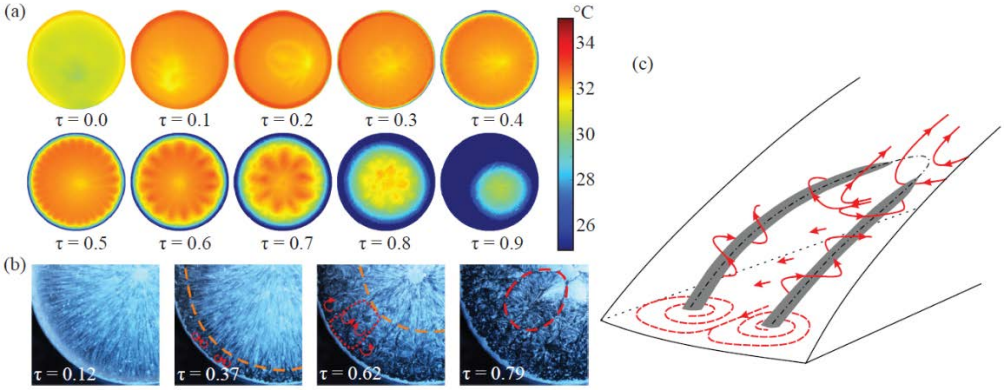

FIG. 1. (a) Instant image of interfacial temperature distribution on the evaporating droplet at the non-dimensional time, τ, (b) instants of the inner flow field from PIV, and (c) schematics to form the deformed Bénard-Marangoni convection cells.

Stability analysis of volatile liquid films in different evaporation regimes

Omair Mohamed[1], Luca Biancofiore[1], and Christian Ruyer-Quil[2]

[1] *Department of Mechanical Engineering, Bilkent University, 06800, Ankara, Turkey,* omair.mohamed@bilkent.edu.tr, luca@bilkent.edu.tr

[2] *Université de Savoie Mont Blanc, CNRS, LOCIE 73000 Chambéry, France,* ruyerquc@univ-smb.fr

Evaporating liquid films have a wide range of important technological applications across several industries, including distillation, combustion, coating and cooling processes, and chemical synthesis. The evolution of the liquid film's interface is tied directly to the performance and efficiency of these systems, and therefore, a better understanding of this evolution can result in large economic and environmental gains.

With this in mind, we investigate the temporal evolution of evaporating liquid films flowing over a heated solid surface, where we study volatile films in two different evaporation regimes, each relevant to a distinct industrial scenario: (i) molecular transfer rate-limited evaporation, and (ii) diffusion-limited evaporation.

In the presence of a gas stream adjacent to the liquid, the evaporation process is limited by the molecular transfer rate across the interface since the role of vapor diffusion is eliminated by the gas flow above the liquid. In this setting, a single-fluid (one-sided) model is appropriate and evaporation effects have been found to be destabilizing [1,2]. We formulate our model by extending the work of Joo *et. al.* [3] to incorporate a shearing gas effect, which is introduced by prescribing a constant shear stress along the liquid interface. This leads to a Benney-like differential equation governing the evolution of the liquid interface under the effects of inertia, hydrostatic pressure, surface tension, thermocapillarity, evaporation, and gas shear.

We employ linear stability theory to derive a dispersion relationship which we use to investigate the temporal and spatiotemporal characteristics of the flow, where we find that the evaporation of the film can cause convective-absolute transitions in the nature of the perturbations, as shown in Fig. 1. We also find that a strong enough counter-flowing shearing gas can suppress the inertial instability, affirming similar conclusions found by previous studies for a strongly confined film [4]. Additionally, we solve the liquid interface's governing equation numerically to simulate the film's evolution subject to finite perturbations, which allowed performing a nonlinear numerical spatiotemporal analysis. We found the wave-front dynamics to be dictated nonlinearly (linearly) for weak (strong) thermal instabilities.

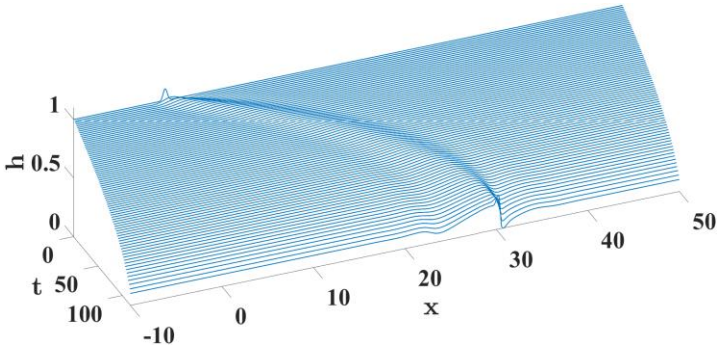

FIG. 1. Spatiotemporal evolution of a perturbed sheared volatile film evaporating in the molecular transfer rate-limited regime. Note the transition of the perturbation from stable to convectively unstable, and finally to absolute instability as the film becomes thinner.

[1] J. P. Burelbach, S. G. Bankoff, and S. H. Davis, Nonlinear stability of evaporating/condensing liquid films, J. Fluid Mech. **195**, 463 (1988).

[2] Margerit, J., Colinet, P., Lebon, G., Iorio, C. S. & Legros, J. C. 2003 Interfacial nonequilibrium and B´enard-Marangoni instability of a liquid vapor system. Phys. Rev. E **68**.

[3] S. W. Joo, S. H. Davis, and S. G. Bankoff, Long-wave instabilities of heated falling films: Two-dimensional theory of uniform layers, J. Fluid Mech. **230**, 117 (1991).

[4] G. Lavalle, Y. Li, S. Mergui, N. Grenier, and G. F. Dietze, Suppression of the Kapitza instability in confined falling liquid films, J. Fluid Mech. **860**, 608 (2019).

On the other hand, we study the evolution of liquid films where the diffusion of vapor into the gas domain plays a significant role, e.g., the evaporation of a liquid film into a static ambient environment. To model this setting, we combine the liquid film model of Joo *et. al.* [3] with the generalized evaporation model of Sultan *et. al.* [5], which we modify to account for the change in base state height due to the mass loss. Notably, the effects of evaporation are stabilizing in the diffusion-limited regime [5]. We form a coupled liquid-vapor model which we reduce using long-wave theory to again derive a differential equation governing the evolution of the liquid interface under the relevant physical effects. Notably, transfer rate-limited evaporation can still be recovered using this formulation under a variable transformation.

Once more we use linear stability theory to investigate the temporal stability of the flow, where we find that under diffusion-limited evaporation, the thermocapillary instability is augmented by an additional effect emanating from the vapor mass flux perturbation. Moreover, we observe the complete suppression of the thermocapillary instability by the stabilizing evaporation effects when vapor diffusion is significant, as shown in Fig. 2. Finally, we numerically solve the coupled liquid-vapor system to simulate the system's evolution subject to finite perturbations, where we observe rich and dynamic film evolution, including harmonic changes in the temporal growth rate as the film evaporates.

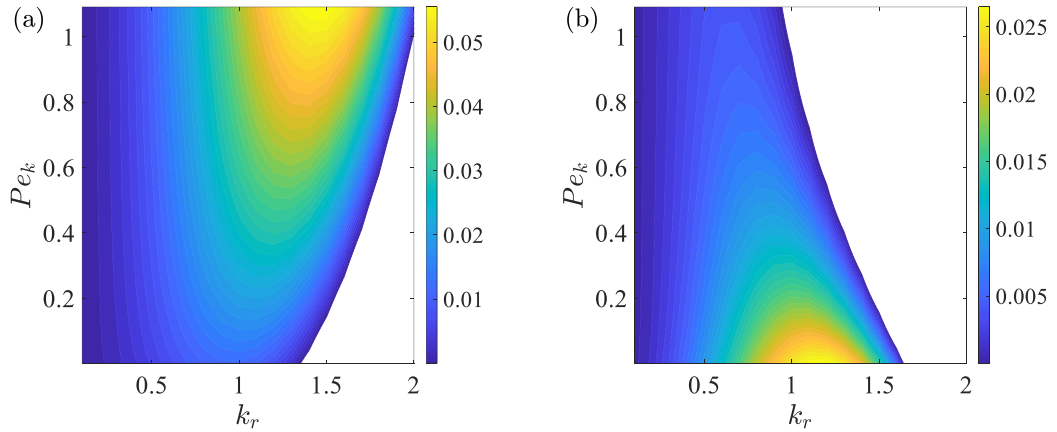

FIG. 2. Contour plots of the temporal growth rate ω_i in the (Pe_k, k) parameter space for two different values of the vapor recoil parameter V_r, where Pe_k is a kinetic Péclet number determining the evaporation regime, and k is the dimensionless wave number. (a) $V_r = 0.5$. (b) $V_r = 1.5$. White regions correspond to stable flow. Notice the suppression of the thermocapillary instability at $Pe_k \approx 1$ in figure (b), due to the increased stabilizing action of vapor recoil.

[5] E. Sultan, A. Boudaoud, and M. B. Amar, Evaporation of a thin film: Diffusion of the vapour and Marangoni instabilities, J. Fluid Mech. **543**, 183 (2005).

Experimental study of thermocapillarity–induced deformation of evaporating films on structured copper surfaces

Robin Behle, Peter Stephan and Tatiana Gambaryan-Roisman

Institute for Technical Thermodynamics, TU Darmstadt, Darmstadt, Germany, behle@ttd.tu-darmstadt.de

Thin liquid films are widely used in energy and chemical technology due to their ability to dissipate heat through evaporation. Such films are also essential in cooling systems for both ground and space applications, where high heat transfer densities are required. The behavior of thin films on heated surfaces is governed by the Marangoni effect, which arises from inhomogeneities in surface tension. This effect not only enhances convective heat transport, but also causes potential liquid film rupture, leading to dry patches and decreased heat transfer. Theoretical and numerical studies have shown that using surfaces with topography can induce Marangoni stresses, allowing for better control of the flow pattern, liquid topology, and heat transfer. This study experimentally investigates the thermocapillary-induced deformation and rupture of a thin liquid film on a surface with topography.

A series of experiments have been conducted in the framework of the preparation of the "Marangoni in Films" experiment on board the International Space Station (ISS). The experimental setup includes a copper substrate with sinusoidal grooves, where the wavelength of the topography is much larger than its amplitude. The substrate is placed in a test cell filled with a mixture of nitrogen gas and vapor of the fluorinert fluid HFE 7100. The thin liquid film on the substrate also consists of HFE 7100. The nitrogen pressure, initial vapor concentration, and substrate temperature can be varied. The deformation of the thin liquid film is measured using Fourier-Deflectometry, and the data is analyzed to evaluate the Marangoni-driven long-wave film deformation and to detect film rupture. Additionally, the evaporation rate of the liquid is determined by measuring the change in pressure.

It has been shown that using a structured substrate, such as the one with sinusoidal grooves in the experiment, induces controlled film deformation. This is due to thermocapillary stresses created by the temperature non-uniformity at the liquid-gas interface. The flow of the film results in local thinning over the crests and thickening over the valleys of the grooves, which is consistent with predictions from the long-wave theory [1].

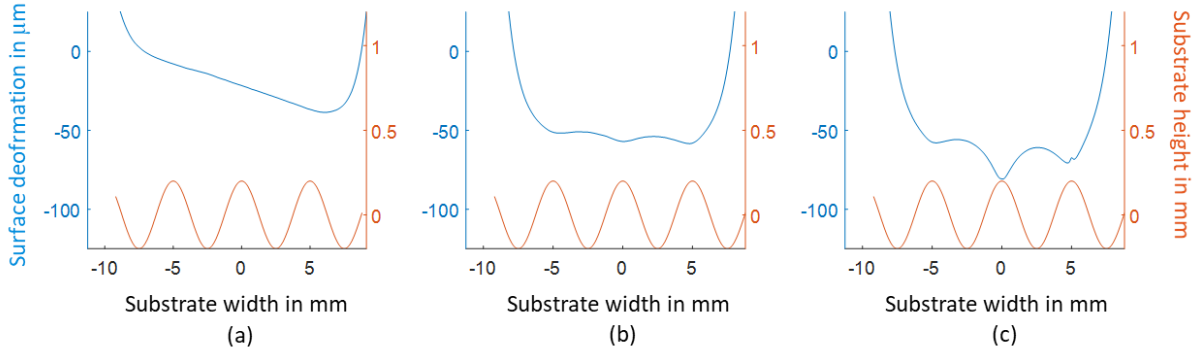

FIG 1. Evolution of liquid surface deformation (blue) over substrate geometry (orange). Deformation measured with Fourier-Deflectometry (side view)*;* (a) after film injection and settling, (b) during onset of surface deformation, (c) approaching film rupture

[1] A. Bender, P. Stephan and T. Gambaryan-Roisman, Numerical investigation of the evolution and breakup of an evaporating liquid film on a structured wall, Int. J. Heat Fluid Flow **70**, 104-113 (2018)

In Fig. 1, the profile of the liquid film deformation is illustrated at three distinct stages: immediately after film injection and settling (a), the onset of surface deformation (b), and the advanced stage of deformation approaching film rupture (c). Furthermore, the controlled rupture of the film at the crests of the topography is observed.

This work was supported by the European Space Agency (ESA) and the German Aerospace Center (DLR) in the framework of the “Verständnis und Beeinflussung von Marangoni-Strömungen und Transportprozessen unter μ-g Bedingungen: “Marangoni in Films”” project, grant no.50WM2047. The evaporation chamber setup was provided by Redwire Space and the Fourier-Deflectometry by Lambda-X.

Experimental investigation on evaporation of pinned nanofluid sessile droplet on heating PTFE surface

Yuequn Tao[1*], Jun Qin[1,2] and Qiusheng Liu[1,2*]

[1] *Institute of Mechanics, Chinese Academy of Sciences, Beijing 100190, China*
[2] *University of Chinese Academy of Sciences, Beijing 100049, China*
*taoyuequn@imech.ac.cn, liu@imech.ac.cn

Nanofluid droplet evaporation has gained much audience nowadays due to its wide applications in painting, coating, surface patterning, particle deposition, etc[1]. The evaporation and dryout of nanofluid solutions is a far-from-equilibrium process where several possible underlying mechanisms (including hydrodynamic instabilities of the continuous liquid phase, nucleation and growth of dewetting holes, and spinodal dewetting) can be responsible for observed pattern formations[2]**Erreur ! Signet non défini.Erreur ! Signet non défini.**. The relative importance of the mechanisms and the conditions under which they occur are far from being fully understood.
Experimental investigations of Al_2O_3-H_2O nanofluid sessile droplet evaporation into air on heating PTFE substrates are reported in this study. A circle groove with inner diameter of 4mm was machined on the substrate, which lead to contrived effect on the contact angle and contact line. The evolution of the droplets shape with time is recorded by side-view CCD and the evaporation rate is deduced from the image analysis of the evolution of volume in time. The study is focused on the effect of nanoparticles addition on the evaporation process and the effects of substrate temperature, initial droplet volume, nanopariticle concentration, etc. Results indicate that the droplets containing nanoparticles show a great variation in motion of the contact line, evaporation rate, evaporation regimes and flow dynamics in comparison with pure liquid droplets. Nanofluid droplets show stronger pinning along the droplet perimeter and, upon evaporation, leave a ring-shaped nanoparticle stain. During the "pinning" phase and contrary to what is expected, the presence of nanoparticles leads to a reduction of the evaporation rate compared to the base fluid. The overall evaporation time for base fluid droplets is found to be longer than for nanofluid ones.

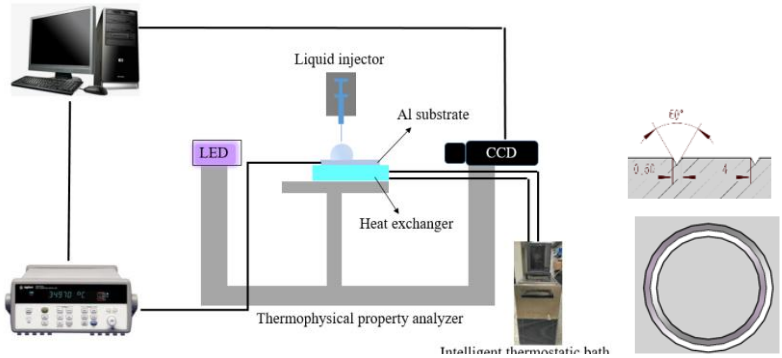

FIG. 1. Left: Experimental setup; Right: The heating substrate

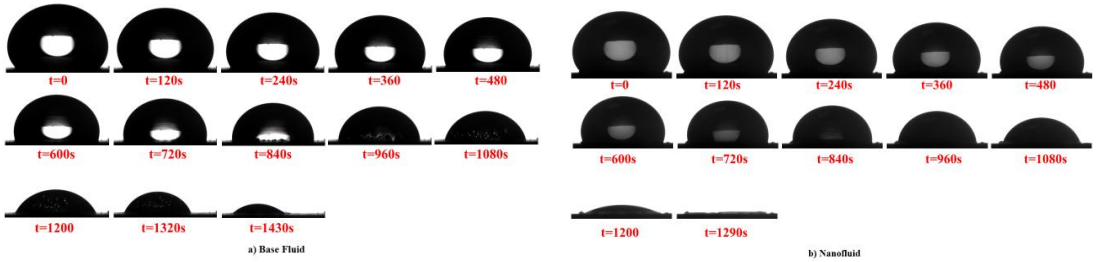

FIG. 2. Left: Evaporation procesof base fluid with time; Right: Evaporation process of nanofluid.

ACKNOWLEDGEMENTS : This work was financially supported by Bureau of International Cooperation, The Chinese Academy of Sciences (No.115111KYSB2020008), Key Research and Development Plan of

[1]A. A. Mehrizi, H. Karimi-maleh, M. Naddafi et al. Evaporation characteristics of nanofuel droplets: A review, Fuel.**319**, 123731(2022)
[2] J.H Ren, A. Crivoi, F. Duan. Disk-Ring Deposition in Drying a Sessile Nanofluid Droplet with Enhanced Marangoni Effect and Particle Surface Adsorption. Langmuir. 36, 15064-15074(2020).

Influence of g-jitters on the vapour of an evaporating sessile droplet: masking of Marangoni effect

Senthil Kumar Parimalanathan[1], Hatim Machrafi[2], Adam Chafai[1], Alexey Rednikov[1] and

Pierre Colinet[3]

[1]*TIPs Laboratory, Université libre de Bruxelles, Brussels, Belgium* sparimal@ulb.ac.be
[2]*Institute of Physics, Université de Liège, Liège, Belgium,* h.machrafi@uliege.be
[3]*TIPs Laboratory, Université libre de Bruxelles, Brussels, Belgium* pcolinet@ulb.ac.be

The study of fundamental physics in microgravity has recently gained significant importance. The European Space Agency (ESA) has identified the understanding of vapour dynamics surrounding an evaporating sessile droplet in reduced gravity as a crucial area of research. This is because the processes of evaporation in microgravity have many applications, including material processing, additive manufacturing, cooling systems, and pharmaceutical industries. As, in pure zero-gravity, buoyancy-driven convections are zero in both the sessile droplet and its vapour, the dominant surface tension gradients resulting from evaporation give rise to 'Marangoni Convection'. This phenomenon could affect not only the evaporation rates but also the distribution of the vapour cloud, as we have demonstrated in our previous studies using sounding rocket experiments [1]. However, in our recent study, we show for the first time that, in some cases, residual gravity, in the form of g-jitters, can have an effect on the evaporation rates of microliter sessile droplets. The analysis has been performed by using a combination of experiments and an axisymmetric numerical model using COMSOL. A numerical model has been developed in order to understand the mechanisms that are responsible for what we observe in the vapour cloud, focusing on the interplay between the Marangoni flow and g-jitters. In both the vapour and liquid phases, the model solves for the Navier-Stokes equations and energy balance, with also the species balance in the gas phase. The evaporation is represented by an evaporation flux that generates a concentration gradient in the gas phase and, through cooling of the droplet surface, temperature gradients in both the liquid and gas phases. This drives the Marangoni mechanism. The effect of the g-jitter is assessed by including buoyancy.

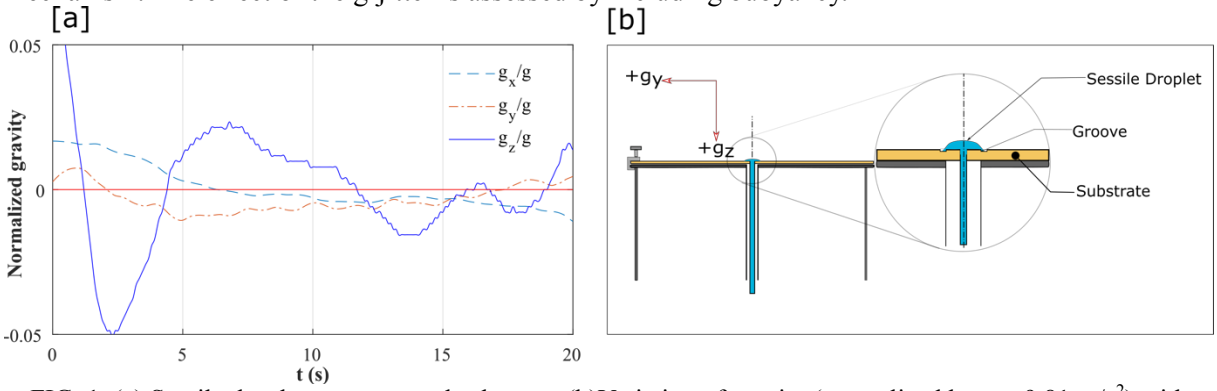

FIG. 1. (a) Sessile droplet on a grooved substrate. (b)Variation of gravity (normalized by g = 9.81 m/s^2) with time during the microgravity phase of a typical parabolic maneuver.

The evaporation dynamics of HFE-7100 sessile droplets on a grooved silicon substrate (shown in FIG. 1(a)) were studied in a sophisticated experimental setup developed at TIPs laboratory, ULB. The experiments were conducted during the 78th Parabolic flight campaign organized by ESA at Novespace. To visualize and characterize the vapour cloud surrounding the droplets, Mach-Zehnder interferometry [2] was used. One of the main drawbacks of parabolic flight tests over drop tower and sounding rocket is the presence of fluctuations in gravity, known as g-jitters, during the microgravity phase. The temporal variation of gravity during the microgravity phase of a typical parabolic maneuver (Day 1, Parabola, 28) is shown in FIG. 1(b). The arrow marks indicate the directions of the g_z (vertical component, being positive downwards) and g_y (horizontal component, being positive from right to left). The third horizontal component g_x is in the direction perpendicular to the screen, so it is considered only to affect the height of the vapour cloud. These directions indicate how the vapour cloud tends to fluctuate with the variation of the g-jitter data.
Despite these fluctuations being small (in the present case, the maximum variation being ±0.05g, g =

9.81 m/s^2), it has been observed that they significantly affect the shape of the vapour cloud surrounding the sessile droplet. The temporal variation of the vapour cloud shapes (phase-wrapped images) for the gravity data presented earlier is shown in FIG. 2(a). In order to compare the experimental results with simulations, the concentration plots were converted to phase-wrapped images using Abel's transform [2]. The converted phase-wrapped images have been presented in FIGS. 2 (b-d). The numerical results shown in FIG. 2(b) incorporate both the effect of g-jitters and the Marangoni stresses. The comparison is quite good except for the asymmetry in the experimental vapour cloud attributed to the g- jitters in the horizontal directions. Therefore, it is interesting to compare the present vapour cloud shapes to an ideal condition when no gravity is present. Therefore, simulations have been performed with gravity effects turned off (FIG. 2(c)), which resulted in different vapour cloud shapes. Even in the absence of gravity, the vapour cloud rises as a plume due to the influence of the Marangoni stresses in the liquid phase. However, the size grows monotonically with an increase in time. Therefore, it was necessary to study if the Marangoni stresses have any consequences on the vapour cloud shapes in the presence of g-jitters. In FIG. 2(d), the temporal evolution of the vapour cloud in the numerical model has been obtained by decoupling the gas flow velocities from the Marangoni stress-induced velocity in the liquid phase (assuming a zero tangential velocity component on the surface from the gas side). Surprisingly, coupling or decoupling the Marangoni stresses with the gas phase does not play a significant role in characterizing the vapour cloud shapes in the presence of dominant g-jitters. Even though the Marangoni stresses may be dominant in the liquid phase, the effects are masked by the g-jitters, which significantly influence the vapour phase. We also observed that g-jitter not only modified the shape of the vapour cloud but also influenced the evaporation rates. These findings have important implications for designing and operating experiments conducted in microgravity, particularly those involving evaporation dynamics.

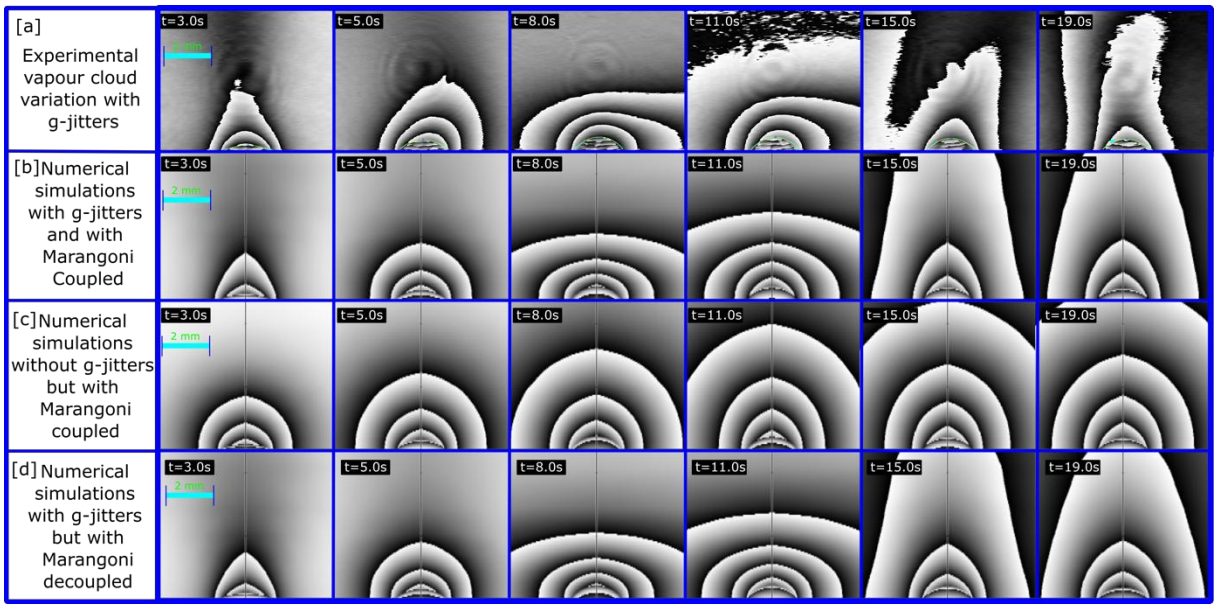

FIG. 2. Variation of vapour cloud shapes in reduced gravity (a) Experimental data (b) Numerical simulation results incorporating Marangoni and g-jitter effects. (c) Numerical simulations without any g-jitter but with Marangoni stress coupled to gas-phase. (d) Numerical simulations with g-jitter but without coupling the Marangoni stresses to the gas phase.

Acknowledgements: The authors are grateful for the support and funding from ESA and BELSPO PRODEX (Evaporation and Heat Transfer) and the Fonds de la Recherche Scientifique-F.N.R.S.

[1] Dehaeck S., Rednikov A.Y., Machrafi H., Garivalis A.I., Di Marco P., Parimalanathan S.K. and Colinet P., Vapor clouds with Marangoni jets and electroconvection off sessile droplets on a sounding rocket, to be submitted to Langmuir (2023).
[2] Dehaeck S., Rednikov A. and Colinet P., Vapor-based interferometric measurement of local evaporation rate

Session 11 – Thin films

Thursday June 22, 9:00–10:30

Modelling the Continuous Hydraulic Jump and Vortex Structure

Roger Khayat, Wenxi Wang and Abdelkader Baayoun

Department of Mechanical and Materials Engineering, Western University, Canada rkhayat@uwo.ca

We examine the structure of the circular hydraulic jump and the recirculation appearing for a jet impinging on a disk. We use a composite mean-field thin-film approach [1], which consists of subdividing the flow domain into three regions of increasing gravity strength: a developing boundary layer near impact, an intermediate supercritical viscous layer leading up to the edge of the jump, and a region comprising the jump and subcritical flow. The flow is assumed to drain at the edge of the disk (figure 1).

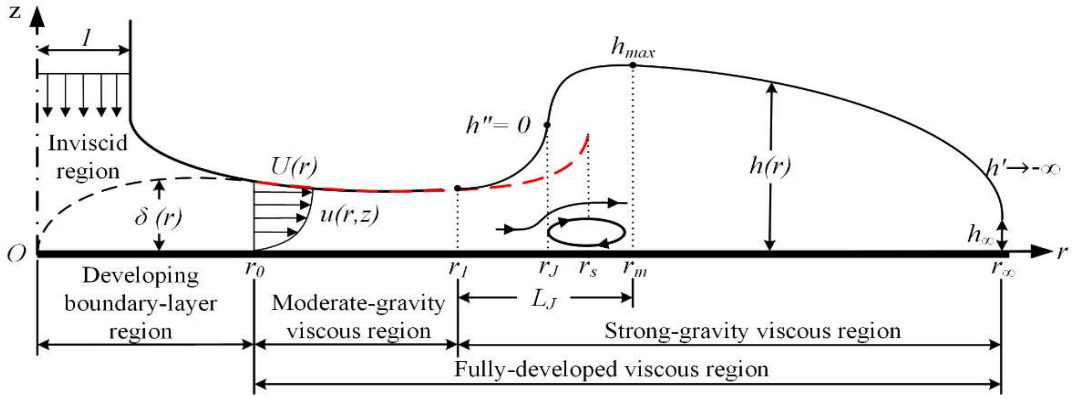

Figure 1. Schematic illustration of the axisymmetric jet flow impinging on a flat stationary disk and the hydraulic jump of type I with one vortex downstream. Shown are the developing boundary-layer region $\left(0 < r < r_0\right)$ and the fully-developed viscous region $\left(r_0 < r < r_\infty\right)$. All notations are dimensionless. In this case, the jet radius is equal to one. The film is allowed to fall freely over the edge of the disk where an infinite slope in the film thickness occurs, $h'\left(r = r_\infty\right) \to -\infty$. Shown in dashed-red curve is the schematic film-thickness profile reflecting the approach of Wang & Khayat (2019), terminating with a singularity at a finite radius denoted here by r_s. The jump location coincides with $h''\left(r_J\right) = 0$, and $h\left(r_m\right) = h_{max}$.

Unlike existing formulations [2] that capture the continuous jump profile and the recirculation zone, the present approach does not require any empirically or numerically adjustable boundary conditions. The governing boundary-layer equations for the thin film are elliptic given the presence of the hydrostatic pressure gradient [1], thus resulting in a two-point boundary value problem, requiring upstream and downstream boundary conditions, particularly at the edge of the disk. We demonstrate that the stress or corner singularity for a film draining at the edge is equivalent to the infinite slope of the film surface, which we impose as the downstream boundary condition. The present approach is validated against numerical solutions of the boundary-layer equations and Navier-Stokes equations, showing excellent agreement, as well as against existing models of the averaged film equations. Comparison against existing measurements of the film profile and jump radius also showed close agreement and/or equally accurate predictions as existing numerical solutions. We derive a scaling law from momentum conservation across the jump and lubrication flow for the jump height: $r_J\left[\ln\left(r_\infty / r_J\right)\right]^{1/8} = 2/3 \mathrm{Fr}^{1/4}\,\mathrm{Re}^{3/8}$. This scaling is similar to that proposed by Duchesne *et al.* [3] but has no empirical basis. It generalizes that of Bohr *et al.* [4] to include the effect of the disk size.

[1] Y. Wang & R. E. Khayat The role of gravity in the prediction of the circular hydraulic jump radius for high-viscosity liquids. *J. Fluid Mech*. **862**, 128–161 (2019).

[2] S. Watanabe, V. Putkaradze & T. Bohr Integral methods for shallow free-surface flows with separation. *J. Fluid Mech.* **480**, 233-265 (2003).

In an effort to stimulate further experimental work, we examined the influence of flow rate (inertia) in some detail, over the same range of experimental conditions of Duchesne *et al*. [1, 3]. We examine the film profile and vortex structure, the flow at the edge, the jump length, and energy dissipation and conjugate depth ratio. In particular, we show that the predicted edge thickness follows closely the behaviour $h_\infty \approx (27/70)^{1/3} (Fr/r_\infty)^{2/3}$ established from the Gibbs free energy minimization. In contrast to channel flow, the energy dissipation exhibits a maximum at some flow rate, which we showed to result from the non-monotonic distribution of the film thickness with distance in the supercritical region. The film profile was found to have a significant influence on the jump size and vortex structure. This connection was missed in the existing literature, particularly studies on channel flow or flows where the developing boundary-layer and viscous-film regions were not fully accounted for in the supercritical formulation. The conjugate depth ratio was predicted to monotonically decrease with the Froude number due to the linearly growing film profile upstream. One of the difficulties facing theory and experiment has been the identification of the jump location, which we assumed to coincide with the change in the film surface concavity. We showed that this assumption is accurate as the predicted jump radius is very close to the critical radius based on the local Froude number.

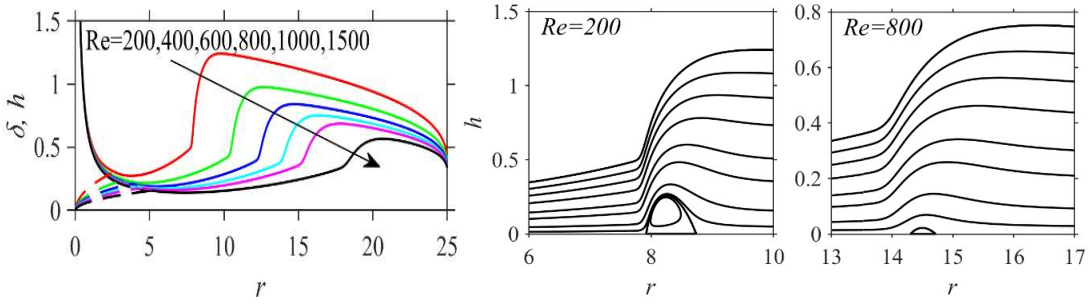

Figure 2. Influence of Re (viscosity) on the free surface profile (solid curves) the boundary-layer thickness (dashed curves). Also shown are the streamlines around the jump region for Re = 200 and 800. Here, Fr = 10 and $r_\infty = 25$.

The influence of the viscosity is depicted in figure 2, where Re is varied and Fr is fixed. As expected, a larger Re (lower fluid viscosity) results in a thinner boundary-layer and film thickness in the developing boundary-layer region (figure 2a). In contrast to the effect of gravity, the supercritical flow is sensibly dependent on viscous effects, as depicted by the dependence of the film (figure 2a) and stress profiles (not shown). As Re increases, the film profile becomes flatter, with a weakening of the supercritical minimum and subcritical maximum film thickness, as the jump is pushed towards the disk edge. The growth of the jump radius with Re is consistent with the scaling law above. The jump becomes essentially nonexistent at a relatively large value of Re. Simultaneously, the vortex diminishes in size as Re increases, and vanishes at a Re much smaller than that corresponding to the vanishing of the jump. This clearly shows that the existence of a jump is not necessarily accompanied by the formation of a vortex (figures 2b/c). Finally, it is interesting to observe that the strength of the singularity of the stress (equivalently of the film slope) at the edge weakens considerably with Re.

[3] A. Duchesne, L. Lebon & L. Limat. Constant Froude number in a circular hydraulic jump and its implication on the jump radius selection. *Europhys. Lett.* **107**, 54002 (2014).

[4] Bohr, T., Dimon, P. & Putzkaradze, V. 1993 Shallow-water approach to the circular hydraulic jump. *J. Fluid Mech.* **254**, 635-648.

The Effect of a Non-Uniform Heating in Axisymmetric Rayleigh-Bénard Instability

Dilara Özev[1], François Gallaire[2] and Luca Biancofiore[1]

[1] *Department of Mechanical Engineering, Bilkent University 06800 Bilkent, Ankara, Turkey*
[2] *Laboratory of Fluid Mechanics and Instabilities, Ecole Polytechnique Federale de Lausanne, Lausanne 1015, Switzerland*

I. INTRODUCTION

In a dynamical system, instability arises when a slight perturbation to one solution of the state does not disappear but instead grows, pushing the entire system towards another solution. In the context of fluid instabilities, the Rayleigh-Bénard problem is one of the well-studied convective systems where fluid movements are induced by a density variation in the presence of gravity [1].

The Rayleigh-Bénard instability with uniform constant temperature boundaries has been thoroughly studied in experimental, theoretical, and numerical studies [2, 3]. However, introducing a non-uniform heating at the bottom wall is still an area of inquiry, which can enlighten the behavior of the fluid and provide a comprehensive understanding of the stability mechanism in more realistic applications such as optically manipulated fluids [4]. The objective of the present study is to investigate the instability of a thin infinite fluid layer with a normal (Gaussian) distributed temperature field at the bottom.

II. GOVERNING EQUATIONS AND NUMERICAL METHOD

The Navier-Stokes equations are coupled with the energy equation using the Boussinesq approximation, i.e. $\rho = \rho_0[1 - \beta(T - T_0)]$, where ρ is the fluid density, ρ_0 the reference density, β the thermal expansion and T_0 is the reference temperature. The governing equations for 2D steady state base flow are

$$\boldsymbol{\Delta} \cdot \mathbf{u} = 0, \tag{1}$$

$$\mathbf{u} \cdot \boldsymbol{\Delta}\mathbf{u} = -\boldsymbol{\Delta}\mathrm{p} + \mathrm{Pr}\boldsymbol{\Delta}^{\mathbf{2}}\boldsymbol{u} + PrRa\theta\mathbf{e_z}, \tag{2}$$

$$\mathbf{u} \cdot \boldsymbol{\Delta}\theta = \boldsymbol{\Delta}^{\mathbf{2}}\theta, \tag{3}$$

where p, θ and $\boldsymbol{u} = (u_r, u_\varphi, u_z)$ are dimensionless pressure, temperature and velocity.

Dimensionless parameters present are the Rayleigh number, $Ra = \frac{\beta g d^3 \Delta\theta}{\kappa\nu}$, and the Prandlt number $Pr = \nu/\kappa$, where $g, d, \kappa, \nu, \Delta\theta$ represent the gravitational acceleration, the spacing between parallel plates, the thermal diffusivity, the kinematic viscosity and the mean temperature difference between plates respectively. The Rayleigh number measures the relative importance between the buoyant and viscous forces.

The top and bottom walls are assumed to be no slip and kept at constant temperatures.

$$\mathbf{u} = 0, \quad \theta = \theta_b(r) \quad \text{at } z = 0, \tag{4a}$$

$$\mathbf{u} = 0, \quad \theta = 0 \quad \text{at } z = 1. \tag{4b}$$

The bottom wall temperature $\theta_b(r)$ is

$$\theta_b(r) = \frac{2}{\sqrt{\pi}} \frac{\Gamma\sqrt{\frac{1}{2\sigma^2}}}{\mathrm{erf}(\Gamma\sqrt{\frac{1}{2\sigma^2}})} e^{-\frac{r^2}{2\sigma^2}}, \tag{5}$$

where σ is the standard deviation of the temperature at the wall and $\Gamma = \mathrm{R}/\mathrm{d}$ is the aspect ratio, i.e. length R over height d of the domain. $\theta_b(r)$ satisfies for all values of σ that

$$\int_0^\Gamma \theta_b(r)\, dr = 1 \text{ and } \Delta\theta = 1. \tag{6}$$

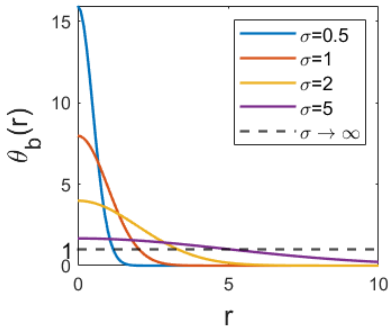

FIG. 1. The bottom wall temperature θ_b as a function of σ and r.

We illustrate in Fig. 1 the temperature distribution $\theta_b(r)$ on r for different values of σ. Since we work in cylindrical coordinates, the symmetry axis boundary conditions are defined as

$$\mathrm{u_r} = \frac{\partial \mathrm{u_z}}{\partial \mathrm{r}} = 0, \quad \frac{\partial \theta}{\partial \mathrm{r}} = 0 \quad \text{at } r = 0. \tag{7}$$

The outer boundary is

$$\mathbf{u} = 0, \quad \frac{\partial \theta}{\partial \mathrm{r}} = 0 \quad \text{at } r = \Gamma. \tag{8}$$

A linear stability analysis (LSA) is conducted to investigate the stability of 2D axisymmetric base flow solution $(\boldsymbol{u}, p, \theta)$ under 3D small perturbations.

III. RESULTS AND DISCUSSIONS

FreeFem++ [5] is the software used for solving equations numerically using the Finite Elements approach. The Newton-Raphson iteration method is used for computing the base flows. The critical Rayleigh number Ra_c , i.e. the onset of instability, for uniform bottom heating (i.e. $\theta_b = 1$) is 1708 [2]. In the present study, the Rayleigh number is set to $Ra = 1000$, which is then stable for $\theta_b = 1$, to investigate how changing the distribution of $\theta_b(r)$ effects the stability of the system by changing σ. The Prandlt number is set to $Pr = 1$.

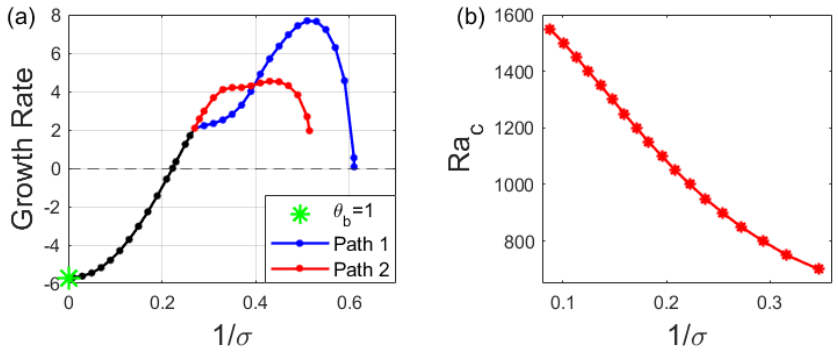

FIG. 2. (a) $m = 0$ mode LSA results for $Ra = 1000$; (b) The critical Rayleigh number Ra_c vs $1/\sigma$.

We illustrate in Fig. 2 (a) the growth rate of the azimuthal wave number $m = 0$ mode in function of $1/\sigma$. It appears that the system gets unstable when $1/\sigma = 0.223$ is exceeded at $Ra = 1000$, which is much smaller than the critical Rayleigh number for the classic Rayleigh-Bénard problem.

We found that there exist two different base flow solutions satisfying the same set of governing equations and boundary conditions if $1/\sigma > 0.27$, similarly to what found by Boronska & Tuckerman [2]. These two solution branches are indicated as path 1 and path 2. Both branches tend to achieve a maximum in the instability before a clear stabilization for relatively large values of $1/\sigma$. A careful analysis of the initial guess of the Newton-Raphson iteration is needed to follow one of the two paths.

The neutral curve representing the threshold of instability is shown in Fig. 2 (b). We observe that the critical Rayleigh number varies with $1/\sigma$ before reaching a saturation around $Ra = 700$. At Rayleigh numbers lower than that of the saturation, the system is stable for all values of σ. This means that for $Ra < 700$, the destabilization is no longer triggered by the changes in the bottom wall heating concentration.

We have shown that introducing a non-uniform heating, such as Gaussian distribution for temperature at the bottom wall can trigger the instabilities at Rayleigh numbers smaller than those of the classic Rayleigh-Bénard convection with a saturation limit.

[1] E. L. Koschmieder, Instabilities in fluid dynamics, *Synergetics,* 70–78. (1977).

[2] M. Wanschura, H. Kuhlman and H. Rath, Three-dimensional instability of axisymmetric buoyant convection in cylinders heated from below, *Journal of Fluid Mechanics, 326,* 399-415 (1996).

[3] K. Boronska and L. Tuckerman, Standing and travelling waves in cylindrical Rayleigh–Bénard convection*, Journal of Fluid Mechanics*, 559, 279 (2006)

[4] S. M. Mousavi, I. Kasianiuk, D. Kasyanyuk, S. K. Velu, A. Callegari, L. Biancofiore and G. Volpe, Clustering of janus particles in an optical potential driven by hydrodynamic fluxes, *Soft Matter, 15*(28), 5748–5759 (2019).

[5] P. Meliga, and F. Gallaire, Control of axisymmetric vortex breakdown in a constricted pipe: Nonlinear steady states and weakly nonlinear asymptotic expansions, *Physics of Fluids, 23(*8), 084102 (2011).

Kapitza instability of Nusselt's condensation film

Simeon Djambov[1] and François Gallaire[1]

[1] *Laboratory of Fluid Mechanics and Instabilities, École Polytechnique Fédérale de Lausanne, 1015 Lausanne, Switzerland,* simeon.djambov@epfl.ch, francois.gallaire@epfl.ch

A quiescent, saturated vapour condenses onto a uniformly cooled, inclined plate and forms a laminar, incompressible, gravity-driven film flow of Newtonian liquid of constant material properties (fig. 1). We set out to investigate the linear stability of Kapitza waves on this film's free surface [1]. We perform our analysis in the framework of the one-sided model, whereby we consider the vapour phase as mechanically passive [2].

In Nusselt's pioneering theory, the effect of condensation is twofold: with respect to energy conservation, through its associated latent heat, and, crucially, with respect to mass conservation, where it acts as a source. This makes the basic flow one of a spatially developing nature – the film's thickness scales as the streamwise position to the power of *1/4* [3].

We make the problem dimensionless by rescaling all distances with a characteristic length H_N, which we choose as the equality of the streamwise position with the film thickness at that position (fig. 1); we use a hydrostatic pressure scale, a viscous velocity scale from Poiseuille's law, and recast the temperature field from *0* on the wall to *1* on the interface.

As regards the local linear stability, *i.e.* in the quasi-parallel approximation, condensation appears to damp perturbations. Since thinner liquid layers promote heat transfer, vapour tends to condense more in the perturbation's throughs rather than on the crests, thus stabilising the system. The threshold for the onset of local linear instability corresponds to larger Reynolds numbers, comparing the flow's inertia and viscosity, than in the classical thin-film flow, without condensation.

A higher Jakob number, measuring sensible to latent heat, which characterises a cooler plate and, hence, improved condensation, increases the critical Reynolds number. Nevertheless, it also ensures that the basic flow thickens – and reaches this local instability criterion – faster, ultimately shortening the critical streamwise distance for the emergence of waves.

Thanks to the convective nature of the instability, the spatial problem is well-posed. We seek to establish the system's response to a harmonic forcing of real angular frequency ω. The linearised, quasi-parallel perturbation evolution equations are a quadratic eigenvalue problem for the wave number k, the solution

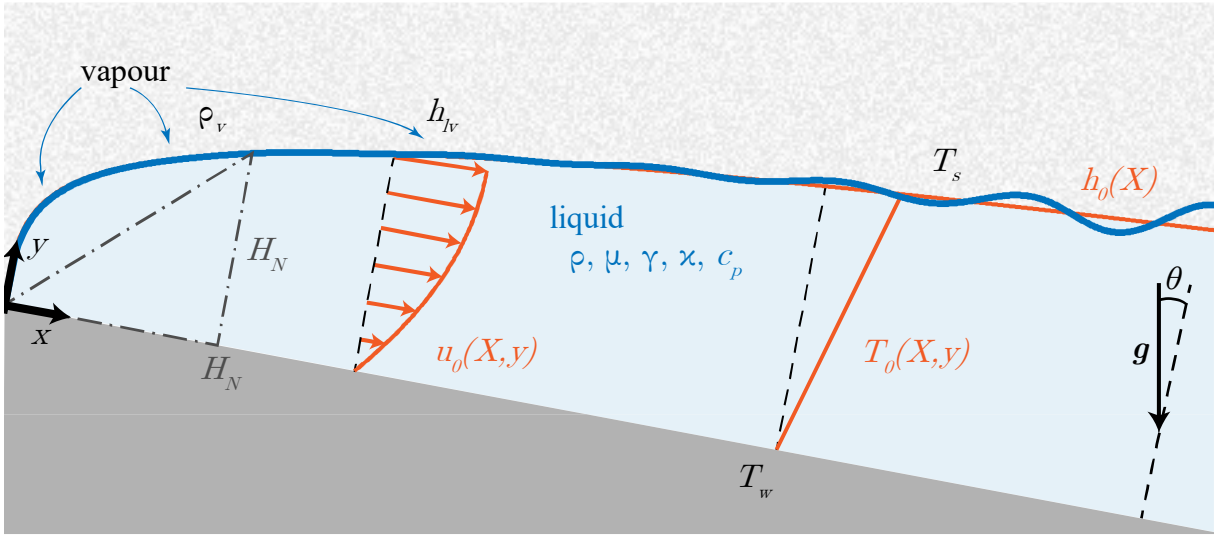

FIG. 1 A sketch of the problem at hand. The basic flow is represented in orange.

[1] P. L. Kapitza, *Wave flow of thin layers of viscous fluid: I. Free flow*, Zh. Eksp. Teor. Fiz. **18**, 3 – 18 (1948).

[2] A. Oron, S. H. Davis, S. G. Bankoff, *Long-scale evolution of thin liquid films*, Rev. Mod. Phys. **69**(3), 931 – 980 (1997).

[3] W. Nusselt, *The surface condensation of water vapour*, Z. Ver. Dtsch. Ing. **60**(27), 541 – 546 (1916).

to which produces the spatial dispersion relation. For waves propagating in the direction of the flow, the negative imaginary part of the wave number is the spatial growth rate, and vice versa. It turns out that only one spatial branch, associated to downstream-propagating waves, becomes locally linearly unstable. This is the spatial Kapitza instability.
The analysis also shows that the forcing frequency, to which the system is locally most receptive, increases downstream, while the associated wave number remains almost constant. Furthermore, a separation of scales between these perturbation wavelengths and the basic flow's evolution length makes the weakly non-parallel approach suitable. We introduce a "slow" streamwise coordinate X, which captures the basic flow's streamwise dependence, and integrate the locally computed, quasi-parallel spatial dispersion relations along it (fig. 2). Before reaching the critical streamwise distance, the perturbations decrease in magnitude (see inset). This critical distance is longer for larger forcing frequencies. After the onset of instability, the perturbations grow in a sub-exponential manner, as the local spatial growth rates decrease downstream. One by one, larger forcing frequencies take precedence. Thereafter, following the WKB method [4], a first order expansion in the slow streamwise coordinate produces a correction to these spatial gains, which we compare to a global resolvent analysis, similar to Viola *et al.* (2016) for the growth of instabilities in spatially developing swirling wakes [5]. This enables us to predict the linearly most amplified inlet forcing frequency.
The approach can also be extended to other weakly non-parallel thin film flows, for instance a rain-fed falling film, the thickness of which scales as the streamwise position to the power of *1/3*.

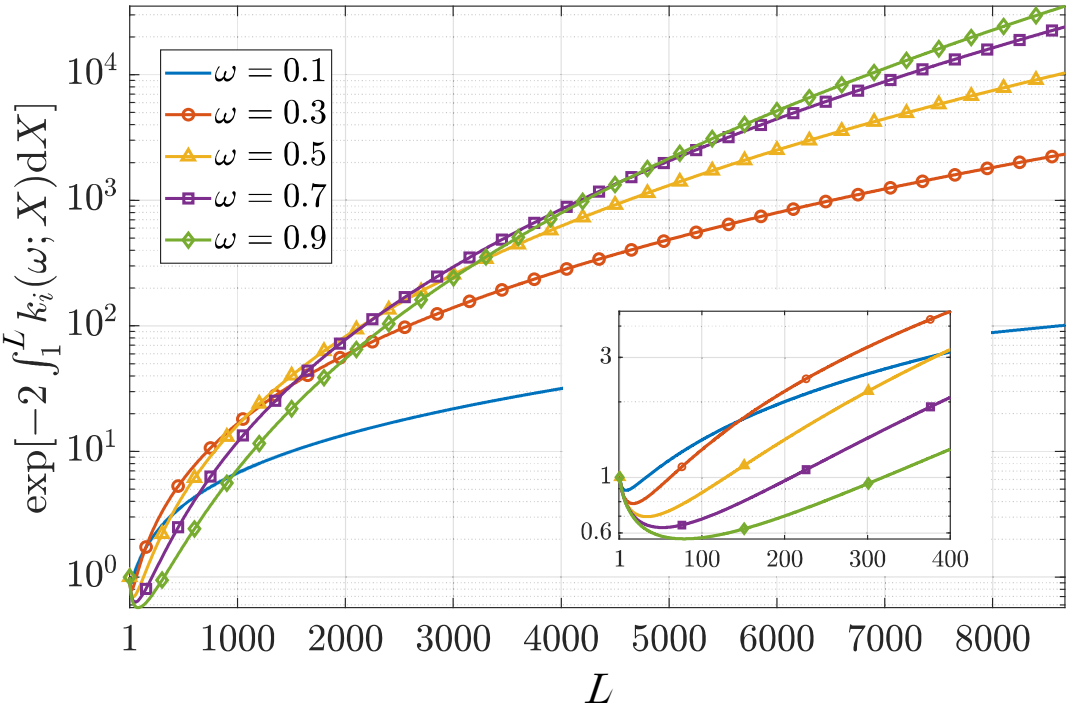

FIG. 2 Spatial gain. Material properties of water, inclination angle $\theta = \pi/4$, Jakob number $Ja \approx 18$, describing a cooling of *10*K. $\omega = 0.1$ corresponds to around $80\mathrm{s}^{-1}$ and the largest dimensionless plate length $L \approx 8700$ scales to *1*m.

[4] P. Huerre, M. Rossi, *Hydrodynamic instabilities in open flows*: "Hydrodynamics and Nonlinear Instabilities", edited by C. Godrèche and P. Manneville, 81 – 294 (1998).
[5] F. Viola, C. Arratia, F. Gallaire, *Mode selection in trailing vortices: harmonic response of the non-parallel Batchelor vortex*, J. Fluid Mech. **14**(790), 523 – 552 (2016).

A thin film model for surfactant-mediated electrowetting: Role of bulk and surface charges

Shreyank Goel[1] and Dipin S. Pillai[2]

[1] *Department of Chemical Engineering, IIT Kanpur, 208016, India shreyank20@iitk.ac.in*
[2] *Department of Chemical Engineering, IIT Kanpur, 208016, India dipinsp@iitk.ac.in*

I. Abstract

Miniaturization is a necessity in today's world. Size reduction through the advent of microfluidics has facilitated the integration and intensification of multiple processes over a single microfluidic chip. In droplet-based microfluidics, the incorporation of an external electric field provides control over the mixing, transport, and manipulation of droplets. The electrowetting behavior of a charge-carrying, surfactant-loaded sessile droplet is important for applications like point-of-care diagnostics. In biomedical assays, droplets with charged molecules like dissolved ions, proteins, and DNA are often used. In addition, the majority of biological samples examined during point-of-care diagnostics are biofluids with dissolved salt and surfactants, e.g. respiratory droplets comprising protein (mucin), salt (NaCl), and surfactant (dipalmitoylphosphatidylcholine) in addition to water, which is anticipated to have a significant impact on electrowetting. In this work, we develop two reduced-order models for electrowetting of a sessile droplet under a closed co-planar configuration. The weighted residual integral boundary layer (WRIBL) method is used to obtain evolution equations that describe how the liquid-air interface and the depth-integrated flow rate change over time and space. The solutions to the evolution equations are obtained numerically using the spectral collocation method.

In the first part, we investigate the role of domain charges, characterized by the Debye length, on droplet wetting. Under low relaxation time scales, both droplet deformation and wetting alteration under an AC field are shown to be equivalent to that under a root-mean-square (RMS) DC field. We show that a charge-carrying electrolytic sessile droplet can exhibit a larger deformation in comparison to the two asymptotic limits of a perfect-conductor and perfect-dielectric droplet, corresponding respectively to very low and high Debye lengths. The effect of several other parameters such as the inherent equilibrium wettability, permittivity ratio, and electric field strength are also investigated.

In the second model, an insoluble surfactant-laden leaky dielectric droplet is considered. We show that the competition between the charge relaxation and forcing timescales governs the charge buildup at the interface, and consequently determines the equivalence between periodic and steady forcing. The presence of surfactants and the associated Marangoni flow is shown to delay the interfacial charge buildup. While the mean droplet deformation under AC forcing remains the same as that under DC forcing, the amplitude of droplet oscillation is shown to be significantly damped by the surfactants.

II. Figures

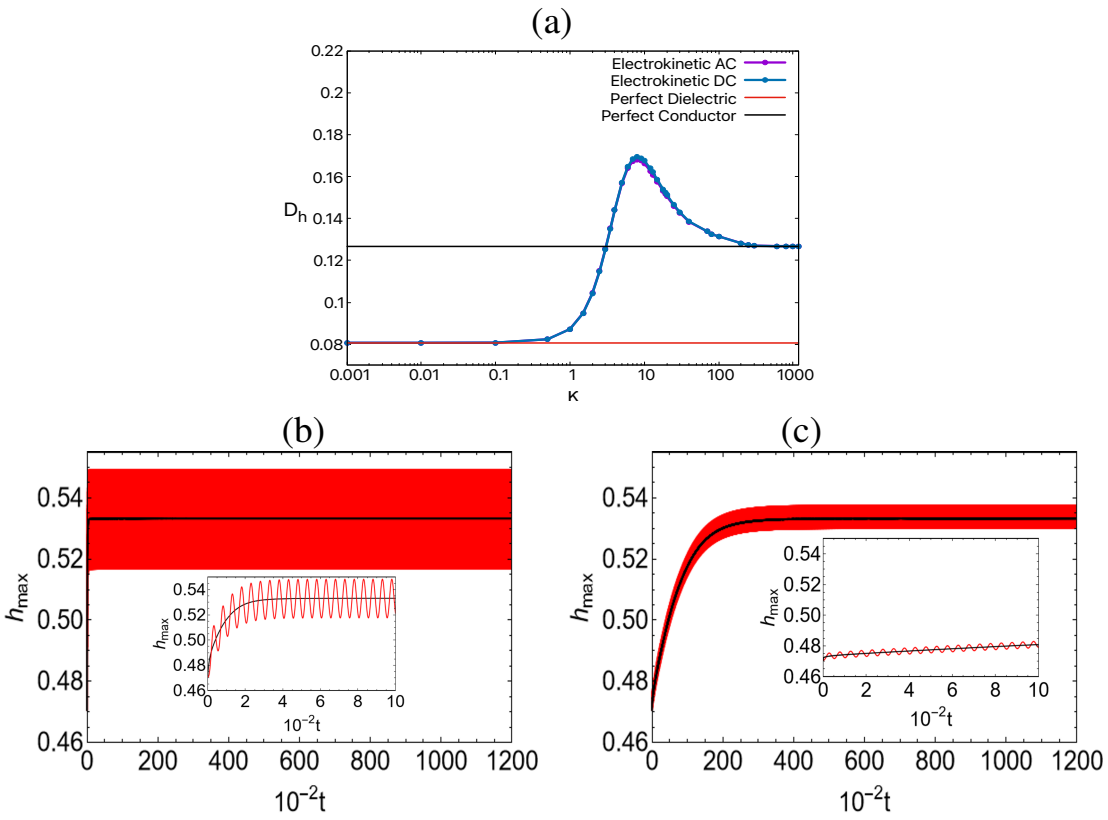

Figure 1: **(a)** Variation in droplet deformation (D_h) with inverse Debye length (κ) for AC and RMS DC forcing. The two asymptotic limits of perfect dielectric (PD) and perfect conductor (PC) are also depicted. The dimensionless parameters are $Re = 1,\ S = 20,\ E = 10\ (AC),\ E = 5\ (DC),\ \varepsilon_{12} = 6,\ \kappa = 0.001\ (PD),\ \kappa = 1000\ (PC)$. The temporal variation of maximum droplet height for both AC and DC forcing is plotted for **(b)** $Ma = 0$, **(c)** $Ma = 3$. It can be seen that the presence of surfactants decreases the amplitude of oscillations and delays the time to achieve steady state. However, the steady mean amplitude achieved by the droplet is unaffected. The dimensionless parameters are $Re = 0.1,\ E = 5(DC),\ E = 10(AC),\ S = 20,\ Ca = 1,\ Pe = 300,\ Oc = 0.01,\ \sigma = 10,\ \varepsilon_{12} = 2$.

Nonlinear dynamics and control of a thin liquid film on a spinning ellipsoid

Selin Duruk[1], Ross Shepherd[1], Mathieu Sellier[1] and Edouard Boujo[2]

[1] *Department of Mechanical Engineering, University of Canterbury, Christchurch, New Zealand*
Mathieu.sellier@canterbury.ac.nz
[2] *Laboratory of Fluid Mechanics and Instabilities, EPFL, Lausanne, Switzerland*

Covering a surface with a thin coating layer which may serve a protective, a functional, or a decorative purpose is routine in many industrial processes. Many coating processes have been optimized to obtain quality coatings on flat, rigid surfaces. In spin coating, for example, the centrifugal force is used to distribute the dispensed fluid uniformly on a rotating surface. Spin coating on a flat surface has benefited from decades of research is therefore a well-established process [1]. Achieving a quality coating on a complex-shaped substrate is, however, more challenging because of the interplay between the fluid film, the substrate shape and its motion kinematics resulting from translation and/or rotation. We are interested here in the dynamics of a thin liquid film on an arbitrary-shaped surface subject to rotation around a vertical axis.

The goal of this study is to extend the work presented in [2] considering the dynamics of a thin film on an axisymmetric spinning spheroid to non-axisymmetric substrates. The governing equations for a thin liquid film deposited on a smooth closed surface of a substrate rotating around its vertical axis at constant angular velocity are presented and the corresponding lubrication model is derived as an extended version of the equation presented in [3]. These governing equations are solved numerically in the commercial Finite Element package COMSOL 5.6 using the General Form PDE interface.

We particularly focus on the thin film flow on a spinning ellipsoid as an archetypical example of a non-axisymmetric and non-constant curvature substrate. A parametric analysis is also performed to shed light on the effect of the centrifugal force on two basic ellipsoidal substrates, namely a disk-like and a rugby ball-like substrate.

As an illustration of the capability of the model we developed and implemented, FIG. 1 shows the contours of film thickness on a rugby ball like substrate for increasing rotation starting from the stationary case. The results confirm that in the absence of rotation, the fluid thins in the upper hemisphere and thickens in the southern one as substrate curvature and gravity compete to redistribute the fluid around the “rugby ball”. Clear minima and maxima develop on the prime meridian of the surface. Introducing rotation is seen to move the maxima closer to the equator and to increase the magnitude of the peak as the angular velocity is increased. These peaks would eventually develop into liquid ligament as the angular velocity is further increased which would eventually break-up into satellite droplets.

In this talk, we will also propose a methodology to evaluate the required body force vector that would lead a uniform thin liquid film coating on an arbitrary substrate. We present a generic equation to test the linear stability of the homogeneously disturbed film on a substrate of arbitrary shape and define the stability criteria with respect to the forcing term in the normal direction. This could inform future strategies to develop coating processes leading to a uniform film thickness on complex-shaped surfaces.

[1] Sahu, N., Parija, B., & Panigrahi, S. (2009). Fundamental understanding and modeling of spin coating process: A review. Indian Journal of Physics, 83(4), 493-502.

[2] Duruk, S., Boujo, E., & Sellier, M. (2021). Thin liquid film dynamics on a spinning spheroid. Fluids, 6(9), 318.

[3] Thiffeault, J. L., & Kamhawi, K. (2006). Transport in thin gravity-driven flow over a curved substrate. arXiv preprint nlin/0607075.

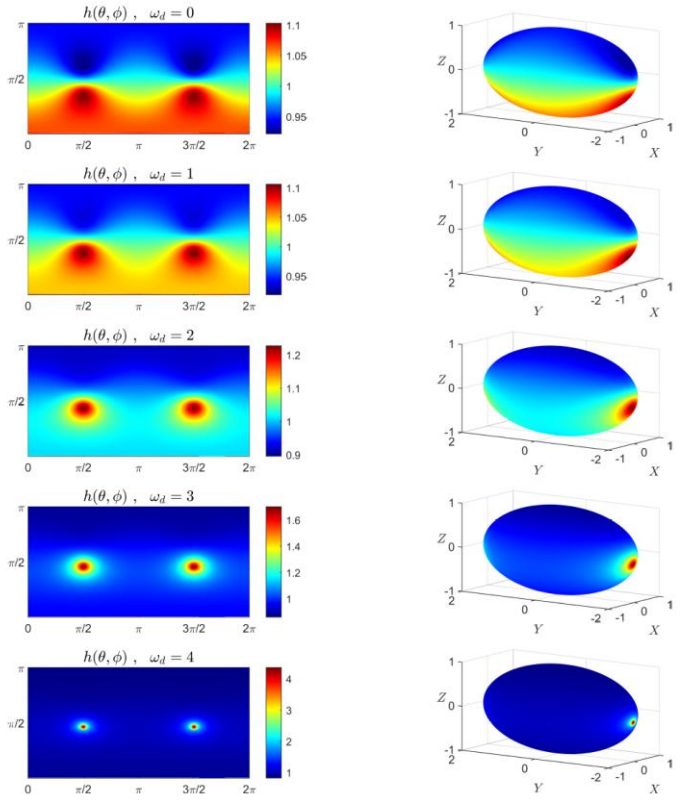

FIG. 1: Steady film thickness distribution on a rotating non-axisymmetric rugby ball-like substrate, for increasing angular velocity $\omega_d = 0, 1, 2, 3, 4$ (top to bottom). Left: in the (θ, ϕ) plane. Right: Film thickness contours on the substrate.

Steady Flows Generated by Oscillations of Centrifuged Liquid–Liquid Interface in Rotating Cylinder

Olga Vlasova[1], Ivan Karpunin[1] and Nikolai Kozlov[1]

[1] *Laboratory of Vibrational Hydromechanics, PSHPU, 614990, Perm, Russia,* kozlovn@pspu.ru

Oscillations of interface between two immiscible phases noticeably affect the mass transfer by steady streaming [1, 2]. The oscillations themselves may occur in the form of waves or, for instance, quasi-stationary ("frozen") relief. The fluid motion that follows produces an inhomogeneity in the velocity distribution along the interface resulting in the generation of the average vorticity in the boundary layers adjacent to the interface.

In rotating fluids the forces of inertia play an important role in the excitation of fluid inertial oscillations. In the cylindrical core-annular flow rotating about a horizontal axis, radial core shift is observed [3, 4]. This leads to the generation of steady streaming [4, 5], which brings the interface in the lagging differential rotation with respect to the container. The driving force in this case is the gravity whose rotation relative to the container makes the fluid oscillate. The theoretical findings [1, 2] predict the appearance of tangential velocity discontinuity at the oscillating interface, on the limits of the boundary layers.

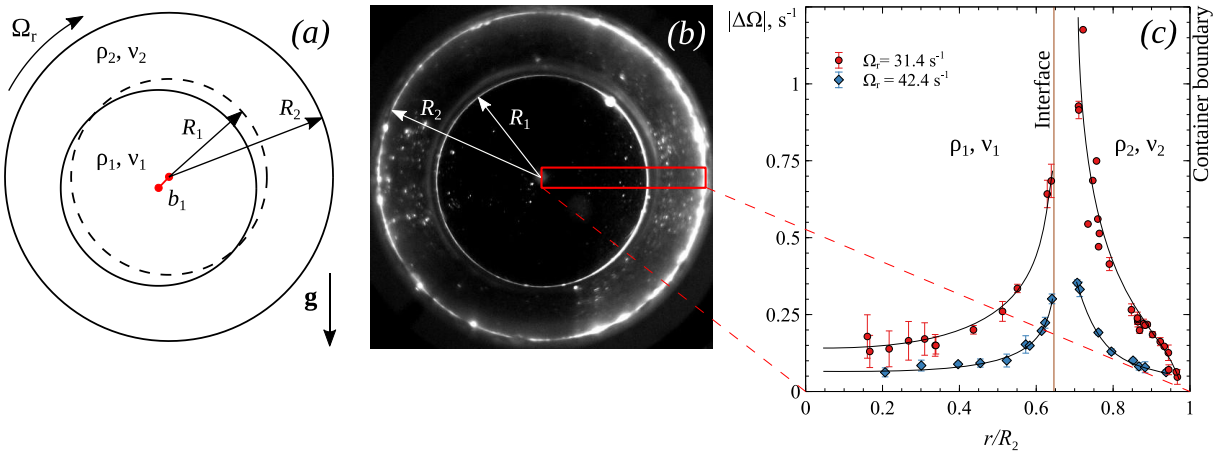

FIG. 1. *a*) Schematic of the steady radial displacement of the light liquid column (b_1 is exaggerated). *b*) Photograph of the centrifuged two-liquid system illuminated with a laser light sheet, viewed along the cylinder axis. The container is rotating clock-wise with $\Omega_r = 31.4\ \mathrm{s}^{-1}$, the relative core volume is $R_1^2 / R_2^2 = 0.40$. *c*) Profiles of the angular velocity of the azimuthal steady streaming. Experimental points are fitted with Bézier curves that serve to guide the eye.

In the present work the steady flows are studied experimentally in a rotating two-phase system formed by centrifuged immiscible liquids (Fig. 1). The cylindrical container is oriented horizontally, so that the gravity vector is perpendicular to the rotation axis (Fig. 1(*a*)). The rotation rate Ω_r is set sufficiently high so as to maintain the core-annular distribution of liquids and circular shape of the interface (Fig. 1(*b*)). The images of the liquids are taken with a high-speed camera through the

[1] D. Dore, On mass transport Induced by interfacial oscillations at a single frequency, Proc. Camb. Phil. Soc. **74**, 333–347 (1973).

[2] D. V. Lyubimov, T. P. Lyubimova and A. A. Cherepanov, *Dynamics of interfaces in vibration fields*, FizMatLit, Moscow (2003) (in Russian).

[3] O. M. Phillips, Centrifugal waves, J. Fluid Mech. **7** (3), 340–352 (1960).

[4] N. V. Kozlov, A. N. Kozlova and D. A. Shuvalova, Dynamics of immiscible liquids in a rotating horizontal cylinder, Phys. Fluids **28**, 112102 (2016).

[5] R. F. Gans, On steady flow in a partially filled rotating cylinder, J. Fluid Mech. **82** (3), 415–427 (1977).

transparent front flange of the cylindrical container. Laser light sheet and the PTV technique are applied to obtain the radial profiles of the fluid angular velocity after subtracting the container angular velocity: $\Delta\Omega = \Omega_{\text{fluid}} - \Omega_{\text{r}}$ (Fig. 1(*c*)). The observation shows that the tracers are moving azimuthally, along the circular trajectories about the core axis.

The most interesting feature of the velocity profiles is that the maxima of $\Delta\Omega$ are not equal in the two liquids. The annular flow rotates faster. The gap between these maxima is approximately the width of the dynamic viscous boundary layer $\sqrt{2\nu_2 / \Omega_{\text{r}}}$. This means that the fluid velocity drop is formed on the limits of the boundary layer. This result is in good qualitative agreement with the theoretical predictions [1, 2]. As the results indicate, the cylindrical boundary layer at the interface is formed on the side of the outer liquid. Liquid in the annulus oscillates about the core while the latter moves almost solid-like. However, the core velocity profile reveals that its rotation is not solid-like, and this effect is attributed to the Ekman pumping generated by the flanges.

The results obtained may potentially find application in the intensification of mass transfer between fluids or the control of species distribution.

The work was financially supported by the Russian Science Foundation (grant 18-71-10053).

Session 12 – Acoustics and optomechanics

Thursday June 22, 11:00–12:30

The sound of a bursting soap bubble

Adrien Bussonnière[1], Arnaud Antkowiak[2], François Ollivier[2], Michaël Baudoin[3], Régis Wunenburger[2]

[1] *Matière et Système Complexes, Université Paris Cité, CNRS, UMR 7057, Paris, France*
adrien.bussonniere@cnrs.fr
[2] *Institut ∂'Alembert, Sorbonne Université, CNRS, UMR 7190, Paris, France*
[3] *IEMN, Univ. Lille, CNRS, ECLille, ISEN, Univ. Valenciennes, UMR 8520, Lille, France*

Many familiar events feature a distinctive sound: paper crumpling or tearing, squeaking doors, rain drumming on the ground or the characteristic bubbling sound of boiling water. Though hardly noticeable in our daily environment, these common place sounds carry a profusion of information about the fleeting physical processes at the root of acoustic emission.

In this talk we investigate the popping sound emitted by a bursting soap bubble [1,2] seen as a paradigm of violently evolving liquid interfaces; by making use of acoustic antennae, high speed cameras (see figure) and taking advantage of aeroacoustics conceptual framework [3], we reveal how the forces due to capillarity, Marangoni flow and out-of-equilibrium dynamics of surfactants [4] shape the acoustic signature of bursting bubbles [5]. This study provides new information on the forces exerted by interfaces, paving the way for a complement tool to study violent events.

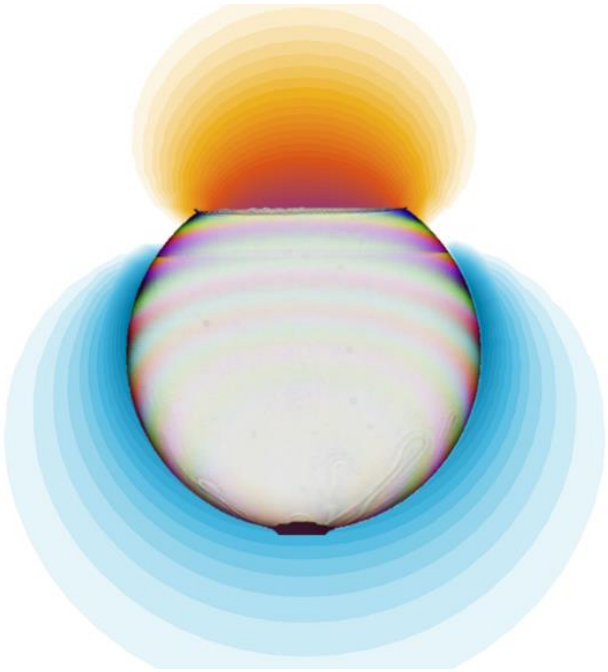

Figure: Snapshot of a soap bubble bursting associated to the acoustic field emitted: compressions are show in red scale and dilatations in blue scale.

[1] F. E. C. Culick, Comments on a ruptured soap film, J. Appl. Phys. **31**, 1128 (1960).
[2] W. R. McEntee, K. J. Mysels, The Bursting of Soap Films. I. An Experimental Study, J. Phys. Chem., **73**, 3018 (1969).
[3] M. S. Howe, Theory of Vortex Sound, Cambridge University Press, Cambridge, England, (2002).
[4] S. Frankel, K. J. Mysels, The Bursting of Soap Films. II. Theoretical Considerations, J. Phys. Chem., **73**, 3028 (1969).
[5] Bussonniere, A., Antkowiak, A., Ollivier, F., Baudoin, M., & Wunenburger, R. Acoustic sensing of forces driving fast capillary flows. Phys. Rev. Lett., **124**, 084502 (2020).

Phase Separation of Oil-in-Water Emulsion with Surface Acoustic Wave

Yifan Li[1], Joseph D'Addesa[2], Fasano Mark[2], Javier A. Diez[3], Linda J. Cummings[2],

Lou Kondic[2] and Ofer Manor*[1]

[1]*The Wolfson Faculty Department of Chemical Engineering, Technion — Israel Institute of Technology, Haifa 3200003, Israel * manoro@technion.ac.il*

[2]*Department of Mathematical Sciences, New Jersey Institute of Technology, Newark, New Jersey 07102, USA*

[3] *Universidad Nacional del Centro de la Provincia de Buenos Aires, (UNCPBA), Pinto 399, 7000, Tandil, ARGENTINA*

I. Phase Separation with SAW

We successfully separate the oil phase out of stable oil-in-water emulsion using MHz-frequency surface acoustic waves (SAWs). We place a droplet of oil-in-water emulsion atop a piezoelectric actuator – a SAW device – which supports the formation of a surface acoustic wave near the surface of the device upon the application of weak power (1 Watt). We observe the extraction of oil from the drop in a form of a film, which spread atop the SAW device, while the drop becomes increasingly transparent owing to the reduction in oil droplet concentration therein.

We successfully carried out proof-of-concept experiments with emulsion: We place 10μl drops of 10-40% oil-in-water emulsion, which are stabilized with SDS and Tween-20 (two types of surfactants), on a flat horizontal SAW device in 85% relative humidity and ambient (40-50% relative humidity) environments; see for example FIG. 1 for a 40% oil in water drop in 85% relative humidity environment. Following 6.5 minutes from the excitation of SAW in the SAW device (In addition to approximately 10 minutes in which we let the humidity equilibrate in the humidity chamber before applying SAW), we observe a 20 μm thick film of oil leave the drop and spread upon the SAW device mostly opposite to the path of the SAW. During this time, the initially opaque drop becomes continuously transparent and shrinks in size.

We find that regardless of the presence of SAW in the solid substrate (SAW device), oil droplets in the emulsion adsorb atop the solid and free surfaces of the drop to form oil films due to the oil's low surface energy. The application of SAW extract oil off the drop by the acoutowetting phenomenon: the oil film spread due to SAW induced acoustic radiation pressure and acoustic flow. Over time, we observe an increasing quantity of oil film outside the drop.

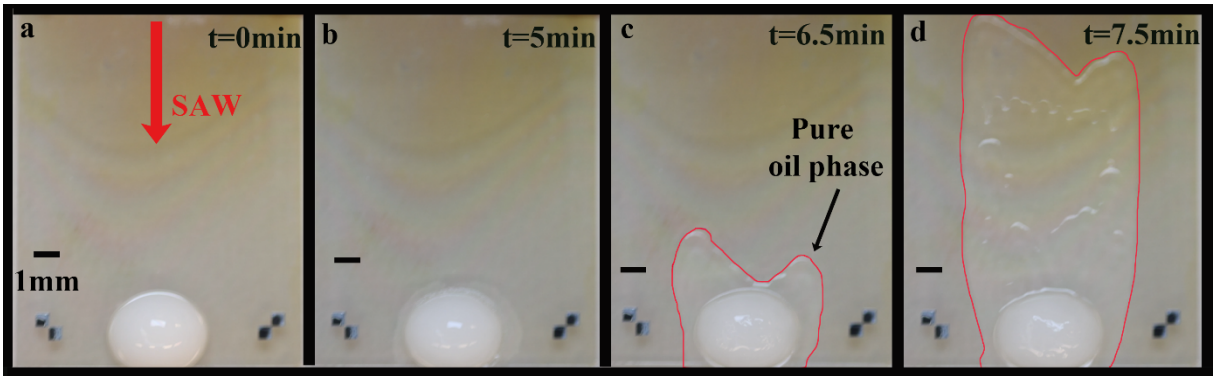

FIG. 1. Top view time laps of a sessile drop of an oil-in-water emulsion in the presence of a 20 MHz-frequency propagating surface acoustic wave (SAW) in the solid substrate (SAW device). The SAW extracts an oil film out of the drop, which continuously spreads over the substrate.

Drop impact on liquid pool: acoustics and effect of surfactants

V. Gourmandie[1], J. Pierre[2], V. Leroy[3], C. Derec[4]
[1] *Matière et Systèmes Complexes – Université Paris Cité, 75205 Paris, France* vincent.gourmandie@u-paris.fr
[2] *Institut Jean le rond d'Alembert, 75252 Paris, France* juliette.pierre@cnrs.fr
[3] *Matière et Systèmes Complexes – Université Paris Cité, 75205 Paris, France* valentin.leroy@u-paris.fr
[4] *Matière et Systèmes Complexes – Université Paris Cité, 75205 Paris, France* caroline.derec@u-paris.fr

When a drop impacts a bath an air cavity develops underwater which sometimes leads to the entrapment of a bubble when it suddenly retracts. This phenomenon is associated with a powerful acoustic emission, which everyone has experienced when dealing with a dripping faucet. It also has implication on the sound of rain [1]. The exact mechanism leading to the formation of the bubble is still unclear. It appears that the bubble is formed only for a limiting range of drop diameters and heights of fall: if the drop arrives with a speed that is too low or too high, there is no bubble. Another observation found in the literature is that the phenomenon disappears when surfactants are added to the liquid. But this effect has not been the object of a systematic study yet.

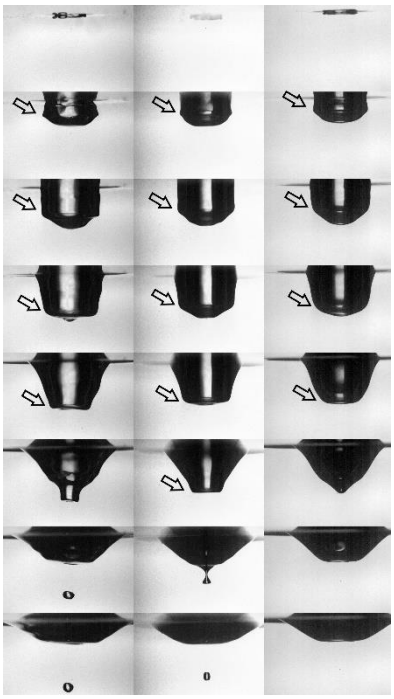

FIG. 1. Snapshots of the underwater air cavity after the impact of a 3 mm diameter droplet falling from 12 cm. The time between two successive images is 3 ms.
First column: distilled-water, 72 mN/m.
Second column: Water-ethanol mixture, 41 mN/m (15 %w).
Third column: Sodium Dodecyl Sulfate and water mixture, 65 mN/m (1.5 mM)
Arrows show the wave-like form propagating along the surface of the cavity.

We have developed an experimental setup combining fast camera recording synchronized with acoustic underwater measurement with a hydrophone. The drop velocity is modified by changing the height of fall, and systematic experiments were performed with 3 mm drops and different solutions for the drop and the bath: distilled water, water-ethanol mixtures of various concentrations, SDS-water mixtures with various concentrations. The surface tension of each solution was measured in-situ during the experiment.

Snapshots of the underwater air cavity are shown in Fig.1 during its development and its retraction, for an impacting drop of same velocity but different solutions: distilled-water (1st column), water-ethanol mixture (2nd column) and SDS mixture (3rd column). During the development of the cavity, it seems that a wave propagates along its surface (arrows) and finally focuses at its bottom. The delicate timing

[1] Pumphrey, H. C., Crum, L. A. & Bjo/rno/, L. Underwater sound produced by individual drop impacts and rainfall. The Journal of the Acoustical Society of America 85, 1518–1526 (1989).

between these two phenomena may be the key to understand bubble entrapment [2]: if the wave focuses too early or to late no bubble entrapment occurs.

Figure 1 also highlights that for the same drop diameter and impact velocity, the dynamics is modified: the entrapped bubble may have a different size or even disappear, and the wave is smoothed for SDS mixture, even for a very low concentration (much smaller than the cmc). With systematic experiments on both mixtures at various concentrations, we show that the change in the dynamics of the bubble entrainment cannot be explained by a simple modification of the surface tension.

[2] Morton, D., Rudman, M. & Jong-Leng, L. An investigation of the flow regimes resulting from splashing drops. Physics of Fluids 12, 747–763 (2000).

The Stability of a Bubble in a Power-law Liquid Subject to an Acoustic Field

S. Ilke Kaykanat[1] and A. Kerem Uğuz[2]

[1] *Department of Chemical Engineering, Bogazici University, 34342, Istanbul, Turkey,* seymenilke.kaykanat@boun.edu.tr

[2] *Department of Chemical Engineering, Bogazici University, 34342, Istanbul, Turkey,* kerem.uguz@boun.edu.tr

Ultrasound-mediated microbubble therapy is a non-invasive medical treatment. One of the main advantages of microbubble therapy is that it allows for the targeted delivery of drugs, thereby reducing the side effects of conventional treatment methods. Due to the volume oscillations of the microbubbles under the effect of an acoustic field, the permeability of blood vessels is temporarily increased, which increases the uptake of drugs into cells [1, 2]. Microbubbles are encapsulated in a lipid or protein shell to increase their lifetime in blood. In this study, the dynamics of a bubble in blood is investigated. The bubble is in an unbounded liquid (blood) and encapsulated with a shell as shown in FIG.1. For blood and bubble shell, power-law and Kelvin-Voigt constitutive laws are employed, respectively. It is assumed that blood is a compressible liquid. An external acoustic field is applied to obtain volume oscillations. In the case of small disturbances, the dispersion relation is found from the Rayleigh and energy equations. The effects of the frequency, the power-law index, and the apparent viscosity on the critical acoustic pressure amplitude, above which the bubble is unstable, are investigated.

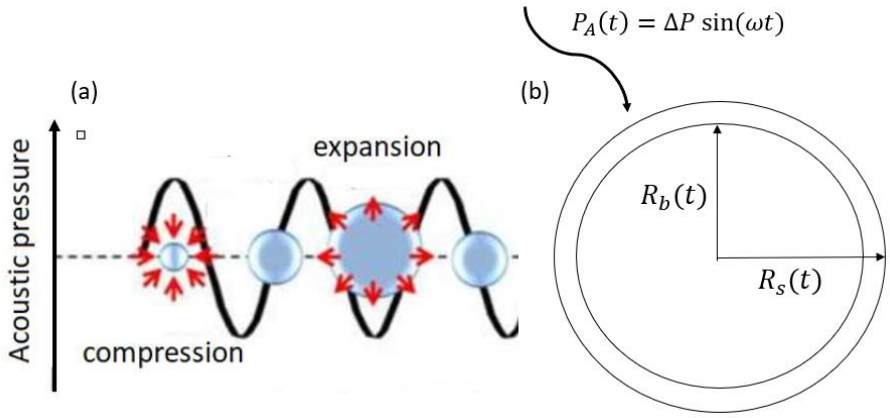

FIG. 1. Graphical illustration of (a) stable bubble oscillation under the effect of acoustic field [3] and (b) bubble encapsulated with a shell.

[1] M. Wang, Y. Zhang, C. Cai, J. Tu, X. Guo and D. Zhang, Sonoporation-induced cell membrane permeabilization and cytoskeleton disassembly at varied acoustic and microbubble-cell parameters. Scientific reports, 8(1), 3885 (2018).

[2] O. E. Mussenden, Clinical diagnosis of the extracranial cerebrovascular disease. Revista Cubana de Angiología y Cirugía Vascular, 15(2) (2014).

[3] H. L. Liu, C. H. Fan, C. Y. Ting and C. K. Yeh, Combining microbubbles and ultrasound for drug delivery to brain tumors: current progress and overview. Theranostics, 4(4), 432 (2014).

Acoustic Flow in Porous Media

Ofer Manor

Department of Chemical Engineering, Technion – Israel Institute of Technology, Haifa, Israel
manoro@technion.ac.il

We study the steady acoustic flow – acoustic streaming – to appear along the path of an acoustic stimulus – a propagating planar acoustic wave – in porous media [1]. We give new insights to previous findings of acoustic contributions to mass transport in porous media in geological (Elkhoury et al. 2006; Hamida & Babadagli 2008) and unit operation (Poesio et al. 2002; Yao et al. 2012) length scales as well as in smaller length scales of submicron- and nano-channels on lab on a chip platforms (Miansari & Friend, 2016; Guttenberg et al., 2004; Xu, 2018; Connacher et al., 2018; Ang et al., 2017; Martinez et al., 2010; Ho et al., 2011; Parolo & Merko ̧ci, 2013).

The theory is conducted by a detailed calculation of the transport of mass through cylindrical pores of arbitrary azimuth compared to the acoustic path. We consider limits of large, medium, and small pore diameters compared to the thickness of the viscous boundary layer. The boundary layer is invoked by interactions between the acoustic wave and the surface of the pores and introduces surface contributions to the overall mass transport through a porous medium. See illustration in Fig 1.

We find that for same acoustic properties in fluid and solid, the acoustic forcing for flow is equivalent to the pressure forcing throughout a porous medium in the Darcy equation in addition to a correction to account for the azimuth between the acoustic path and pores. However, in the general case, where the acoustic properties of the fluid deviate from the solid, the acoustic forcing for flow is further associated with surface effects. The latter render the similarity to the Darcy equation non-trivial. The rate of acoustic streaming in the rigid porous frame limit is found to be connected to the Strouhal number and acoustic Reynolds number.

Recent experiment, which was inspired by the theory, shows flow in paper based porous media along the path of a MHz-frequency acoustic wave.

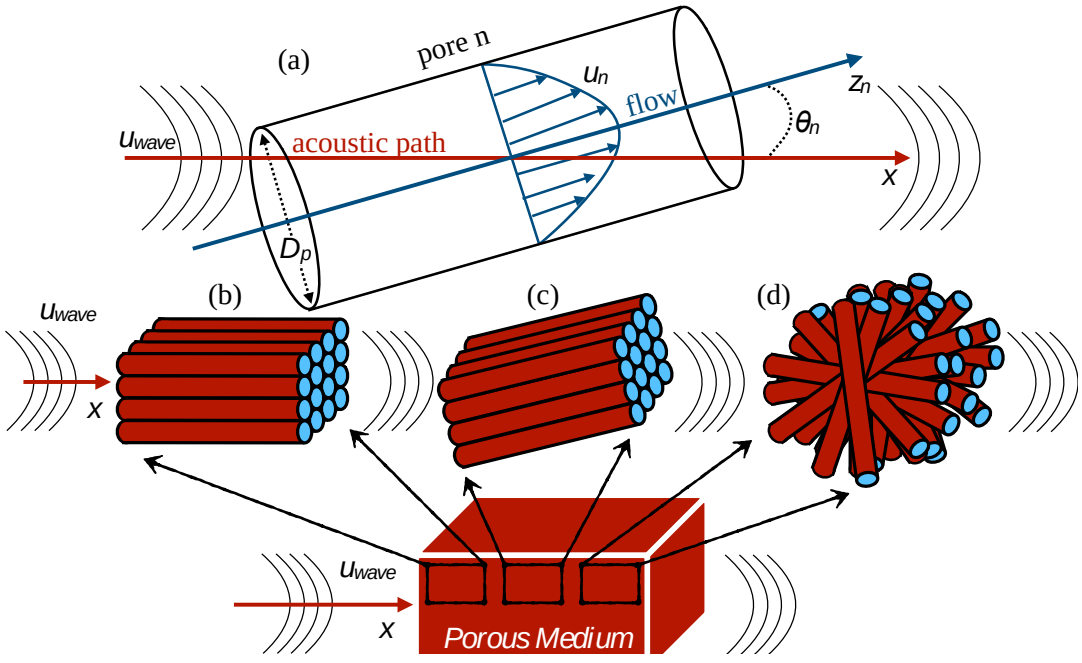

Fig 1: An illustration of (a) pore n, of diameter D_p, which is oriented along the axial axis, z_n, and supports an axial flow component, u_n; both are at an angle, θ_n, with respect to the path of an acoustic wave, x; stack of pores may be aligned (b) along (c) askew, or (d) randomly with respect to the acoustic path.

[1] O. Manor, Acoustic flow in porous media, J. Fluid Mech. **920**, A11 (2021).
doi:10.1017/jfm.2021.436

Opto-capillary deformation of fluid interfaces

David Rivière, Matthieu Robert de Saint Vincent, Hamza Chraibi, Ulysse Delabre and Jean-Pierre Delville

Univ. Bordeaux, CNRS, LOMA, UMR 5798, Talence F-33400, France, jean-pierre.delville@u-bordeaux.fr

Deformations of liquid free surfaces, resulting from the tangential stresses triggered by a thermal gradient, are known for decades[1] with applications in micro-flows[2] and welding.[3] For instance, assuming a negative variation of the surface tension with temperature, Marangoni stresses produce a dimple in the liquid. The extension to an interface separating two liquids has been much less investigated; depending on the fluids, thermocapillary stresses may induce either a dimple or a bump. We would like to rationalize this general situation using continuous lasers as local heating sources. Lasers are indeed very appealing to trigger thermocapillary flows because (i) optical focusing at absorbing liquid interfaces can be strong and then produce very large thermal gradients while keeping reasonable overheating and, (ii) laser excitation is contactless and easy to displace so that the method offers a lot of versatility. We used either a visible laser after adding a dye in the solution or directly an infrared laser when water was involved. We investigate Marangoni deformations either of interfaces at rest (Figure 1) or interfaces flowing in a microchannel (Figure 2). After describing laser heating,[4] we show analytically and numerically,[5] and demonstrate experimentally[6] that interface deformations triggered by opto-capillarity depend on both the viscosity contrast and the ratio between the liquid layer heights. Finally, we show that the large thermal gradients offered by laser light excitation allow to break the stability on an interface, either at rest by forming a thermocapillary jet, or when flowing by controlling the thread-to-droplet transition for digital microfluidics.

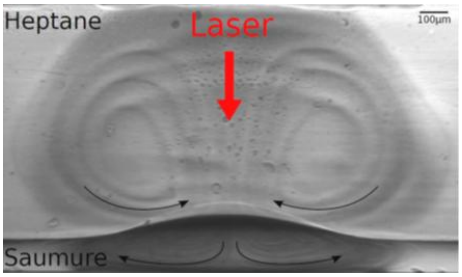

FIG. 1: Opto-capillary interface deformation triggered by an infrared laser-heating of a brine layer in contact with a non-absorbing alkane layer.

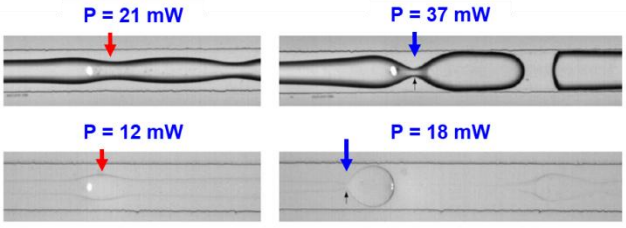

FIG. 2: Opto-capillary interface pinching and bumping of a water-in-oil liquid thread flowing in a microchannel, when varying the viscosity ratio or the confinement: thick threads pinch while thinner ones bulge, as indicated by the red arrows.

[1] J. C. Loulergue, P. Manneville, Y. Pomeau. Interface deflections induced by the marangoni effect: an application to infrared visible image conversion. J. Phys. D 14, 1967 (1981).
[2] A. A. Darhuber, S. M. Troian. Principles of microfluidic actuation by modulation of surface stresses. Annu. Rev. Fluid Mech., 37, 425-455 (2005).
[3] A. P. Mackwood, R. C. Crafer. Thermal modelling of laser welding and related processes: a literature review. Opt. Laser Technol. 37, 99 (2005).
[4] D. Rivière, B. Selva, H. Chraibi, U. Delabre, J. P. Delville. Convection flows driven by laser heating of a liquid layer. Physical Review E, 93(2), 023112 (2016).
[5] H. Chraïbi, J. P. Delville, Thermocapillary flows and interface deformations produced by localized laser heating in confined environment. Physics of Fluids, 24(3), 032102 (2012).
[6] M. Robert de Saint Vincent, H. Chraibi, J. P. Delville. Optical flow focusing: Light-induced destabilization of stable liquid threads. Physical Review Applied, 4(4), 044005 (2015).

Session 13 – Thermal effects

Thursday June 22, 14:00–16:00

Mathematical Model for a Non-Isothermal Dense Nanofluid

Raj Gandhi[1], Alexander Oron[2], and Alexander Nepomnyashchy[1]

[1] *Department of Mathematics, Technion-Israel Institute of Technology, 3200003, Haifa, Israel,*
raj.gandhi@campus.technion.ac.il (R. Gandhi), nepom@technion.ac.il (A. Nepomnyashchy)
[2] *Department of Mechanical Engineering, Technion-Israel Institute of Technology, 3200003, Haifa, Israel,*
meroron@technion.ac.il (A. Oron)

Abstract

Nanofluids are engineered colloidal mixtures made of nanoparticle (1-100nm diameter) suspension in a base liquid. We develop a mathematical model for dense nanosuspension subjected to temperature and bulk nanoparticle concentration gradients in the presence of the Soret effect in the gravity field. A highly concentrated configuration of alumina nanoparticles suspended in water is considered in this work. The nanoparticles in a dense concentration configuration interact with each other via the van der Waals force. The nanoparticle interaction contributes to the governing equations as the osmotic pressure. In our model, we neglect the contribution of the viscosity gradient and shear-induced particle migration due to $Pe \ll 1$, and that of the shear rate to the particle flux. It is inferred from the literature that all thermophysical properties of a nanofluid strongly depend on the bulk nanoparticle concentration, and these experimental data are incorporated into our mathematical model.

We consider a nanofluid layer deposited on a planar horizontal solid substrate and heated by a specified heat flux, as shown in fig.1. The layer is exposed to the ambient atmosphere at its free deformable interface. Nanoparticles are present in the bulk and on the interface, and their dynamics are linked by interfacial kinetics. Due to the presence of the Soret effect, the gradients of temperature and bulk nanoparticle concentration are coupled. We exemplify the thermosolutal coupled quiescent steady states for pressure, temperature, and bulk nanoparticle concentration, presented in fig.2. We find that for low values of the heat flux introduced to the system, the variations of the steady state components are linear with height. However, these variations become nonlinear when this heat flux increases. Furthermore, we illustrate a non-zero effect of nanoparticle interactions on the interfacial pressure.

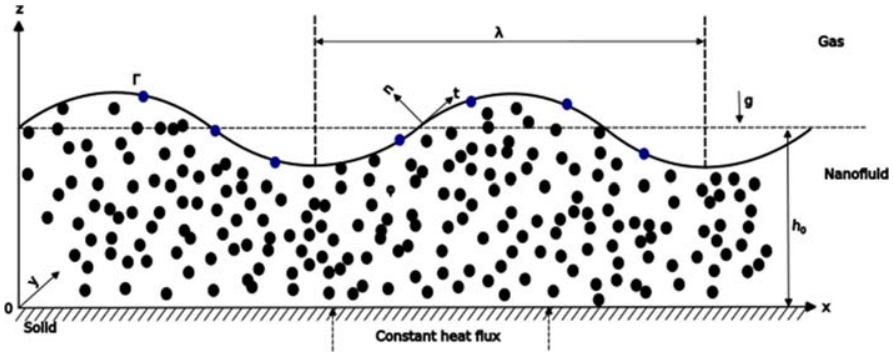

FIG. 1. Sketch of the nanofluid layer on the solid substrate subjected to a constant heat flux through the substrate.

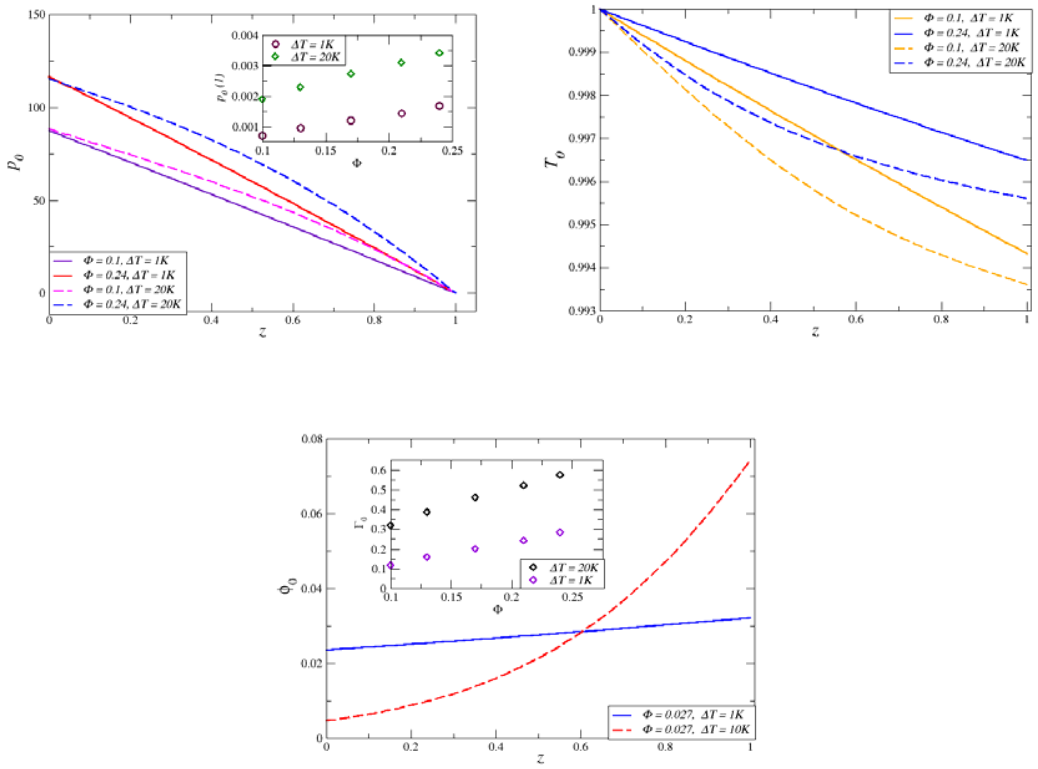

FIG. 2. Variation of the quiescent steady state components of the system with height z. Top row: pressure p_0 (left) and temperature T_0 (right) for the average bulk nanoparticle concentration $\Phi = 0.1$ and $\Phi = 0.24$ at $\Delta T = 1$K and $\Delta T = 20$K. Inset: interfacial pressure variation $p_0(1)$ with the average bulk nanoparticle concentration Φ ; Bottom row: bulk nanoparticle concentration Φ_0 for the average bulk nanoparticle concentration $\Phi = 0.027$ at $\Delta T = 1$K and $\Delta T = 10$K. Inset: variation of the interfacial nanoparticle concentration Γ_0 with the average bulk nanoparticle concentration Φ.

Acknowledgments. This research has been funded by the European Union's Horizon 2020 research and innovation program under the Marie Skłodowska-Curie grant agreement No 955612.

Joule heating-induced thermal convection in a three-layer liquid system

Harunori N. Yoshikawa,[1] Anupam Hiremath[2] and Innocent Mutabazi[2]

[1] *Université Côte d'Azur, CNRS, Institut de Physique de Nice, 06100 Nice, France* harunori@unice.fr
[2] *Normandie Université, UNIHAVRE, CNRS UMR 6294, Laboratoire Ondes et Milieux Complexes, 76058 Le Havre, France*

Research interest in liquid metal batteries has been renewed because of its high potential as an efficient and durable energy storage device [1]. A battery consists of two liquid-electrode layers separated by an intermediate electrolyte layer. During charging and discharging operations of a battery, stationary liquid layers are subject to different instability mechanisms: magnetohydrodynamic [2 , 3] and thermal [2 , 4] ones due to electric current flowing through the layers. The characterizations of these instabilities are of primordial importance for efficient and safe operation of this promising energy storage device.

We investigate the thermal instability provoked by the temperature gradient that is generated by the Joule heating in the electrolyte layer (Fig. 1). A linear stability analysis is performed to determine the critical values of the Rayleigh number

$$\mathrm{Ra} = \frac{\alpha \Delta T g (H/2)^3}{\nu \kappa} \quad \text{with} \quad \Delta T = \frac{J_0^2 H^2}{4\sigma\lambda},$$

and the critical eigenfunctions, where α is the coefficient of thermal expansion of the electrolyte. The impact of the thermal Marangoni effect will be discussed.

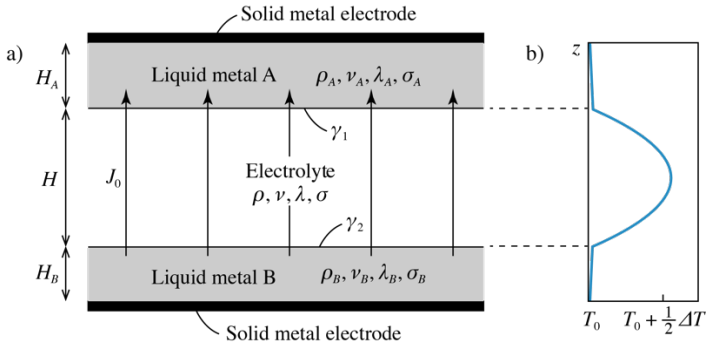

FIG. 1. A considered liquid-layer system subject to an electric current density J_0. a) a schematic illustration of a liquid battery. The densities, kinematic viscosities, thermal conductivities, and electric conductivities of liquids are denoted by ρ, ν, λ, and σ, respectively. b) The temperature profile in the conduction state.

[1] S. Zhang, Y. Liu, Q. Fan, C. Zhangn T. Zhou, K. Kalantar-Zadeh and Z. Guo, Liquid metal batteries for future energy storage, Energy Environ. Sci., **14**, 1754-5692 (2021).
[2] D. H. Kelley and T. Weier, Fluid mechanics of liquid metal batteries, Appl. Mech. Rev., **70**, 020801 (2018).
[3] N. Weber, P. Beckstein, V. Galindo, W. Herreman, C. Nore, F. Stefani, T. Weier, Metal pad roll instability in liquid metal batteries, Magnetohydrodynamics, **53**, 3-13 (2017).
[4] Y. Shen and O. Zikanov, Thermal convection in a liquid metal battery, Theor. Comput. Fluid Dyn. **30**, 275-294 (2016).

Pattern transitions and evolutions of Marangoni flow in a Czochralski configutation with deformed free surfaces

Chunmei Wu[1], *Ruiqi Huang*[1], *Lin Ding*[1], *Xiyuan Xue*[1], *Junfeng Shen*[1], *Yourong Li*[1]

[1] *Key Laboratory of Low-grade Energy Utilization Technologies and Systems of Ministry of Education, School of Energy and Power Engineering, Chongqing University, Chongqing 400044, China*

E-mail:chunmeiwu@cqu.edu.cn

Pattern transitions and evolutions are ubiquitous in spatiotemporal dynamical systems in nature and industry. As a rich territory for studies of pattern formation during surface tension driven convections, thermcapillary flow has attained much attention and become one of the research focuses for its widely existence in various fields. In indusrty, Czochralski technology is an important method for growth crystal, where the melt is contained in a crucible. In the past few decades, many scholars have been focused on thermocapillary convection in the model of Cz configuration with a assumption of flat free surface. However, surface deformation in inevitable in industrial production process, which has significantly influence on thermocapillary convection and often be ignored by scholars. The effect of wall wetbility and crystal growth angle may make the surface deform to be convex or concave. Such surface deformation and the temperature oscillations during thermocapillary convection are strongly coupled.

In order to gain a fundamental understanding on the pattern transitions and evolutions of thermocapillary flow in a Czochralski configutation with curved free surfaces, a series of unsteady three-dimensional numerical simulations were carried out by using the finite volume method. Silicon melt with Prandtl number of 0.011are chosen as the working fluids. The contact angle ranges from 90 ° to 8 °, growth angles are set at 90 ° and 11°. The volume ratio V_r is adopted to charactize the effect of surface deformation. Results show that the basic flow is axisymmetric and steady at small temperature gradient in different surface shapes. With the increase of the thermocapillary Reynolds number, the flow will undergos several types of transition to three-dimensional steady flow or three-dimensional oscillatory flow, which significantly dependent by volume ratio, as shown in Figure 1. When the growth angle is considered to be 90 °, the flow pattern transition is almost the same as that of flat surface. Once the the thermalcapillary Reynolds number exceeds a critical value, the flow bifurcates to three-dimensional steady flow. As the thermalcapillary Reynolds increases further, the flow evolves into three-dimensional oscillatory flow, and finally become chaos. When the effect of growth angle is considered, as the increase of thermocapillary Reynolds number, the basic flow directly transit into the three-dimensional oscillating flow, and the oscillation is only oppear near the crystal. When the volume ratio is less than 1.2, a reversed pattern transition occurs in the liquid pool.

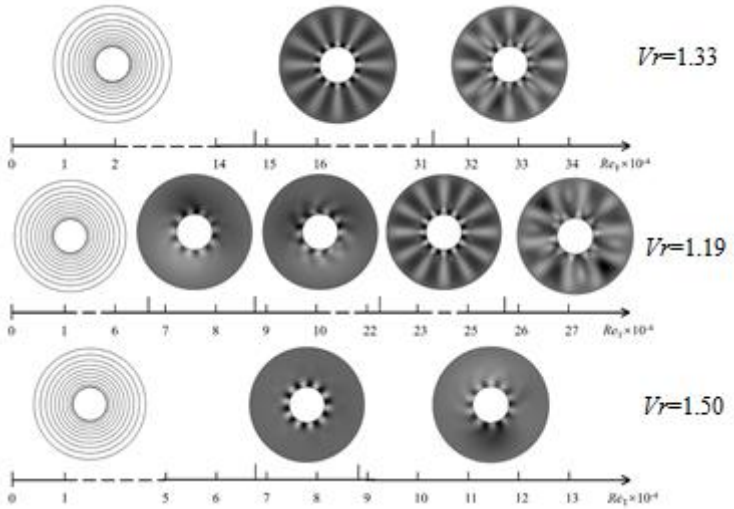

FIG. 1. Evolutions of the surface temperature patterns with the increasing thermocapillary Reynolds number.

Effect of temperature on flowing water film

Simon Brient[1], Thomas Séon[1], Axel Huerre[2], Christophe Josserand[3] and Laurent Duchemin[4]

[1] *Institut Jean Le Rond ∂'Alembert, CNRS, Sorbonne Université, Paris, France*
[2] *Matières et Systèmes Complexes, Université Paris Diderot, CNRS, Paris, France*
[3] *Laboratoire d'Hydrodynamique (LadHyX), CNRS, Ecole Polytechnique, IP Paris, Palaiseau, France*
[4] *Physique et Mécanique des Milieux Hétérogènes, CNRS, ESPCI Paris, Université PSL, Sorbonne Université, Université de Paris*

Flowing film are ubiquitous in nature and technology, from falling film condenseurs to surface coating. There are numerous studies concerning the stability or waves propagation on such films, but really few on the form of free flowing film. These lasts exhibit a particular braided structures with nodes, as shown on the left image figure 1., resulting from an interaction between surface tension and inertia [1]. We noticed that this shape is affected if a temperature difference is imposed between the flowing water and the substrate. Indeed, nodes start to drift downward the flow when the plate is cooled, figure 1. To study the effect of temperature on the shape of flowing water film, a special set-up has been build.

The experimental set-up consists in a closed loop of water in which liquid is set into motion by a chiller, that also serves as temperature controller. The substrate is made of an aluminium plate which can be cooled or heated thanks to a cooling bath. Water flowing on the plate comes from an overflowing water tank built to avoid any fluctuations of flow rate, ruled by hydrostatic pressure. This allows us to avoid the initial meandering instability. We record with a thermal camera the evolution of the shape of the film and get the profile with image analysis.

Initially, an isothermal free film flow is produced and reaches after certain time a mechanical equilibrium. Then, the plate is cooled down whereas water temperature is kept constant. Thus, a temperature difference is created between water and the aluminum substrate that triggers a change in water film shape, figure 1. Thermal images point out a significant thermal transverse gradient in the film, from a warm center to cooler edges, figure 2. This results in a surface tension gradient and then to a Marangoni force towards lower surface tension areas ie. edges of the film. This film widening leads to the observed nodes displacement.

In this talk, we will describe the dynamics of this change in form of water film due to cooling.
First, we will prove that this evolution can't be explained by a simple temperature dependency of contact angle. Afterward, we will exhibit two temporal regimes. The first one, fast, seems largely due to a Marangoni effect whereas the second one, that can persist during several hours, is closely linked to a coupled evaporation-condensation effect near the contact line [2, 3]. By adding thermocapillary effects in a coupled set of ODEs already describing the isothermal free flow [1], we will propose a numerical model of the first regime and discuss its agreement with experiments. We will then interpret the final shape reached after several hours of condensation and its stability.

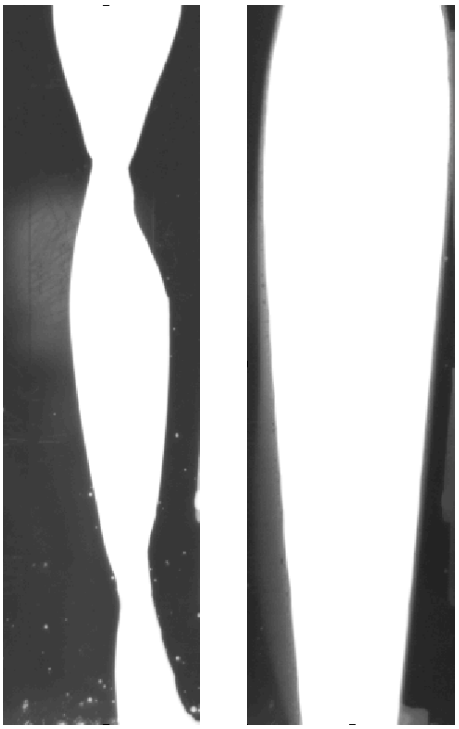

FIG. 1. Evolution of the shape of the film. Left: Isothermal film at $T_{water} = T_{plate} = 45°C$. Right: Non-isothermal case with $T_{water} = 45°C$ and $T_{plate} = 25°C$ after $2h$ of experiment

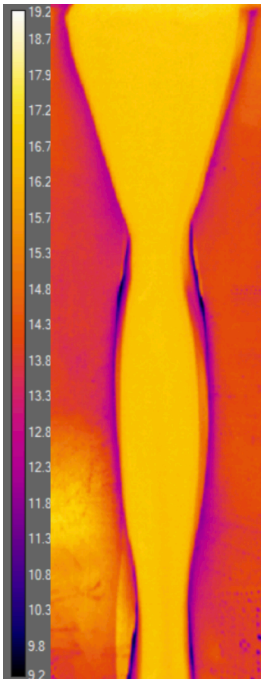

FIG. 2. Thermal image of a warm free film flowing on a cold substrate (orange corresponds to warm areas, purple to cold ones)

[1] Mertens, K., Putkaradze, V., & Vorobieff, P. (2005). Morphology of a stream flowing down an inclined plane. Part 1. Braiding. *Journal of Fluid Mechanics*, *531*, 49-58..

[2] Wayner Jr, P. C. (1993). Spreading of a liquid film with a finite contact angle by the evaporation/condensation process. *Langmuir*, *9*(1), 294-299

[3] Mehrizi, A. A., Liu, Q., & Wang, H. (2021). Nanoscale morphology of thin liquid films near the advancing contact line during condensation. *Physics of Fluids*, *33*(7), 072109.

Experimental investigation on behavior of particles constituting coherent structure in a high-aspect-ratio liquid bridge

Shin Noguchi[1] and Ichiro Ueno[2]

[1] *Div. of Mech. Aerospace Eng., Graduate School of Sci. and Tech., Tokyo Univ. Science, Japan*
7522703@ed.tus.ac.jp

[2] *Dept. of Mech. Aerospace Eng., Graduate School of Sci. and Tech., Tokyo Univ. Science, Japan,*
ich@rs.tus.ac.jp

We conduct experimental research on the coherent structures of low-Stokes-number particles in a thermocapillary liquid bridge. These structures, known as particle accumulation structures (PASs), occur in traveling-wave convection [1]. The formation of PASs is influenced by variations in the shape of the liquid bridge, particularly its aspect ratio. Gravity plays a major role in shaping liquid bridges on Earth, which is why previous experimental studies have primarily focused on liquid bridges with low aspect ratios. We discover a PAS with an azimuthal wave number of $m = 1$ in a high aspect ratio liquid bridge of $O(10^{-3}$ m), which has a distinct spatial structure from those previously reported in prior research. The experiment utilizes particles that are heavier than the test liquid. By tracking individual particles of Stokes number St = $O(10^{-5})$, we were able to observe their spatial and temporal behaviors as they form coherent structures. We reveal that two major coherent structures simultaneously emerge within the liquid bridge of $\Gamma = 1.6$ aspect ratio. The Poincaré sections of these structures qualitatively match the predictions made by Barmak et al. [2 , 3].

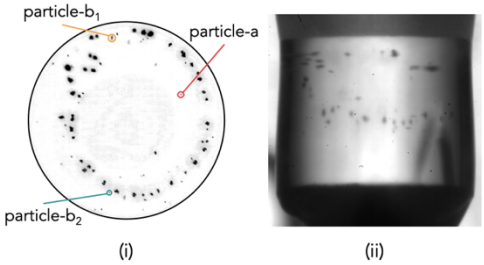

FIG. 1. Particle images of PAS under $\Delta T = 40$ K or Ma = 3.3×10^4: (i) illustrate the particle image observed through the upper rod (Top view image), (ii) exhibit the particle image monitored through the external shield (Side view image).

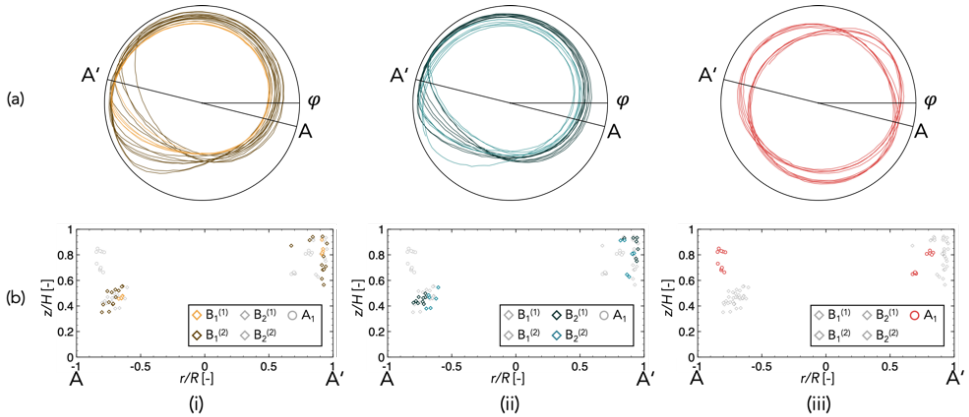

FIG. 2. Row (a): top view of coherent structures by (i) and (ii) particles 'b_j' and (iii) particle 'a'. Row (b) Poincaré section at A-A' cross-section shown in Row (a). Column (i) and (ii) consists of the trajectories (i) '$B_1^{(1)}$' (in orange) and '$B_1^{(2)}$' (in brown) by the particle 'b_1' and (ii) '$B_2^{(1)}$' (in deep blue) and '$B_2^{(2)}$' (in light blue) by the particle 'b_2' and Column (iii) consists of the trajectories (i) 'A_1' (in red) by particle 'a'. Corresponding Poincaré points in Row (b) are plotted in the same color as in Row (a).

We acknowledge financial support by Grant-in-Aid for Challenging Research (Exploratory) (grant number: 20K20977) from the JSPS.

[1] D. Schwabe, P. Hintz, and S. Frank, New features of thermocapillary convection in floating zones revealed by tracer particle accumulation structures (PAS), Microgravity Sci. Technol. Vol. **9**, No. 1-2, 163-168 (1996).

[2] I. Barmak, F. Romanò, and H. C. Kuhlmann, Particle accumulation in high-Prandtl-number liquid bridges, Proc. Appl. Math. Mech. **19**, e201900058 (2019).

[3] I. Barmak, F. Romanò, and H. C. Kuhlmann, Finite-size coherent particle structures in high-Prandtl-number liquid bridges, Phys. Rev. Fluids **6**, 084301 (2021).

Study of vapor condensation heat transfer on nanostructured and hierarchical microporous-nanostructured superhydrophobic surfaces

Xin Wang [1] and Zhenqian Chen [2]

[1] *Southeast University, School of Energy and Environment, Nanjing, 210096, P.R. China*
xin_wang@seu.edu.cn

[2] *Southeast University, School of Energy and Environment, Nanjing, 210096, P.R. China zqchen@seu.edu.cn*

Abstract: A new hierarchical superhydrophobic surface with micropores and nanoblades (MN SHS) is proposed to strengthen the jumping ability of droplets and maintain the high-efficiency droplet jumping condensation at the larger subcoolings. The results demonstrate that the jumping frequency and the proportion of multidroplets merging (n≥8) on the MN SHS are higher than those on the nanostructured superhydrophobic surfaces (Nano SHS). Moreover, the maximum diameter of condensate droplets is only 150μm, which is approximately 50% smaller compared to the Nano SHS. Spontaneous jumping of condensate droplets is observed on the 40PPI MN SHS (PPI: the average number of pores per inch.) at a subcooling of 16K; while the droplet jumping condensation occurs at a maximum of 5K on the Nano SHS. As the subcooling ranges from 5K to 16K, the heat transfer coefficient of MN SHS is increased by at least 26.4% compared to the Nano SHS. In addition, lattice Boltzmann model is adopted to simulate the self-propelled jumping behaviors on different structured surfaces. The energy conversion efficiency of drops on the MN SHS is higher compared to that on the Nano SHS. This work will contribute to the potential development of dropwise condensation in energy utilization, petrochemical engineering, thermoelectric cooling and aerospace thermal management systems.

Keywords: Condensation heat transfer, Hierarchical superhydrophobic surface, Droplet jumping, Surface energy, Lattice Boltzmann method

In the past two decades, due to the promising applications in self-cleaning [1, 2], anti-icing/frosting [3, 4], water harvesting [5] as well as hotspot cooling of electronics [6-8], spontaneous jumping behaviors of droplets merging have attracted much attention. For droplet jumping condensation, the heat transfer is significantly higher compared to that of conventional dropwise condensation; however, it is limited by the lower surface subcooling. As the subcooling degree is larger, the smaller nucleation radius and larger population density cause the condensate to flood the surface. The condensation mode transits to dropwise condensation or even filmwise condensation, which deteriorates the heat transfer efficiency. Therefore, it is urgent and significant to implement the efficient and continuous droplet jumping condensation under the larger subcoolings.

In this work, a hierarchical SHS decorated with micropores and nanoblades is proposed to enhance dropwise condensation heat transfer. The size distribution and heat transfer characteristics on the MN SHS are compared to the Nano SHS at different subcooling degrees. Besides, the lattice Boltzmann method is adopted to simulate the self-propelled jumping behaviors of drops caused by merging on the different textured surfaces. It is demonstrated that both MN and Nano SHS can maintain the high-efficiency droplet jumping condensation at the low subcooling degree (ΔT<5K). The jumping frequency and the proportion of multi-droplets merging on the MN SHS are higher over those on the Nano SHS. Accordingly, the maximum and average diameters on the Nano SHS are significantly smaller. Furthermore, a smaller PPI contributes to enhancing heat transfer. At the larger subcooling (ΔT≤16K), the condensation mode on the Nano SHS changes to the normal dropwise condensation. As well, condensate droplets can only be removed by gravity induced sliding. In contrast, droplet can still coalesce to jump from the MN SHS. As the removal behaviors of droplets change from self-propelled jumping to gravity induced sliding, the critical departure size is raised by order of magnitude. The thermal resistance due to the larger droplets on the Nano SHS deteriorates the heat transfer performance. Due to jumping out of plane, the heat transfer coefficient of MN SHS is increased by at least 26.4% compared the Nano SHS. The theoretical analysis reveals that the solid-liquid adhesion dissipative energy is extremely low because the droplets penetrated into nanoblades while suspended on the micropores. Even though the droplet is in the composite wetting state on the MN SHS, the jumping velocity is slightly lower than that in the Cassie state. In addition, the jumping velocity predicted by LBM agrees well with the data from previous experiments and simulations. For Oh≤0.0373, the jumping velocity of droplets on the curved substrate is greatly higher over that on the flat substrate. As the Oh number decreases, the surface curvature plays an increasingly significant role. When the Oh number is 0.00997 ($2r$=140μm), the energy conversion efficiency of coalesced drops on the curved substrate is 23% higher over that on the flat substrate. This work will provide new perspectives into the design of advanced functional surfaces for micro/nano structures to enhance condensation heat transfer.

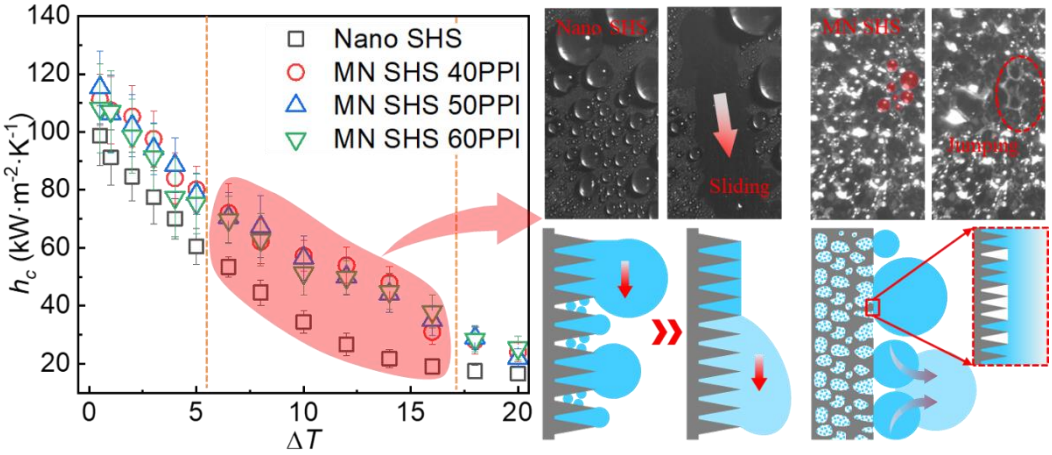

Figure 1. Variation of heat transfer coefficient with surface subcooling on the different structured surfaces

References:

[1] Wisdom, K. M.; Watson, J. A.; Qu, X.; Liu, F.; Watson, G. S.; Chen C. H. Self-Cleaning of Superhydrophobic Surfaces by Self-Propelled Jumping Condensate. *Proc. Natl. Acad. Sci. U. S. A.* 2013, 110, 7992-7997.

[2] Watson, G. S.; Gellender, M.; Watson, J. A. Self-Propulsion of Dew Drops on Lotus Leaves: A Potential Mechanism for Self-Cleaning. *Biofouling* 2014, 30, 427-434.

[3] Zhang, H.; Zhao, G.; Wu, S.; Alsaid, Y.; Zhao, W.; Yan, X.; Liu, L. Zou, G.; Lv, J.; He, X.; He, Z.; Wang, J. Solar Anti-Icing Surface with Enhanced Condensate Self-Removing at Extreme Environmental Conditions. *Proc. Natl. Acad. Sci. U. S. A.* 2021, 118 (18), e2100978118.

[4] Boreyko, J. B.; Collier, C. P. Delayed Frost Growth on Jumping-Drop Superhydrophobic Surfaces. *ACS Nano* 2013, 7, 1618-1627.

[5] Huang, W.; Tang, X.; Qiu, Z.; Zhu, W.; Wang, Y.; Zhu, Y. L.; Xiao, Z.; Wang, H.; Liang, D.; Li, J.; Xie, Y. Cellulose-Based Superhydrophobic Surface Decorated with Functional Groups Showing Distinct Wetting Abilities to Manipulate Water Harvesting. *ACS Appl. Mater. Interfaces* 2020, 12, 40968-40978.

[6] Oh, J.; Birbarah, P.; Foulkes, T.; Yin, S. L.; Rentauskas, M.; Neely, J.; Pilawa-Podgurski, R. C. N.; Miljkovic, N. Jumping-Droplet Electronics Hot-Spot Cooling. *Appl. Phys. Lett.* 2017, 110, 123107.

[7] Wiedenheft, K. F.; Guo, H. A.; Qu, X.; Boreyko, J. B.; Liu, F.; Zhang, K.; Eid, F.; Choudhury, A.; Li, Z.; Chen, C. H. Hotspot Cooling with Jumping-Drop Vapor Chambers. *Appl. Phys. Lett.* 2017, 110, 141601.

[8] Foulkes, T.; Oh, J.; Sokalski, P.; Li, L.; Sett, S.; Sotelo, J.; Yan, X.; Pilawa-Podgurski, R.; Castaneda, A.; Steinlauf, M.; Miljkovic, N. Jumping Droplets Electronics Cooling: Promise versus Reality. *Appl. Phys. Lett.* 2020, 116, 203701.

Brownian Motion as a Probe of Complex Surfaces

Nicolas Fares[1], Maxime Lavaud[1,2], Thomas Salez[1] and Yacine Amarouchene[1]

[1]*Bordeaux Univ., CNRS, LOMA, UMR 5798, F-33400, Talence, France.*

[2]*EPOC, CNRS-UMR 5805, Bordeaux-INP, University of Bordeaux, 33600, Pessac, France.*

In blood vessels, red blood cells flow further away from the vessels' walls than their white counterparts, the former being softer. Understanding and harvesting such elastohydrodynamic-related effects could lead to contactless ways to probe complex materials. To address this matter, a novel method based on Mie holography and stochastic inference was recently developed in the group [1]. In a nutshell, the 3D trajectory of a Brownian micro-sphere diffusing in salted water on top of a charged rigid glass surface is recorded and analyzed. Specifically, the 3D position of the sphere is measured down to a 10-nanometer resolution while surface forces are measured down to a few femtonewtons, only limited by thermal noise (see Fig. 1, left-hand side). In addition, local diffusion profiles, as well as relevant probability density functions and high-order cumulants [2], are extracted from the statiscal analysis of trajectories, leading to a precise measurement of fine deviations from the standard Gaussian statistics of displacements. Finally, this method, being contactless and relying only on a thermal excitation, is promising to cope with soft and fragile materials. Experiments are currently run on elastomeric ones. Interestingly, the local diffusion profile corresponding to the perpendicular motion shows clear deviations from the previous rigid-confinement scenario (see Fig. 1, right-hand side). For now, those deviations are interpreted as an effective giant slippage, potentially related to the softness of the investigated materials.

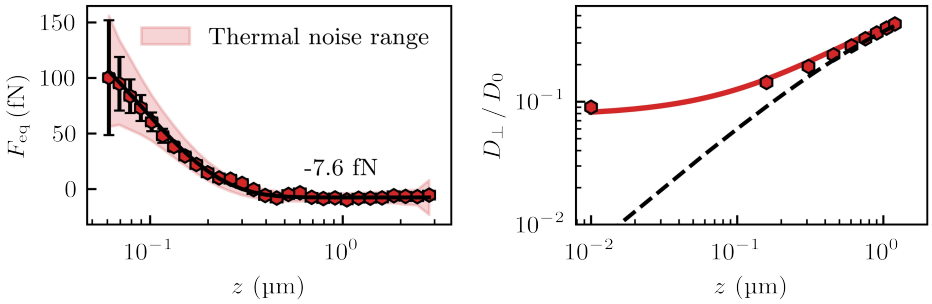

FIG. 1. Left: Equilibrium force F_{eq} as a function of the separation distance z between a Brownian sphere diffusing in salted water and a glass wall. The force includes electrostatic repulsion and weight. The red dots correspond to experimental data, the solid line to the theoretical expectation, and the red-colored region to the theoretical thermal-noise limit; Right: Local diffusion coefficient $D_\perp$, normalized by the bulk one D_0, as a function of the separation distance z between the Brownian sphere and an elastomeric wall. The red dots correspond to experimental data, the red solid line to a theoretical fit, and the black dashed line to the rigid-confinement scenario.

[1] Lavaud, M., Salez, T., Louyer, Y. & Amarouchene, Y. Stochastic inference of surface-induced effects using Brownian motion. Physical Review Research 3. Publisher: American Physical Society, L032011 (July 2021).

[2] Alexandre, A., Lavaud, M., **Fares, N.**, *et al*. Non-Gaussian diffusion near surfaces. Accepted in Physical Review Letters (December 2022).

Poster session

Thin-film Rayleigh–Taylor instability in the presence of a deep periodic corrugated wall

T. Corbin[1], B. Dinesh[2] and R. Narayanan[1]

[1] *Department of Chemical Engineering, University of Florida, Gainesville, FL 32611, USA,* tcorbin@ufl.edu, ranga@ufl.edu

[2] *Department of Chemical Engineering and Technology, Indian Institute of Technology-BHU, Varanasi, UP 221005, India*
dinesh.che@iitbhu.ac.in

This study examines the Rayleigh-Taylor (R-T) instability of a thin liquid film overlying a passive fluid when the film is attached to a periodic wavy deep corrugated wall. By using a reduced-order long-wave model, we demonstrate that the wavy wall amplifies the instability, particularly when the interface pattern is sub-harmonic to the wall pattern. We derive an expression for the growth constant of the instability for any wall amplitude in the specific case involving two full waves in the wall and a full wave at the interface. Nonlinear computations reveal that the sliding motion of the interface is arrested by the wavy wall when a single liquid film is present but not necessarily when a bilayer system is considered. The interface evolution shows the development of primary and secondary troughs that subsequently slide along the flat wall due to symmetry breaking. However, it is found that the sliding motion can be ultimately arrested by the top wavy wall, depending on the fluids' holdup. A critical value of the interface position is identified, beyond which the onset of sliding motion is observed, while below this value, sliding is always prevented.

Acknowledgements

The authors acknowledge funding from NSF via grant number # 2025117

Perturbation method applied to interfacial three dimensional waves in the presence of a parallel current

Soraya Salmi[1], Nabil Allalou[2] and Mohamed Debiane[2]

[1] *Département de physique, Faculté des sciences, Université M'Hamed Bougara de Boumerdes, Route de la gare Ferroviaire, Boumerdes 35000, Algeria,* s.salmi@univ-boumerdes.dz

[1] *Laboratoire revêtements, Matériaux et Environnement, Université M'Hamed Bougara de Boumerdes, Avenue de l'indépendance, Boumerdes 35000, Algeria*

[2] *Faculté de physique, Laboratoire mécanique des fluides théoriques et appliqués, Université des Sciences et de la Technologie Houari Boumediene, B.P.32 El Alia*

I. Abstract

Weakly non-linear behaviour of interfacial short-crested waves with current is presented in this paper. a perturbation method was applied to determine fifth-order solutions. The advantage of this method is that it allows for the determination of the harmonic resonance condition which is one of the major short-crested waves characteristics. We have shown that there is a critical current beyond which steady wave solutions cannot exist. This critical current is associated with the emergence of instability.

II. Introduction

We consider a two layer unbounded fluid system with parallel uniform current U as shown in Fig. 1a. The top layer has a density of ρ_1 and the lower has density ρ_2. The two layers are supposed to be horizontal with infinite depths. The defined cartesian coordinates system is composed of the horizontal plane (xOy) and the z-axis which is pointed vertically upward. Its origin is placed on the unperturbed interface between the two layers as shown in Fig. 1a. Herein, short crested-wave field are generated from the non-linear interaction of two wave trains propagating toward each other with the same characteristics. L is the incident wave's wavelength, θ is the angle between its direction of incidence and the normal to the wall as shown in Fig. 1b. The two fluids are assumed inviscid, incompressible, homogeneous and the motion is irrotational. Both fluids are considered to be stably stratified by gravity, *i.e.* $\rho_1 < \rho_2$.

.

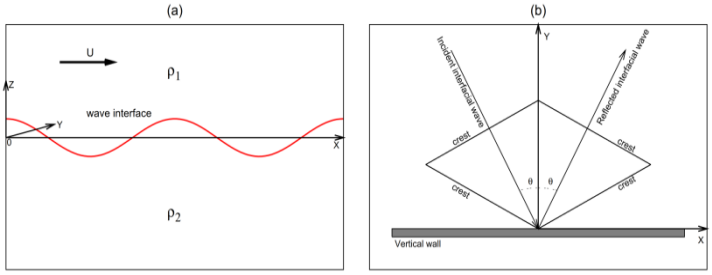

FIG. 1. (a) Schematic representation of an interfacial wave in the presence of a current parallel to the Ox axis. (b) Reflection of a plane wave from a vertical wall

II. Results and discussion

- *Dynamical Limit*

The *dynamical limit* is associated with the existence of a critical current beyond which the problem does not admit a steady wave solutions. The linear critical current is defined when $\omega_0^+ = \omega_0^-$, it is given by the following expression :

$$U_{lc} = \frac{\sqrt{\mu(1-\mu^2)}}{\mu p},$$

where the second subscript l stands for the linear case. In this case, we have :

$$\omega_0^+ = \omega_0^- = \frac{\mu p U_{lc}}{\mu + 1}.$$

The sign of ω_2 in the (μ, θ) plane for a current $U = 1$ is shown in Fig. 2. The dynamical condition above which steady solutions do not exist is also represented. There are two regions for which ω_2 can be negative or positive. These two regions are separated by a line corresponding to $\omega_2 = 0$. Along this line $\omega = \omega_0$ and therefore ω is independent of the wave steepness h. On the other hand, for $\omega_2 < 0$, the frequency ω is a decreasing function of the wave steepness h whereas for $\omega_2 > 0$, ω increases with h.

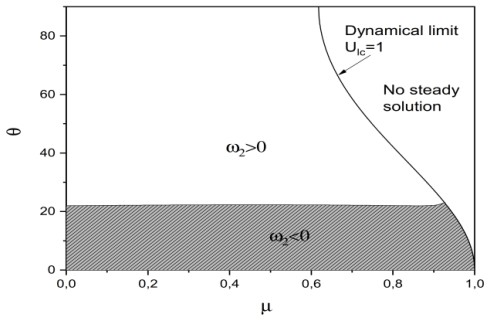

FIG. 2. The sign of ω_2 in the (μ, θ) plane for $U_{lc} = 1$.

- *The Influence Of current On Interfacial Profile*

Representative three dimensional profiles and their cross-sectional view $Y = 0$ and $X = 0$ for interfacial short crested wave in the presence of a current are illustrated in Fig. 3. It is seen that for low values of current $U = 1$ the profile is typical of a short-crested wave with a sharp crest and a rounded trough. As the current U increases, the crest becomes more flattens as it seen for $U = 3.09$. As the critical current is reached $U \approx U_{lc}$.

$[U = 1]$

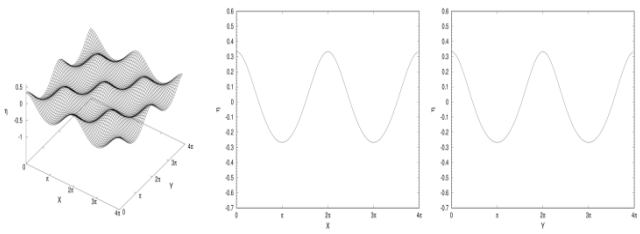

$[U = 3.09838]$

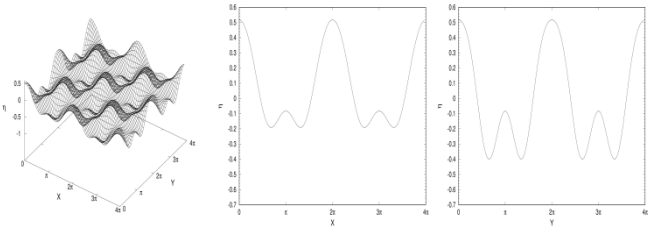

FIG .3. 3D wave profile and their cross-sectional view $Y = 0$ and $X = 0$ on two wavelengths for selected value of current U and for fixed values of $h = 0.30$, $\mu = 0.2$ and $\theta = 45^\circ$.

III. REFERENCES

[1] P.G. Saffman, and H. Yuen," Finite-amplitude interfacial waves in the presence of a current,"

[2] N. Allalou, M. Debiane and C. Kharif, "Three-dimensional periodic interfacial gravity waves: Analytical and numerical results," *Eur. J. Mech. B Fluids* **30** 371(2011).

Electrically modulated directional switching of a compound droplet in micro-confined oscillatory flow

Tanoy Kahali[1], Somnath Santra[2], and Suman Chakraborty[1]

[1]*Department of Mechanical Engineering, Indian Institute of Technology; Kharagpur, Kharagpur, West Bengal-721302, India suman@mech.iitkgp.ac.in*
[2]*Universite Grenoble Alpes, CNRS, LIPhy, Grenoble, France somnathme1028@gmail.com*

ABSTRACT

Electric field-mediated droplet manipulation has emerged as an integral part in applications spanning chemistry, biotechnology, different industries, and engineering sectors. Here, we demonstrate a means for controlling the cross-stream trajectory of a compound droplet in a microfluidic channel under the combined influence of an oscillatory axial pressure gradient and a transverse electric field. This study illustrates the role of flow pulsation in delaying the drop's attainment of a steady-state transverse position. Our findings reveal that with an enhancement in the frequency of oscillation, both the axial and transverse movement of the drop is preferentially attenuated, with its dynamic traversal occurring in a locus offset to the central axis which can be further overcome by employing a transverse electric field. Further, our findings delineate that a viscosity ratio below unity between the inner to outer droplet phases delays the transverse migration of the compound drop, whereas the converse enhances the same. In addition, we observe that a leaky-dielectric compound drop, suspended in another leaky medium having the respective electrical conductivity ratio of the inner-to-outer droplet phase surpassing their respective electrical permittivity ratio not only provides a suitable handle for selectively altering the direction of the resulting drop trajectory from towards the channel centreline to away from the same but at the same time provides a precise settling of the same at an intermediate transverse location by harnessing the interplay of electrical and hydrodynamic shear. Moreover, we have identified the key parameters responsible for the directional switching and assumed via a regime map delineating three different directions of motion of the droplet. We envisage that these findings will open up novel perspectives of controllable maneuvering of the double emulsion system in a confined microfluidic environment bearing decisive implications in engineering and biology.

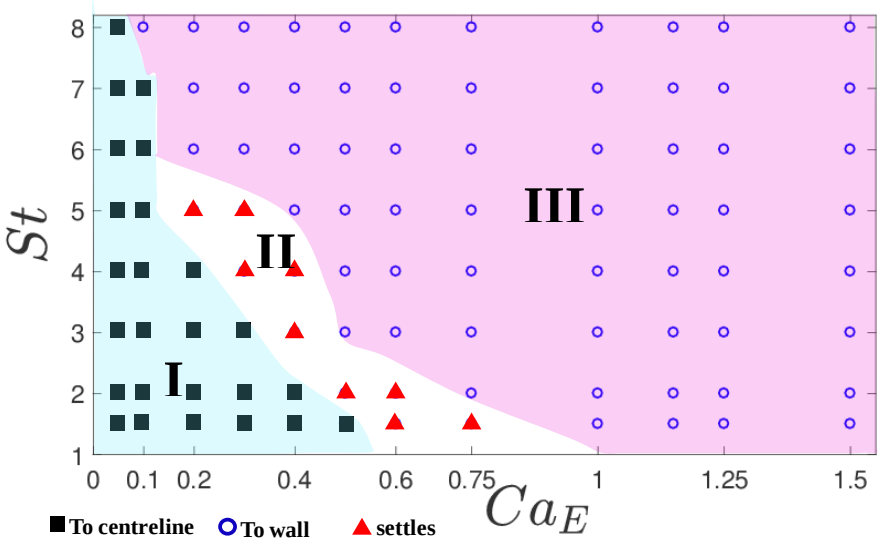

FIG. 1. Regime diagram showing three distinct parametric spaces of *St* and Ca_E, corresponding to the system-*A*. Regime-I features the drop migration towards the channel central axis, as marked by black coloured square markers. Regime-II features the settling region represented by red coloured triangles. Regime-III features the drop migration towards the wall electrode, indicated by the blue coloured ring markers.

REFERENCES

[1] K. Chaudhury, S. Mandal, and S. Chakraborty, "Droplet migration characteristics in confined oscillatory microflows," Phys. Rev. E 93, 023106 (2016).

Influence of the solvent nature on the optical rotatory dispersion of poly(propylene oxide) in solutions determined from channeled spectra

Cristina M. Pavel[1], Camelia Hulubei[2], Andreea I. Barzic[2], Raluca M. Albu[2], Dan G. Dimitriu[1] and Dana O. Dorohoi[1]

[1] *Faculty of Physics, Alexandru Ioan Cuza University, 700506, Iasi, Romania* dimitriu@uaic.ro

[2] *Department of Physical Chemistry of Polymers, "Petru Poni" Institute of Macromolecular Chemistry, 700487, Iasi, Romania,* irina_cosutchi@yahoo.com

Investigation of water-soluble polymers for biomedical applications is of high interest in science [1]. A special attention is given to the optical properties of the macromolecular compounds, which are essential for the interaction of the materials with electromagnetic fields. In particular, polymers exhibiting optical activity are intensely investigated since the drug release rate from them can be easily monitored through optical rotation measurements [2]. This phenomenon is associated with the circular birefringence of the polymer solution, which is strongly influenced by the wavelength of the incident radiation [3].

Poly(propylene) oxide (PPO) is an optically active polyether with a good solubility in a wide range of solvents, exhibiting a linear optical rotatory dispersion (ORD).

The method of channeled spectrum is a fast and efficient method to characterize the anisotropy of transparent layers. The channeled spectrum is a succession of minima and maxima of the optical flux density, as a result of phase difference introduced between light components propagating with different velocities in the anisotropic layer. The method was first applied to anisotropic polymer foils [4], liquid crystals [5], and inorganic crystals [6] for estimation of the linear birefringence, then extended to polymer solutions [7] for determination of optical rotatory dispersion.

Here we report on the investigation of the optical rotatory dispersion of PPO solutions in benzene, benzonitrile, carbon disulfide, chloroform, ethyl acetate, pyridine, tetrachloroethylene, carbon tetrachloride, methylene chloride and p-dioxane, respectively. The used experimental device consists of two crossed polarizers, between which a cell containing the polymer solution is introduced. The device is illuminated with electromagnetic radiation in the visible range of spectrum (light). Because the polymer solution rotates the polarization plane of radiation, the flux density after the second polarizer will be different from zero. Channeled spectra are recorded by a spectrophotometer. As an example, Fig. 1a shows the channeled spectrum of PPO in chloroform, while Fig. 1b shows the circular birefringence of the same solution. The data depends on the concentration of PPO in solution, as well as on the length of the cell containing the solution.

The obtained results are in good agreement with those existing in literature [8] and obtained by a different method. They offer important information on the influence of the solvent nature on the optical rotatory dispersion of PPO in solutions.

Acknowledgment: This work was co-funded by the European Social Fund, through Operational Program Human Capital 2014-2020, project number POCU/993/6/13/153322, project title *Educational and training*

[1] V. G. Kadajji and G. V. Betageri, Water soluble polymers for pharmaceutical applications, Polymers **3**, 1972 – 2009 (2011).

[2] S. Mallakpour and A. Zadehnazari, Advances in synthetic optically active condensation polymers – A review, Express Polym. Lett. **5**, 142 – 181 (2011).

[3] S. Ioan, A. I. Cosutchi and D. O. Dorohoi, Optical rotatory dispersion for polymers, Rom. J. Phys. **53**, 85 – 90 (2008).

[4] V. Pop, D. O. Dorohoi and E. Cringeanu, A new method for determining the birefringence dispersion, J. Macromol. Sci. B **33**, 373 – 385 (1994).

[5] S. Picos, G. Amarandei, I. Diaconu and D. O. Dorohoi, The birefringence of thin films of some nematic liquid crystals, J. Optoelectron. Adv. Mater. **7**, 787 – 793 (2005).

[6] D. G. Dimitriu and D. O. Dorohoi, New method for determining the optical rotatory dispersion of inorganic crystals applied to some samples of Carpathian quartz, Spectrochim. Acta A **131**, 674 – 677 (2014).

[7] A. I. Barzic, D. G. Dimitriu and D. O. Dorohoi, New method for determining the optical rotatory dispersion of hydroxypropyl cellulose polymer solutions in water, Polym. Eng. Sci. **55**, 1077 – 1081 (2015).

[8] Y. Kumata, J. Furukawa and T. Fueno, The effect of solvents on the optical rotation of poly(propylene oxide), Bull. Chem. Soc. Jpn. **43**, 3663 – 3666 (1970).

support for PhD students and young researchers in preparation for insertion into the labor market.

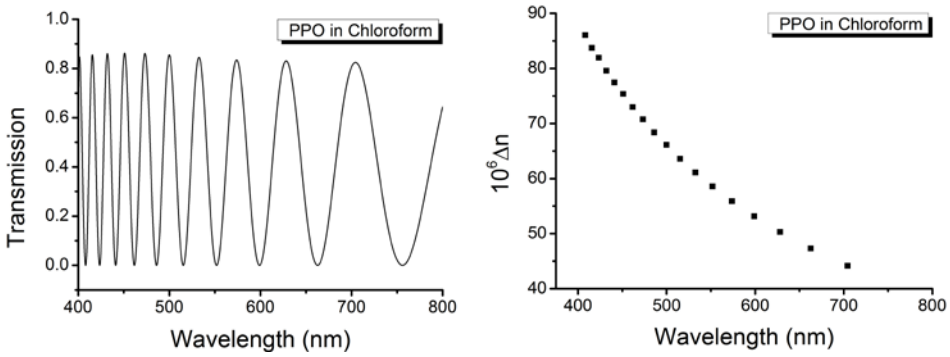

(a) (b)

FIG. 1. Channeled spectrum (a) and circular birefringence (b) of PPO in chloroform.

Solvatochromic analysis of surfactant binary mixtures

Alexandru Zara, Cristina M. Pavel, Ecaterina Ambrosi, Dan G. Dimitriu and Dana O. Dorohoi

Faculty of Physics, Alexandru Ioan Cuza University, 700506, Iasi, Romania dimitriu@uaic.ro

The preparation of microemulsions often involves binary mixtures of a surfactant with an alcohol [1]. The interactions in such solvents mixtures are complex, since the solute is surrounded preferentially by the component solvents, but also the complex formed by the two solvents. However, to understand the role of solvation in the chemical processes, it is important to know what type of specific and nonspecific interactions take place in such systems, and to estimate the strength of these interactions.

Solvatochromism is a rather simple method to investigate the solute-solvent interactions in the binary mixtures [2]. The dependence of the solute's absorption spectral bands positions on the nature of the solvent is the basis of this method. The shift of the absorption band of the solute is strongly influenced by the interactions of the solute's molecule with the solvents molecules existing in its cybotactic region (first solvation shell). Several theoretical models estimate the composition of the first solvation shell of the solute's molecule, the most used being the statistical cell model of ternary solutions [3], Suppan model [4], and Bosch-Rosés model [5].

Here we report on the solvatochromic investigation of surfactant binary mixtures obtained from polyethylene glycol p-(1,1,3,3-tetramethylbutyl)-phenyl ether (Triton X-100) and water, methanol, ethanol and 1-propanol, respectively. Triton X-100 is a nonionic surfactant with a rigid hydrophobic molecular segment and a flexible polar head, widely used to lyse cells to extract proteins or organelles or to permeabilize the living cells membranes [6]. Different dyes were used as probes (solutes), their absorption spectral bands being recorded for different mole ratios between Triton X-100 and water/alcohols.

Kamlet-Abboud-Taft model [7] was applied to estimate the contribution of each type of intermolecular interactions to the total spectral shift of the electronic absorption band of the solute. The composition of the first solvation shell of solute was comparatively estimated by using the three above-mentioned models. Bosch-Rosés model also provided important information on the (1:1) complex formed between Triton X-100 and water/alcohols in the binary mixtures. The statistical cell model of ternary solutions allowed the calculation of the interaction energy between two molecules in pairs solute-solvent.

The obtained results were compared with similar results existing in literature [8], a good agreement being found.

Acknowledgment: This work was co-funded by the European Social Fund, through Operational Program Human Capital 2014-2020, project number POCU/993/6/13/153322, project title *Educational and training support for PhD students and young researchers in preparation for insertion into the labor market.*

[1] R. Zana, Aqueous surfactant-alcohol systems: a review, Adv. Colloid Interface Sci. **57**, 1 – 64 (1995).

[2] S. Nigam and S. Rutan, Principles and applications of solvatochromism, Appl. Spectrosc. **55**, 362A – 370A (2001).

[3] V. Pop. D. O. Dorohoi and M. Delibas, Considerations on the statistical model of intermolecular interactions in ternary solutions, An. Stiint. Univ. Al. I. Cuza s.Ib **32**, 79 – 84 (1986).

[4] P. Suppan, Local polarity of solvent mixtures in the field of electronically excited molecules and exciplexes, J. Chem. Soc. Faraday Trans. 1 **83**, 495 – 509 (1987).

[5] E. Bosch and M. Rosés, Relationships between E_T polarity and composition in binary solvent mixtures, J. Chem. Soc. Faraday Trans. **88**, 3541 – 3546 (1992).

[6] M. Poša, D. Škorić and A. Pilipović, Binary mixtures (1:1) of Triton X-100 and Propanolol hydrochloride in an aqueous solution of NaCl: Whether mixed micelles are formed, possible clarification in ^{1}H DOSY NMR experiment, J. Mol. Liq. **369**, 120870 (2023).

[7] M. J. Kamlet, J. L. M. Abboud and R. W. Taft, An examination of linear solvation energy relationships, in *Progress in Physical Organic Chemistry*, vol. 13, ed. by R. W. Taft, Wiley Interscience, New York (1981), pp. 485 – 630.

[8] M. Kohantorabi, H. Salari, M. Fakhraee and M. R. Gholami, Surfactant binary systems: Ab initio calculations, preferential solvation, and investigation of solvatochromic parameters, J. Chem. Eng. Data **61**, 255 – 263 (2016).

Microfluidics-based experimental study of the yield stress fluids effect for soil remediation

Amine Ben Abdelwahed[1], Antonio Rodriguez De Castro[1] and Henri Bertin[2]

[1] *I2M, Arts et Métiers Institute of Technology, CNRS, Esplanade des Arts et Métiers, 33405 Talence Cedex, France, amine.ben-abdelwahed@ensam.eu; antonio.rodriguez-de-castro@u-bordeaux.fr*

[2] *I2M, CNRS, Esplanade des Arts et Métiers, 33405 Talence Cedex, France, henri.bertin@u-bordeaux.fr*

The remediation of polluted soils by the injection of complex fluids is a cost-effective strategy allowing in situ decontamination with minimal environmental and economic impact. The use of polymers such as xanthan gum and polyacrylamide in hydrolyzed form (HPAM) allows to increase the efficiency of the macroscopic scanning of a pollutant thanks to the optimization of the viscosity ratio of the injected and displaced fluids [1, 2]. Although significant progress in this field has recently been made, the dynamics of immiscible flows of pollutants by a shear-thinning fluid remains very limited. This can be explained by the difficulties of assessing the influence of the dynamic viscosities and interfacial tensions at the pore scale.

In this work, a series of microfluidic experiments (FIG. 1) were performed to identify those microscopic mechanisms of displacement and to quantify their impact on scanning efficiency. In order to achieve this goal, concentrated xanthan gum solutions with concentrations ranging from 2,000 to 8,000 ppm developing a yield stress will be used as blocking agents. The yield stress fluid is injected through previously "Lab on Rock" microfluidic chips at their residual pollutant saturation. We will present an overview on recent experimental data and the theoretical analysis on this topic.

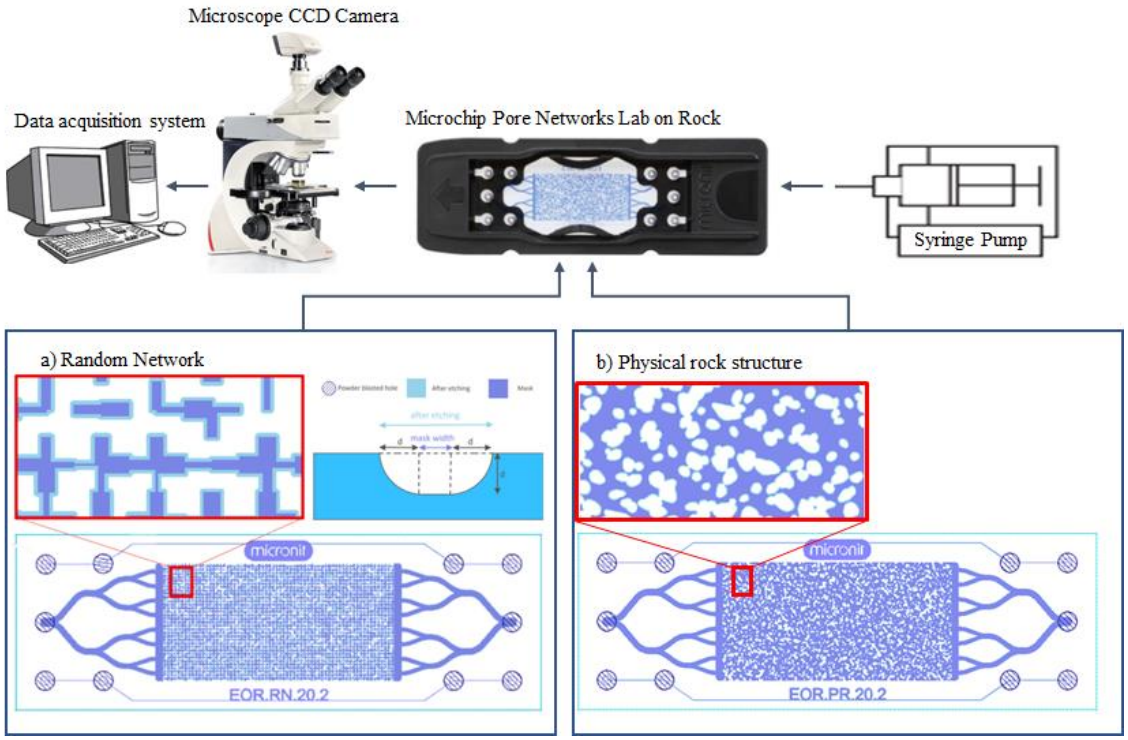

FIG. 1. Schematic drawing of the experimental apparatus and the microfluidic borosilicate glass chips (based on the drawing on the website of Micronit Company). The chips are 10 mm × 20 mm: a) Random network channels have widths of 50, 70, 90, 110 and 130 µm and the depth of the channels is 20 µm, b) Physical rock structure with a 150 µm wide crack

[1] I. Bouzid, N. Fatin-Rouge. *Assessment of shear-thinning fluids and strategies for enhanced in situ removal of heavy chlorinated compounds-DNAPLs in an anisotropic aquifer*. J. Hazard. Mater. **432**, 128703 (2022).

[2] A. Rodriguez De Castro, A. Ben Abdelwahed, H. Bertin. *Enhancing pollutant removal from contaminated soils using yield stress fluids as selective blocking agents*. J. Contam. Hydrol. **255**, 104142 (2023).

Experimental study on coherent structures by particles suspended in high-aspect-ratio ($\Gamma \geq 2.5$) thermocapillary liquid bridges of high Prandtl number

Keiichiro Kato[1,*], Shin Noguchi[1], Shogo Sensui[1], Kizuku Kurose[2] and Ichiro Ueno[2,**]

[1] Division of Mechanical and Aerospace Engineering, School of Science and Technology, Tokyo University of Science, Japan, *7519029@alumni.tus.ac.jp

[2]Department of Mechanical and Aerospace Engineering, Faculty of Science and Technology, Tokyo University of Science, Japan, **ich@rs.tus.ac.jp

I. INTRODUCTION

Schwabe et al. [1] discovered a phenomenon in which tracer particles suspended in a thermocapillary liquid bridge accumulate in traveling-wave-type oscillatory convection. This phenomenon is called the "particle accumulation structure (PAS)." Its occurring condition and the spatial structures have been investigated mainly for the convective structures induced by the hydrothermal wave (HTW) instability with moderate azimuthal wavenumbers $2 \leq m_{\mathrm{HTW}} \leq 5$. In these two decades the PAS in the HTW of $m_{\mathrm{HTW}} = 1$ has been investigated extensively [2 , 3], notwithstanding that their existence range in Marangoni number is extremely limited [4]. In this study, we focus on the PAS, or the coherent structures, formed by low-Stokes-number particles in high-aspect-ratio liquid bridges, in which the HTW of $m_{\mathrm{HTW}} = 1$ is steadily realized. Through the ground experiments, we unravel the PASs in the liquid bridges of the aspect ratio $\Gamma = H/R \geq 2.5$, where H and R are the height and the radius of the liquid bridge, respectively. Via three-dimensional reconstruction of the particle behavior, the correlation between the spatio-temporal motion of the particles and the coherent structure is investigated.

II. EXPERIMENTS

Left panel in Fig. 1 shows a schematic diagram of the experimental apparatus. Detailed view of the liquid bridge is illustrated in right panel. A designated amount of the test liquid 'bridges' between upper and lower coaxial rods to form a liquid column with a free surface. The radius of the end surfaces of the rods is of 0.75 mm. The upper rod is heated and the lower one is cooled to generate the temperature difference between the end surfaces of the liquid bridge. The upper rod is made of sapphire, through which the particle images are detected by the high-speed camera (Camera 1). The liquid bridge is coaxially surrounded by the cylindrical external shield. The particles in the liquid bridge are observed simultaneously from the side by another high-speed camera (Camera 2) through the external shield. Simultaneous tracking the particles by the synchronized high-speed cameras leads the three-dimensional reconstruction of the particles position. A CaF_2 window is partially installed in the external shield to detect the surface temperature of the liquid bridge via the infrared (IR) camera. Ambient gas flow is added in between the liquid bridge and the external shield under designated flow rate to vary the heat transfer through the free surface. Silicone oil of 2 cSt and the air are used as the test liquid and gas, respectively. The Prandtl number of the test liquid is of 28.6 at 25 °C. Gold-coated acrylic particles of 10 μm in diameter are employed as the test particles. Fluorescence particles of 13 μm in diameter are also employed.

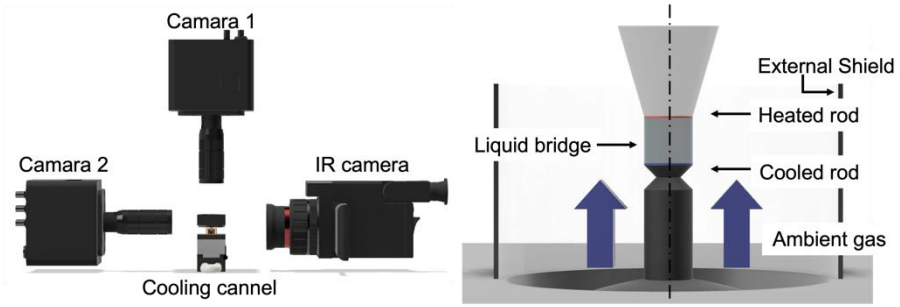

FIG. 1. (Left) Schematic diagram of the experimental apparatus, and (Right) detailed view of liquid-bridge sustaining part.

III. RESULTS

Figures 2 show the particle behaviors and the reconstructed coherent structure in the rotating frame of reference in the liquid bridges of $\Gamma = 2.8$: (a) and (b) frames indicate the path lines of the fluorescent particle observed by the top-view camera (Camera 1) and by the side-view camera (Camera 2),

respectively. Those images are obtained by stacking 1500 images corresponding to a period of 6 s. Each particle exhibits an ordered motion at a constant turnover period. (c), (d) illustrates a typical example of the reconstructed path line of a single particle in the rotating frame of reference. The initial point of the reconstructed particle position is indicated by the star. The star indicates the position of the trajectory where the particle locating near the cooled disk. Suppose this instant is defined as $t = 0$ s. The particle rises inside the liquid bridge following the return flow from the cold disk toward the hot disk by changing its azimuthal position. When the particle reaches closest to the free surface, the particle travels along the free surface toward the cold disk. The particle keeps traveling along the free surface, but it becomes invisible in the top-view image at the bottom region of the liquid bridge due to the convex shape of the liquid bridge. It reappears in the top-view image. However, the particle reappears and then rise again, following the return flow by exhibiting a helical motion. In this presentation, we will show the spatio-temporal variation of the coherent structures in the liquid bridges of different Γ.

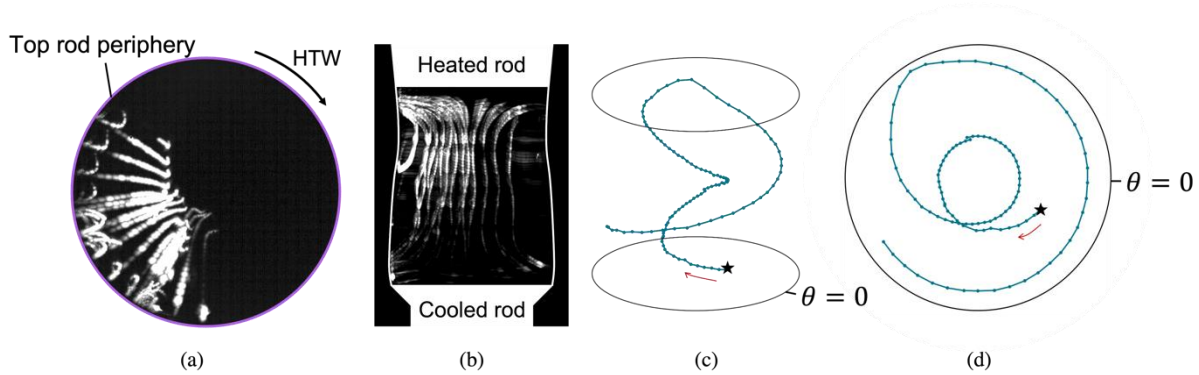

FIG. 2. Typical example of particle motion forming PAS in liquid bridge of Γ = 2.8: (a) particle image observed from above, (b) particle image observed from side, (c) reconstructed trajectory of a single particle, and (d) projected one in rotating frame of reference. The initial point of the reconstructed particle position is indicated by the star. The corresponding instant of this initial point is defined at $t = 0$ s.

ACKNOWLEDGEMENTS: This work was partially supported from the Japan Society for the Promotion of Science (JSPS) by Grant-in-Aid for Challenging Research (Exploratory) (grant number: 20K20977).

IV. REFERENCES

[1] Schwabe, D., Hintz, P. and Frank, S., New features of thermocapillary convection in floating zones revealed. by tracer particle accumulation structures (PAS), Microgravity sci. technol. Vol. 9, No. 1–2 (1996), pp. 163–168.

[2] Sasaki, Y., Tanaka, S. and Kawamura, H., Particle Accumulation Structure in Thermocapillary Convection of. Small Liquid Bridge, Transactions of the Japan Society of Mechanical Engineers Series B, Vol. 70 (2004).

[3] Sayo Terasaki and Shogo Sensui and Ichiro Ueno, Thermocapillary-driven coherent structures by low-Stokesnumber particles and their morphology in high-aspect-ratio liquid bridges, International Journal of Heat and Mass Transfer (2023)

[4] Schwabe, D., Mizev, A. I., Udhayasankar, M. and Tanaka, S., Formation of dynamic particle accumulation. structures in oscillatory thermocapillary flow in liquid bridges, Physics of Fluids, Vol. 19 (2007), 072102

Melting in microgravity of phase change materials in axisymmetric systems with thermocapillary effects: melting bridges and spherical drops

A. Borshchak Kachalov, R. Varas, P. Salgado Sánchez, U. Martinez, D. Gligor,
J. M. Ezquerro and J. Porter
E-USOC, Center for Computational Simulation, Escuela Técnica Superior de Ingeniería Aeronáutica y del Espacio, Universidad Politécnica de Madrreid, Madrid, Spain. pablo.salgado@upm.es

Due to its relevance to recent microgravity research [1,2], we numerically investigate the thermocapillary-driven melting of the organic phase change material n-octadecane in weightlessness. The effect of thermocapillary flows on heat transport is analyzed in two axisymmetric configurations: a melting bridge [3] and a spherical drop; see the sketches of Fig. 1. The solid/liquid transition is studied by varying key dimensionless parameters including the Marangoni number (Ma), which is selected by the applied temperature(s), and geometry, which is characterized by the dimensionless volume V and aspect ratio $\Gamma = L/R$, if applicable. For the melting bridge system, we first consider the case of cylindrical geometry with $V = 1$ and analyze the effect of Ma and Γ on heat transport and the type of oscillatory flow that appears in the liquid phase during the melting process. These basic results are compared with those obtained in rectangular containers [4], with an improvement in the heat transfer rate of approximately 50% seen for the melting bridge configuration. The analysis is then extended to noncylindrical bridges with $V \neq 1$, and to spherical drops; these drops may result from the destabilization and break-up of a liquid bridge that experiences strong perturbations (accelerations). Melting is analyzed in both cases for varying Ma and/or V.

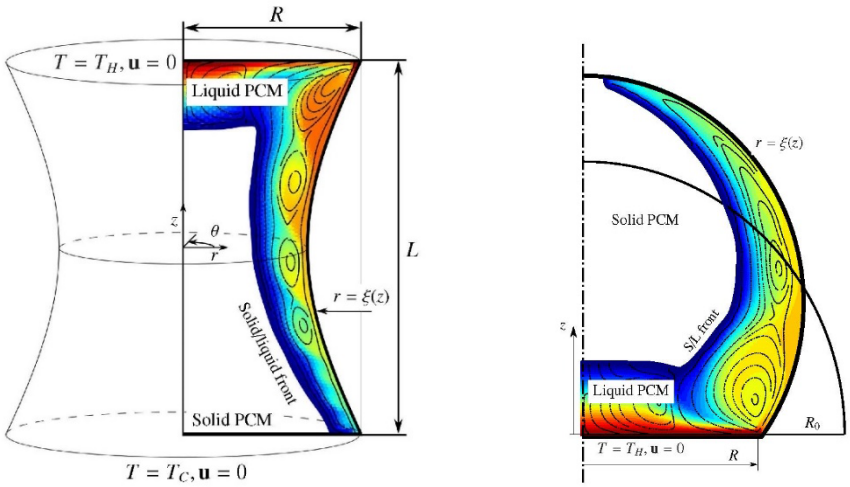

FIG. 1. Sketch of the axisymmetric systems modelled numerically: (left) melting bridge, (right) spherical drop.

[1] J. M. Ezquerro, P. Salgado Sánchez, A. Bello, J. Rodríguez, V. Lapuerta, and A. Laverón-Simavilla. Experimental evidence of thermocapillarity in phase change materials in microgravity: measuring the effect of Marangoni convection in solid/liquid phase transitions. *International Communications in Heat and Mass Transfer* **113**, 104529 (2020).

[2] J. Porter, A. Laverón-Simavilla, M. M. Bou-Ali, X. Ruiz, F. Gavalda, J. M. Ezquerro, P. Salgado Sánchez, U. Martínez, D. Gligor, I. Tinao, J. Gómez, J. Fernández, J. Rodríguez, A. Borshchak Kachalov, V. Lapuerta, B. Seta, J. Massons, D. Dubert, A. Sanjuan, V. Shevtsova, and L. García-Fernández. The “Effect of Marangoni Convection on Heat Transfer in Phase Change Materials” experiment. Submitted to *Acta Astronautica*, under review.

[3] R. Varas, P. Salgado Sánchez, J. Porter, J. M. Ezquerro, and V. Lapuerta. Thermocapillary effects during the melting in microgravity of phase change materials with a liquid bridge geometry. *International Journal of Heat and Mass Transfer* **178**, 121586 (2021).

[4] P. Salgado Sánchez, J. M. Ezquerro, J. Fernández, and J. Rodríguez. Thermocapillary effects during the melting of phase change materials in microgravity: heat transport enhancement. *International Journal of Heat and Mass Transfer* **163**, 120478 (2020).

Occurrence of Convective Formations in Ternary Gas Systems Containing Greenhouse gases

Vladimir Kossov[1], Olga Fedorenko[1,2], Dauren Zhakebayev[3] and Mansiya Asembaeva[4]

[1] *Department of Physics, Institute of Mathematics and Informatics, Abai Kazakh National Pedagogical University, 050010, Almaty, Kazakhstan,* kosov_vlad_nik@list.ru

[2] *Institute of Experimental and Theoretical Physics, al-Farabi Kazakh National University, 050040, Almaty, Kazakhstan,* fedor23.04@mail.ru

[3] *Faculty of Mechanics and Mathematics, al-Farabi Kazakh National University, 050040, Almaty, Kazakhstan,* dauren.zhakebayev@gmail.com

[4] *Institute of Experimental and Theoretical Physics, al-Farabi Kazakh National University, 050040, Almaty, Kazakhstan,* m.asembaeva@physics.kz

The presence of several mechanisms of heat and mass transfer (convection, thermal conductivity, diffusion, thermal diffusion, and diffusion thermal conductivity) and the need to take into account cross effects determine the difficulties in describing multicomponent mixtures [1]. To manage the behavior of such systems, new understanding of the characteristics of combined mass transfer must be acquired, in not only the diffusion or convective stages of mixing but also at the interface between these regimes. Such systems may exhibit monotonic and oscillatory instabilities, as evidenced by the findings of a study of convective stability in multicomponent systems in a non-uniform temperature field in vertical cavities [2]. For such situations, the equations of motion and mass transfer of components, in which the effects of cross-diffusion are insignificant, were used to solve the stability problem. Due to thermal diffusion, the component with a negative separation coefficient moves to a more heated wall, which leads to the development of instability accompanied by an increase in the flow intensity and a sharp decrease in the concentration difference between the upper and lower boundaries, which is explained by the appearance of convection. However, as studies conducted in [3] have shown, concentration gravitational convection can also manifest itself in a strictly isothermal case. The seeming paradoxical nature of the emerging movement is explained by the unstable stratification of at least one of the components of the system. Due to the difference in the diagonal and cross diffusion coefficients, the spatial redistribution of dissolved substances in the gravity field occurs, followed by the release of the potential energy of the component with the highest molecular weight, which is converted into the energy of the moving medium.

The paper presents experimental and numerical research on the study of the change of "diffusion - concentration gravitational convection" modes in an isothermal three-component gas mixture, in which the diffusion coefficients of the components differ distinctively from each other. Ternary mixtures in which at least one of the components is a greenhouse gas are considered. Mixing occurs at room temperature and at elevated pressures. It is assumed that the results obtained in model situations will make it possible to develop recommendations that, when followed, can achieve the mode of preferential transfer of a component with given thermophysical properties, which seems to be relevant for systems containing greenhouse gases.

Figure 1 shows a schematic problem statement for a flat vertical channel (Fig. 1a), experimental data for the 0.570 He + 0.430 C_3H_8 – 0.403 C_3H_8 + 0.597 N_2O system in which the diffusion–convection transition was studied at various pressures and room temperature (Fig. 1b), shadow patterns of convective flows (Fig. 1c), the experimental data reconstructed in terms of the Rayleigh numbers and their location relative to the critical stability line (Fig. 1d).

Experiments in the systems He + C_3H_8 – C_3H_8 + N_2O, He + CO_2 – N_2, He + Ar – N_2, and CH_4 + R12 – n-C_4H_{10} revealed a nonlinear dependence of total transfer on pressure for the components with the highest molecular weight. The dependence shown in Fig. 1b is not typical for diffusion, in which a monotonic decrease in the intensity of mixing with increasing pressure is observed. Linear stability analysis makes it possible to satisfactorily determine the critical values of the Rayleigh numbers at which convection begins (Fig. 1d), which is fixed by the shadow method (Fig. 1c). As the intensity of the convective motion increases, the deviations from the linearized model increase and the profiles of the velocity and concentrations of the components given within the framework of the linear approach no longer agree with the real situation.

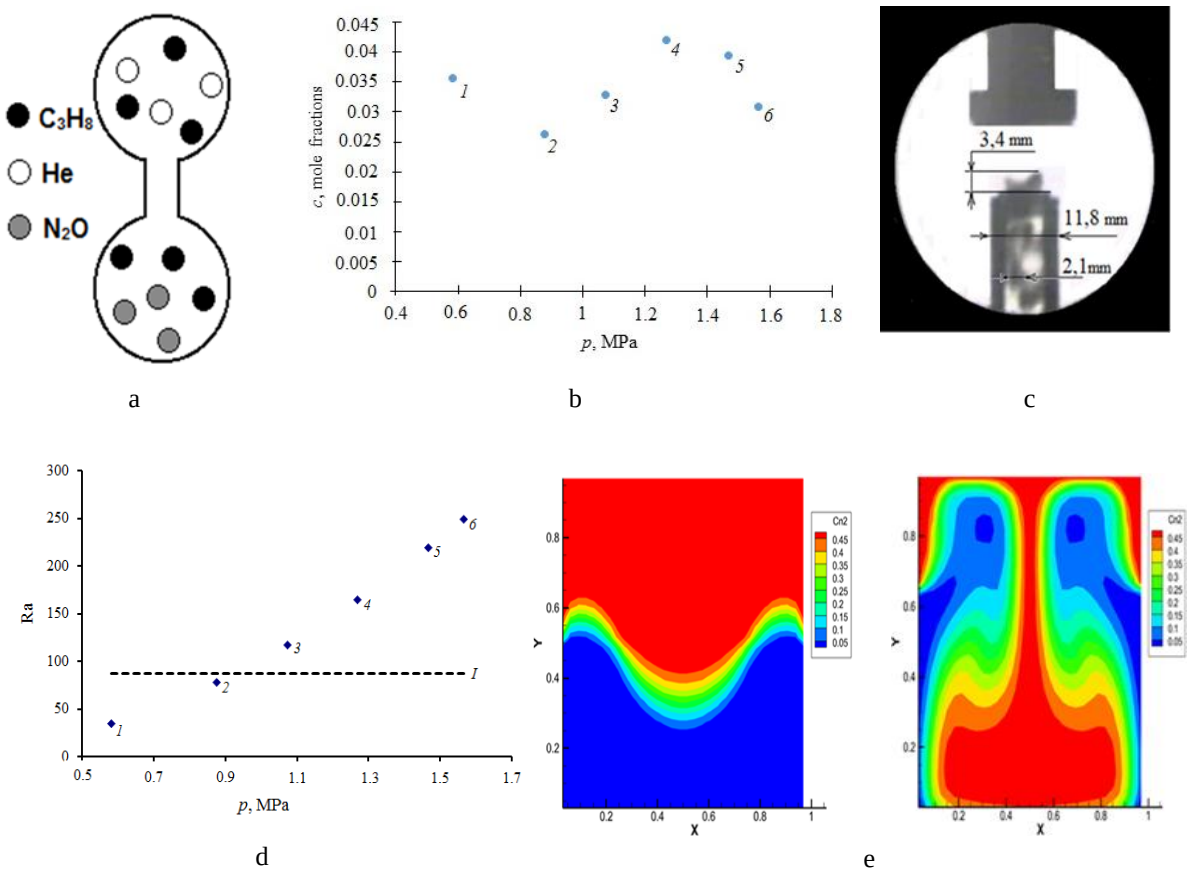

FIG. 1. Diffusion and convective regimes in isothermal ternary gas mixtures: a: Scheme of an experimental diffusion cell of the two-flask method [4]; b: Nitrous oxide concentrations transferred to the upper flask of the apparatus as a function of pressure for the system 0.293 He + 0.707 C_3H_8 – 0.697 C_3H_8 + 0.303 N_2O. Points refers to 1 – 0.487; 2 – 0.582; 3 – 0.683; 4 – 0.780; 5 – 0.926 MPa [4]; c: Shadow picture of convective formation in the upper flask of the diffusion cell; d: The dependence of the partial Rayleigh number on pressure for the system 0.570 He + 0.430 C_3H_8 – 0.403 C_3H_8 + 0.597 N_2O. Points ♦ are the experimental Rayleigh numbers at various pressures: 1 – p = 0.583, 2 – 0.876, 3 – 1.074, 4 – 1.27, 5 – 1.467, 6 – 1.565 MPa. I is a critical line [4]; e: Isoconcentration lines of carbon dioxide for the system 0.5 He + 0.5 CO_2 – N_2, p = 1.0 MPa, T = 298.0 K. Characteristic mixing times are equal to 0.76 s and 1.90 s respectively.

In this case, to study the evolution of convective flows in the initial stage of development is possible numerically within the framework of nonlinear approximations. Moreover, a matrix of transfer coefficients was used in the equations of multicomponent diffusion, i.e., the movement of one solute along its concentration gradient causes a flow of other solutes either along or against. In this case, the mixture separation boundary can be destabilized, and hydrodynamic instabilities arise due to the cross diffusion. The concentration distributions of the components were obtained at different times (Fig. 1f), on the basis of which the conditions for the occurrence of convective formations were studied, and their characteristics were explained using the cross-diffusion model.

The Committee of Science of the Ministry of Science and Higher Education of the Republic of Kazakhstan has supported this work (the project number: AP14870237).

[1] I. I. Ryzhkov and V. M. Shvetsova, On thermal diffusion and convection in multicomponent mixtures with application to the thermogravitational column, Phys. Fluids **19**, 027101 (2007).
[2] N. A. Zhubova and T. P. Lyubimova, Soret-induced convection of binary and ternary mixtures in square cavity heating from above, Bulletin of Perm University. Physics **2(36)**, 74-82 (2017).
[3] V. Kossov, O. Fedorenko, A. Kalimov and A. Zhussanbayeva, Diffusion mechanisms for the occurrence of the instability of mechanical equilibrium of a ternary gas mixture containing carbon dioxide, Fluids **6(5)**, 177 (2021).
[4] V. N. Kossov, O. V. Fedorenko, M. K. Asembaeva and V. Mukamedenkyzy, Changing diffusion-convection modes in ternary mixtures with a diluent gas, Theor. Found. Chem. Engin. **54(2)**, 289-296 (2020).

Generating electrokinetic ion resonance in an electrical double layer using MHz-frequency surface acoustic waves in the underlying substrate

Oles Dubrovsky, Sudeepthi Aremanda, and Ofer Manor*

Department of Chemical Engineering, Technion – Israel Institute of Technology, Haifa, Israel

manoro@technion.ac.il

We employ for the first time a MHz-frequency mechanical vibration, i.e., a Rayleigh type surface acoustic wave (SAW) in a solid substrate, to dynamically excite the electrical double layer of ions (EDL) in the neighboring electrolyte solution.

The EDL, to appear next to charged surfaces in electrolyte solutions, is an electrical surface phenomenon in which an artificially or naturally charged surface in an electrolyte solution attracts a cloud of ions that introduce osmotic and electrical effects in its vicinity. The EDL is fundamental across countless natural and artificial systems and may considerably vary in properties between one system to another. Its applications range from supporting electrophoresis and electro-wetting to governing the kinetics of particulate coagulation, folding structures of proteins, surface properties of membranes, and particulate adsorption onto an underlying substrate. The generic nature of the EDL and the interplay between physical mechanisms therein alongside its short length scales of usually several nanometers and a relaxation time scale of nano- to micro-seconds render the EDL and the interplay between its different subcomponents an enigma, even now more than a century since it was discovered.

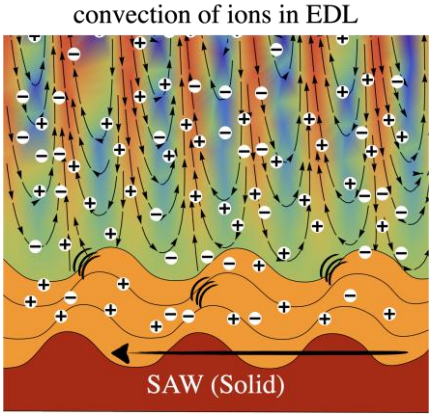

Fig. 1: A schematic illustration of positive (+) and negative (–) ions in an EDL within an electrolyte solution, where the underlying solid supports a SAW, which imposes a periodic and oscillatory convective flow within the SAW evanescent viscous penetration length into the solution, which may be comparable to the Debye length of the EDL. The flow is indicated using streamlines, which are calculated using theory for the generation of acoustic flow by a propagating SAW [2], where arrows indicate flow direction and the red and blue colors indicate high and low flow intensity, respectively

The experiment, which we will present in our talk and is illustrated in Fig. 2, is inspired by a theory [1] for the near equilibrium distortion of the EDL by MHz-frequency surface acoustic waves (SAWs) in the solid. The SAW excitation renders dynamic variations in the ion density and a partial electrical discharge in the EDL, which supports the leakage of a measurable electrical field off the EDL. The electrical field leakage corresponds to an array of mechanical-electrical responses therein. We show that the measurement agrees to leading order with a dedicated theory for the near equilibrium distortion of the EDL. The agreement facilitates a mean for deciphering the measured signal to potentially give new and direct insights about dynamical effects in EDLs. In the measurement, we observe resonance effects in the excited EDL to result from a periodic motion of ions and which are akin to resonance in an equivalent RLC electrical circuit.

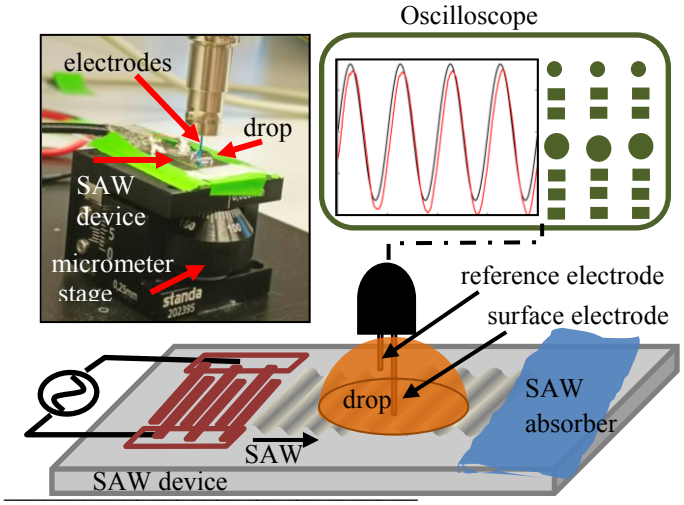

Fig. 2: A photo and a schematic of the experimental system, where we place a drop atop a SAW device while using a surface and reference electrodes, connected to an oscilloscope to measure the electrical field that leak off the SAW excited EDL

[1] O. Dubrovski and O. Manor. Revisiting the electroacoustic phenomenon in the presence of surface acoustic waves, Langmuir, **37**,14679–14687 (2021)

[2] O. Manor, L.Y. Yeo, and J.R. Friend, The appearance of boundary layers and drift flows due to high-frequency surface waves, J. Fluid Mech. **707**, 482–495 (2012).

Generating resonance effects in electrical double layers via MHz-frequency surface acoustic wave-excitation

Sudeepthi Aremanda[1] and Ofer Manor[1]

[1] *The Wolfson department of Chemical Engineering, Technion-IIT, 3200003, Haifa, Israel*
asudeepthi@campus.technion.ac.il

I. INTRODUCTION

The electrical double layer of ions (EDL) - the arrangement of ions at the solid-electrolyte interfaces - appears across numerous systems and finds applications in diverse fields. The research on EDLs has advanced swiftly over the past decades. Nevertheless, close probing of EDLs remains a challenge to date because of their short length and time scales, typically characterized by a Debye length of several nanometers and a relaxation time of nanoseconds to microseconds, respectively. We propose here an experimental technique that employs time dynamic measurements to scrutinize EDLs closely by utilizing MHz-frequency surface acoustic waves (SAWs). For this purpose, we excite the EDL at its length and time scales with SAW and capture its response as an electrical frequency spectrum. To go into detail, SAW upon interacting with the electrolyte solution generates a transient periodic flow at its frequency in the electrolyte solution within the viscous penetration depth. A recent theoretical study [1] suggested that the SAW-driven fluid flow in the electrolyte next to the solid surface can potentially alter the equilibrium arrangement of ions in the EDL and cause leakage of the electric field out of the EDL owing to the overlap of the characteristic length and time scales of the EDL and SAW. Furthermore, the study highlighted that the leaked electrical potential carries structural information and properties of the EDL. Therefore, in practice one may obtain information about EDLs by measuring the electrical potential leakage out of the SAW-excited EDLs. In this work, we aim to measure the electrical potential leakage away from the SAW-excited EDLs experimentally and obtain structural information and properties of the EDLs, subsequently.

II. EXPERIMENTAL DETAILS

We generate SAW in a Lithium Niobate substrate which supports the formation of an EDL in a neighboring electrolyte drop of 20 μl volume as shown in fig. 1a. We used two univalent (near ideal) electrolyte solutions: $NaNO_3$ and KCl at ionic strengths (I) ranging from 0.5 to 6 mM and applied SAW signals at 20 MHz frequency (f) in the voltages (ψ_i) ranging from 20 to 100 mV. Two microelectrodes

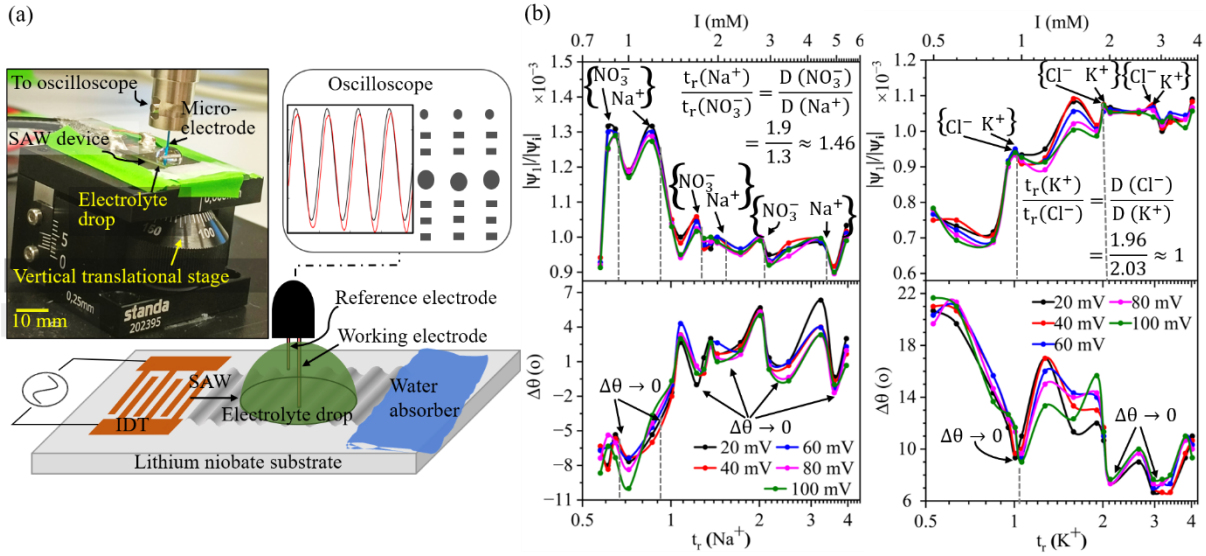

FIG. 1. (a) Schematic illustration and real image of the experimental setup; (b) Magnitude and phase of the electrical potential leakage from SAW-excited EDLs in NaNO3 and KCl solutions

of 250 μm diameter were positioned in the electrolyte drop to measure the electrical potential leakage (ψ_1). As the leaked electrical potential is expected to disperse at distances larger than a SAW wavelength

away from the solid surface, we positioned the first electrode (the surface electrode) at a distance of one-fifth of the SAW wavelength (40 μm) from the solid surface. The second electrode which is the reference electrode was set in the bulk of the drop at a distance of several SAW wavelengths away from the solid surface. Therefore, the electrical potential leakage is measured against the electrical potential in the bulk of the electrolyte drop. Finally, the electrodes were connected to a lock-in amplifier via BNC connectors for the measurement.

III. RESULTS AND DISCUSSION

We present our experimental results in fig. 1b wherein we show the magnitude of scaled electrical potential leakage $\left(\frac{|\psi_1|}{|\psi_i|}\right)$ and its phase $(\Delta\theta)$ relative to the SAW-excitation signal at various power levels of the SAW for $NaNO_3$ and KCl solutions as a function of ionic strength (I) and time-ratio (t_r) values. Here, the time ratio is defined as the ratio of the characteristic time scale of SAW to the EDL relaxation time scale, i.e., $t_r \equiv \frac{\omega^{-1}}{(\sigma^2/D_j)}$, where ω is the angular frequency of SAW, D_j is the diffusion coefficient of the ion 'j' in EDL, and σ is the Debye length. We evaluated Debye lengths using the expression, $\sigma = \sqrt{(\varepsilon_0\varepsilon_r RT)/2000F^2}\ 1/\sqrt{I}$, where ε_0 and ε_r are the permittivity of the vacuum and relative permittivity of the electrolyte solution respectively and $R,\ T,\ F$ are the gas constant, temperature, and Faraday constant respectively [2]. The $t_r$values along the x-axes in fig. 1b are derived based on the diffusion coefficients of the positive ions in the respective electrolyte solutions. We noticed in fig. 1b that the magnitude of electrical potential is maximized for the t_r values that correspond to the ratio of the diffusion coefficients of positive and negative ions in the respective electrolyte solutions and the phase difference approaches zero $(\Delta\theta \to 0)$ at these points. The results resemble the behavior of series RLC (resistor-inductor-capacitor) circuits at resonance. In literature, EDLs are often modeled as simple RLC circuits [2]. Therefore, we attribute the peaks in fig. 1b (the top layer -the electrical frequency spectrum) to the resonance of ions in the EDL to the SAW excitation. For the $NaNO_3$ solution, we observe a maximum of $\frac{|\psi_1|}{|\psi_i|}$ in fig. 1b at $t_r(Na^+) \approx 1$ i.e., when the relaxation time scale of Na^+ matches the characteristic time scale of the EDL. Further, theoretically, we can write $\frac{t_r(Na^+)}{t_r(NO_3^-)} = \frac{D_{NO_3^-}}{D_{Na^+}} = \frac{1.9}{1.3}$ which is ≈ 1.46. In fig. 1b (top left) we see that the peak on the left of the peak at $t_r(Na^+) \approx 1$ corresponds to $t_r \approx 0.7$ and the ratio turns out to be $\approx \frac{1}{0.7} \approx 1.44$ which is $\approx \frac{D_{NO_3^-}}{D_{Na^+}}$. This signals that the peak at $t_r \approx 0.7$ corresponds to the resonance of NO_3^- ions in the EDL to the SAW excitation. Moreover, the phase difference $(\Delta\theta)$ between the excitation signal and the response of the EDL approach zero at these points (bottom left of fig. 1b). Similarly, for KCl we can write $\frac{t_r(K^+)}{t_r(Cl^-)} = \frac{D_{Cl^-}}{D_{K^+}} = \frac{1.96}{2.03}$ which is ≈ 1. Hence, we expect the resonance peaks that correspond to $K^+$and Cl^- to occur close by in this case. Confirming this, in the case of KCl we observe only one peak at $t_r(K^+) \approx 1$ in fig. 1b (top right). We believe that the resonance peaks for $K^+$and Cl^- are engulfed into a single peak in this case. In addition, we see the phase difference $(\Delta\theta)$ between the excitation SAW signal and the response of the EDL to approach zero at this point (bottom right of fig.1b). Therefore, there is ample evidence to believe that the ions in the EDL resonate with the SAW excitation when their relaxation time scales match the characteristic time scale of SAW. Further, we speculate that the residual peaks appearing in the electrical frequency spectrum (the top layer of fig. 1b) correspond to the higher harmonics as the t_r values at these points appear to be integer multiples of the t_r values of the fundamental resonance points. Thus, it is possible to identify the type of ions in the EDL by observing the resonant effects in the electrical frequency spectrum since the resonant frequencies are a function of the diffusion coefficients of the ions. Further, we acquired the structural information about the EDL by applying the RLC circuit analogy to the SAW-excited EDLs and computing the equivalent circuit elements- the resistance experienced by the ions in the EDL due to viscous dissipation (the equivalent of R) and the measure of charge (the equivalent of C) in the EDL.

[1] O. Dubrovski and O. Manor, "Revisiting the Electroacoustic Phenomenon in the Presence of Surface Acoustic Waves," *Langmuir*, vol. 37, no. 50, pp. 14679–14687, 2021, doi: 10.1021/acs.langmuir.1c02414.

[2] R. J. Hunter, *Foundations of colloid science*. Oxford University Press, 2001.

An experimental study on the role of heat generation on the morphology and microstructure in thin-layer electrodeposition instability

Sarathy K. Gopalakrishnan[ab], Pinar Eribol[c], Diwakar. S. Venkatesan[d], Abdelkrim Talbi[c], Ranga Narayanan[a], Kirk J. Ziegler[a], Farzam Zoueshtiagh[c]

[a]*Department of Chemical Engineering, University of Florida, Gainesville, Florida 32611, USA*
[b]*Department of Materials Science and Engineering, University of Florida, Gainesville, Florida 32611, USA*
[c]*University of Lille, CNRS, UMR 8520, IEMN, F-59000 Lille, France*
[d]*Engineering Mechanics Unit, JNCASR, Jakkur, Bangalore, 560064, India*

Metal deposits during electrodeposition can lead to well-defined patterns due to morphological instability. However, the underlying instability is often obscured by the growth of dendritic branches due to non-linear interactions. These non-linear interactions can take the form of coupled phenomena like convection, ohmic heating, and localized pH or concentration changes in the electrolyte solution. Infrared thermography mapping during thin-layer electrodeposition showed that the ohmic heating from the growth of patterns substantially increases the temperature of the electrolyte. In this work, we studied the effect of the initial electrolyte concentration on the temporal evolution of the temperature profile within the electrochemical cell during electrodeposition (see Figure 1). Our results show that the temperature distribution within the cell depends on various coupled factors like the initial bulk concentration and pH of the solution, as well as dynamic transitions in the morphology and microstructure of the growing deposits. Understanding these coupled phenomena is essential to predicting the growth patterns during electrodeposition, which can be important to heat management problems associated with battery safety and performance.

Acknowledgment: We acknowledge support from NSF 2004527

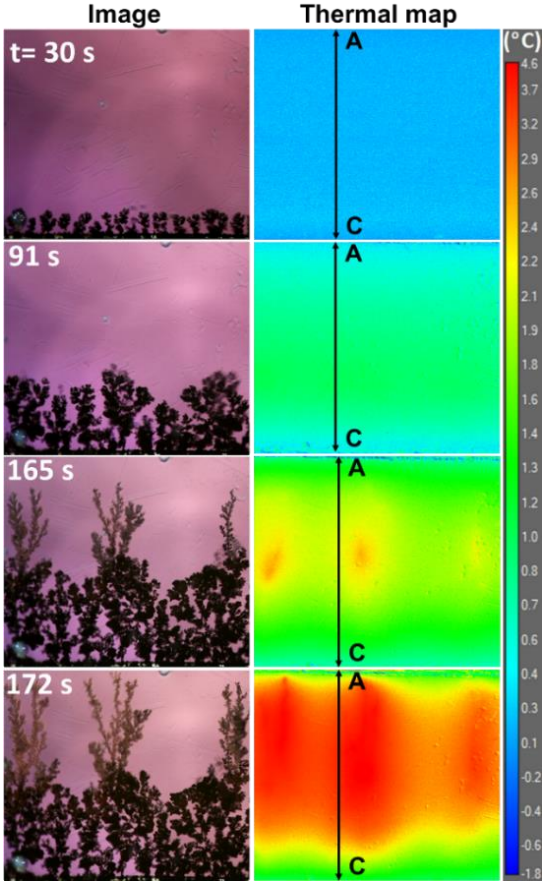

Figure 1. The evolution of electrodeposited morphology and the corresponding thermal map at an electrolyte concentration of 5 mM for |AC| = 6mm (A: anode, C: cathode).

Formation of Faraday waves on a liquid in a librating annular channel

S. Richter[1], I. D. Borcia[1], R. Borcia[1], M. Bestehorn[1], F.-T. Schön[2] and U. Harlander[2]

[1] *Department of Theoretical Physics, BTU, 03044, Cottbus, Germany*
[2] *Department of Fluid Mechanics, BTU, 03044, Cottbus, Germany*

Referring to recent experimental studies [1 , 2], we simulate the spatio-temporal evolution of a three-dimensional liquid residing in a large open vessel with the geometry of an annular channel, i.e., the liquid is bounded on the bottom side by a solid and flat substrate, on the top by its free surface and in radial direction by two curved solid sidewalls with different radii (Fig. 1).

The system is excited by time-periodic oscillations of the channel around its center, engendering the formation of horizontal Faraday instabilities. In the case of excitations breaking the horizontal mirror symmetry, a non-vanishing mean flow is observed.

We compare our results with both the data obtained from the experiments and the findings of a previously employed direct numerical simulation [3], which follows the same approach as the present method but is limited to two dimensions.

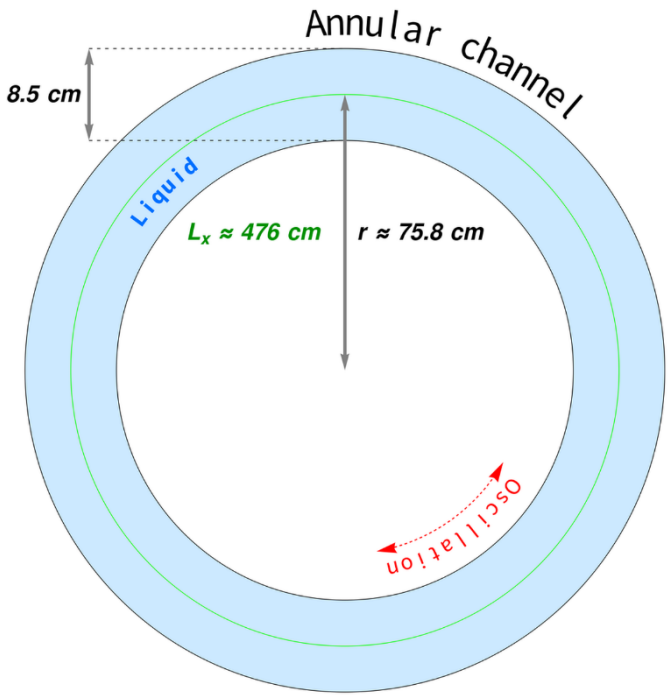

FIG. 1: Plan view of simulated domain (gravity points into the plane). The average circumference of the channel is $L_x \approx 4.76$ m and the mean depth is about 3 cm to 6 cm. This corresponds to the parameters used in the experiment. The system performs librations (oscillatory rotations) around the center causing wave formation.

[1] I. D. Borcia, R. Borcia, W. Xu, M. Bestehorn, S. Richter, and U. Harlander, "Undular bores in a large circular channel", Eur. J. Mech. B Fluids **79**, 2020.
[2] I. D. Borcia, R. Borcia, S. Richter, W. Xu, M. Bestehorn, and U. Harlander, "Horizontal faraday instability in a circular channel", PAMM **19**, 2019.
[3] S. Richter and M. Bestehorn, "Direct numerical simulations of liquid films in two dimensions under horizontal and vertical external vibrations" , Phys. Rev. Fluids **4**, 2019.

Prandtl Number Dependence of Instability of Thermocapillary Convection in an Annular Pool with a Heated Inner Cylinder

Li Zhang[1] and You-Rong Li[2]

[1] Chongqing City Management College, 401331, Chongqing, China, zhanglizl@cqu.edu.cn
[2] School of Energy and Power Engineering, CQU, 400044, Chongqing, China, liyourong@cqu.edu.cn

ABSTRACT

Thermocapillary convection is driven by the thermal capillary force from the tangential temperature gradient. It widely exists in many industrial production processes, such as crystal growth, the melting and solidification of phase change materials, evaporation, and condensation. Various flow patterns appear in the thermocapillary convection, which attracts a lot of researchers to reveal the underlying mechanisms. The existing experiments and numerical simulations mostly focus on the thermocapillary flow in an annular pool heated from its outer wall. There are few researches on the annular pool heated from the inner wall. However, in microgravity experiments on thermocapillary flow in the annular pool in China Space Station, the inner cylinder is heated in order to reduce the heat flux. This paper presented a set of direct numerical simulations on Prandtl number dependence of the instability of thermocapillary flow in an annular pool with a heated inner cylinder. The Prandtl number of the working fluids varies from 0.01 to 28.01. The radius ratio of the annular pools is fixed at 0.2 and the aspect ratio is 0.5. It was found that with the increase of the Prandtl number, the critical Marangoni number of the flow destabilization increases. Therefore, for higher Prandtl number fluids, the thermocapillary convection becomes more stable. After the flow destabilizes, the concentric ring, the cellular structure, the rotating petal-like, and the spoke pattern appear respectively in the annular pool depending on the Prandtl number.

Keywords: Thermocapillary convection; numerical simulation; instability; Prandtl number; annular pool

A mesh refinement approach for the Volume of Fluid Method

R. Dachsel[1] and M. Bestehorn[2]
[1]*Department of Medical Physics*
Carl-Thiem-Klinikum Cottbus, 03048 Cottbus, Germany
[2]*Department of Theoretical Physics*
BTU Cottbus-Senftenberg, 03044 Cottbus, Germany

The volume of fluid (VOF) method is a free-surface modelling technique for tracking and locating the free surface or fluid–fluid interface [1]. In this framework, an indicator function has to be defined to track the interface on a fixed grid. The evolution of this indicator function is governed by the transport equation which has to be solved separately from the Navier-Stokes equations. In order to increase the accuracy of the interface, one can either use sophisticated interpolation techniques [2] or refine the grid for the entire framework which includes both the transport equation and as well as the Navier-Stokes equations.

In this work we propose an improvement by using a grid refinement technique that will only affects the indicator function and the transport equation of the framework while the Navier-Stokes equations remains on the unrefined grid. In this way we increase the resolution and accuracy of the interface while the numerical treatment of the linear transport equation on the refined grid does not require an extensive computational effort.

By a detailed evaluation at hand of standard benchmarks and applications from CFD we demonstrate that our approach may yield significant improvements over the none refined framework while similarly fast.

---

[1] W. Noh and P. Woodward: SLIC (Simple Line Interface Calculation), 1976
[2] R. Remmerswaal and A. Veldman: Parabolic interface reconstruction for 2D volume of fluid methods, 2022

Internal Mass Transfer between a Single Particle and Non-linear Extensional Creeping Flow

Jie Chen[1,2], Anjun Liu[2,3] Weipeng Zhang[1,2], Zai-Sha Mao[1,2], Chao Yang[1,2*]

[1] *CAS Key Laboratory of Green Process and Engineering, Institute of Process Engineering, Chinese Academy of Sciences, Beijing 100190, China*

[2] *School of Chemical Engineering, University of Chinese Academy of Sciences, Beijing 100049, China*

[3] *Qilu University of Technology (Shandong Academy of Sciences), Shandong Computer Science Center (National Supercomputer Center in Jinan), Jinan 250101, China*

**Corresponding author: chaoyang@ipe.ac.cn*

The fundamental research on transport phenomena (momentum, heat and mass transfer) of a single particle in non-linear extensional creeping flow is of great importance in practical application in chemical and process industry. The distinctive flow field will exhibit with the variation of nonlinear intensity (E). The mass transfer rate thereupon is influenced greatly by the nonlinear intensity and Peclet number. Based on the flow field, we have simulated numerically the internal mass transfer process and proposed the empirical correlations of the mass transfer rate for a wide range of Peclet number (from 0 to 10,000). The simulation results show that when $E \geq 0$, there are two symmetrical internal circulations in the droplet, which is similar to that in a linear extensional flow. The limit value of mass transfer rate Sh is 15, which is equal to that in a linear extensional flow, no matter how large E is. When $E \leq -3/7$, the number of internal flow circulation of a droplet increase to four and the transfer rate Sh increases. When $E = -1$, the maximum internal transfer rate Sh equals 30, which is twice of that in a linear extensional flow. The generation of new flow circulations in droplets and the circulation positions will enhance mass transfer when $E \leq -3/7$, which provides a new idea for enhancing the internal mass transfer rate of droplets.

Acknowledgement: The National Key Research and Development Program of China (No. 2021YFC2902502), the National Natural Science Foundation of China (22078320, 22035007), the NSFC-EU project (31961133018), and the External Cooperation Program of BIC, Chinese Academy of Sciences (122111KYSB20190032).

Experimental Investigation of Evaporation Droplet Imposed Airflow in Microgravity

Zi-long Li[1,2] , Yu-Qun Tao[1], Qiu-Sheng Liu[1,2*] Jun Qin[1,2], Christophe Minetti[3], Carlo Saverio Iorio[3]

[1] *Institute of Mechanics, Chinese Academy of Sciences, Beijing 100190, China*

[2] *University of Chinese Academy of Sciences, Beijing 100049, China*

*liu@imech.ac.cn

Droplets exposed to airflow is the most common phoenomenon in nature and it also has important application in the field of the microgravity such as environment control and life support system (ECLSS) in space station. There are few studies on the dynamics of droplets in microgravity. Milad and Christoph et.al[1] performed an experiment to study the behavior of droplet shedding by shearing airflow in microgravity, they found that the critical velocity of shedding droplet is lower in microgravity than that in normal gravity.

This wotk performs an experiment in microgravity using parabolic flight to study the interfacial characteristics of droplets subjected to shear flow. For the volume of 18 μL and 25 μL, The difference in microgravity is larger than that in normal gravity under the same wind velocity and with the increase of the airflow velocity, the difference in microgravity increases more rapidly as shown in Fig. 1. The $\theta_a - \theta_r$ and wind speed can be described by the formula

$\sin\frac{\theta_a-\theta_r}{2}=\frac{1}{\sin\theta_0}\frac{C_D}{k}\cdot We$, and this has a good agreement with experiment results in microgravity as shown in Fig 2

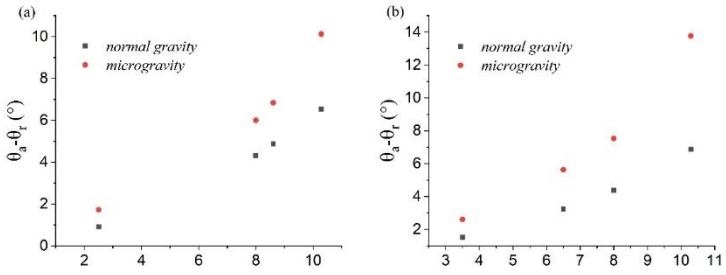

Fig. 1 The difference between advanced and rear contact angle in microgravity and normal gravity

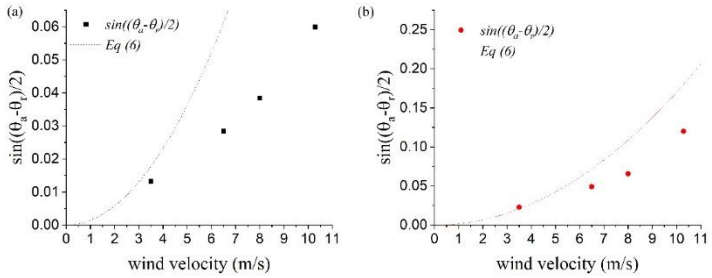

Author Index